Investigating the effect of hypoxia on the JmjC histone lysine demethylase KDM4A

Rebecca Louise Hancock
Linacre College, University of Oxford

Michaelmas Term 2016

A thesis submitted to the board of the Faculty of Physical Sciences of the University of Oxford in partial fulfilment of the requirements for the degree of Doctor of Philosophy

Abstract

The JmjC-histone lysine demethylases (JmjC-KDMs) are epigenetic regulators responsible for the demethylation of methylated lysine residues on the *N*-terminal histone tails. As Fe^{2+} and 2-oxoglutarate dependent oxygenases (2OG oxygenases), the JmjC-KDMs possess an absolute requirement for molecular oxygen and are related to the cellular oxygen sensing HIF hydroxylases, PHD2 and FIH. Several JmjC-KDMs are known HIF target genes, hence are upregulated in hypoxia. Moreover, a number of JmjC-KDMs have been shown to have differential oxygen dependences, while aberrant histone methylation has been observed in both hypoxic cells and disease states such as cancer and cardiovascular disease.

The work described in this thesis aimed to investigate the impact of hypoxia on the JmjC-KDM, KDM4A. *In vitro* kinetic analyses revealed a $K_m^{app}(O_2)$ for recombinant KDM4A of 173 ± 23 μM, which is higher than reported values for the 2OG oxygenases C-P4H, mPAHX and even FIH, and approaching those evaluated for the key oxygen sensor PHD2 (230-1746 μM). These results indicate that KDM4A activity is sensitive to oxygen availability, and has the biochemical potential to act as an oxygen sensor in the context of epigenetic regulation.

Subsequent investigation of the cellular oxygen dependence of KDM4A found that the activity of ectopically expressed KDM4A in U2OS cells demonstrates a graded response to oxygen. Importantly, this trend correlates with the *in vitro* results, providing further evidence that hypoxia may impact upon epigenetic regulation by the JmjC-KDMs.

The various factors that may contribute to the hypoxic inhibition of KDM4A were investigated, both *in vitro* and in cells. The results of these studies suggest that altered concentrations of TCA cycle intermediates, comprising reduced levels of the 2OG oxygenase co-substrate 2OG and increased concentrations of the reported inhibitor 2HG, are likely to have only a minimal effect on the activity of KDM4A in hypoxia. Interestingly, the inhibitory potency of the 2OG oxygenase inhibitor IOX1 against KDM4A was increased under conditions of low oxygen, implying that the use of mixed-mode inhibitors against KDM4A may be of therapeutic benefit in hypoxic disease states. This may be of particular pertinence to cardiac hypertrophy (CH), in which KDM4A activity is reported to have pathophysiological consequences. In a collaboration with Dr Tim McKinsey (University of Colorado, Denver), the KDM4 inhibitor CCT1 was tested in a phenotypic screen of cardiomyocyte hypertrophy, the results of which further support a role for KDM4A in this disease, and suggest that the use of small-molecule inhibitors of KDM4A may be a viable therapeutic strategy in CH.

Finally, the effect of reactive oxygen species, levels of which may be increased in hypoxia, on KDM4A activity was explored. Recombinant KDM4A was found to be acutely sensitive to inhibition by hydrogen peroxide (H_2O_2) when compared to the HIF hydroxylases PHD2 and FIH. These results imply that KDM4A may act as a sensor of oxidative stress at the chromatin level, and further investigation in more biologically relevant contexts is proposed.

Overall, the work described herein demonstrates that the activity of KDM4A is sensitive to oxygen availability, a phenomenon that is likely to have significant implications for epigenetic regulation in hypoxia and the expression of KDM4A-regulated genes in ischaemic diseases.

Acknowledgements

Firstly, I would like to thank Dr Emily Flashman and Dr Akane Kawamura for their support and supervision throughout my entire DPhil, and for being truly excellent mentors. Thank you for trusting me with a challenging and inspiring project, and for always having open office doors. Thanks also to Professor Chris Schofield for his encouragement and having an abundance of interesting ideas while allowing me the freedom to pursue my own. I am grateful to the British Heart Foundation CRE for my funding and to Professor Angie Russell and Professor Shoumo Bhattacharya for this opportunity.

A number of people have contributed directly to the work in this thesis. I am particularly indebted to Dr Norma Masson, Dr Mun Chiang Chan, Monica Esteban, Dr Mark White, Pauline Lang, Dr Louise Walport, Dr Tom McAllister and Dr Adam Hardy for essential materials, protocols and experimental assistance. Thanks also to H. Manso Jubier, Dr Adam Hardy and Wendy Sobey for keeping the lab running smoothly.

My time in the CJS/AK/EF groups has been an absolute pleasure, largely due to my fantastic colleagues. Particular thanks for stimulating conversation, technical wisdom and friendship go to Kate Dunne, Dr Richard Hopkinson, Dr Tom McAllister, Dr Bhaskar Bhushan, Dr Hanna Tarhonskaya, Rachel Shamo-Schiller, Gareth Langley, Dr Sarah Wilkins, Dr Louise Walport and Dr Jurgen Brem. Many others have provided fun and excellent tea-time chat throughout: thank you Cass, Cyrille, David, Hilal, Joanna, Joan, John-Paul, Martine, Ollie, Rachel, Suzana, Yijia, and the others I am bound to have missed. Special thanks for proof-reading go to Rich, Tom, Kate, John-Paul, Hanna, Bhaskar and Sezgi Goksan.

I have been fortunate to have a fantastic support network outside of the lab. My amazing friends have been there to raise a smile and a glass when needed. My parents have been a never-ending source of encouragement. Thank you for looking after me during the lows and celebrating the highs with me. To James and Tom, thanks for keeping things real and reminding me of the world outside academia. Finally, my most heartfelt thanks go to Sam, without whom the last three years would have been impossible. I cannot describe how much your love and support means, nor can I wait for what our future holds.

Declaration

The work described in this report is entirely my own, except where I have directly acknowledged help from a named person or given reference to a published source.

Contents

Abbreviations

ADAM12	*A Disintegrin And Metalloproteinase Domain 12*
ANF	*Atrial Natriuretic Factor*
APS	Ammonium Persulfate
ASCL2	*Achaete-Scute Family bHLH Transcription Factor 2*
ATP	Adenosine Triphosphate
Bis-Tris	Bis(2-hydroxyethyl)-amino-tris(hydroxymethyl)-methane
BCA	Bicinchoninic Acid
BSA	Bovine Serum Albumin
CA9	*Carbonic Anhydrase 9*
CH	Cardiac Hypertrophy
CHCA	α-cyano-4-hydroxycinnamic acid
CHD5	*Chromodomain Helicase DNA Binding Protein 5*
CI	Confidence Interval
Da	Dalton (mass unit)
DAPI	4',6-Diamidino-2-phenylindole
dm	Dimethyl
DMEM	Dulbecco's Modified Eagle Medium
DNA	Deoxyribonucleic Acid
DNMT	DNA Methyltransferase
Dox	Doxycycline
DSBH	Double Stranded Beta Helix
DTT	Dithiothreitol

E. coli	*Escherichia coli*
EDTA	Ethylenediaminetetracetic acid
ESI-MS	Electrospray ionisation MS
FBS	Foetal Bovine Serum
FHL1	*Four and a half LIM Domains Protein 1*
FIH	Factor Inhibiting HIF
Fmoc	Fluorenylmethyloxycarbonyl
FPLC	Fast Protein Liquid Chromatography
GP5	*Glycoprotein V*
HDAC	Histone Deacetylase
HeLa	Henrietta Lacks' Human Cervical Cancer Cell Line
HEPES	4-(2-hydroxyethyl)-1-piperazineethanesulfonic acid
HF	Heart Failure
HIF	Hypoxia Inducible Factor
HPLC	High pressure liquid chromatography
H3	Histone 3
IDH	Isocitrate Dehydrogenase
IF	Immunofluorescence
IOX1	5-Carboxy-8-hydroxyquinoline
IPTG	Isopropyl β-D-1-thiogalactopyranoside
JmjC-KDM	JumonjiC- Domain Containing KDM
KDM	Histone Lysine Demethylase
LC	Liquid Chromatography
LSD	Lysine Specific Demethylase

MALDI-TOF	Matrix-Assisted Laser Desorption Ionisation Time of Flight
MES	2-(*N*-morpholino)ethanesulfonic acid hydrate
MFC	Mass Flow Controller
MS	Mass Spectrometry
MUT	Catalytically Inactive Mutant
M_W	Molecular Weight
NOG	*N*-oxalylglycine
PAGE	Polyacrylamide Gel Electrophoresis
PBS	Phosphate Buffered Saline
PBS-T	Phosphate Buffered Saline (+ 0.1 % Tween 20)
PCR	Polymerase Chain Reaction
PE	Phenylephrine
PHD	Plant Homeodomain
PHD2	Prolyl Hydroxylase Domain 2
PKMT	Protein Lysine Methyltransferase
PMSF	Phenylmethylsulfonyl fluoride
PPIC	*Peptidyl Prolyl Isomerase C*
PRMT	Protein Arginine Methyltransferase
RNA	Ribonucleic Acid
ROS	Reactive Oxygen Species
RT-qPCR	Quantitative Reverse Transcription PCR
sd	Standard Deviation
SDS	Sodium Dodecyl Sulfate
sem	Standard Error of the Mean

SOC	Super Optimal Broth with Catabolite Repression
TEMED	*N*,*N*,*N'*,*N'*-Tetramethyl-Ethane-1,2-Diamine
TET	Ten-Eleven Translocation Enzyme
TFA	Trifluoroacetic Acid
tKDM4A	truncated recombinant $KDM4A_{1-359}$
Tris	Tris(hydroxymethyl)aminomethane
UV	Ultraviolet
U2OS	Human Bone Osteosarcoma Epithelial Cell Line
WT	Wild Type
2HG	2-Hydroxyglutarate
2OG	2-Oxoglutarate
2TY	2-Tryptone Yeast Extract
5caC	5-Carboxycytosine
5fC	5-Formylcytosine
5hmC	5-Hydroxmethylcytosine
5mC	5-Methylcytosine

Common one- and three-letter amino acid abbreviations are used throughout

Chapter 1: Introduction

1.1. Epigenetics – definitions to date

Francis Crick's central dogma of biology states that the cell's genetic material, deoxyribonucleic acid (DNA), provides the code from which all proteins are synthesised *via* the intermediate messenger ribonucleic acid (mRNA) in a linear and non-reversible manner, i.e. 'DNA makes mRNA makes proteins'[1]. Each diploid cell in the human body is derived from the embryonic stem cells, hence possesses the same genotype. However, these cells have differentiated to produce phenotypically distinct cell types, expressing both a common and specialised set of genes depending on their location and function. The gene expression profile of each cell also adapts to environmental changes and is highly dynamic, suggesting that a complex regulatory mechanism must be at play during both cellular differentiation and the normal life of a cell.

In 1942, Conrad Waddington first defined 'epigenetics' as the study of the developmental mechanisms underlying how a genotype gives rise to a phenotype[2]. His definition was largely concerned with cellular differentiation during development, a phenomenon that he likened to a ball rolling downhill into one of a number of inescapable valleys[3]. He envisaged that the undifferentiated cell, a ball, may roll down one of several paths in what Waddington termed the 'epigenetic landscape,' with its ultimate fate being determined by the valley in which it settles. Each valley represents a particular cell lineage, and once differentiated the cell cannot become any other type of cell.

More recently, the term epigenetics has come to be used in relation to any heritable changes in gene expression (and therefore cellular phenotype) that are not due to changes in the underlying DNA base sequence[4]. Subsequent definitions have also considered the

mechanisms mediating epigenetic regulation, including non-coding RNA and modifications to DNA and histone proteins[5,6], aspects of which are discussed below. However, much as the term has been defined, questions remain as to the heritability of epigenetic marks[7]. Indeed, recent discussion has proposed two developmental epigenetic models: the reprogramming model, which largely occurs in gametes whose chromatin states are reset to achieve totipotency upon fertilisation, and the inheritance model, which suggests that chromatin states in embryonic cells are inherited from those in mature germ cells, and direct subsequent developmental transcriptional programmes[8].

1.2. DNA packaging, nucleosomes and histones

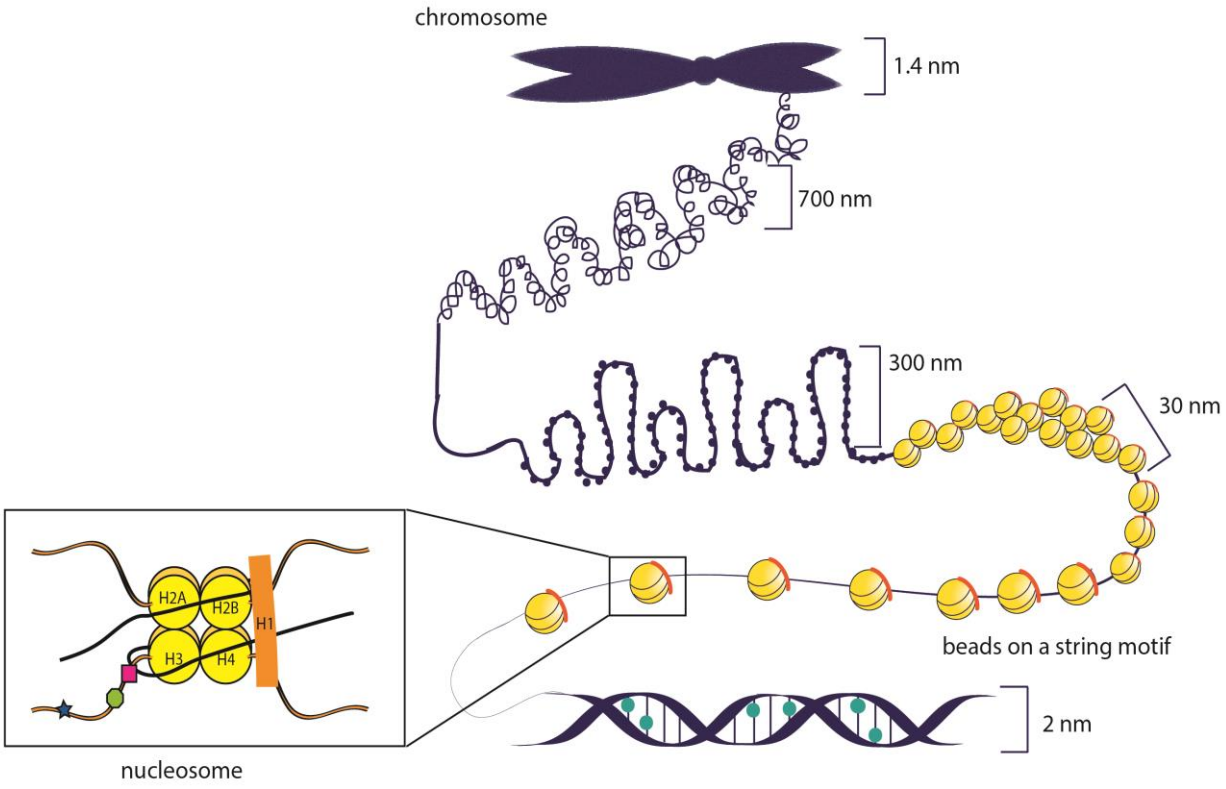

Figure 1.1 Schematic of DNA packaging within the nucleus. The DNA double helix is wrapped around nucleosome units (inset), in a 'beads on a string' motif. These are packed, along with the linker histone H1[12], progressively to form the 30 nm, 300 nm and 700 nm fibres, eventually enabling organisation of DNA into chromosomes and efficient packaging of DNA within the nucleus[23]. Coloured shapes on histone H3 tail (inset) denote possible post-translational modifications (Chapter 1.3.2).

Chromatin is the macromolecular complex that enables the effective compaction of approximately 2 m of DNA in each human cell[9], and is made up of nucleosomes, which consist of 147 base pairs of DNA wrapped around a histone octamer[10] (Figure 1.1, Figure 1.2). The histone octamers are made up of two copies of each of the four histone proteins, histone 2A (H2A), histone 2B (H2B), histone 3 (H3) and histone 4 (H4), which initially form heterodimers: H2A with H2B, and H3 with H4[10,11]. These heterodimers then combine as two H2A/H2B dimers with a H3/H4 tetramer to produce the histone octamer. Individual nucleosomes are spaced along the DNA in a 'beads on a string' motif, with histone 1 (H1) protein acting as a linker to enable condensation of chromatin to produce the 30 nm fibre[12] (Figure 1.1). Histones are positively charged, globular proteins hence form electrostatic interactions with DNA in order to stabilise the nucleosome. The *N*-terminal tails protrude from the nucleosome, and both NMR spectroscopy and ion mobility mass spectrometry studies have shown them to be disordered and dynamic[13,14]. However, their presence appears to be necessary for overall nucleosome stability[15].

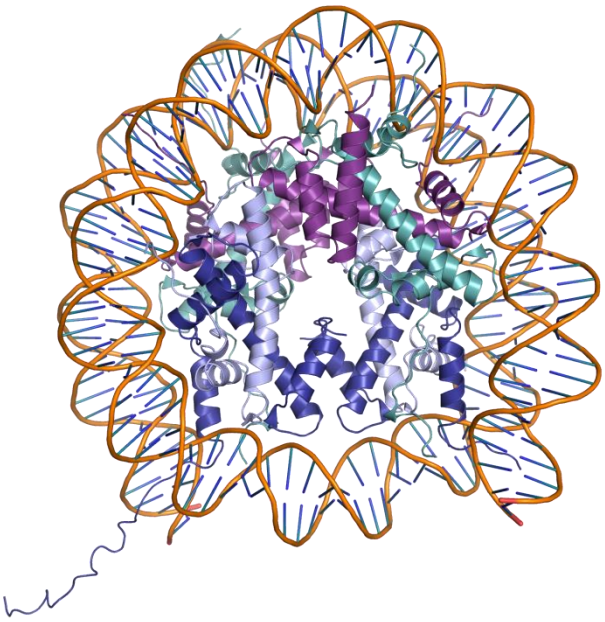

Figure 1.2 View of a crystal structure of a nucleosome. A single nucleosome comprises 147 bp DNA (orange), wrapped around a histone octamer core, which contains two copies of each of the canonical histone subunits: H2A (teal), H2B (purple), H3 (dark blue, protruding *N*-terminal tail visible) and H4 (light blue). The H2A and H2B subunits form a dimer of dimers, while H3 and H4 come together as a tetramer, before assembling to produce the histone octamer[10,11]. Adapted from RCSB Protein Databank (PDB) file ID 1AOI using pyMOL.

In certain contexts, histone proteins, in particular, H2A, H2B and H3, may be substituted by a number of variants, which differ from the canonical histones in size, sequence and chromosomal location[16]. These include H2A.X, which is involved in the response to DNA damage[17], H3t, which is specific to testes[18], and the H3 variant CENP-A, found in centromeric nucleosomes[19]. Inclusion of these variants in the nucleosome is orchestrated by a number of specific chaperone proteins[20], and impacts transcription by altering the stability of the complex[21].

As well as enabling the compaction of DNA in the nucleus, chromatin allows the dynamic, spatiotemporal regulation of gene transcription[22]. Chromatin may take two forms: open, transcriptionally permissive euchromatin or tightly packaged, repressive heterochromatin[23].

Changes to the chromatin structure affect the accessibility of the DNA to the transcriptional machinery and are mediated by thousands of interacting proteins. These proteins are responsible for numerous processes, including ATP-dependent remodelling, substitution of individual histones with histone variants, or post translational modification of the unstructured *N*-terminal histone tails.

1.3. Mechanisms of epigenetic regulation

Epigenetic regulation is achieved through a number of mechanisms. These include the production of noncoding RNA[24] and ATP-dependent remodelling of chromatin[25], as well as the introduction of covalent modifications to both DNA and histone proteins. These modifications generally affect transcription *via* changes to chromatin structure or charge, ultimately disrupting or modulating the interactions between DNA and the transcriptional machinery.

1.3.1. DNA methylation

The first epigenetic modification to be identified was methylation at the 5 position of cytosine residues in DNA (5-methylcytosine, 5mC, Figure 1.3). This modification occurs within cytosine-guanine doublets (CpG), approximately 60-90% of which are methylated within the genome[26], and is associated with transcriptional repression. For instance, in genomic imprinting, one of the two parental alleles of a specific subset of genes is hypermethylated, to ensure expression of only one copy of the gene[27,28], while DNA methylation also contributes to X-chromosome inactivation in females to maintain the sex chromosome:autosome ratio[29,30]. There are two main mechanisms by which DNA methylation is thought to silence gene expression. Firstly, in a 'passive' mechanism, DNA recognition factors associated with active transcription may be prevented from binding[31]. Secondly, specific proteins that recognise methylated cytosine residues are able to bind to the methylated DNA and subsequently recruit transcriptional co-repressors to actively silence the gene in question[32,33].

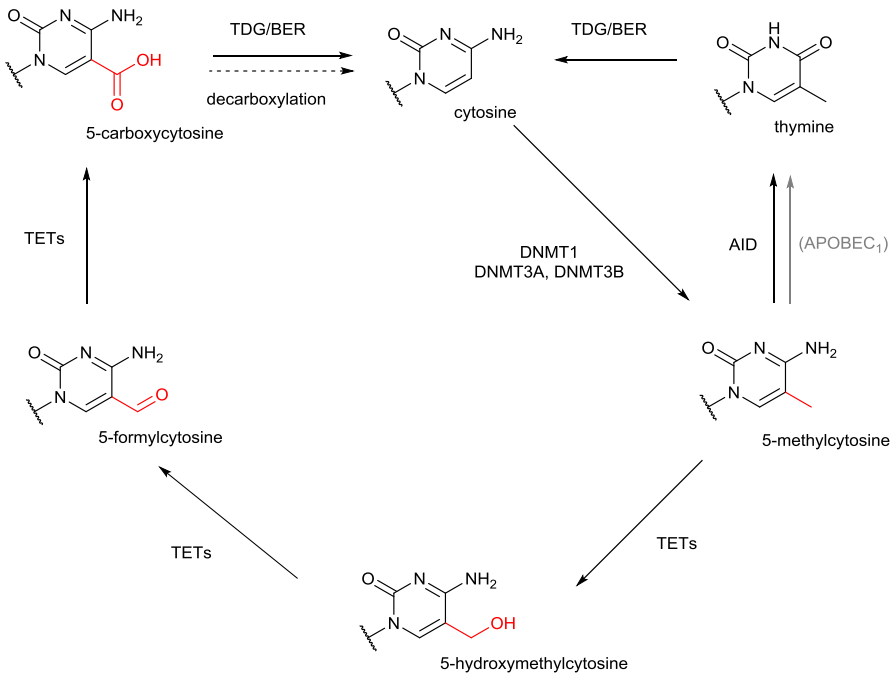

Figure 1.3 Enzymatic modification of cytosine. Several modifications to cytosine, shown in red, are known to occur in humans, and their interconversion is mediated by various families of enzymes. Conversions for which only *in vitro* evidence is available are shown in grey, while dotted lines denote non-enzymatic mechanisms.

De novo DNA methylation occurs in the embryo immediately upon implantation, following global DNA demethylation (a process which confers totipotency) after fertilisation[34], and is mediated by the DNA methyltransferases, DNMT3a and DNMT3b[35,36]. Maintenance of DNA methylation during replication and cell division is then carried out by DNMT1[33]. DNA demethylation is regulated by both active and passive means (Figure 1.3). Passive demethylation may arise due to failure of the DNA methyltransferases to maintain methylation during DNA replication[37], while the enzymatic transformation of 5mC by a number of enzymes also results in its demethylation. Notably, the Ten-Eleven-Translocation (TET) enzymes are able to catalyse successive oxidations of 5mC, resulting in 5-hydroxymethylcytosine (5hmC), 5-formylcytosine and finally 5-carboxycytosine (5caC)[38,39] (Figure 1.3). 5caC may be subject to spontaneous decarboxylation, or excised by thymine-DNA glycosylase (TDG)[40] to enable reintroduction of cytosine by base excision repair (BER)[41]. Two further enzymes have been implicated in the demethylation of 5mC: activation-induced deaminase (AID) has been shown to catalyse the conversion of 5mC to thymine in *E. Coli*, while apolipoprotein B mRNA editing enzyme catalytic polypeptide-like 1 (APOBEC1) displays similar deaminase activity *in vitro*[42]. These transformations are proposed to be followed by the action of TDG/BER to reinstate cytosine[37]; however, subsequent study has shown very low efficiency of these enzymes against 5mC, hence the biological significance of this remains a cause for controversy[43].

Importantly, not all CG-rich regions of DNA are methylated. So-called CpG islands (CGIs) are constitutively unmethylated CpG clusters, usually correlating with transcriptional start sites[44]. CGIs are generally a feature of transcriptionally permissive euchromatin[45] and may arise due to protection against *de novo* methylation during development, or *via* demethylation of previously methylated DNA. However, some CGIs acquire methylation throughout development, leading to stable repression of associated gene regions[45].

1.3.2. Post translational modifications of histone tails

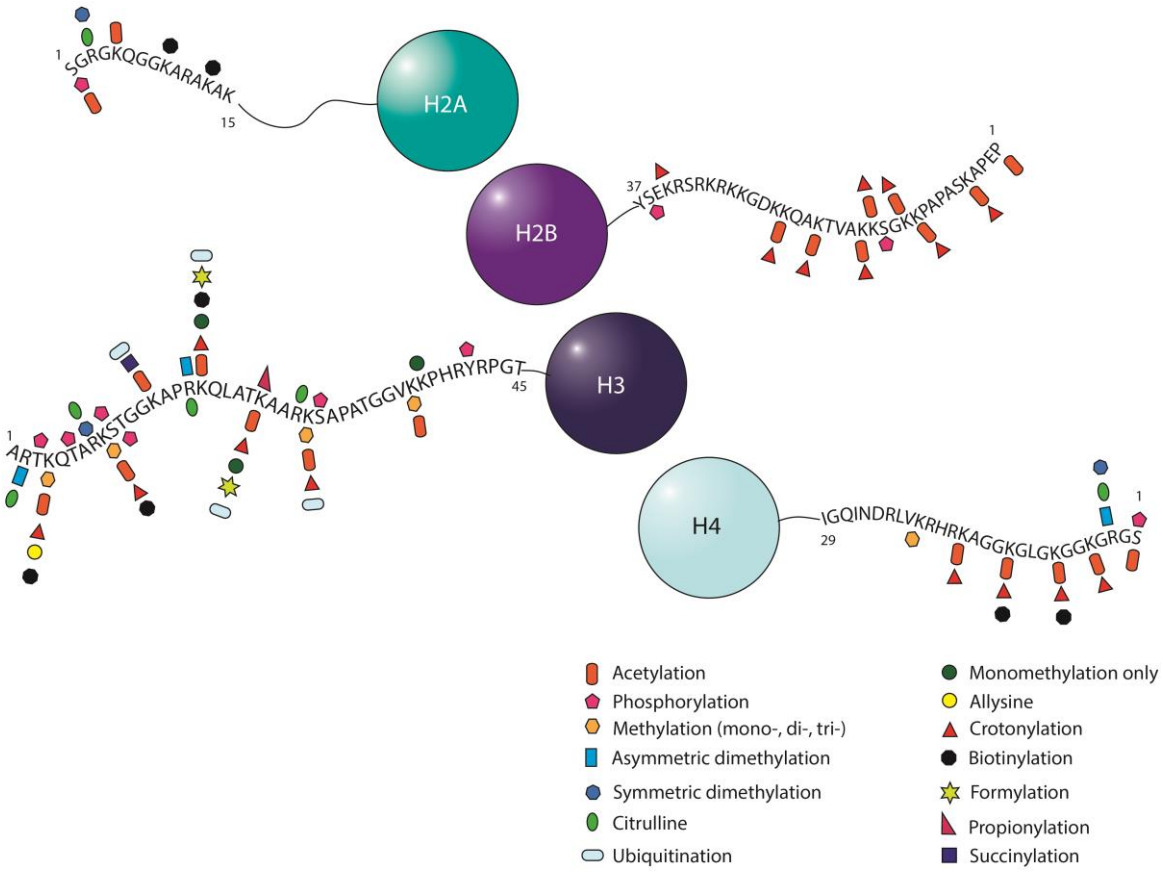

Figure 1.4 Known post-translational modifications of the *N*-terminal histone tails. Scheme showing the covalent modifications that have been characterised on histone tails to date, as defined in the Uniprot database (http://www.uniprot.org/) , or more recently reviewed by Xu *et al.*[52]. Spheres represent the globular cores of the histone proteins**.**

The histones are some of the most post-translationally modified proteins in the proteome. There are an extensive number of covalent modifications that may occur on the unstructured *N*-terminal histone tails (Figure 1.4), altering the charge or size of the nucleosome complex and thereby modulating the association between the histones and DNA, the overall chromatin structure, or the recruitment of proteins required for transcription to the chromatin[46]. A large number of proteins are responsible for 'writing', 'reading' and 'erasing' these marks, providing a highly dynamic method of epigenetic regulation. Multiple marks may occur on histone tails within the same nucleosome, often acting in combination to

produce what is known as the 'histone code', a complex set of signals that collectively dictate the biological outcome downstream of the associated chromatin[47]. There is thought to be a high degree of cross-talk between epigenetic marks: a modification at one position may facilitate binding of an epigenetic modulator and direct its action to a nearby residue, or may inhibit binding to or modification of other residues[48,49]. Well-studied histone modifications include acetylation, phosphorylation and methylation, and are briefly discussed below (Figure 1.4), while advanced mass spectrometry and proteomic techniques have enabled the recent discovery of marks including crotonylation and succinylation of lysine residues[50–52] (Figure 1.4).

Acetylation occurs on lysine residues (Figure 1.5) and is predominantly associated with actively transcribed euchromatin[53]. This mark is 'written' by the histone acetyltransferases (HATs) and removed by histone deacetylases (HDACs), of which there are four main classes: Class I (HDAC1, 2 and 8), Class II (HDAC4, 5 , 7, 9 and 10), Class III (SIRT1-7) and Class IV (HDAC11)[54]. Acetylation neutralises the positive charge found on unmodified lysine residues, resulting in reduced association of the negatively-charged DNA with the nucleosome and producing a more open chromatin conformation that is accessible for binding of transcription factors[55–57].

Phosphorylation of threonine, serine and tyrosine residues (Figure 1.5) in the histone tails is catalysed by protein kinases, while its removal is mediated by histone phosphatases. It has been well-documented that phosphorylation of serine 139 of the histone variant H2A.X is crucial to DNA damage repair[58]. Intriguingly, in the context of transcriptional regulation, phosphorylation of a large number of residues on the canonical histones has been investigated and found to be associated with both active and repressed chromatin regions[59]. Histone phosphorylation also plays a role in chromatin condensation, particularly during meiosis and mitosis[60].

Methylation is a common post-translational modification of histones, and is found on both lysine and arginine residues. Arginine methylation can take mono-, asymmetric di- or symmetric di- forms (Figure 1.5), and is mediated by the protein arginine methyltransferases (PRMTs), all of which utilise the methyl donor *S*-adenosylmethionine (SAM)[61]. A family of enzymes known as the peptidylarginine deiminases (PADIs) is responsible for the deamination of methylated arginine to produce citrulline[62] (Fig 1.5).

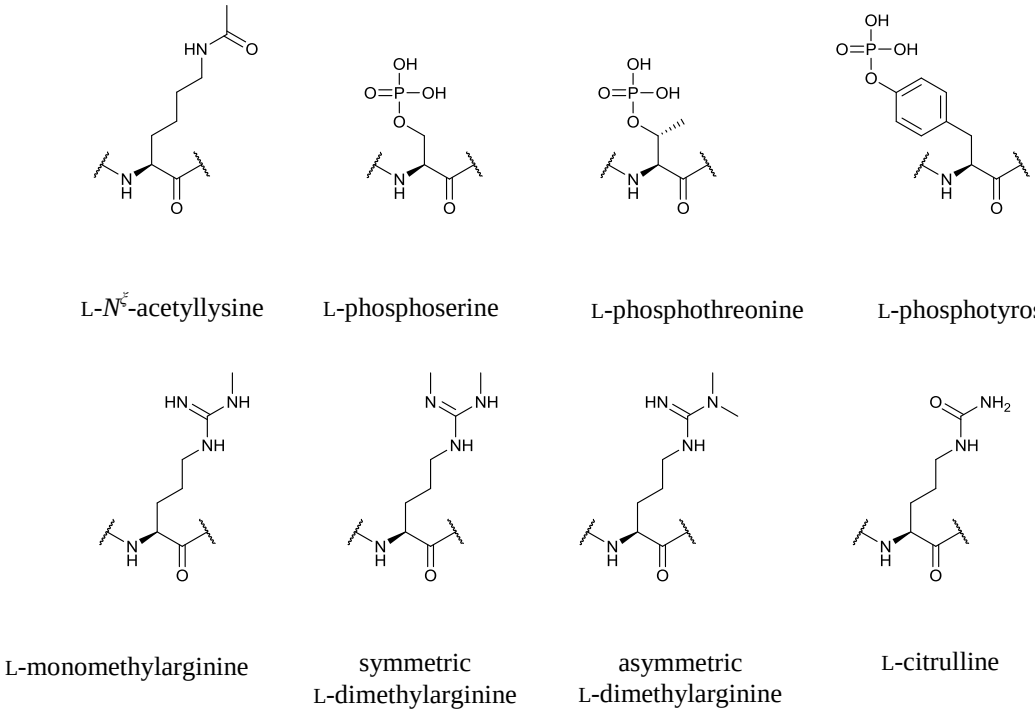

Figure 1.5 Structures of the common post-translational modifications of histone residues (Chapter 1.3.2).

1.3.2.1. Histone lysine methylation

Histone lysine residues may be mono-, di- or tri- methylated (Kme1, Kme2, Kme3, Figure 1.6). Methylation has been characterised on H3K4, H3K9, H3K27, H3K36, H4K20, and the core lysine residue H3K79. These marks maintain the positive charge on the lysine residues, but the position and extent of methylation on these residues contributes to the epigenetic status of the associated gene[63,64]. In general, H3K4, H3K36 and H3K79 methylation signifies

active chromatin, while methylation at H3K9 and H3K27 is repressive, and mostly associated with heterochromatin[65]. These marks are often localised to particular gene regions, with H3K4me3 most often found in promoter regions[66,67], and H3K36 located towards the 3' end of genes[63,65].

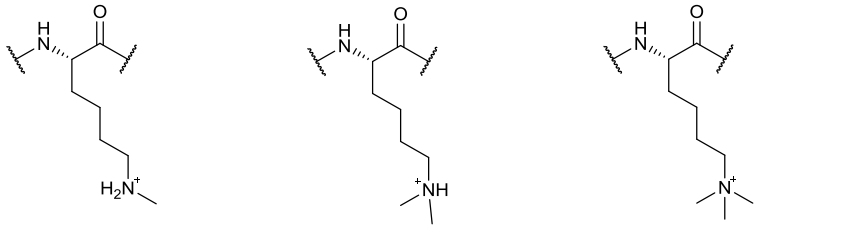

Figure 1.6 Structures of mono-, di- and trimethyllysine (Chapter 1.3.2.1).

As with the PRMTs (Chapter 1.3.2), the enzymes responsible for histone lysine methylation (protein lysine methyltransferases, PKMTs) are SAM-dependent, and most possess a SET domain[68]. These include the H3K9 methyltransferases SUV39H1[69] and G9a[70]. The exceptions to this are the H3K79 methyltransferase, DOT1L, and an H3K4 methyltransferase which is part of the mixed lineage leukaemia protein 1 (MLL1) complex[71]. In general, these enzymes act as part of multiprotein complexes[72], and many histone methyltransferases are also capable of accepting non-histone substrates[73].

Methylation of histone lysine residues was initially believed to be a stable mark, until the discovery of the histone lysine demethylases (KDMs) responsible for its removal. Enzymes of this category belong to two main families. The first to be discovered was Lysine-Specific Histone Demethylase 1, LSD1, also known as KDM1A, a flavin-adenine dinucleotide (FAD) dependent oxidase which catalyses the demethylation of di- and mono-methylated H3K4 *via* formation of an imine intermediate[74,75]. The homolog KDM1B was later discovered through

domain homology and found to have the same substrate specificity as KDM1A, despite a lack of sequence similarity[76].

The second family of KDMs are Jumonji-C (JmjC) domain containing enzymes and are members of the 2-oxoglutarate dependent oxygenase superfamily (Chapter 1.4). Collectively, the KDMs are able to remove mono-, di-, and trimethylation from most known methylated histone lysines, although there is currently no known demethylase of H3K79. However, evidence of the reversibility of H3K79 methylation has been observed, leading to speculation that there is yet a demethylase to be discovered[77].

1.4. The 2-oxoglutarate dependent oxygenases

The JmjC-KDMs are members of the non-haem 2-oxoglutarate and Fe^{2+} dependent oxygenase (2OG oxygenase) superfamily, of which there are over 60 known human enzymes. Members of this family are widespread in nature and known to carry out diverse reactions (Figure 1.7) in a variety of biological pathways across multiple organisms, including those involved in collagen biosynthesis and DNA repair[78–80]. The fact that these enzymes possess such diverse reactivity, substrate specificity and functionality has led to extensive study from structural, mechanistic and functional perspectives.

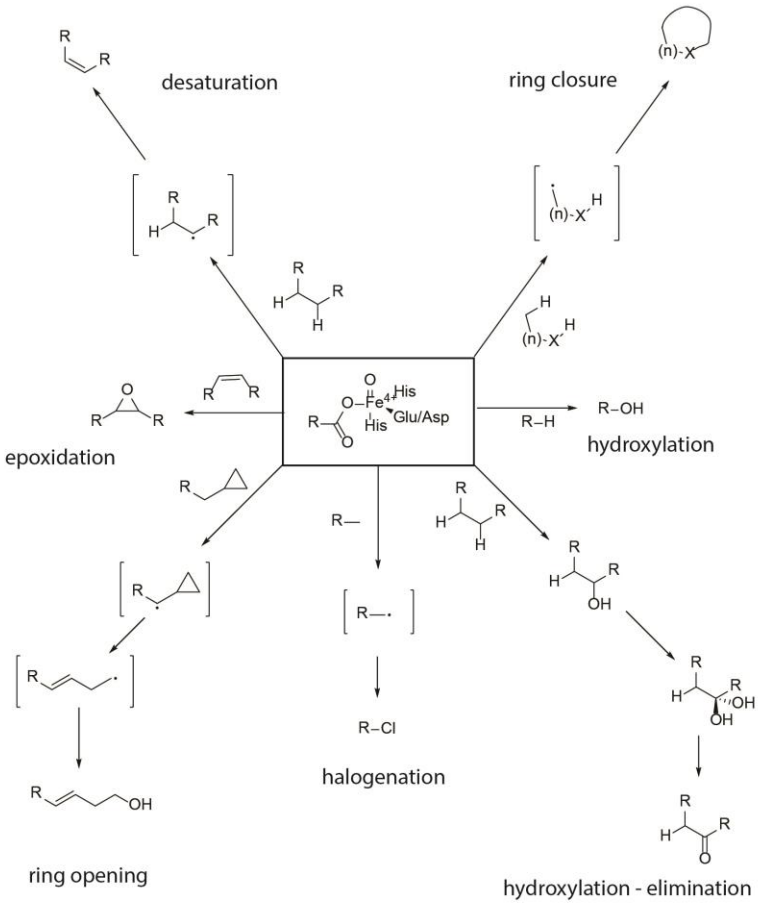

Figure 1.7 Range of reactions catalysed by members of the 2OG oxygenase superfamily of enzymes. Adapted from Clifton *et al.*, copyright 2006[78] with permission from Elsevier.

1.4.1. Structure and mechanism

All members of the 2OG oxygenase superfamily share a conserved structure, comprising a double-stranded beta-helix (DSBH, also known as a cupin fold or jelly roll) and an iron-binding HXD/E…H facial triad in the active site (Figure 1.8). This was first observed in 1995 by Roach *et al.*, upon crystallisation of isopenicillin *N*-synthase (IPNS, Figure 1.8a), a 2OG oxygenase involved in the synthesis of penicillin[81].

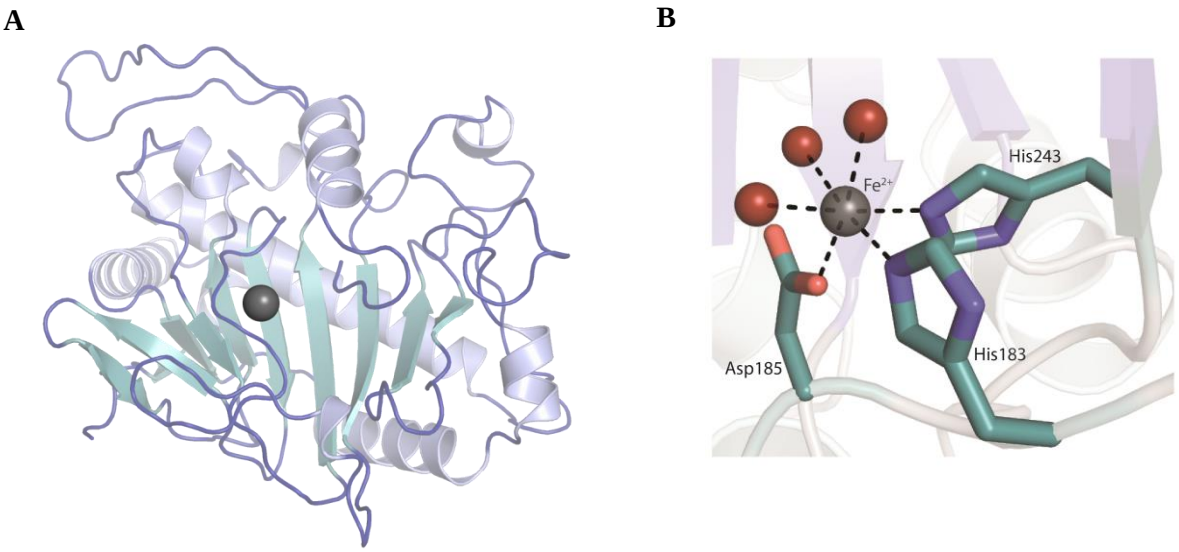

Figure 1.8 Views of crystal structures showing key conserved structural features of 2OG oxygenases. **A)** View of a crystal structure of IPNS, in which the DSBH (light teal) was first observed. Adapted from PDB file 1IPS using pyMOL. **B)** View of a crystal structure of the active site of DAOCS; the iron-binding facial triad of HXD/E…H is shown in dark teal, while three coordinated water molecules complete the octahedral coordination about the Fe^{2+} centre (grey sphere). Adapted from PDB file 1RXF using pyMOL.

Subsequent study of Deacetoxycephalosporin-C synthase (DAOCS), a second 2OG oxygenase involved in penicillin biosynthesis, observed the resting state of the enzyme, with three water molecules coordinated to the active site Fe^{2+} to produce octahedral geometry about the metal centre[82] (Figure 1.8b). These, and further, structural insights, along with kinetic and spectroscopic analyses of a number of enzymes, lead to the proposal of a conserved catalytic mechanism for the 2OG oxygenase superfamily (Figure 1.9).

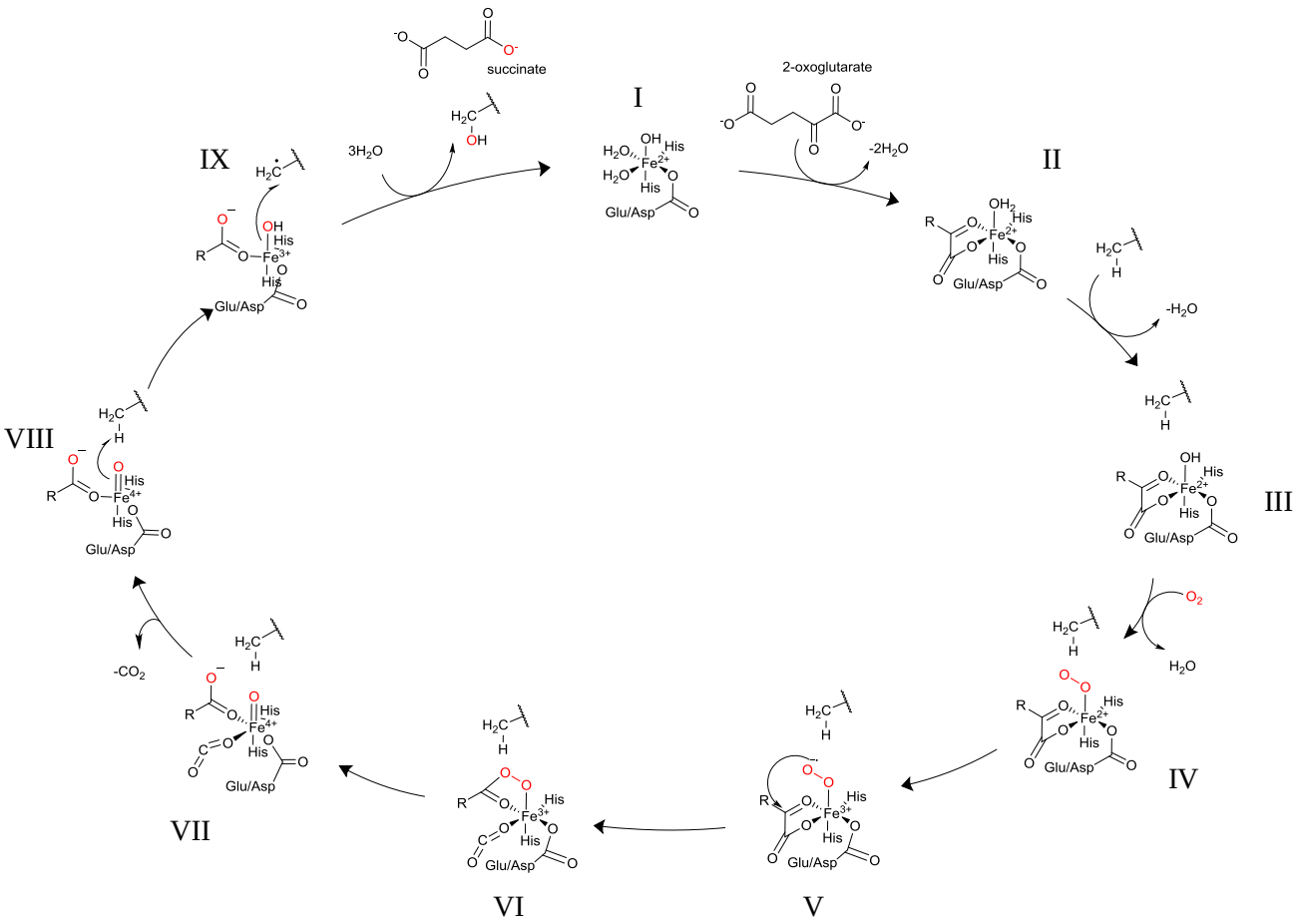

Figure 1.9 Consensus mechanism of the 2OG oxygenases. 2OG binds in a bidentate fashion to the Fe^{2+} catalytic centre, followed by substrate, and finally oxygen. Oxidation of Fe^{3+} produces a highly reactive ferryl-oxo intermediate, which participates in a radical rebound mechanism to hydroxylate the prime substrate. Atoms derived from atmospheric oxygen are highlighted in red.

Binding of 2OG to the active site *via* the ketol group and one of its carboxylate groups[83,84] displaces two water molecules from the Fe^{2+} centre (II), while the second 2OG carboxylate is coordinated by a basic residue (arginine or lysine)[79,82,84]. Prime substrate then binds in the active site[83], weakening the interaction between the Fe^{2+} centre and the remaining water molecule[82], to produce a complex primed for reaction with oxygen (III)[85]. Binding of oxygen leads to oxidation of 2OG to form succinate and carbon dioxide[86], and a highly reactive Fe^{4+}-oxo species (VII); this has been characterised in the bacterial oxygenase TauD[87] and in the viral prolyl collagen hydroxylase P4H[88], using Mössbauer spectroscopy, and is also observable by reductive EPR, Raman and UV/vis spectroscopy[85,88], *via* which a metal-to-ligand charge transfer band may be observed. Finally, abstraction of a proton from the

substrate by the Fe^{4+}-oxo species produces an Fe^{3+}-OH species, which then catalyses hydroxylation of the substrate, also regenerating the Fe^{2+} centre.

Interestingly, while there is no direct role for ascorbate in the catalytic cycle of the 2OG oxygenases, several studies have indicated that ascorbate is necessary for the activity of a number of these enzymes, in particular the collagen prolyl-4 hydroxylase, P4H[89], and the HIF hydroxylases[90,91]. The presence of ascorbate is thought to prevent inactivation of the enzyme *via* maintenance of Fe in the +2 oxidation state[90], although the mechanism of ascorbate involvement in the reactions of 2OG oxygenases is likely to vary across the superfamily.

1.4.2. JmjC histone demethylases

The Jumonji (JmjC) domain was first identified in a gene trap experiment in mice. *JARID2* gene mutation resulted in aberrant neural plate and tube formation, producing abnormal neural grooves resembling a cross; hence the gene was named after the Japanese for cruciform, *Jumonji*[92]. The JmjC-domain was then found to be necessary for demethylation of methylated H3K36me3 by FBXL11, which was subsequently named JmjC domain-containing histone demethylase 1A (JHDM1A), and is now known as KDM2A, the first identified JmjC-KDM[93]. The JmjC domain has since been identified in numerous 2OG oxygenases (>30), although not all of these possess histone lysine demethylase activity. For instance, FIH is a promiscuous protein hydroxylase, capable of the hydroxylation of asparaginyl and prolyl residues in a range of non-histone substrates[94]. Furthermore, several JmjC 2OG oxygenases, including the ribosomal histidyl hydroxylases MINA53 and NO66[95], and the lysyl hydroxlyases JMJD5[96,97] and JMJD6[98] have been controversially assigned as histone demethylases[99–101], albeit as an arginyl, rather than lysyl demethylase in the case of JMJD6[102].

Table 1.1 Substrate specificity and domains of the characterised JmjC-KDMs. Green shading indicates demethylase activity that has been observed both in cells and *in vitro*, grey shading signifies activities that have been demonstrated *in vitro* only, and orange shading indicates controversial assignments of JmjC 2OG oxygenases as histone demethylases. Table adapted with permission of Future Medicine Ltd from Hancock *et al.* (2015)[250].

	H3K4			H3K9			H3K27			H3K36			H3K79			H4K20			H1.4K26			Domains	Refs
	1	2	3	1	2	3	1	2	3	1	2	3	1	2	3	1	2	3	1	2	3		
KDM2A/ FBXL11 KDM2B/ FBXL10																						CXXC PHD FBox LRR	103,104
KDM3A/ JMJD1A KDM3B/ JMJD1B KDM3C/ JMJD1C HR																							105–109
KDM4A/ JMJD2A KDM4B/ JMJD2B KDM4C/ JMJD2C																						JmjN Tudor PHD	110–117
KDM4D/ JMJD2D KDM4A/ JMJD2E																						JmjN	
KDM5A/ JARID1A KDM5B/ JARID1B KDM5C/ JARID1C KDM5D/ JARID1D																						JmjN ARID PHD C5HC2 ZF	118–122
KDM6A/ UTX KDM6B/ JMJD3 KDM6C/ UTY																						TPR	123–128
KDM7A/ KIAA1718 KDM7B/ PHF8 PHF2																						PHD	129–133
KDM8/ JMJD5 MINA53 NO66																							99–101

There are now over 20 known JmjC-KDMs, grouped into six subfamilies based on structural and sequence similarity, and substrate specificity (Table 1.1). In addition to the catalytic JmjC domain, these enzymes also contain multiple 'reader' and/or binding domains, thought

to facilitate substrate specificity (Table 1.1) and protein-protein interaction. For instance, the Plant Homeodomain (PHD) finger of the KDM7 subfamily member PHF8 targets demethylation of H3K9me2 *via* binding to trimethylated H3K4[133], while the ARID domain of the KDM5s is involved in recognition of CG-rich regions of DNA[134,135].

Interestingly, the structure of the JmjC 2OG oxygenases in general differs slightly from that of other superfamily members, in that the 2OG co-substrate is bound in the active site *via* coordination of its C-5 carboxy group with a lysyl, rather than an arginyl residue, which is located on the 4th, as opposed to the 8th strand of the DSBH[79]. However, evidence suggests that the JmjC-KDMs, like all JmjC 2OG oxygenases, share the conserved mechanism of the 2OG oxygenase superfamily (Figure 1.9), producing a hemiaminal species, which then collapses to produce formaldehyde and the demethylated lysine product (Figure 1.10). The hemiaminal intermediate is yet to be directly observed in complex with a JmjC-KDM, but has been isolated in complex with the DNA repair enzyme AlkB[136].

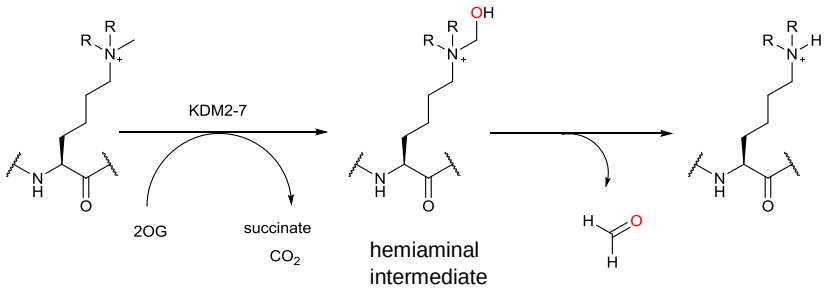

Figure 1.10 Mechanism of demethylation of methylated lysine residues by the JmjC-KDMs. Oxidation of the methyl group *via* the consensus mechanism of the 2OG oxygenases (Figure 1.9), results in a hemiaminal species, which collapses to produce the demethylated product and formaldehyde. Atoms derived from atmospheric oxygen are highlighted in red.

1.4.2.1. KDM4 subfamily

The KDM4 subfamily of JmjC-KDMs comprises five isoforms, KDM4A-E, of which KDM4E is thought to be a pseudogene, i.e. is encoded for in genomic DNA but not expressed in mammalian cells. KDM4A-C demethylate both di-and tri-methylated H3K9 and

H3K36 residues, while KDM4D and KDM4E only accept H3K9me2/3 substrates (Table 1.1). All five subfamily members possess both the JmjN and JmjC domains essential for catalytic activity, but PHD and tandem Tudor domains are present in KDM4A-C (Figure 1.11c). These tandem Tudor domains have been shown to facilitate binding of the enzymes to trimethylated H3K4 and H4K20 residues[137] (Figure 1.11b), each of which is recognised by a distinct set of amino acid residues within the motif[138].

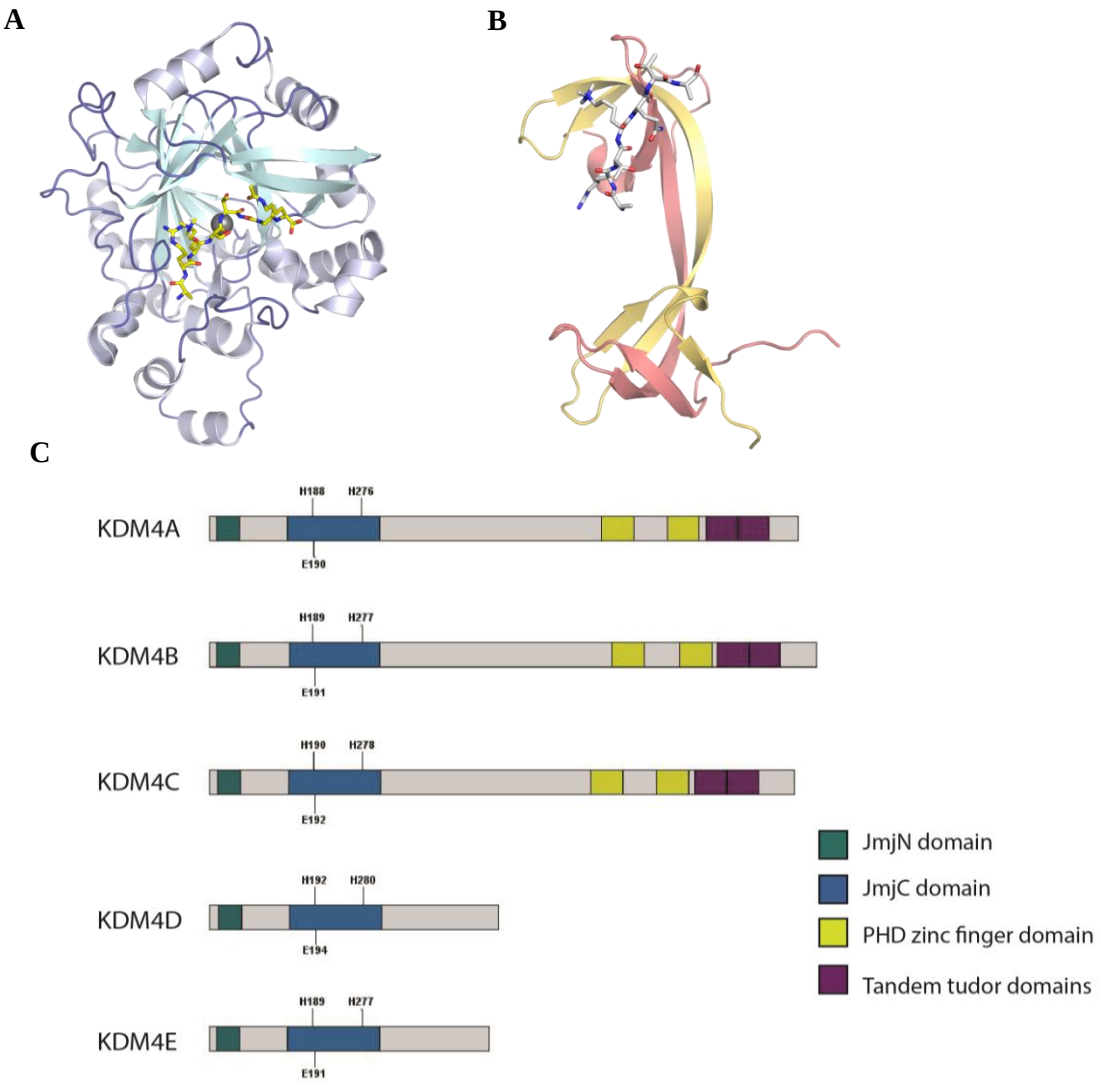

Figure 1.11 Structural features of the KDM4 subfamily of histone demethylases. **A)** View of a crystal structure of KDM4A, showing the conserved double stranded beta helix (pale cyan) with bound H3K9me3 peptide substrate (yellow). Figure produced from RCSB PDB file 2OQ6 using pyMOL. **B)** View of a crystal structure of the tandem Tudor domains of KDM4A, showing the mode of recognition of a bound H3K4me3 peptide (grey). Figure adapted from PDB file ID 2GFA using pyMOL. **C)** Domain architecture of the KDM4 subfamily members. Figure was produced using IBS 1.0[381].

A number of interactions between KDM4 subfamily members and non-histone proteins have been identified. Notably, KDM4A, KDM4C and KDM4D interact with androgen receptor[139,140], and KDM4B interacts with estrogen receptor[141]. These interactions with proteins involved in activation or repression of distinct subset of genes suggest roles for the KDMs in specific transcriptional programmes.

1.4.2.2. KDM4A

KDM4A was first identified as a histone demethylase (then named JHDM3A, as the first member of the third known lysine demethylase subfamily) in 2006 by Klose *et al.*[110]. KDM4A had previously been shown to be involved in transcriptional repression *via* interaction with the N-CoR co-repressor, with a role in regulating the expression of the achaete scute-like transcription factor ASCL2[142]. Prior molecular characterisation had also identified interactions with the retinoblastoma-binding protein (pRb) and HDACs, highlighting a potential role for KDM4A in cell proliferation and oncogenesis[143].

KDM4A was known to possess a JmjC-domain, which was recognised as necessary for the demethylase activity of KDM1A, KDM2A and KDM2B, prompting the investigation of the catalytic activity of KDM4A against methylated histone substrates. These *in vitro* studies demonstrated that recombinant KDM4A was able to demethylate H3K9me3, H3K36me3, and to a lesser extent, H3K9me2 and H3K36me2, with concomitant release of formaldehyde[110]. Furthermore, ectopic expression of the full-length FLAG-tagged protein in NIH3T3 mouse embryonic fibroblast cells revealed similar substrate specificity against native histones, with almost complete loss of H3K9me3 and H3K36me3[110].

Of the four remaining members of the KDM4 subfamily, KDM4B and KDM4C demonstrate the same substrate specificity as KDM4A, while KDM4D and KDM4E only accept H3K9me3/2, and not the H3K36 equivalents[113,144]. Crystallographic and biochemical studies

were mounted to elucidate the basis for these differences and the structural basis for the substrate preferences of the KDM4 subfamily. Initial studies on KDM4A found that the binding of $H3_{7-14}$K9me3 and $H3_{31-41}$K36me3 peptides in the enzyme's active site produces a bent conformation in the substrates (Figure 1.12), enabled by the positioning of glycine and proline residues in relation to the methylated lysine[145]. This conformation can likely not be achieved by H3K4 or H3K27 peptides, whose sequence (Figure 1.4) does not permit the requisite flexibility[145].

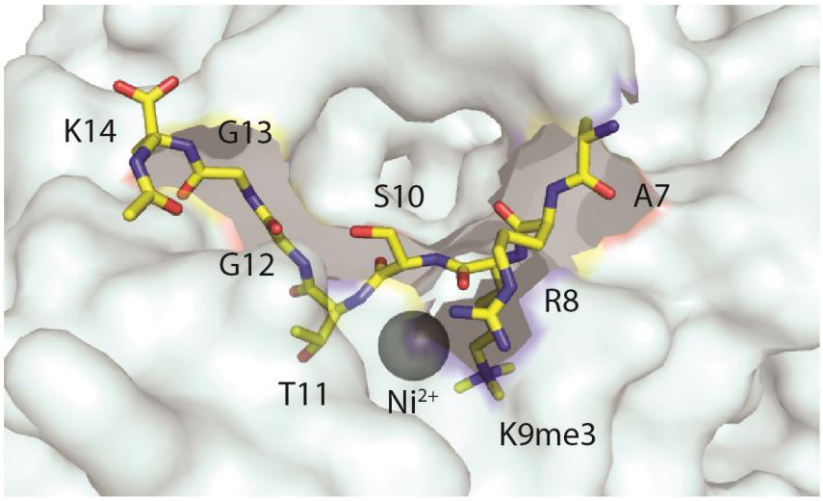

Figure 1.12. View of a crystal structure of KDM4A showing $H3_{7-14}$K9me3 peptide bound in the active site. Ni^{2+} is shown bound in the Fe^{2+} binding site. The 'W' conformation of the peptide appears to be necessary for demethylation and is facilitated by glycine residues 12 and 13 of the peptide, providing a basis for the substrate specificity across the KDM4 subfamily[145]. Figure adapted from PDB file 2OQ6 using pyMOL.

Subsequent studies on the KDM4A-D family members encompassed both kinetic and crystallographic analyses, and found that the reported substrate selectivity observed is likely to arise from both differences in key interactions between the enzyme and substrate throughout the substrate binding pocket, and different rates of reaction once the substrate is bound[144]. As the 2OG oxygenases utilise both 2OG and O_2 as co-substrates, there are numerous factors that may affect the rate of reaction of an enzyme, which can, in turn, contribute to substrate selectivity.

1.5. The cellular response to hypoxia

Oxygen is necessary for most forms of life for numerous cellular processes. In order to maintain oxygen homeostasis, cells must be able to sense and respond to changes in the oxygen concentration in their environment. The mammalian hypoxic response is mediated by the beta loop-helix-loop Per-ARNT-SIM (PAS) domain transcription factor, known as the Hypoxia Inducible Factor, HIF[146]. HIF is a constitutively expressed heterodimer consisting of an alpha and beta subunit[147], which must interact in hypoxia in order to bind to hypoxia regulatory elements (HREs) at specific gene promoters, activating their transcription and facilitating the hypoxic response[148] (Figure 1.13). There are thousands of known HIF target genes involved in multiple biological pathways, notably those involved in angiogenesis, metabolism and transcriptional regulation[148,149], whose activation allows the cell to adapt to hypoxia. Examples include those encoding vascular endothelial growth factor (VEGF), lactate dehydrogenase A (LDHA) and carbonic anhydrase 9 (CA9)[149].

The HIFα subunit exists in three isoforms. HIF-1α and HIF-2α share a high degree of sequence homology[150,151], but are non-redundant, having distinct transcriptional targets and differential expression in different cell types[152,153]. HIF-3α possesses only approximately 57% sequence identity with HIF-1α, and is truncated at the *C*-terminus in comparison, lacking the *C*-terminal activation domain (CAD)[154]. Interestingly, a number of potential HIF-3α variants have recently been identified, apparently with distinct biological functions and target genes[154,155].

HIF levels and activity are modulated by a set of iron and 2-oxoglutarate dependent oxygenases: the HIF hydroxylases Prolyl Hydroxylase Domain 1-3 (PHD1-3) and Factor Inhibiting HIF (FIH), which function as cellular oxygen sensors. As per the 2OG oxygenase consensus mechanism (Figure 1.9), these enzymes possess an absolute requirement for molecular oxygen. This enables them to catalyse the hydroxylation of specific residues in the

constitutively expressed HIFα subunit, signalling for its degradation or ablating its transcriptional activity. The PHD enzymes hydroxylate prolyl residues within the *N*- and *C*-terminal oxygen dependent degradation domains of the HIFα subunit (NODD and CODD, respectively)[156], enabling interaction of HIFα with the von-Hippel-Lindau tumour suppressor-elongin B-elongin C complex (pVHL), ubiquitination and targeting for degradation[157–159]. PHD2 is the most well studied of the PHDs and is proposed to be the most important in normoxia[160]. FIH catalyses the hydroxylation of an asparaginyl residue in the HIFα CAD[161], blocking its interaction with the CH1 domain of the p300/CBP transcriptional co-activators[162], both of which possess acetyltransferase activity[163] and are essential for activation of HIF target genes[164]. In normoxia, the activity of the HIF hydroxylases is unimpaired and HIF is degraded without activating its target genes. In conditions of low oxygen, the activity of these enzymes is reduced, hence their hydroxylation reactions cannot occur[165], HIFα is upregulated and translocates to the nucleus, where it is able to bind to HIFβ and activate the hypoxic response[166] (Figure 1.13).

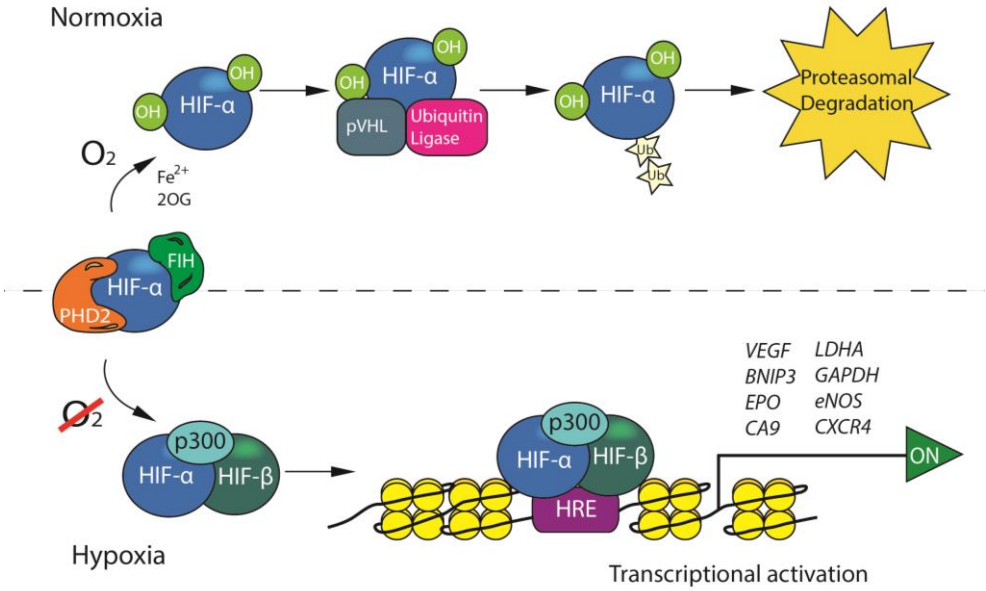

Figure 1.13 The HIF-mediated hypoxic response. The levels and activity of the constitutively-expressed HIF-α subunit are regulated by the HIF hydroxylases. In normoxia, PHD2 and FIH hydroxylate HIF, facilitating binding of the pVHL-elongin B elongin C complex and ubiquitin ligase, which target it for proteasomal degradation. In hypoxia, the activity of PHD2 and FIH is reduced, hence HIFα is upregulated and translocates to the nucleus, where it forms a heterodimer with HIFβ, binds to the CBP/p300 co-activator and activates expression of target genes. Adapted with permission of Future Medicine Ltd from Hancock *et al.* (2015)[250].

Both *in vitro* and cellular studies have demonstrated that the catalytic activity of PHD2, in particular, is highly sensitive to oxygen availability. Steady-state kinetic analyses have determined $K_m(O_2)$ values ranging between 230 and 1746 μM for PHD2[167–171], while pre-steady-state kinetic analysis of recombinant PHD2 also revealed that steps in its catalysis subsequent to addition of oxygen are slow compared to equivalent analyses of TauD and a viral collagen prolyl hydroxylase, vCP4H[85,88,172]. This slow reaction with oxygen is proposed to contribute to its oxygen sensing function[85]. Furthermore, in cells, hydroxylation of HIF prolyl residues P402 & P564 by endogenous PHD2 is inhibited at oxygen concentrations below 1.0%[173]. These features are proposed to underpin PHD2's biological role as an oxygen sensor[85], although the rapid degradation of HIF downstream of its hydroxylation by the HIF hydroxylases also contributes to responsiveness of the HIF pathway. However, it is yet to be established as to whether PHD2 is uniquely capable of oxygen sensing in a biologically relevant context within the 2OG oxygenase superfamily.

1.6. Epigenetics and hypoxia

Hypoxia has been shown to affect epigenetic marks and proteins in a number of studies. Notably, changes to DNA methylation and the enzymes regulating this have been observed in different cell lines and under different conditions. Interestingly, several studies have shown a relationship between DNA methylation, TETs and HIF. Global hypomethylation in colorectal cancer and melanoma cell lines was found to persist in hypoxic tumour xenografts[174], while similar loss of 5mC levels with concomitant increases in 5hmC in sclerotic fibroblasts exposed to 1.0% O_2 was attributed to HIF-1α-dependent induction of TET1[175]. Conversely, global hypermethylation, linked to enhanced DNMT3b expression, was found in PwR-1E prostate epithelial cells following chronic hypoxia[176]. Furthermore, chronic hypoxia also resulted in HIF-dependent elevation of DNMT1 and DNMT3b levels in

patient-derived cardiac fibroblasts, again resulting in global hypermethylation and contributing to the fibrotic phenotype[177].

Gene-specific changes to DNA methylation in hypoxia have also been detected. Hippocampal cell cultures exposed to acute hypoxia demonstrated no overall change to average DNA methylation, but both long-term hypo- and hypermethylation in specific gene regions, which corresponded to respective activation or repression of the affected genes[178]. Moreover, loss of expression of the HIF target gene BNIP3 in pancreatic, colorectal and gastric cancer was found to be due to increased methylation of the *BNIP3* locus. Inhibition of the DNA methyltransferases with the DNMT inhibitor 5-azaC restored BNIP3 expression, and resulted in hypoxia-induced cell death[179,180].

The HIF co-activators CBP and p300 are HATs[163], thereby presenting a direct link between histone acetylation and the hypoxic regulation of genes. Altered expression levels, activity and function of HDACs in hypoxia, leading to changes in histone acetylation status, have also been reported. Hypoxic neonatal rat cardiomyocytes displayed reduced H3K9 acetylation at the promoter of *PGC-1α*, a gene involved in the control of cardiac metabolism[181], while transcriptional repression of the cytokine MCP-1 in HeLa exposed to hypoxia was mediated by HDAC-dependent deacetylation of H4, in cooperation with the transcriptional co-activator/repressor NF-κB[182].

Several studies have linked HDAC activity with stabilisation of HIF or co-activation of HIF target genes. In hypoxic HEK293 cells, HDAC7 was found to act as a transcriptional co-activator of HIF-1α *via* direct interaction of the two proteins[183]. Moreover, Fath *et al.* found that treatment of cells with HDAC inhibitors led to the repression of transactivation of HIF target genes. This was due to apparent disruption of the interaction between HIF-1α and p300, although the exact deacetylation event responsible was not elucidated[184]. In a different mechanism, hypoxic enhancement of HDAC1 and HDAC2 activity was linked to increased

phosphorylation of these HDACs by the protein kinase CK2. Furthermore, CK2 and HDAC activity was found to stabilise HIF-1α in hypoxia, *via* downregulation of pVHL[185]. Similarly, overexpression of HDACs 1-3 in HepG2 cells exposed to 1.0% O_2 appeared to activate angiogenesis *via* downregulation of the tumour suppressor genes p53 and pVHL[186], which is again likely to stabilise HIF. Finally, acetylation of the *N*-terminal region of HIF-1α by HDAC4 was found to stabilise HIF-1α and regulate expression of HIF target genes[187]. These examples illustrate the many roles epigenetic proteins may have, potentially involving non-histone substrates, and the numerous interactions that may be disrupted upon aberrant expression or activity of these enzymes.

1.6.1. Histone methylation and hypoxia

The JmjC-KDMs are epigenetic regulators and, as such, possess the potential to enact changes to transcriptional programmes in response to environmental factors. They are members of the 2OG oxygenase enzyme superfamily, hence are related to the cellular oxygen sensing enzymes, PHD2 and FIH. PHD2 has been shown to be particularly sensitive to oxygen concentration, which is thought to be integral to its function as an oxygen sensing enzyme (Chapter 1.5). However, all 2OG oxygenases require molecular oxygen for their catalytic activity; hence the study of their individual oxygen sensitivities is important in understanding whether the HIF hydroxylases are unique in their oxygen sensing functions, or whether lack of oxygen availability may impact upon the numerous other biological pathways in which the 2OG oxygenases are involved.

Several recent studies have indicated that hypoxia may contribute to dysregulation of epigenetic marks, including histone lysine methylation, while many of the JmjC-KDMs are upregulated in hypoxia. Indeed, reviews by both Melvin and Rocha[188] and Perez-Perri[189] have highlighted the area of hypoxia and epigenetics as one of importance for investigation.

Biochemical studies of the JmjC-KDMs have revealed the potential for differential oxygen sensitivity across the KDM4 subfamily. Kinetic studies of KDM4A, KDM4C and KDM4E using an oxygen consumption assay found $K_m^{app}(O_2)$ values for these enzymes of 57 ± 10, 158 ± 13 and 197 ± 16 μM, respectively[190]. Furthermore, detailed kinetic investigation of recombinant KDM4E used mass spectrometry and UV visible spectroscopy techniques to probe the enzyme's reaction with oxygen. Steady-state analysis revealed that the enzyme's demethylase activity possessed a graded response to oxygen between 0 and 21 % O_2 and, although saturating conditions were not reached due to experimental limitations, the estimated $K_m^{app}(O_2)$ value for the enzyme was > 93 μM[191]. Moreover, pre-steady-state kinetic analysis found a slow rate of reaction with oxygen, similar to that previously observed for PHD2[85,191]. This study further suggested that at least some of the JmjC-KDMs have the potential to act in an oxygen-sensitive manner.

There are numerous reports within recent literature of changes to both global and locus-specific histone methylation status in various cell lines under hypoxic conditions (Table 1.2). In some cases, changes to methylation status at a specific gene locus have been detected and linked to altered expression levels of the gene in question, in line with the so-called histone code (Chapter 1.3.2).

Table 1.2 Cellular hypoxia leads to changes in histone lysine methylation. Both global and gene-specific changes to histone lysine methylation, (gain (↗) and loss (↘)) with associated changes in gene expression, have been observed in cells exposed to hypoxia. NS = not stated, ND = not determined. Table adapted and updated with permission of Future Medicine Ltd from Hancock *et al.* (2015)[250].

Cell line	% O_2	Changes to global methylation	Gene locus and change in expression levels	Altered methylation status at promoter	Reference
A549	NS	H3K9me2 ↗ H3K9me3 ↗	--	--	192
Fetal lung type II	2.0	H3K9me2 ↗	*SP-A* ↗	H3K9me2 ↗	193
A549, HOS, HEK293	0.5	H3K9me2 ↗	*MLH1* ↘, *DHFR* ↘	H3K9me2 ↗	194
Hepa1-6	0.2	H3K4me2 ↗ H3K4me3 ↗ H3K79me2 ↗ H3K27me3 ↘	*AFP* ↘, *ALB* ↘	H3K9me2 ↗ H3K27me2 ↗	195
		H3K9me2 ↘ H3K4me1 ↗	*EGR1* ↗	H3K9me2 ↘, H3K27me2 ↘	
HepG2	0.1-5.0	H3K4me2 ↗ H3K4me3 ↗ H3K9me2 ↗ H3K36me3 ↗	--	--	196
BEAS-2B, A549	1.0	H3K4me3 ↗	--	--	197
RAW264.7		H3K9me2 ↗ H3K9me3 ↗ H3K36me3 ↗	*CCL2* ↘, *CCR1* ↘, *CCR5* ↘	H3K9me2 ↗ H3K9me3 ↗	198
RKO NIH 3T3		H3K9me3 ↗	*PP2A* ↘	H3K9me3 ↗	199
McA-RH7777	1.0 or 5.0	H3K9me3 ↗	--	--	200
IMR-90	<0.5	ND	*INK4a does not change*	H3K27me3 ↗ H3K4me3 ↗	201
RKO	<0.1	ND	*APAK* ↘	H3K9me3 ↗	202
MCF-7 RKO	0.01	ND	*BRCA1* ↘ *RAD51* ↘	H3K4me1/2/3↘	203
HeLa	0.5	None observed	*MCP1* ↘	H3K4me3 ↗ H3K9me2 ↗	182

The activity, localisation and levels of several methyltransferases have also been reported to be altered in hypoxia. Overexpression of the H3K9 histone methyltransferase G9a in hypoxia

leads to reduced levels of H3K9me3, but increased H3K9me2 levels[194,204], while stabilisation of the methyltransferases responsible for H3K9me3, SETDB1 and SUV39H2, was revealed in RKO cells exposed to <0.1% O_2[199]. Furthermore, recruitment of the SUV39H methyltransferases to specific gene elements of the developmental gene *SP-A* has been observed in hypoxic fetal lung cells, with a global increase in H3K9me2 at the *SP-A* promoter[205]. Interestingly, exposure of RKO cells to <0.1% O_2 revealed HIF-independent repression of APAK, a protein involved in regulation of p53[202]. This was found to be due to increased levels of H3K9me3 at the APAK locus mediated by SETDB1[202]. However, levels of SETDB1 were only moderately increased in hypoxia, indicating that binding of SETDB1 at the H3K9me3–enriched region of the *APAK* locus is responsible for the changes to H3K9me3 levels observed[202].

There is substantial evidence to show that altered JmjC-KDM expression levels may also contribute to the global and specific methylation changes described. Multiple studies have shown that several (but not all) of the JmjC-KDMs, including *KDM3A, KDM4B, KDM4C, KDM5B* and *KDM5C* are HIF-1α target genes[196,203,206–211]. Hypoxic upregulation of *KDM6B* is mediated by both HIF-1α[212] and HIF-2α[213]. Furthermore, several others are upregulated in hypoxia at the transcript level, apparently independently of HIF[188,196].

Importantly, differential cellular oxygen dependences of these JmjC-KDMs, despite the fact that they are known HIF targets, have been demonstrated in a number of studies. Beyer *et al.* showed that in cells, KDM3A activity was maintained at 0.2% oxygen, whereas KDM4B demethylase activity was significantly reduced under the same conditions[206]. Similarly, in LNCaP cells, KDM3A was active below 0.5% oxygen, whereas KDM5B was inhibited, and the activity of KDM4C was reduced below 3.0%[212]. Hypoxic inhibition of the activity of KDM5A, KDM5B and KDM6B has also been reported[197,201,214]. HIF-dependent upregulation of JmjC-KDMs has been postulated as a compensatory mechanism due to their reduced

activity in conditions of low oxygen[196,206]. However, the fact that several demethylases are able to act on the same methylated lysine substrate and the existence of multiple isoforms within the same KDM subfamily raises the important question of redundancy between these enzymes, and suggests that the relationship between KDM levels and activity in hypoxia is likely to be highly complicated[208], necessitating detailed biochemical and cellular studies.

Table 1.3 Several JmjC-KDMs are upregulated in hypoxia (Hypoxic induction +). Of these, several are HIF target genes (HIF regulation +). KDM3A, KDM4C and KDM6B are reported to interact with HIF at specific gene regions, with consequent changes to HIF target gene expression (HIF binding/ cooperation +). Table adapted and updated with permission of Future Medicine Ltd from Hancock *et al.* (2015)[250].

	Hypoxic induction	**HIF regulation**	**HIF binding/ cooperation**	**References**
KDM2A/FBXL11/JHDM1A	+			196
KDM2B/FBXL10/JHDM1B	+			196
KDM3A/JMJD1A	+	+	+	196,206–210,215
KDM3B/JMJD1B	+			196
KDM3C/JMJD1C	+			196
HR				
KDM4A/JMJD2A				
KDM4B/JMJD2B	+	+		196,206,208,209,211
KDM4C/JMJD2C	+	+	+	196,206,208,216
KDM4D/JMJD2D				
KDM4A/JMJD2E				
KDM5A/JARID1A/RBP2	+			196
KDM5B/JARID1B/PLU1	+	+		196,203,214
KDM5C/JARID1C/SMCX	+	+		196
KDM5D/JARID1D/SMCY	+			196
KDM6A/UTX	+			196
KDM6B/JMJD3	+	+	+	196,212,213
KDM7A/KIAA1718	+			196
KDM7B/PHF8	+			196
PHF2	+			196

Intriguingly, a number of the JmjC-KDMs have been shown to affect the expression of HIF target genes in hypoxia, in some cases due to cooperation with HIF. In HCT116 cells, KDM3A had a direct effect on expression of a specific subset of HIF target genes, including *ADM*, *HMOX1* and *GDF15*, *via* demethylation of H3K9me2 in the promoter regions of these genes[210]. Furthermore, KDM3A and HIF were found to cooperate in HEK293, HeLa and HUVEC cells, resulting in changes to histone methylation at the enhancer of *SLC2A3*, a

hypoxic response gene involved in the glycolytic pathway[215]. Similarly, direct interaction between HIF-1α and KDM4C in breast cancer cells was found to enhance activation of genes including *BNIP3* and *LDHA*, as well as those involved in cancer metastasis, *via* demethylation of the repressive H3K9me3 mark in these gene promoters to enhance HIF binding to the HRE[216]. Finally, an interesting relationship between the apparent HIF-2α target JmjC-KDM KDM6B and activation HIF-2α target genes was recently reported. KDM6B and HIF-2α were co-precipitated from HEK293 cells subjected to 1.0% O_2 for 24 h, while knockdown of KDM6B in HepG2 cells produced a marked reduction in the activation of the HIF-2α target gene EPO in hypoxia[213].

1.6.2. Histone methylation and the JmjC-KDMs in hypoxic diseases

Increased expression and altered catalytic activity of several JmjC-KDMs in hypoxia, along with effects on HIF target genes, have been demonstrated in numerous studies (Chapter 1.3.1). This is likely to have implications for epigenetic regulation in hypoxic disease states. Solid tumours possess hypoxic regions due to abnormal vascularisation[217,218], and hypoxia is also linked to tumour aggressiveness and resistance to treatment[217–219]. Hypoxia and ischaemia are also a feature of many cardiovascular disease states, including anaemia[220] and atherosclerosis[221], and may result in an ostensibly cardio-protective remodelling of cardiac metabolism, which can eventually prove maladaptive[222]. For instance, upregulation of HIF has been shown to activate genes involved in glycolysis and lipid anabolism in cardiac hypertrophy[223], a disorder in which vascularisation is decreased due to increased cardiomyocyte size and fibrosis[224].

The dysregulation or mutation of many epigenetic proteins has been observed in numerous types of cancer[225], while an altered epigenetic landscape and consequent changes to gene expression have been linked to cancer occurrence and progression, and are often associated with poor prognosis[226]. The involvement of JmjC-KDMs, including those regulated by HIF

(Chapter 1.3.1) in numerous types of cancers has been well documented (Figure 1.14), and several JmjC-KDMs have been identified as oncogenes[227].

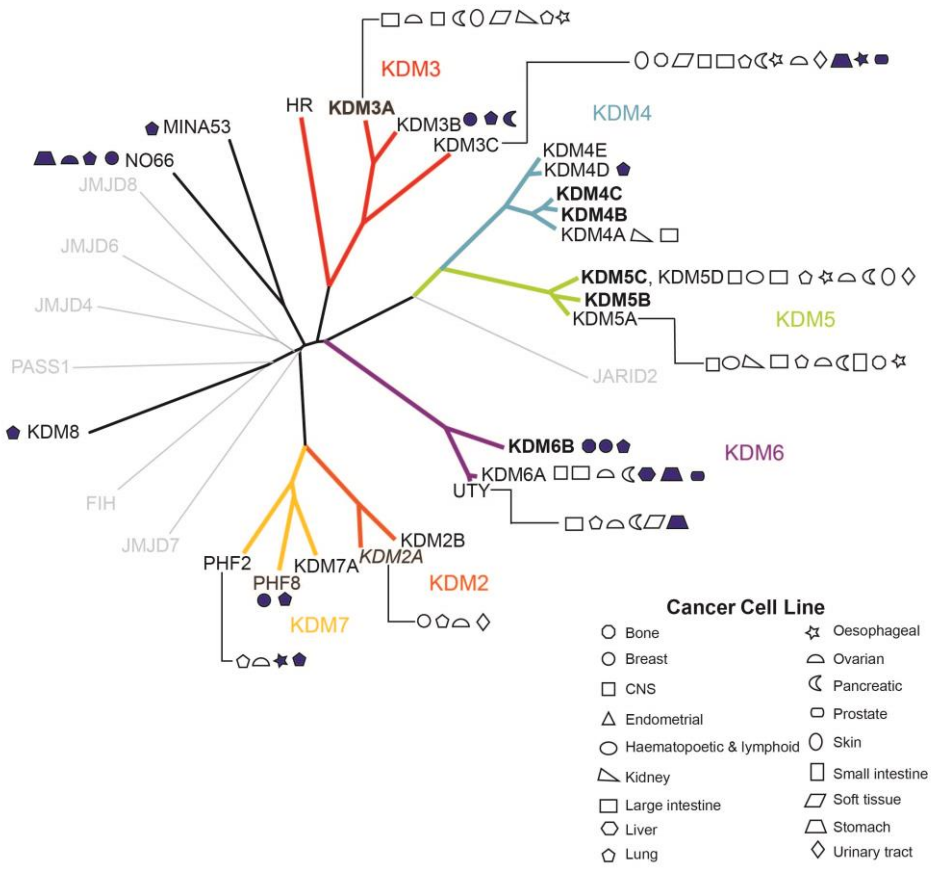

Figure 1.14 JmjC-KDMs in cancer. Multiple JmjC-KDMs have been implicated in various cancers. HIF-upregulated JmjC-KDMs are highlighted in bold. Filled shapes denote JmjC-KDMs overexpressed (mRNA data) in specific cancer cell lines. Open shapes indicate cancer cell lines vulnerable to ≥ 2 shRNAs for a specific JmjC-KDM (log2-fold change ≤-2). Data was generated using the SGC Chromohub, which extracts data from the Cancer Cell Line Encyclopaedia, www.cancerRXgene.org and the Integrative Genomics Portal.

Many cardiovascular diseases, including cardiac hypertrophy, myocardial ischaemia and cardiomyopathy, converge on heart failure[228,229], which is characterised by altered cardiac gene expression. Changes such as a shift in metabolism from oxidation of fatty acids to glycolysis and the activation of fetal genes, including atrial natriuretic factor (*ANF*) and brain natriuretic factor (*BNF*)[230,231], have been proposed as a cardio-protective mechanism, aimed at increasing cardiac efficiency and output in response to stress[232]. However, these

changes are, in fact, maladaptive; hence understanding the factors contributing to this common pathway is necessary to enable therapeutic intervention.

Recent studies have focussed on the epigenetic contribution to cardiovascular disease. Analysis of both genome-wide and gene-specific changes to epigenetic modifications, including histone lysine methylation, has been carried out in disease states such as cardiac hypertrophy, cardiomyopathy and heart failure (Table 1.4). Interestingly, renal failure has been shown to impact upon acetylation, phosphorylation and methylation of cardiac H3 in diabetic mice, with changes to the expression levels of various cardiomyopathy-related genes[233]. In samples from human cardiomyopathic hearts, increased levels of H3K36me3 were correlated with increased expression of non-coding RNA, while at the *DUX4* locus, loss of H3K36me3 and increased DNA methylation corresponded to reduced expression of DUX4, a double homeobox transcription factor[234]. Furthermore, analysis of myocardium from patients with either ischaemic or dilated cardiomyopathy showed increased H3K27ac and loss of H3K9me2/3, with reduced binding of heterochromatin protein 1 (HP1), at the *BNF* promoter region[235].

Kaneda *et al.* determined global changes to H3K4me3 and H3K9me3 in failing murine hearts, subsequently mapping these changes to clusters of genes involved in cardiac function[236]. More detailed global analysis of seven histone modifications including methylation at H3K4, H3K9 and H3K27, in hypertrophic cardiomyocytes revealed a distinct epigenetic signature for cardiac hypertrophy[237]. Moreover, these epigenetic changes were found in both gene promoters and gene enhancing regions, suggesting that aberrant epigenetic regulation may not only be a result of disease, but may drive changes to gene expression and contribute to the disease phenotype[237].

The JmjC-KDMs have been investigated and implicated in several of the disease states discussed above. Overexpression of KDM3A, KDM4A and KDM4B was found in both

ischaemic and dilated cardiomyopathy and correlated to increased expression of the fetal genes *ANF* and *BNF via* changes to H3K9 methylation status and increased recruitment of KDM4A to the *ANF* promoter[235]. The upregulation of these JmjC-KDMs was found not to be solely due to pressure overload[235], suggesting involvement of an alternate stimulus or more complex mechanism. Both KDM3A and KDM4B are HIF target genes, although KDM4A is yet to be identified as such[196,203,206–211], hence hypoxic upregulation of these enzymes in cardiovascular disease is possible.

Table 1.4 Changes to histone lysine methylation and involvement of JmjC-KDMs in cardiovascular disease. Several gene- specific changes to histone lysine methylation, (gain (↗) and loss (↘)) with associated changes in gene expression, have been observed in cardiovascular diseases. Furthermore, a number of JmjC-KDMs have also been implicated in these indications, Table adapted and updated with permission of Future Medicine Ltd from Hancock *et al.* (2015)[250].

Disease state	Changes to lysine methylation status	Gene locus and change in expression level	JmjC-KDM implicated?	Reference
Cardiomyopathy	H3K36me3 ↘	*DUX4* ↘	--	234
Cardiomyopathy	H3K9me2/3 ↘	*ANF* ↗ *BNF* ↗	KDM3A ↗ KDM4A ↗ KDM4B ↗	235
Heart failure	H3K4me3 H3K9me3	Global study	--	236
PTIP k/o mouse (reduced global H3K4me3 model)	H3K4me3 ↘ (globally induced)	*Kcnip2* ↘	--	238
Cardiac hypertrophy	H3K9me3 ↘	*FHL1* ↗	KDM4A ↗	239

Increased levels of KDM4A protein have also been found in samples from hypertrophic cardiomyopathy patients[239]. In mice, heart-specific knock-out of KDM4A blunted the hypertrophic response following TAC-induced cardiac pressure overload, while heart-specific KDM4A overexpression produced no changes to the baseline phenotype, but exacerbated the development of cardiac hypertrophy under pathological conditions[239].

KDM4A was found to bind to the promoter, and activate expression *via* demethylation of H3K9me3, of *FHL1*, which codes for the biomechanical stress sensor FHL1[239]. The results from this study suggest that pharmacological targeting of JmjC-KDMs may be beneficial in cardiac hypertrophy, although further investigation is required to validate KDM4A as a therapeutic target.

1.7. Thesis objectives

Taken together, the evidence to date suggests that the relationship between HIF, hypoxia and the JmjC-KDMs is highly complex (Figure 1.15). Biochemical analysis of individual JmjC-KDMs is required to further elucidate the differences between hypoxic increases in levels and loss of catalytic activity that have been reported in previously published literature, and the true impact of oxygen availability on epigenetic regulation in hypoxia. This is of importance, as the effect of hypoxia on JmjC-KDMs is likely to contribute to both global and gene-specific changes observed in various hypoxic disease states including cancer and cardiovascular disease (Chapter 1.6.1).

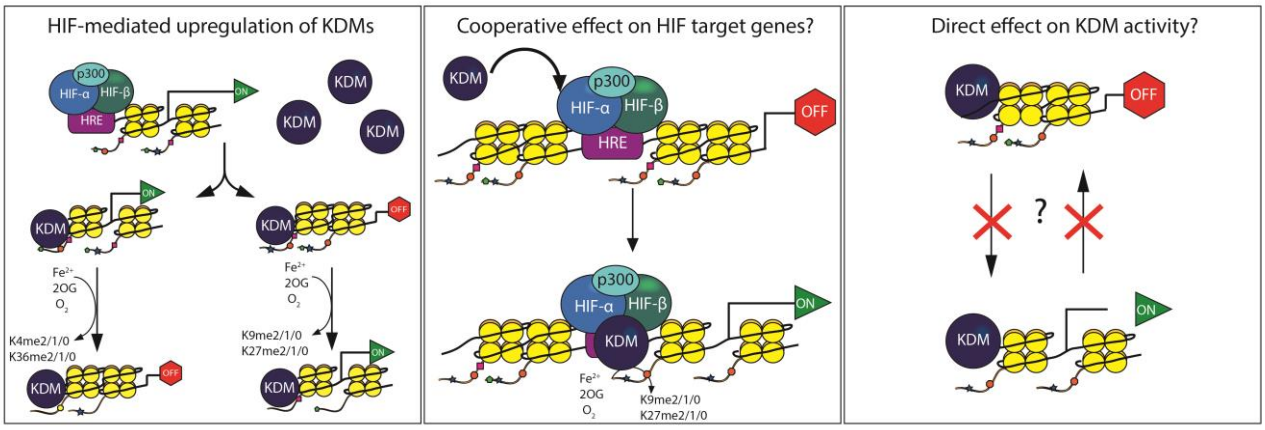

Figure 1.15 Possible mechanisms of hypoxically-induced changes to epigenetic regulation by the JmjC-KDMs. Figure adapted with permission of Future Medicine Ltd from Hancock *et al.* (2015)[250].

The aim of the work described in this thesis was to investigate the effect of hypoxia on the activity of the JmjC-KDM KDM4A using both biochemical and cellular analyses. To enable this, the following specific research questions were outlined for investigation.

- How does the catalytic activity of isolated KDM4A respond to changes in oxygen concentration?
- Does oxygen availability affect the cellular demethylase activity of KDM4A?
- Do physiological changes under hypoxia other than reduction in oxygen availability (e.g. changes to metabolism, production of reactive oxygen species) affect KDM4A activity in cells?
- Do hypoxic changes to histone lysine methylation affect downstream expression of target genes?
- Is KDM4A an oxygen sensor in the context of epigenetic regulation?

The experimental work carried out in relation to these questions is described in Chapters 2, 3, 4 and 5.

A secondary aim of this thesis project was to address the reported role of KDM4A in cardiac hypertrophy, and evaluate its potential as a therapeutic target in this disease state. To this end, various inhibitors of 2OG oxygenase enzymes were tested against KDM4A in cells, while a collaborative project with Dr Tim McKinsey (University of Colorado, Denver) was also established to enable pharmacological targeting of KDMs in a cellular model of cardiac hypertrophy. The results of these investigations are detailed in Chapter 4.

Chapter 2: The *in vitro* oxygen dependence of KDM4A

2.1. Introduction

2.1.1. Michaelis-Menten enzyme kinetics

The Michaelis-Menten model of enzyme kinetics was devised experimentally in 1913 by Maud Menten and Lenor Michaelis[240]. Their analysis of the inversion of sucrose by invertase tested the theory that the reaction rate was proportional to the concentration of the enzyme-substrate complex[240,241]. From this, they not only laid the foundations for the subsequently-defined steady-state kinetic model, but developed understanding of more complex phenomena, such as competitive and product inhibition[241,242].

The steady-state model of enzyme kinetics[243] defines the enzyme reaction as:

$$E+S \underset{k_r}{\overset{k_f}{\rightleftharpoons}} ES \xrightarrow{k_{cat}} E+P \qquad \textbf{2.1}$$

where E = enzyme, ES = enzyme substrate complex, S = substrate and P = product.

The model assumes that the concentration of both enzyme and product is much lower than that of substrate, the product is not reverted to substrate, and the reaction has not reached equilibrium, i.e. is in the steady-state. Under these assumptions in the initial stages of the reaction, the rate is

$$\frac{dP}{dt} = V = k_{cat}[\mathrm{ES}] \qquad \textbf{2.2}$$

Rearrangement of this incorporating the steady-state assumptions detailed above produces Michaelis-Menten equation:

$$V = V_{max}\left(\frac{[S]}{[S]+K_m}\right) \quad \textbf{2.3}$$

where K_m is the Michaelis Constant.

$$K_m = \frac{k_r + k_{cat}}{k_f} \quad \textbf{2.4}$$

The Michaelis constant, K_m, is the concentration of substrate at which the rate of catalysis is half its maximum value. The Michaelis constant can be derived empirically by evaluating the initial (steady-state) reaction rate under different concentrations of substrate. Fitting the data to the Michaelis-Menten equation (Equation 2.3) then enables various parameters, including V_{max} (maximal rate) and K_m, to be determined (Figure 2.1).

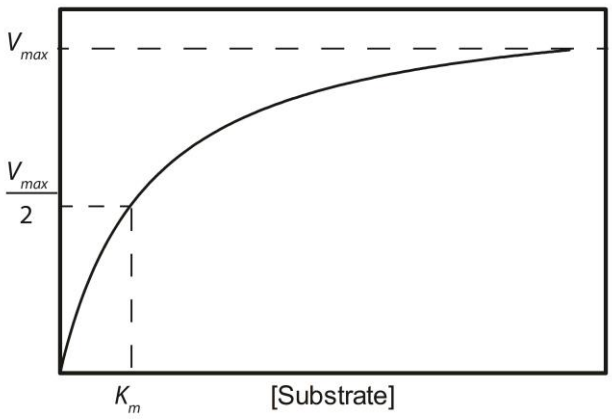

Figure 2.1 Example Michaelis-Menten plot. Plotting the initial rate of reaction against the concentration of variant substrate enables determination of the maximal rate, V_{max} and the Michaelis constant, K_m.

In practice, empirical evaluation often produces the apparent K_m, K_m^{app}, defined as the Michaelis constant "*as observed under conditions…that would hinder the determination of its true value; in the case of a two-substrate enzyme, the Michaelis constant measured under the particular conditions of a defined concentration of the invariant substrate*[244]." The 2OG oxygenases perform multi-substrate reactions; hence all *in vitro* assays result in the evaluation of K_m^{app} values with respect to any of these substrates, and must use saturating concentrations of all other substrates and co-factors to mimic Michaelis-Menten kinetics.

2.1.2. Kinetic studies of the oxygen dependence of 2OG oxygenases

Table 2.1 Differential *in vitro* oxygen sensitivity of 2OG oxygenases. $K_m(O_2)$ values have been determined for a number of 2OG oxygenases using various methods. Adapted and updated from Hancock *et al.*[250].

Enzyme	$K_m(O_2)$/ µM	Substrate	Assay method & references
$PHD2_{181-426}$	230-1746	HIF-$1\alpha_{556-574}$ CODD	O_2 consumption[169], radioactive 2OG turnover[167], MALDI-TOF MS[171],TR-FRET[170]
C-P4H	40	Pro-Pro-Gly	radioactive 2OG turnover[167]
mPAHX	93 ± 43	Isovaleryl CoA	O_2 consumption[169]
TauD	76 ± 17	Taurine	O_2 consumption[169]
FIH	90 -150	HIF-$1\alpha_{788-822}$ CAD	O_2 consumption [169], radioactive 2OG turnover[168] MALDI-TOF MS[245]
FIH	110 ± 73	HIF-$2\alpha_{832-866}$ CAD	O_2 consumption[169]
FIH	100 ± 10	HIF-$2\alpha_{832-866}$ CAD	MALDI-TOF MS[245]
FIH	40 –120	Non-HIF substrates	MALDI-TOF MS[245]
$KDM4A_{1-359}$	57 ± 10	$H3_{7-14}K9me3$	
$KDM4C_{1-366}$	158 ± 13	$H3_{7-14}K9me3$	O_2 consumption[190]
$KDM4E_{1-337}$	197 ± 16	$H3_{7-14}K9me3$	
$KDM4E_{1-337}$	>93	$H3_{7-14}K9me3$	MALDI-TOF MS[191]

The 2OG oxygenase superfamily comprises enzymes involved in many biological processes, from the biosynthesis of collagen to the metabolism of fatty acids. Of significance are the HIF hydroxylases, 2OG oxygenases involved in the cellular response to hypoxia (Chapter 1.5). These enzymes, in particular PHD2, are known as the cellular oxygen sensors and, as such, their reaction with oxygen has been well-studied. Several groups have performed steady-state analyses using a variety of methods, including radioactive 2OG turnover[167], oxygen consumption[169], mass spectrometry[171] and FRET-based assays[170], to yield high $K_m^{app}(O_2)$ values (Chapter 2.1.1) for PHD2 ranging from 230 to 1746 µM[167,169–171] (Table 2.1). Similar investigations on other members of the 2OG oxygenase family, including FIH, the collagen prolyl hydroxylase CP4H, and the plant phytanoyl coenzyme-A hydroxylase mPAHX have attempted to understand the relative sensitivity of these enzymes to oxygen availability (Table 2.1) and have revealed a range of oxygen dependences across the

superfamily. PHD2's high sensitivity towards oxygen availability, as indicated by the high K_m values obtained, has been hypothesised to underlie its biological role as an oxygen sensor.

Moreover, recent studies have assessed the oxygen dependence of several members of the KDM4 subfamily of JmjC-KDMs. The experiments yielded a range of $K_m^{app}(O_2)$ across the subfamily, in parallel to the differences seen across the superfamily. Furthermore, the $K_m^{app}(O_2)$ values obtained for KDM4C and KDM4E are higher than those obtained previously for CP4H, PAHX and FIH (Table 2.1), indicating that the activity of these enzymes is highly sensitive to oxygen availability. This suggests that oxygen concentration may be limiting in the context of epigenetic regulation by these enzymes in hypoxia, although the degree of redundancy, and therefore compensation under compromising conditions, between isoforms in the same KDM subfamily is yet to be determined[246–248].

The studies detailed above employed a variety of methods to assess the oxygen sensitivity of the 2OG oxygenases. There are merits and disadvantages to each of these methods, which must be critically assessed to enable comparisons between the $K_m^{app}(O_2)$ values obtained to be drawn. Several studies have used continuous methods, including an oxygen consumption assay. Continuous methods generally involve a spectrophotometric, fluorescence or colourimetric output, allowing the convenient monitoring of the rate of enzymatic reaction over time, hence facile calculation of the rate of reaction and precise identification of the linear range of the reaction in question. However, measurement of the rate of oxygen consumption or 2OG turnover in the case of the 2OG oxygenase enzymes may result in overestimation of kinetic parameters, due to the possibility of uncoupled turnover of 2OG by these enzymes. Uncoupled turnover is the 'unproductive' enzyme-catalysed oxidative decarboxylation of 2OG, without concomitant oxidation of prime substrate[249].

Conversely, radioactive 2OG turnover and mass spectrometry based end-point assays are used when there is no easily observable output to indicate the progress of the reaction. These are more labour-intensive, as each individual experiment measures the amount of product formed, or substrate used, after a finite period. Each experiment produces only a single data point, and the rate of reaction is calculated from the gradient at the linear range of the timecourse. Therefore, it is often necessary to perform additional control experiments to ensure that data is collected within the linear range of the enzyme reaction. Moreover, in the case of radioactive 2OG turnover assays, the same caveats regarding uncoupled turnover of 2OG apply in the case of the 2OG oxygenases as those discussed above with regard to continuous O_2 consumption assays.

The mass spectrometry-based assays used by Tarhonskaya *et al.*[171,245] and Sanchez *et al.*[191] have the advantage of direct assessment of the amount of product generated, thereby allowing assessment of the kinetics of productive enzyme reactions, mitigating the impact of uncoupled turnover. Matrix Assisted Laser Desorption Ionisation Time-of-Flight (MALDI-TOF) mass spectrometry (MS) enables the ratio of substrate peptide to product peptide, hence percentage demethylation, in a sample to be calculated and is both quick and relatively high-throughput.

2.1.3. Chapter aims

The work detailed in this chapter aimed to assess the *in vitro* oxygen sensitivity of recombinant KDM4A. This was performed using an end-point, mass spectrometry-based assay to enable direct comparison with values obtained previously within the group for PHD2 and FIH (Table 2.1)[171,245]. Overall, this study aimed to aid in the understanding of the extent to which PHD2 and FIH are unique in their biochemical sensitivity towards oxygen and the potential for differential oxygen sensitivity across the 2OG oxygenase superfamily (Table 2.1). The oxygen sensitivity of PHD2, in particular, is thought to be integral to its

function as an oxygen sensor in the HIF pathway[85], hence similar oxygen dependence displayed by other 2OG oxygenases could indicate that they possess a potential oxygen sensing role within the biological pathway they participate in. In the case of the KDMs, reduced activity in hypoxia may result in changes to histone lysine methylation, which can have a direct impact on gene transcription. Therefore, the experiments described herein aimed at understanding the biochemical relationship between KDM4A activity and oxygen availability, in order to establish whether reduced histone lysine demethylation by the KDMs in hypoxia may contribute to the aberrant epigenetic signatures observed in numerous cell lines[189,250] and hypoxic disease states[250] (Chapter 1.6).

Calibration of the oxygen concentrations produced using the Mass Flow Controller was previously performed by Ben Greenfield during his time as a Part II student in the group. Aspects of the work described in this chapter have been published. Figures from this publication are reprinted or adapted with permission from Hancock et al.[251]*, Copyright (2017), American Chemical Society, and acknowledged in the appropriate figure legend.*

2.2. Preparation of materials for *in vitro* experiments

All *in vitro* assays used recombinant *N*-His_6-tagged $KDM4A_{1-359}$ (tKDM4A), which was overexpressed and purified from *E. coli* following a procedure from Ng *et al.*[145] (Chapter 7.1.2). Briefly, tKDM4A was overexpressed in BL21 (DE3) *Escherichia Coli* cells and purified from the lysate *via* Fast Protein Liquid Chromatography (FPLC). Lysate was first purified using immobilised metal affinity chromatography on a 5 mL Ni^{2+} HisTrap fast flow column (General Electric) in 10 mM HEPES pH 7.5 buffer containing increasing concentrations of imidazole (Chapter 7.1.2). The ultraviolet (UV) trace obtained during FPLC purification (Figure 2.2a) and Sodium Dodecyl Sulfate-Polyacrylamide Gel Electrophoresis (SDS-PAGE) analysis (Chapter 7.1.3) was used to select protein fractions of sufficient purity (>80%, Figure 2.2a), which were then pooled, concentrated using a

centrifugal filter membrane (30 kDa MW cut off, Amicon) and submitted to size exclusion chromatography on a Superdex S200 300 mL column (General Electric). Protein fractions were eluted in 10 mM HEPES pH 7.5, 500 mM NaCl, 5 % glycerol, and the UV trace and SDS-PAGE analysis used to select fractions of sufficient purity (>80%, Figure 2.2b) for use as enzyme stock. Selected fractions were concentrated as previously and flash frozen in liquid nitrogen, before storage at –80°C. Liquid chromatography MS (LC-MS) analysis revealed the purified protein to have a mass of 44,273 Da (Figure 2.2c), confirming it as tKDM4A (theoretical mass = 44, 265 Da).

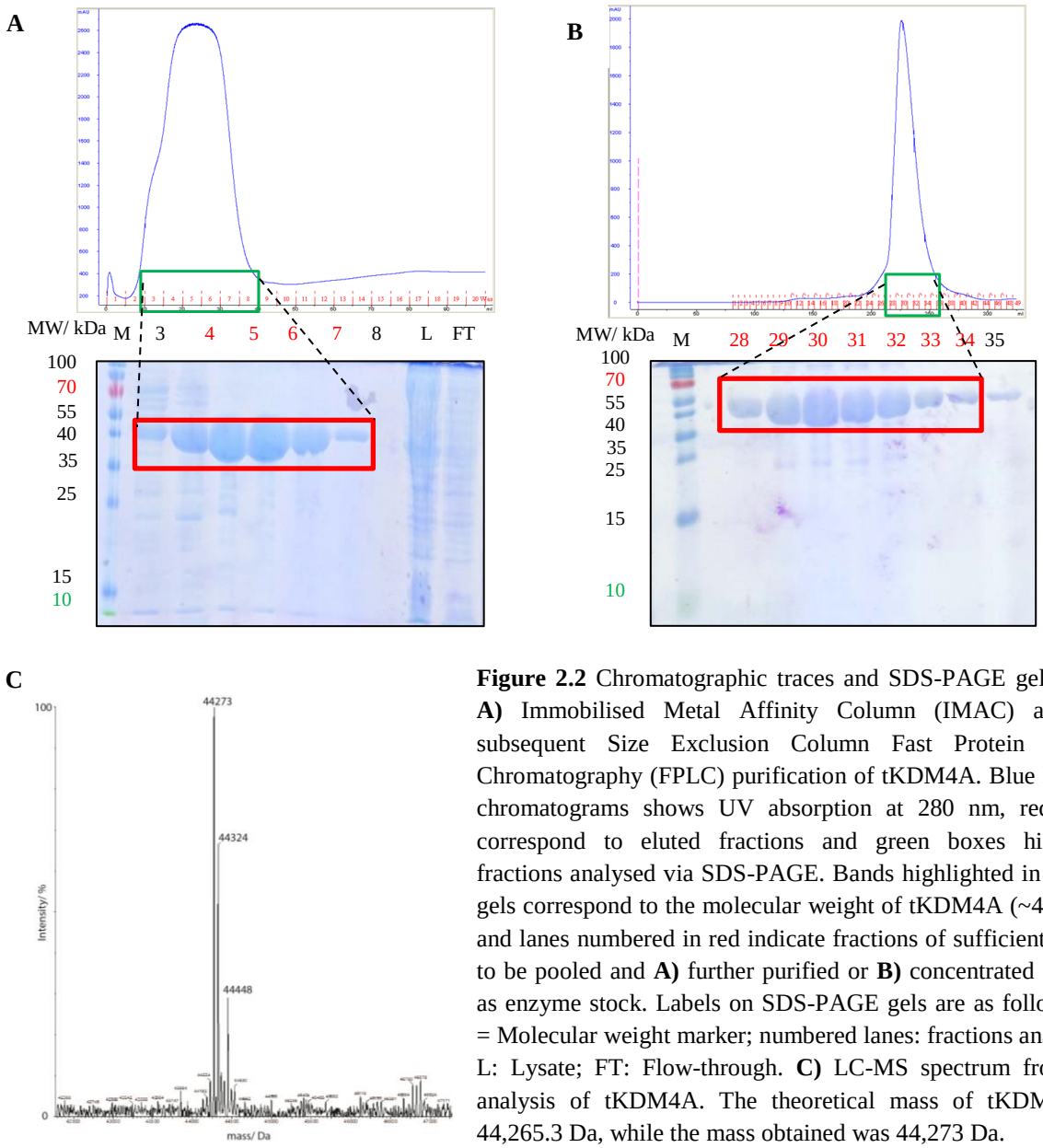

Figure 2.2 Chromatographic traces and SDS-PAGE gels from **A)** Immobilised Metal Affinity Column (IMAC) and **B)** subsequent Size Exclusion Column Fast Protein Liquid Chromatography (FPLC) purification of tKDM4A. Blue line on chromatograms shows UV absorption at 280 nm, red lines correspond to eluted fractions and green boxes highlight fractions analysed via SDS-PAGE. Bands highlighted in red on gels correspond to the molecular weight of tKDM4A (~44 kDa) and lanes numbered in red indicate fractions of sufficient purity to be pooled and **A)** further purified or **B)** concentrated for use as enzyme stock. Labels on SDS-PAGE gels are as follows: M = Molecular weight marker; numbered lanes: fractions analysed; L: Lysate; FT: Flow-through. **C)** LC-MS spectrum from the analysis of tKDM4A. The theoretical mass of tKDM4A is 44,265.3 Da, while the mass obtained was 44,273 Da.

Peptides that have previously been described in the literature as KDM4A substrates[144] were synthesised with a *C*-terminal amide group in-house using a solid-phase microwave peptide synthesiser (Liberty Blue, Chapter 7.1.4). Both a 8mer peptide ($H3_{7-14}$K9me3, ARKme3STGGK, Table 2.2) and a 15mer peptide ($H3_{1-15}$K9me3, ARTKQTARKme3STGGKA, Table 2.2) were produced, and MALDI-TOF mass spectrometry (Figure 2.4) and High Performance Liquid Chromatography (HPLC)-MS analyses (Appendix 1) revealed the peptides to be of sufficient peptidic purity (>90 %) to be suitable for use in *in vitro* assays.

Table 2.2 Sequences and masses of peptides used in the *in vitro* assays described in this chapter.

Peptide	Sequence	Molecular weight/ Da	
		Calculated	Found
$H3_{7-14}$K9me3	ARKme3STGGK	845	845.9
$H3_{1-15}$K9me3	ARTKQTARKme3STGGKA	1602	1603.1

2.2.1. MALDI-TOF mass spectrometry enzyme activity assay

Having prepared the necessary materials, a MALDI-TOF MS assay (Chapter 7.1.5) was performed to assess the activity of the enzyme against these substrates. tKDM4A (1 μM) was incubated with a mixture of H3K9me3 peptide substrate (100 μM), 2OG (100 μM), L-ascorbate (100 μM) and Fe^{2+} (100 μM) in 50 mM HEPES buffer pH 7.5 at 37°C. Samples were taken from the reaction at specific time intervals and quenched with an equal volume of methanol, then submitted to analysis by MALDI-TOF mass spectrometry. This method uses a crystalline matrix, α-cyano-4-hydroxycinnamic acid (CHCA) to facilitate ionisation of the sample from a steel plate, and enables assessment of the enzyme activity *via* accurate determination of the mass of the peptide substrate. Demethylated product peptide is identifiable as a decrease in mass of 14 Da relative to the mass of the substrate peptide

(Figure 2.3). In the case of tKDM4A, the enzyme is able to accept both the original H3K9me3 peptide and, to a lesser extent, the H3K9me2 product peptide[110], hence two product peaks, corresponding to H3K9me2 and H3K9me1 product peptides are observed in the mass spectrum (Figure 2.3), at -14 Da, and -28 Da, respectively. Calculation of the relative intensities of these peaks enables the percentage demethylation of the peptide by tKDM4A to be calculated (Equation 2.5).

$$\% \text{ demethylation} = 100 \times \left(\frac{(I_{-14\ Da} + I_{-28\ Da})}{(I_{substrate} + I_{-14\ Da} + I_{-28\ Da})} \right) \qquad \textbf{2.5}$$

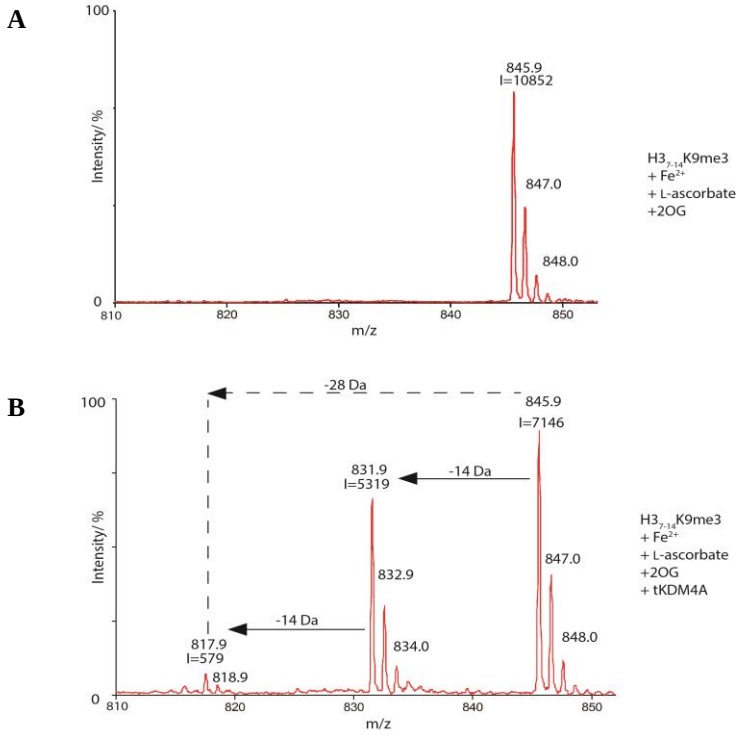

Figure 2.3 Example MALDI-TOF MS spectra of H3$_{7-14}$K9me3 peptide upon addition of **A)** Fe^{2+}, 2OG and L-ascorbate and **B)** Fe^{2+}, 2OG and L-ascorbate, plus tKDM4A. Demethylase activity by the tKDM4A produces two mass peaks, one at -14 Da (831.9 Da), and one at -28 Da (817.9 Da) from the substrate peak (845.9 Da). The intensities of these peaks are used to calculate percentage demethylation using equation 2.19.

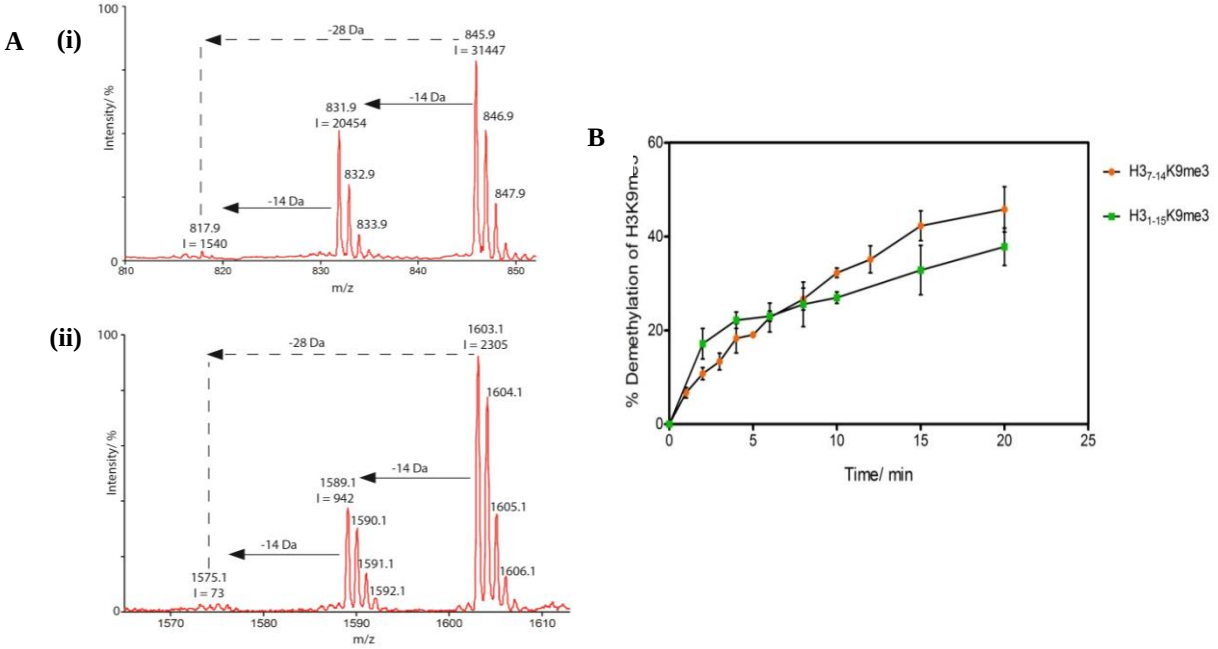

Figure 2.4. **A)** MALDI-TOF spectra for (i) H3K$_{7-14}$K9me3 and (ii) H3$_{1-15}$K9me3 assays after 10 min reaction time. **B)** Calculated percentage demethylation of H3K$_{7-14}$K9me3 (orange circles) and H3$_{1-15}$K9me3 (green squares) peptides plotted against time. Graph was plotted in GraphPad Prism v5.04, error bars represent standard deviation (sd), n = 3 technical repeats.

The MALDI-TOF MS assay (Chapter 7.1.5) was used to test the activity of the purified tKDM4A against the two synthesised peptide substrates. The results of these assays demonstrated both that the purified tKDM4A possessed demethylase activity (Figure 2.4) and that the H3K9me3 peptides synthesised were viable substrates. Therefore, these materials were taken forward for use in the *in vitro* assessment of KDM4A described in this chapter.

2.3. Calculation of Michaelis-Menten constants for 2OG and peptide substrates

The assessment of oxygen dependence requires the maintenance of a desired oxygen concentration, which is usually not possible when using a plate reader or similar to monitor a continuous output, hence *post hoc* measurement of the extent of reaction *via* mass spectrometry was deemed necessary to ensure precise control of oxygen concentration throughout the experiment. Experiments were performed to determine the linear range of reaction and saturating conditions with respect to prime substrate and the 2OG co-substrate, prior to development and optimisation of an oxygen dependence assay. Detailed kinetic analysis of tKDM4A with respect to both prime substrate and 2OG co-substrate was carried

out using the MALDI-TOF mass spectrometry assay described above. It was necessary to evaluate K_m^{app} values for all (co-)substrates using the same assay method, to ensure that saturating conditions of these components were used in the oxygen dependence assay. To evaluate the K_m^{app} values for peptide and 2OG, the concentration of the component in question was varied while maintaining saturating conditions of all others (Table 2.3). As the enzymatic reaction proceeds with a 1:1 stoichiometry of 2OG and peptide, in experiments testing higher concentrations of either substrate, increased concentrations of the other (co-)substrate were used to ensure that turnover was unhindered by lack of (co-)substrate, and that the reaction component under analysis was the only limiting factor.

Table 2.3 Reaction conditions used to determine K_m^{app} values of 2OG and H3K9me3 peptides.

Reaction component	**Concentration in K_m^{app}(2OG) determination/ µM**	**Concentration in K_m^{app}(peptide) determination/ µM**
tKDM4A	1	1
Fe^{2+}	10	10
L-ascorbate	100	100
2OG	Varied: 0-200	100, 150 for [peptide] >100
Peptide	100	Varied: 0-300

For each concentration of the (co-)substrate analysed, samples were taken at multiple timepoints between 0.5 and 10 minutes (Figure 2.5 c, d), and the extent of demethylation and reaction rate were evaluated at each of these, in order to ensure that the maximum initial rate (i.e. rate within the linear range of the reaction) was used in steady-state analyses.

The MALDI-TOF MS assay used for these analyses did present some challenges to the determination of the initial rate of tKDM4A-catalysed demethylation, as the mass spectra produced using this method show the relative amounts of substrate and product in the sample. When a high concentration of substrate is present, the relative ratio of product at early timepoints, often during the steady-state linear range of the reaction, is low, and may be difficult to measure accurately relative to the substrate peak (Figure 2.5a). Conversely,

when a low concentration of substrate is used, the absolute amount of product will be very low, hence difficult to detect and quantify accurately in the presence of a high degree of inherent noise (Figure 2.5b). Therefore, the initial rate of the reaction must be calculated at a time within the linear range of the reaction, but also when sufficient turnover has occurred to ensure accurate measurement of the percentage conversion of the substrate.

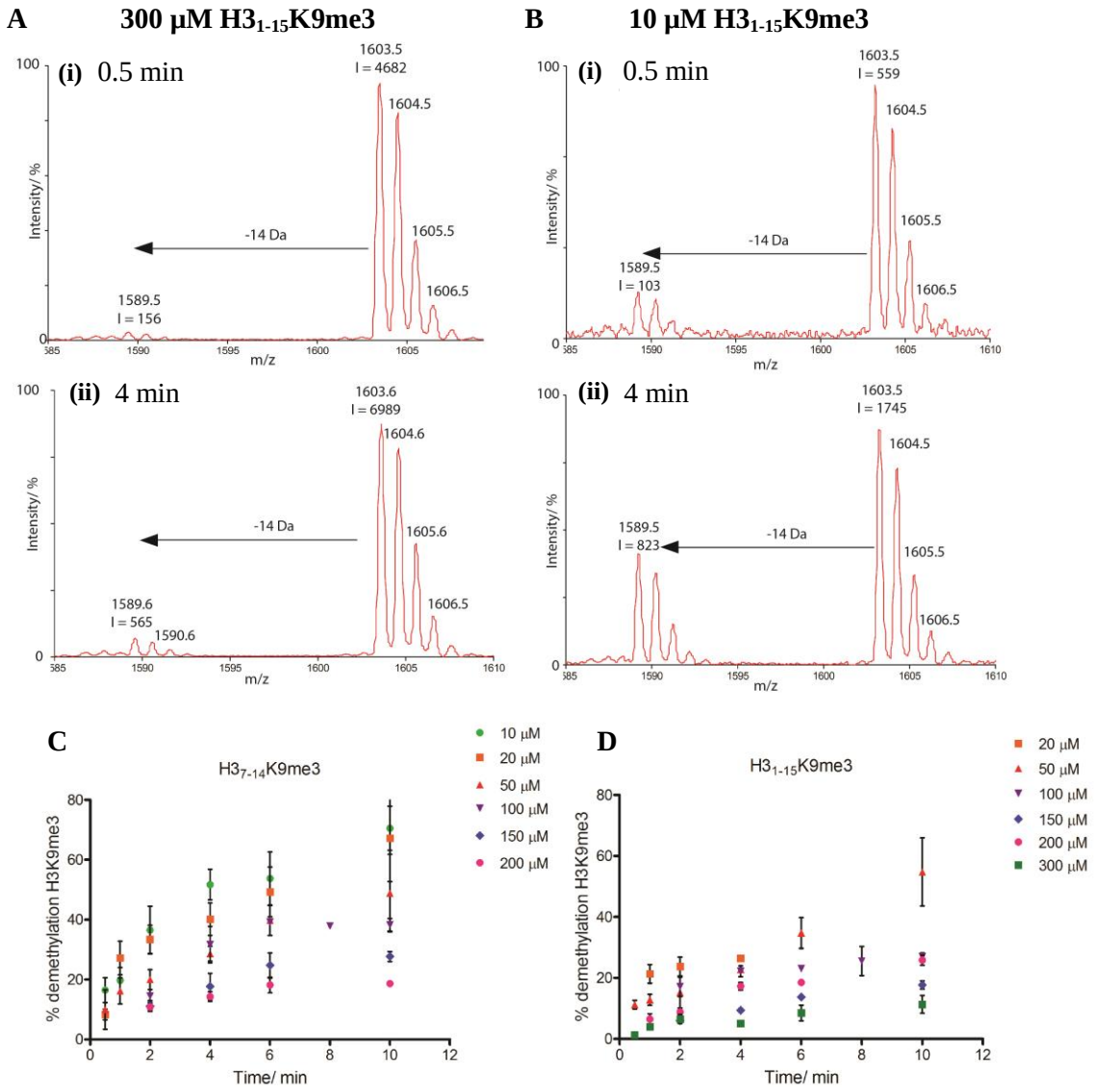

Figure 2.5 Example MALDI-TOF MS spectra of **A)** 300 µM and **B)** 10 µM H3$_{1-15}$K9me3 peptide after (i) 0.5 and (ii) 4 min reaction with tKDM4A. **C)** and **D)** Timecourses used to calculate the initial rate of reaction of tKDM4A with varying concentrations of **C)** H3$_{7-14}$K9me3 and **D)** H3$_{1-15}$K9me3 peptide substrates. Graphs were plotted using GraphPad Prism v5.04 and show the percentage demethylation of the substrate, as calculated from MALDI-TOF MS analyses between 0.5 and 10 min. Error bars denote sd, n = 3 technical repeats.

For both H3K9me3 peptides, the reaction rate was linear and appreciable turnover was achieved for all concentrations tested at timepoints between 4 and 6 minutes (Figure 2.5 c, d), hence rates calculated at these timepoints were used in the K_m^{app} calculations (Figure 2.6). For K_m^{app}(2OG) determination (Figure 2.6 c, d), the rate of reaction at 5 min was calculated for each concentration of 2OG, as this was in the linear range for each peptide substrate in the presence of 100 or 150 µM 2OG (Figure 2.5 c, d). Therefore, at lower concentrations of 2OG, when the rate would be expected to be lower, this would still be in the linear range. The percentage demethylation was corrected by subtraction of the percentage intensity of the -14 Da peak in a no-enzyme control experiment (Figure 2.3b), before calculation of the initial rate of reaction. GraphPad Prism version 5 was used to plot data and fit resultant curves using the Michaelis-Menten equation (Equation 2.3, Figure 2.6).

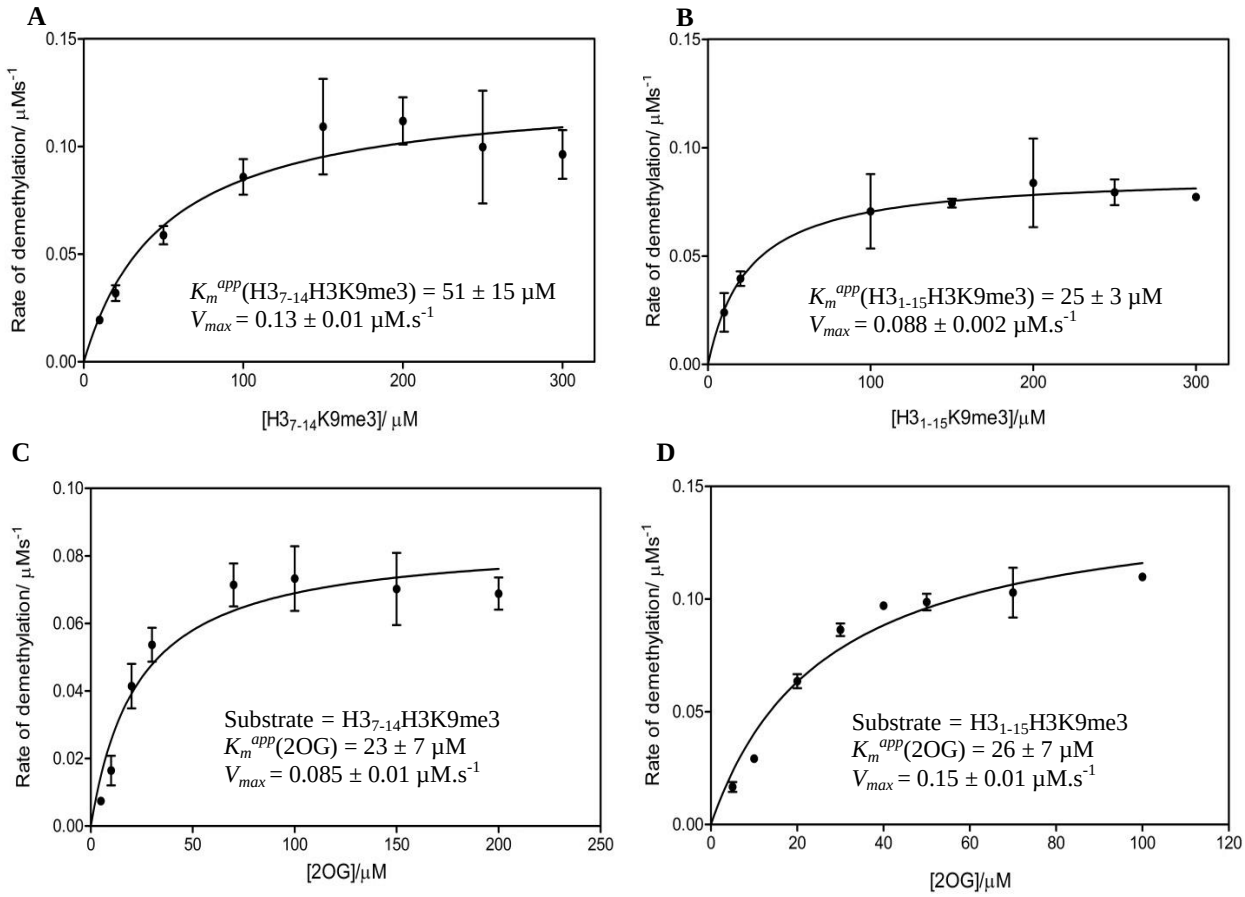

Figure 2.6 Initial rate curves used to evaluate K_m^{app} values for **A)** $H3_{7-14}$K9me3 peptide and **B)** $H3_{1-15}$K9me3 peptide, **C)** 2OG with $H3_{7-14}$K9me3 prime substrate and **D)** 2OG with $H3_{1-15}$K9me3 prime substrate. Curves were fitted to a Michaelis-Menten model using GraphPad Prism v5.04. Error bars represent sd, n = 3 technical repeats. **B)** and **D)** are adapted with permission from Hancock *et al.*[251], Copyright (2017), American Chemical Society.

The experiments detailed above yielded kinetic parameters that were within the same order of magnitude as previously reported values obtained using alternative methods (Table 2.4). Moreover, the use of two different peptide substrates resulted in K_m^{app}(2OG) that did not differ within experimental error. These results demonstrate that the MALDI-TOF MS assay used is appropriate for kinetic evaluation of KDM4A activity. Any differences from literature values are likely to be due to the use of alternative assay methods and conditions, including different peptide substrates, enzyme:substrate ratios[252] and co-factor ratios[253] highlighting the importance of the use of the same method throughout a study.

Table 2.4 K_m^{app} values for (co-)substrates evaluated using the MALDI-TOF MS assay, and previously reported literature values. Differences may arise due to the different assay methods used: *a* = formaldehyde release assay[252].

Reaction component	K_m^{app} by MALDI-TOF MS / μM	Reported K_m^{app} /μM
2OG	23 ± 7 26 ± 7	6[a254]
$H3_{7\text{-}14}$K9me3	51 ± 15	45 ± 7[a,144]
$H3_{1\text{-}15}$K9me3	25 ± 3	17.4 ± 3[a,253]

2.4. Development of a MALDI-TOF MS assay for the O_2-dependence of tKDM4A

2.4.1. Assay design

The kinetic parameters evaluated for tKDM4A with 2OG and the two H3K9me3 peptides enabled saturating conditions of these reaction components to be determined for use in the oxygen dependence assay. Concentrations of 2OG and peptide of at least 2 x the K_m^{app} values obtained (Table 2.4) were used to ensure that only variation of oxygen concentration was limiting. Namely 100 μM 2OG, 100 μM $H3_{7\text{-}14}$K9me3 and 200 μM $H3_{1\text{-}15}$K9me3 were used, along with the Fe^{2+} and L-ascorbate concentrations used in the experiments described above (Table 2.3).

2.4.2. Control of oxygen concentration using a Mass Flow Controller

The MALDI-TOF MS assay described above (Chapter 2.2.1) had to be adapted so that oxygen concentrations could be precisely controlled, necessitating the use of sealed reaction vials (Hichrom Ltd). A Mass Flow Controller (MFC, Brooks Instruments) was used to establish the O_2 concentrations between 0 and 80%. The MFC enables precise control of the percentage flow of two or more gases using thermodynamic principles. Gas flows over two temperature sensors which are separated by a heating element, creating a temperature gradient, which is detected and used to adjust the flow rate of the gas as per equation 2.6:

$$\Delta T = APC_p m \qquad \textbf{2.6}$$

where:

ΔT = temperature difference (K)

A = proportionality constant ($K^{2.} s^{-2.} kJ^{-2}$)

P = power of heating element ($kJ.s^{-1}$)

C_p = specific heat capacity of the gas at constant pressure ($kJ.kg^{-1}.K^{-1}$)

m = mass flow ($kg.s^{-1}$)

The use of two MFCs, one controlling O_2 and the other N_2, enabled a precise mixture of the two gases, corresponding to a partial pressure, pO_2, to be introduced to sealed reaction vials containing the peptide substrate and 50 mM HEPES pH 7.5.

Previous work in the group by Ben Greenfield had investigated the output of the MFC with the use of an aluminium-caged fibre optic oxygen electrode (FOXY, OceanOptics). This has previously been used in oxygen consumption assays[169], and enabled the calculation of the absolute concentration of O_2 (ppm) introduced to the vials under each pO_2. The FOXY electrode works on the principle of fluorescence, and consists of a ruthenium complex embedded in a sol-gel matrix on the end of a fibre-optic cable. Excitation of the ruthenium complex with a pulse of light at 475 nm results in fluorescence emission at 600 nm.

Molecular oxygen is in the triplet spin state, hence a good fluorescence quencher. Quenching of the 600 nm fluorescence can be used to calculate the concentration of the quencher according to the Stern-Volmer equation (Equation 2.7).

$$\frac{I_f^0}{I_f} = 1 + k_q \tau_0 . [Q] \qquad \textbf{2.7}$$

where:

I_f^0 = initial fluorescence intensity

I_f = fluorescence intensity upon quenching

k_q = rate constant of quenching

τ_0 = lifetime of the excited state

[Q] = concentration of quencher

Loss of fluorescence emission in this case corresponds to the concentration of dissolved oxygen. Prior to use for measurement of oxygen concentration, the FOXY must also be calibrated using solutions of known oxygen concentration. Oxygen-depleted buffer (0 ppm O_2) was produced *via* the addition of crystalline sodium sulfite (Na_2SO_3) followed by vacuum degassing, while an air-saturated solution, known to correspond to 7.2 ppm[255], resulted from bubbling compressed air through MilliQ water at room temperature.

The FOXY electrode was then used to measure the concentration of O_2 in buffer equilibrated at pO_2 0-80% using the MFC. The MFC output was used to equilibrate 100 µL 50 mM HEPES pH 7.5 in a sealed glass vial, with the use of a 21-gauge needle. A second needle was used to release gas from the vial, maintaining ambient pressure. The gas flow was maintained for 10 min, during which the vial was incubated at 37 °C. After 10 min the MFC output and depressurising needle were removed, and the FOXY electrode introduced into the solution with the use of a third 21-gauge needle. The measured concentration of O_2 in ppm was then converted to µM, producing a calibration curve (Figure 2.7) which was used in all oxygen dependence assays described in this chapter. This calibration curve was also used in

published analyses of the oxygen dependence of PHD2 and FIH using MALDI-TOF MS assays[171,245], enabling direct comparison of the data obtained herein with these prior experiments.

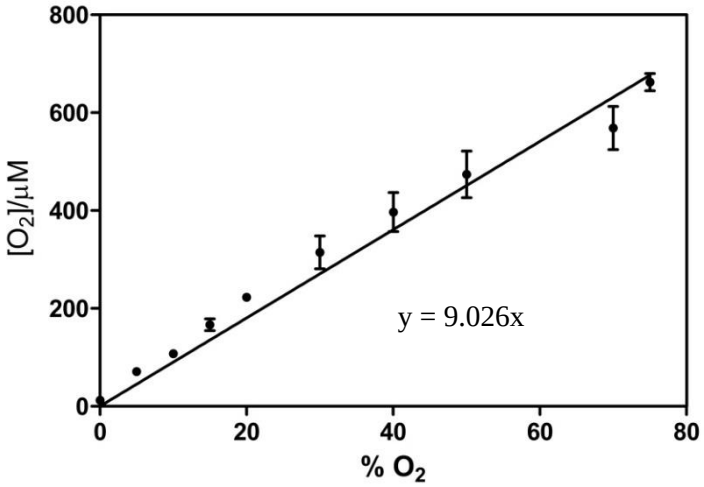

Figure 2.7 Calibration curve used to calculate the concentration of O_2 (µM) in solutions equilibrated at a particular pO_2 using the mass flow controller apparatus. A FOXY electrode was used to measure the absolute oxygen concentration. Error bars denote sd, N = 3 biological repeats, GraphPad Prism v5.04 was used to fit the data to a linear regression model. Adapted with permission from Hancock *et al.*[251], Copyright (2017), American Chemical Society.

This prior work to investigate and optimise the use of the MFC to control oxygen concentrations in the oxygen dependence assays also highlighted some important points for consideration. The availability of only one MFC apparatus meant that only a single vial could be equilibrated at any one time; hence each data point in the oxygen dependence assay was to be collected individually. This necessitated precise and consistent use of the MFC and careful assay design. The introduction of the gas mixture to the vial was a concern, as the fast gas flow was likely to disperse the solution up the sides of the vessel, reducing the bulk volume in which the reaction was to take place and affecting the concentrations therein. Therefore, for each point, the needle from the MFC output was inserted into the vial so that its tip rested approximately 1 cm above the buffer, with the pressure release needle also resting above this point. Further points for consideration are discussed below.

2.4.3. Development of the oxygen dependence assay protocol

The use of sealed vials and prolonged incubation times in the oxygen dependence assay necessitated careful design of the assay protocol, to ensure consistency throughout the experiment. Due to the length of time necessary to equilibrate the reaction to the desired O_2 concentration (10 min), it was decided that only the peptide and buffer should be equilibrated at the desired oxygen concentration using the MFC, before individual and sequential addition of the remaining reaction components. This was to avoid the possibility of unwanted reactions of the co-factors and co-substrates prior to the enzymatic reaction. In particular, previous work within the group (Dr Amjad Khan) had shown that L-ascorbate and 2OG may react over time to form hydrogen peroxide (H_2O_2), which may result in a reduced concentration of 2OG and L-ascorbate being used in the experiment. H_2O_2 is also an inhibitor of KDM4A (Chapter 5), hence could affect the activity of tKDM4A, and impact on the $K_m^{app}(O_2)$ value obtained. Furthermore, prolonged exposure of Fe^{2+} to increased oxygen concentrations may cause its oxidation to Fe^{3+}, again resulting in an altered reaction composition and hindering the reaction.

In order to perturb the oxygen concentration as little as possible, minimal relative volumes (< 10% of the total volume) of the remaining components were added after equilibration of the peptide and buffer, using gas-tight Hamilton syringes to avoid introduction of air bubbles. Specifically, 96 µL of buffer and peptide were equilibrated at the desired pO_2 and 37°C for 10 min, prior to the addition of 1- 2 µL of each of 2OG (10 mM), L-ascorbate (10 mM) and Fe^{2+} (0.5 mM), with final addition of 2 µL tKDM4A (0.05 mM) to initiate the reaction, which was incubated at 37 °C. The reaction was quenched with 100 µL of methanol, and samples taken for MALDI-TOF MS analysis.

The MFC apparatus allowed for only one assay point at a time to be equilibrated, precluding the use of timecourses to establish the linear range of the reaction at different time points, as

had been performed previously (Figure 2.5). Therefore, for the oxygen dependence assay, a single time point of 5 min was chosen, as the KDM4A demethylase reaction had been found to be in the linear range at this time point in the presence of the concentrations of both $H3_{7-14}$K9me3 and $H3_{1-15}$K9me3 peptides (Figure 2.5c, d) and 2OG (Chapter 2.3) to be used in the oxygen dependence assay. Given that the prior experiments were performed at 21% O_2, the reaction could be expected to be in the linear range at oxygen concentrations below this to be surveyed. Moreover, a 5 min reaction time would result in an appreciable amount of demethylation of the H3K9me3 peptide (Figure 2.5a, b) allowing accurate determination of the extent of reaction by MALDI-TOF MS.

Initial experiments used stock concentrations of each component that were kept on ice throughout the experiment. However, the low-throughput nature of the assay meant that these stock solutions were kept on ice for a number of hours and in preliminary experiments, it was noticed that there was precipitation of the tKDM4A solution (data not shown). Therefore, to minimise the possibility of loss of tKDM4A activity during the experiment, in subsequent experiments, 'neat' tKDM4A that had been stored after purification was aliquoted into 2 µL volumes and flash-frozen in liquid nitrogen at the beginning of the experiment, then stored at –80°C throughout the experiment. One aliquot was then thawed and diluted in HEPES buffer to the required stock concentration using a pipette that was set to dispense the required volume and not changed throughout the experiment. Each aliquot of tKDM4A was used for a set of technical triplicates for a specific oxygen concentration, and was therefore kept on ice for a maximum time of 45 minutes to minimise precipitation and loss of activity. This appeared to result in a greater degree of consistent activity of the tKDM4A throughout the experiment, so was incorporated into the final protocol (Figure 2.8, Chapter 7.1.5).

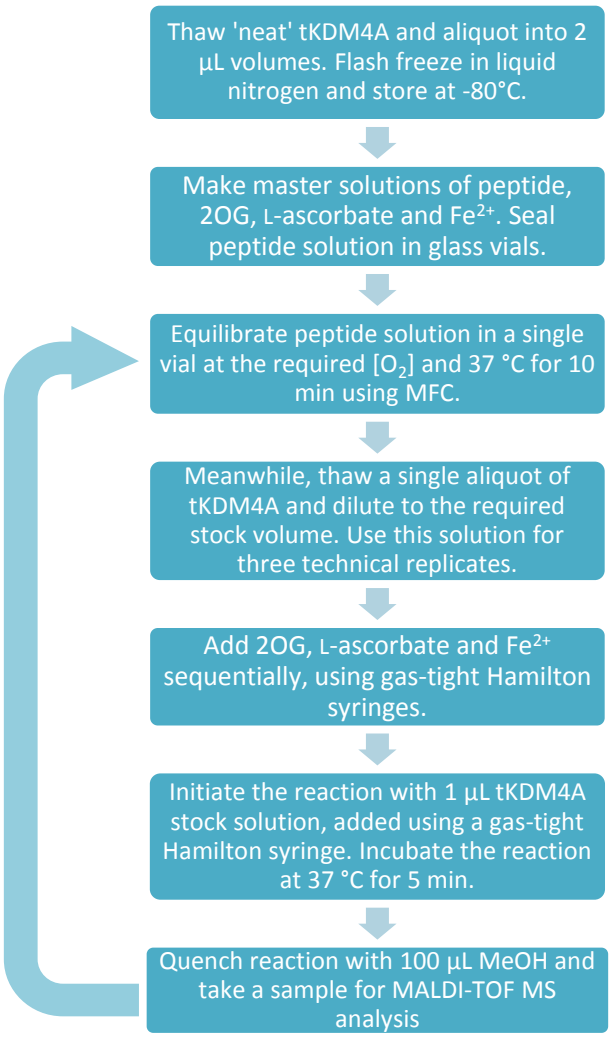

Figure 2.8 Scheme detailing the final procedure used in *in vitro* oxygen dependence assays of tKDM4A.

2.4.4. The oxygen dependence of tKDM4A

Having established the oxygen dependence assay, it was then used to evaluate the $K_m^{app}(O_2)$ for tKDM4A using both of the H3K9me3 peptides synthesised (Chapter 2.2). The initial rate of the enzymatic demethylation reaction was determined at oxygen concentrations between 0 and 80% O_2 (0-722 µM, Chapter 2.4.2), and calculated in the same manner as in the experiments used to evaluate K_m^{app} values of 2OG and the peptide substrates (Chapter 2.3). Only mono-demethylation was taken into account and the extent of demethylation was corrected using a control experiment in which no enzyme was used. The initial rates were plotted against [O_2] and fitted to a Michaelis-Menten model using GraphPad Prism v5.04 (Figure 2.9).

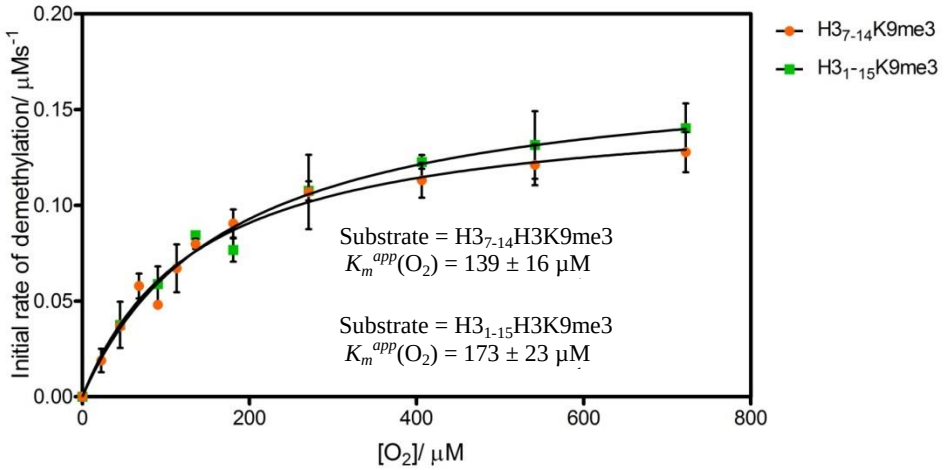

Figure 2.9 Initial rate curves used to evaluate K_m^{app} values for O_2 with $H3_{7\text{-}14}K9me3$ prime substrate (orange circles) and $H3_{1\text{-}15}K9me3$ prime substrate, (green squares). Resultant curves were fitted to a Michaelis-Menten model using GraphPad Prism v5.04. Error bars represent sd, N = 3 biological repeats.

Intriguingly, the experiment using the $H3_{7\text{-}14}K9me3$ peptide resulted in a $K_m^{app}(O_2)$ value of 139 ± 16 µM, while use of the $H3_{1\text{-}15}K9me3$ peptide produced a higher $K_m^{app}(O_2)$ of 173 ± 23 µM (Figure 2.9), a trend also seen in the V_{max} values of 0.154 and 0.174 $\mu M.s^{-1}$, respectively, obtained. These differences may be due to the different lengths of the peptides, which would result in different binding interactions with the protein. The shorter 8mer peptide is likely to have fewer interactions with the tKDM4A, resulting in a more open conformation of the enzyme:substrate complex, while the longer $H3_{1\text{-}15}K9me3$ peptide may produce a less accessible conformation. The consensus mechanism for the 2OG oxygenases proposes that the prime substrate binds to the active site prior to oxygen[82,83,85], hence the binding of the substrate may well affect the ingress of oxygen to the active site. This has been proposed to be the case for PHD2, for which molecular dynamics simulations (Dr C Domene, C Jorgensen, Kings College London, unpublished data) suggested that O_2 enters the PHD2 active site *via* the interface between the HIF substrate and a flexible β2β3 substrate binding loop, before residing in a stable 'E cluster' prior to entering the active site. Further site-directed mutagenesis and steady-state kinetic analysis (L Taylor Kearney, Flashman Group, University of Oxford) indicated that the E cluster is not likely to hinder the

reaction of PHD2 with O_2, thereby suggesting that events during the uptake of O_2 to this site *via* the substrate-enzyme interface are limiting. Inefficient binding of substrate or potential different binding modes of the two peptides investigated may therefore affect oxygen binding, altering the overall rate of reaction. While this phenomenon is yet to be studied in detail for any other 2OG oxygenases, and requires further experimental verification, a similar relationship between the histone substrate and the route of O_2 entry in KDM4A may explain the subtle differences in the $K_m^{app}(O_2)$ values obtained using different substrates. Indeed, a recent computational study on KDM4A has highlighted the importance of both the methylated lysine substrate and the protein environment in providing favourable energetic interactions with oxygen[256]. Kinetic evaluation using longer substrates, and pre-steady-state analyses would help to elucidate this further but were beyond the scope of this thesis.

2.5. Discussion

This chapter describes the successful development and use of a MALDI-TOF MS assay to evaluate the $K_m^{app}(O_2)$ for tKDM4A. The $K_m^{app}(O_2)$ values obtained with both an 8mer peptide and a 15mer peptide were relatively high when compared with those evaluated for other 2OG oxygenases (Table 2.1). Interestingly, the $K_m^{qpp}(O_2)$ value for KDM4A lies between those determined for the cellular oxygen sensing HIF hydroxylases, FIH and PHD2, using the same MALDI-TOF MS assay (Table 2.6). Moreover, the $K_m^{app}(O_2)$ values obtained for additional 2OG oxygenases, including C-P4H and mPAHX, using alternative methods (Table 2.1) are substantially lower than that evaluated for KDM4A (Chapter 2.4.4). Taken together, these comparisons indicate that KDM4A is, indeed, one of the more oxygen-sensitive members of the 2OG oxygenase superfamily.

Table 2.6 $K_m^{app}(O_2)$ values evaluated for KDM4A, PHD2 and FIH using a MALDI-TOF MS assay.

Enzyme	$K_m^{app}(O_2)$/ µM	Substrate
$PHD2_{181-426}$	> 450[171]	HIF-1$\alpha_{556-574}$ CODD
$KDM4A_{1-359}$	139 ± 16	$H3_{7-14}$K9me3
	173 ± 23	$H3_{1-15}$K9me3
FIH	100 ± 10[245]	HIF-2$\alpha_{832-866}$ CAD
$KDM4E_{1-337}$	>93[191]	$H3_{7-14}$K9me3

While the responsiveness of the HIF system to hypoxia is due to a complex relationship between the rapid degradation of HIF and the activity of the HIF hydroxylases[149], the biochemical oxygen sensitivity of these enzymes, particularly PHD2, is thought to be integral to their oxygen-sensing function[85]. Cellular experiments revealed that the biochemical oxygen sensitivities of the HIF hydroxylases were reflective of their relative cellular oxygen dependences, with FIH maintaining activity against endogenous HIF at oxygen concentrations below 1.0%, while the activity of PHD2 was impaired[173]. Therefore, it is likely that the high degree of oxygen sensitivity displayed by isolated KDM4A is indicative of its behaviour in cells and suggests that KDM4A possesses the biochemical potential for an oxygen sensing role in the context of chromatin. Should the catalytic activity of KDM4A be impaired under conditions of low oxygen in cells, this may ultimately result in altered epigenetic regulation and aberrant histone lysine methylation. These mechanisms may underlie changes to the expression of disease-related genes in hypoxic disease states, such as cancer and cardiovascular disease. Therefore, the results from the experiments described in this chapter prompted further study of the oxygen sensitivity of KDM4A in a cellular context (Chapter 3, Chapter 4), to ascertain whether the *in vitro* oxygen sensitivity described here is also apparent in a biological setting.

Chapter 3: The cellular oxygen dependence of KDM4A

3.1. Introduction

The *in vitro* investigation of the oxygen dependence of KDM4A detailed in Chapter 2 revealed that the activity of isolated tKDM4A was highly sensitive to oxygen availability in comparison to many of the 2OG oxygenases. This suggests that KDM4A may be capable of a biological oxygen sensing function similar to the related HIF hydroxylases, prompting investigation into the oxygen dependence of the enzyme in a cellular context.

A number of studies have assessed the cellular oxygen sensitivity of several 2OG oxygenases, including the HIF hydroxylases, PHD2 and FIH, several of the JmjC-KDMs, and the TET enzymes. Experiments in pVHL-deficient RCC4 cells, in which HIF is not degraded[157], enabled analysis of the hydroxylation levels of endogenous HIF-1α by the HIF hydroxylases under different oxygen concentrations. Hydroxylation of Asn803 by FIH was maintained under oxygen concentrations as low as 0.25%, whilst hydroxylation of Pro402 and Pro564 by PHD2 was significantly reduced at oxygen levels below 1.0%[173]. This differential oxygen sensitivity of the catalytic activities of the HIF hydroxylases in cells is reflective of the trends observed in *in vitro* experiments. MALDI-TOF MS assays using the recombinant enzymes evaluated $K_m^{app}(O_2)$ values of 110 ± 30 μM for FIH[245] and >450 μM for PHD2[171], indicating much higher oxygen sensitivity for PHD2.

A recent investigation attributed loss of 5hmC in cancer cell lines incubated in hypoxia and hypermethylation of CpG-rich regions in hypoxic tumours to loss of TET activity under hypoxia[257]. The same study assessed the $K_m^{app}(O_2)$ for recombinant TET1 and TET2, which

were found to be 0.31% and 0.53% O_2, respectively[257]. According to the oxygen calibration experiments performed within the group (Ben Greenfield, Chapter 2.4.2), these measurements correspond to approximately 3-5 μM O_2, depending on the reaction conditions used. While these values are significantly lower than those evaluated for PHD2, FIH, KDM4E and KDM4A (>450 μM[171], 100 μM[245], >93 μM[191] and 173 μM, Chapter 2.4.4) in the Schofield/Kawamura/Flashman Laboratories, the *in vitro* analyses of the TET enzymes revealed that they displayed a graded response to oxygen concentration, similar to the other 2OG oxygenases surveyed. Further analysis demonstrated that potential limiting factors in hypoxia, including the production of reactive oxygen species (Chapter 5) and a reduction in 2OG levels (Chapter 4), were not likely to contribute to the hypoxic loss of 5hmC in cancer cell lines[257], indicating that lack of oxygen availability is likely the factor limiting TET activity in hypoxia.

Similar studies of the oxygen dependence of some of the HIF-upregulated KDMs have been conducted in cells. Beyer *et al.* compared the cellular activity of ectopically expressed KDM3A with that of KDM4B under hypoxia (0.2% or 1.0% O_2), and found that, although the activity of both enzymes was maintained at 1.0% O_2, KDM4B activity was greatly reduced at 0.2% O_2, while KDM3A-mediated demethylation of H3K9me2 remained unhindered[206]. In concordance with this, the activity of KDM4C and KDM5B was inhibited below 0.5% O_2 in LNCaP cells, while KDM3A maintained demethylation of H3K9me2 even in severe hypoxia, specifically at the enhancer region of the prostate specific antigen (*PSA*), increasing its expression in cooperation with HIF-1α and androgen receptor (AR)[214]. The varying impact of reduced oxygen availability on the catalytic activity of these KDMs implies that their HIF-induced upregulation may not be purely a compensatory mechanism for loss of activity in hypoxia, but is likely more complex and dependent on their individual involvement in specific transcriptional programmes.

A recent study demonstrated that KDM4A-mediated demethylation of H3K9me3 and H3K36me3 promoted transient site-specific copy gain, a phenomenon characteristic of certain cancers[258]. Subsequent investigation demonstrated that KDM4A retained sufficient activity in cells exposed to 1.0% O_2 to promote copy gain, although the extent of demethylation in these cells was reduced compared to normoxia[259]. Interestingly, in concordance with previous reports, KDM4A levels were found not to increase at the transcript level in hypoxia[196,206,208,259], although stabilisation of the protein was observed, and attributed to a reduced interaction with the SCF-ubiquitin ligase complex responsible for its degradation[259,260].

3.1.1. Chapter aims

The aim of the experiments described in this chapter was to thoroughly evaluate the impact of cellular hypoxia on the catalytic activity of KDM4A against its native substrates, in order to determine whether the cellular oxygen sensitivity correlates with the *in vitro* results obtained (Chapter 2) and to help elucidate the complex relationship between JmjC-KDM levels and activity in hypoxia highlighted by the studies described above.

pcDNA3 constructs encoding full length N-terminally FLAG-tagged KDM4A WT and KDM4A MUT were originally donated by Professor Rob Klose (Department of Biochemistry, University of Oxford) and supplied for use by Dr Louise Walport (Schofield Laboratory, University of Oxford) . U2OS cells stably overexpressing doxycycline-inducible, full-length FLAG-KDM4A WT (F-KDM4A U2OS cells) used in immunofluorescence and western blot experiments described in Chapter 3.3 were kindly donated by Dr Norma Masson (Ratcliffe Laboratory, NDM, University of Oxford). The qPCR primers used to evaluate levels of β-actin in analyses detailed in Chapter 3.4.1) were provided by Dr Andrew Mun Chiang Chan (Ratcliffe Laboratory, NDM, University of Oxford). Immunofluorescence

experiments to assess the cellular oxygen dependence of TET1 (Chapter 3.5) were performed with Dr Akane Kawamura (Department of Chemistry, University of Oxford).

Aspects of the work described in this chapter have been published. Figures from this publication are reprinted or adapted with permission from Hancock et al.[251]*, Copyright (2017), American Chemical Society, and acknowledged in the appropriate figure legend.*

3.2. Optimisation of an O_2-dependence assay in HeLa cells

3.2.1. Development of the experimental protocol

In order to probe the oxygen dependence of cellular KDM4A activity, an immunofluorescence assay in HeLa cells, as described previously[261] (Chapter 7.2), was adapted. HeLa cells were transfected using FuGENE® HD (Promega) with a pcDNA3 vector encoding full-length, wild type *N*-terminally FLAG-tagged KDM4A (KDM4A WT)[110]. An inactive variant, in which the Fe^{2+}-binding His188 residue is mutated to an alanine (KDM4A MUT)[110], was used as a control. After 4 h, the media was replaced on the cells, which were then incubated under normoxia or hypoxia in a hypoxic workstation (Invivo$_2$ 400, Baker Ruskinn) for 24 h before being fixed with 4% paraformaldehyde and stained using antibodies against FLAG and H3K9me3 (Chapter 7.2.5). 4,6-Diamidino-2-phenylindole dihydrochloride (DAPI) was used to verify the nuclear location of ectopically expressed KDM4A. Cells were imaged using an Operetta high-content imaging system (PerkinElmer) and analysed using Harmony® software.

On preliminary analysis of the images procured in this experiment, it was apparent that the transient transfection protocol used resulted in heterogeneous overexpression of KDM4A in the HeLa cells (Figure 3.1a-e). Comparison of the number of cells imaged, as identified using DAPI staining (blue, Figure 3.1a-d) with the number demonstrating FLAG staining (orange, Figure 3.1a-d) revealed that not all cells treated with the FuGENE®:DNA mix

overexpressed KDM4A. High levels of overexpression of KDM4A were necessary to be able to observe global changes to H3K9me3 levels. Therefore, the intensity of the FLAG fluorescence signal was used to identify a smaller and more homogeneous population of cells overexpressing high levels of KDM4A (Figure 3.1). In each experiment, cells that had not been treated with the FuGENE® HD-DNA mix (non-transfected control, NTC) were used as a control. The maximum FLAG fluorescence in these cells was used as a baseline (Figure 3.1e, lower dashed line) and only cells in transfected wells with a FLAG fluorescence intensity of greater than 2.5 x this baseline level were included for analysis (Figure 3.1e, green squares). Normalisation of the average FLAG fluorescence intensity in the selected cells overexpressing KDM4A WT against that of KDM4A MUT-overexpressing cells incubated at the same oxygen concentration revealed that the level of KDM4A WT overexpression in cells selected for analysis was equivalent in normoxia and hypoxia, within experimental error (Figure 3.1c).

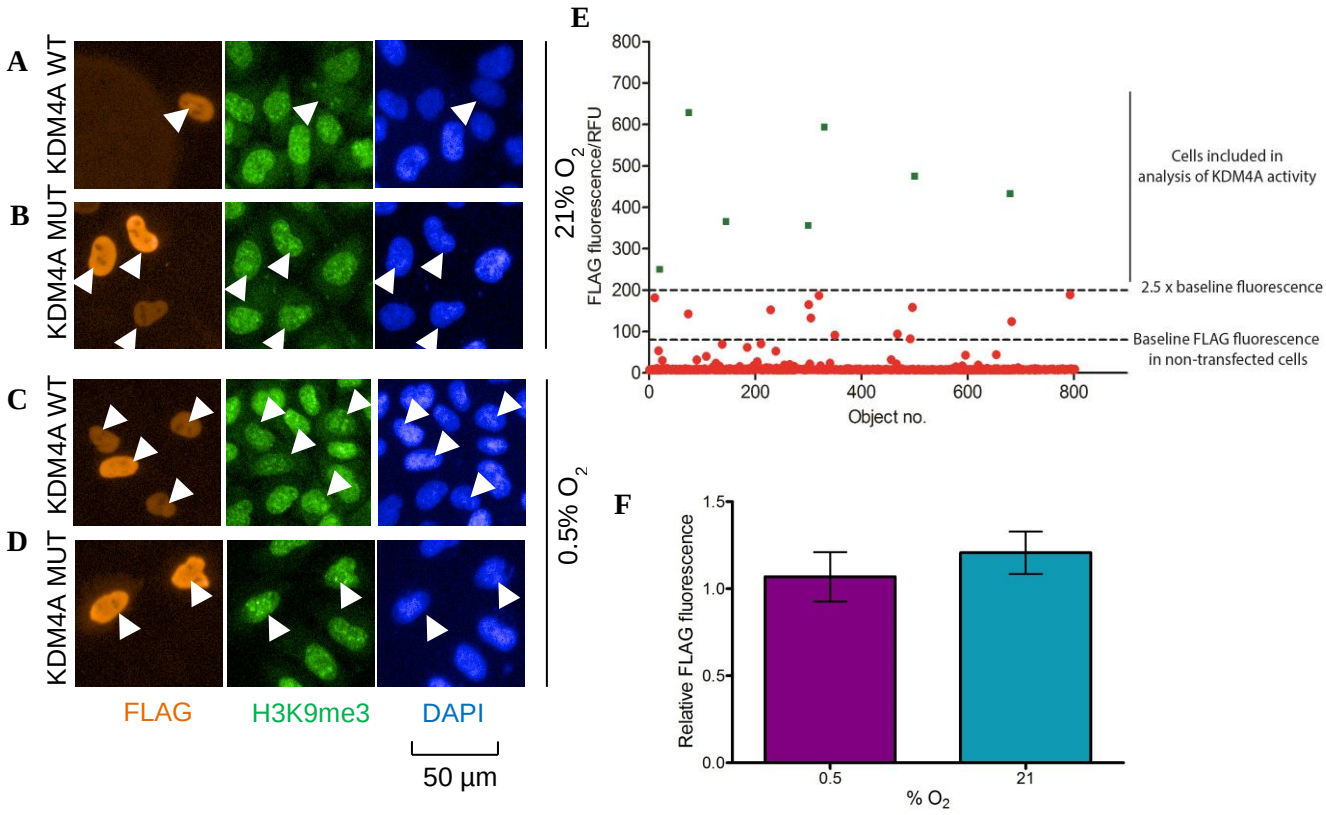

Figure 3.1.A-F). Selected images from immunofluorescence analysis of the effect of hypoxia on the cellular activity of KDM4A. HeLa cells were transiently transfected with FLAG-KDM4A WT **(A, C)** or catalytically inactive KDM4A MUT **(B, D)**, then incubated for 24h at 21% **(A, B)** or 0.5% O_2 **(C, D).** Images were processed and analysed at the same time, using the same fluorescence intensity signal window. Selection of KDM4A-overexpressing cells from immunofluorescence experiments in transiently transfected HeLa cells (depicted using white arrows) was achieved using analysis of FLAG fluorescence**. E)** Example graph depicting FLAG levels (relative fluorescence units, RFU) in cells treated with FuGENE® HD transfection reagent and pcDNA3 encoding FLAG-KDM4A WT. Maximum FLAG fluorescence in non-transfected cells (not depicted) was ascribed as baseline fluorescence, and cells with FLAG levels > 2.5 x the baseline fluorescence (green squares) were chosen for use in analysis of cellular KDM4A activity. **F)** FLAG fluorescence in the selected population of FLAG-KDM4A WT transfected cells was normalised against that in FLAG-KDM4A MUT cells incubated at the same O_2 concentration. Error bars denote sd, n > 20 cells per treatment.

Having identified a population of transfected cells, analysis of global H3K9me3 fluorescence (relative fluorescence units, RFU) in both KDM4A WT- and KDM4A MUT-overexpressing cells (Figure 3.1 a-d) then enabled calculation of KDM4A demethylase activity (Figure 3.2). As expected, KDM4A WT overexpressing cells possessed apparently reduced levels of H3K9me3, while KDM4A MUT-transfected cells showed no difference in H3K9me3 fluorescence (Figure 3.1b, d). This indicates that loss of H3K9me3 in KDM4A WT-transfected cells (Figure 3.1a, c) was due to KDM4A WT catalytic demethylase activity, rather than overexpression of the protein alone. Therefore, H3K9me3 fluorescence in

KDM4A WT-overexpressing cells was normalised against that in KDM4A MUT-overexpressing cells incubated in the same O_2 concentration (Equation 3.1). The ectopically expressed KDM4A WT was ascribed as having 100% activity in normoxia, resulting in maximum loss of H3K9me3, hence relative KDM4A activity in hypoxia could be calculated using equation 3.2.

$$\%\ \text{demethylation H3K9me3} = 100\left(1-\left(\frac{\text{H3K9me3 fluorescence}_{WT}}{\text{H3K9me3 fluorescence}_{MUT}}\right)\right) \qquad \textbf{3.1}$$

$$\text{Relative KDM4A activity} = \left(\frac{\%\ \text{demethylation H3K9me3}_{0.5\%\ O_2}}{\%\ \text{demethylation H3K9me3}_{21\%\ O_2}}\right) \qquad \textbf{3.2}$$

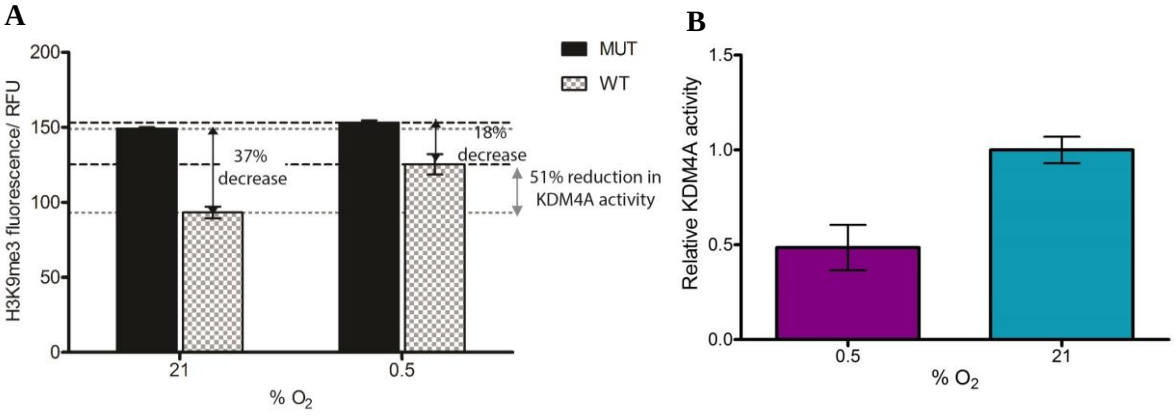

Figure 3.2.A) Scheme depicting calculation of percentage demethylation and relative loss of KDM4A activity in transiently transfected HeLa cells. Raw mean fluorescence intensity (RFU) of H3K9me3 in KDM4A WT transfected cells was normalised against that in KDM4A MUT-transfected cells incubated at the same O_2 concentration. Loss of H3K9me3 in 21% O_2 was ascribed as maximum KDM4A activity, and used to calculate relative KDM4A activity in hypoxia. **B)** Relative KDM4A activity in hypoxia (0.5% O_2) and normoxia, as calculated from the immunofluorescence experiment in transiently transfected HeLa. Data was plotted and analysed using GraphPad Prism v5.04, error bars denote sd, n >20 cells.

Demethylase activity of the WT enzyme in 21% O_2 led to reduction of H3K9me3 levels of 37 ± 2.6% compared to those in the KDM4A MUT-overexpressing cells (Figure 3.2a). In hypoxia, an 18 ± 4.5% reduction in H3K9me3 fluorescence was observed, which corresponded to an approximately 51% loss in KDM4A activity (Figure3.2b).

3.2.2. Optimisation of the transfection protocol

Although this assay enabled evaluation of the cellular activity of KDM4A WT in normoxia and hypoxia, very few KDM4A WT-transfected cells were available for analysis under the selection criteria described: 49 KDM4A WT-transfected cells were selected in normoxia, and 24 in hypoxia. Therefore, experiments to optimise transfection efficiency were explored. Initial investigations were mounted to explore the impact of transfection time on the transfection efficiency. Cells were treated with the FuGENE® HD transfection reagent and FLAG-KDM4A WT or FLAG-KDM4A MUT DNA, and then incubated for 4 or 24 h. The media was then changed to remove the transfection reagent, and the cells incubated for a further 24 h prior to fixing, staining and imaging as described above. FLAG fluorescence signal was used to identify highly transfected cells and calculate percentage transfection efficiency in the entire population of imaged cells.

Table 3.1 Transfection efficiency of FLAG-KDM4A WT using FuGENE ® HD incubation times of 4 and 24 h. 9 fields were imaged per well of a 96-well plate at 20 x magnification.

Transfection time	DNA	Total number of cells	Number of transfected cells	Transfection efficiency
4h	KDM4A WT	16490	92	0.6
	KDM4A MUT	15490	2081	13.4
24 h	KDM4A WT	12272	307	2.5
	KDM4A MUT	8076	2247	27.8

These results revealed increased transfection efficiency in cells transfected for 24 h (Table 3.1), hence the assay protocol was adapted to include a 24 h transfection period. However, these efficiencies were still very low, particularly in relation to the KDM4A WT DNA, prompting further optimisation. The experiments described above had used a FuGENE HD:DNA ratio of 3:1, according to the manufacturer's protocol (Chapter 7.2.2). Different

ratios of FuGENE:DNA (2.5:1, 3:1 and 4:1) were investigated, in an effort to improve the low transfection efficiency. After 24 h transfection, the media was replaced on the cells, which were incubated for a further 24 h at 21% O_2. Cells were stained, imaged and analysed as described above.

Table 3.2 Transfection efficiency of FLAG-KDM4A WT using different ratios of FuGENE ® HD:DNA. Each condition was tested in 3 wells of a 96-well plate. 9 fields of cells were imaged per well at 20 x magnification.

Protocol	Total number of cells	Number of transfected cells	Transfection efficiency
FuGENE® HD:DNA 2.5:1	14501	659	4.5
FuGENE® HD:DNA 3:1	13481	1836	13.6
FuGENE® HD:DNA 4:1	14483	38	0.3

The results from this experiment (Table 3.1) revealed that a FuGENE:DNA ratio of 3:1 resulted in a transfection efficiency of 13.6% (1836 KDM4A WT-overexpressing cells), compared to 4.5% for a 2.5:1 ratio and 0.3% for a 4:1 ratio. This demonstrated some variability in the transfection protocol using a 3:1 ratio of FuGENE HD:DNA, and that altering this ratio would not be beneficial in improving the transfection efficiency. Therefore, subsequent experiments used a 24 h transfection time, with a FuGENE HD:DNA ratio of 3:1.

3.2.3. The oxygen dependence of KDM4A in HeLa cells

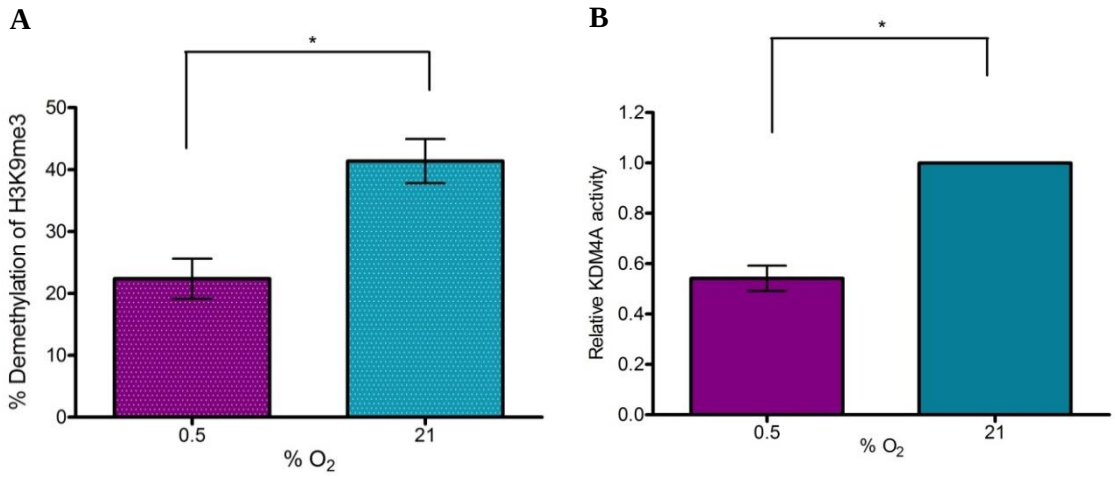

Figure 3.3 A) Loss of H3K9me3 and **B)** relative KDM4A activity in HeLa cells transiently transfected with FLAG-KDM4A WT and incubated in 0.5 (purple) or 21% (teal) O_2 for 24 h, as calculated using equations 3.1 and 3.2. Data was plotted and Student's t test was performed in GraphPad Prism v5.04, N = 3 biological repeats, error bars represent sd. $P < 0.05$.

Using the optimised protocol, three biological repeats (i.e. three identical experiments performed on different days) of the immunofluorescence experiment to analyse the effect of hypoxia on KDM4A activity against H3K9me3 were performed. Overexpression of FLAG-KDM4A WT in HeLa cells was found to result in 41 ± 3.6% loss of global H3K9me3 in normoxia, while in hypoxia, only a 22 ± 3.2% reduction in H3K9me3 levels was observed (Figure 3.3a). This corresponded to a 46 ± 8% ($P < 0.05$) relative loss of KDM4A activity in cells exposed to 0.5% O_2 compared to that in normoxia (Figure 3.3b). Given that the expression levels of FLAG-KDM4A WT were similar in both hypoxia and normoxia (Figure 3.1), these results indicate that hypoxia had an impact on loss of H3K9me3 levels due to an effect on the activity, rather than expression levels of KDM4A.

The same immunofluorescence protocol as described above was adapted in order to assess the effect of 0.5% O_2 on demethylation of endogenous H3K36me3 by overexpressed KDM4A. An antibody against H3K36me3 (rabbit α-H3K36me3, Abcam ab9050) was used instead of the α-H3K9me3 antibody, which necessitated fixing of the cells with ice-cold

MeOH, rather than 4% paraformaldehyde (Chapter 7.2.6). Cells were imaged and analysed in the manner described above.

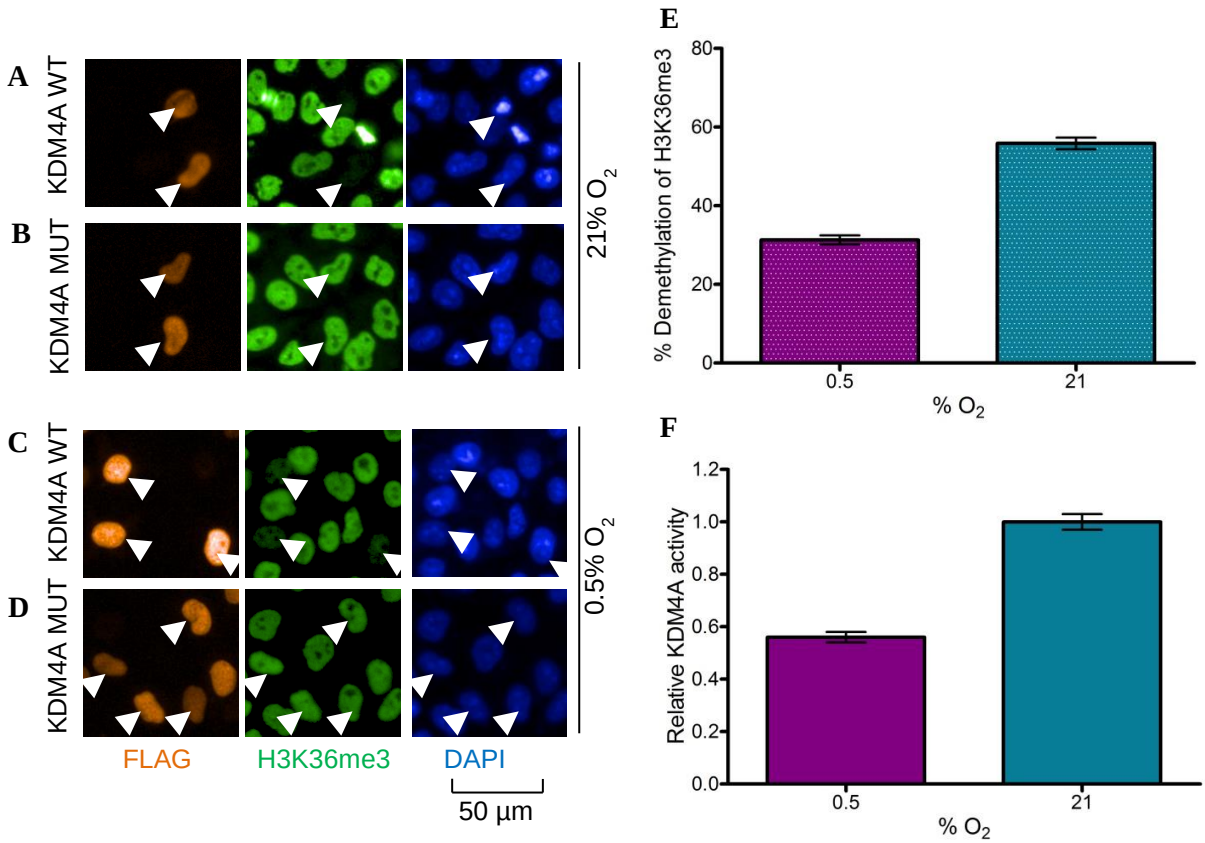

Figure 3.4.A-D). Selected images from immunofluorescence analysis of the effect of hypoxia on the cellular activity of KDM4A against H3K36me3. H3K36me3 levels (green) were quantified in HeLa cells transiently transfected with FLAG-KDM4A WT (orange, **A, C**) or catalytically inactive KDM4A MUT (orange, **B, D**), then incubated for 24h at 21% (**A, B**) or 0.5% O_2 (**C, D**). Images were processed and analysed at the same time, using the same fluorescence intensity signal window. **E)** Demethylation of H3K36me3 and **F)** relative KDM4A activity against H3K36me3 in HeLa cells transiently transfected with FLAG-KDM4A WT and incubated in 0.5 (purple) or 21% (teal) O_2 for 24 h, as calculated using equations 3.1 and 3.2. Data was plotted and analysed in GraphPad Prism v5.04, n >20 cells, error bars represent standard error of the mean (sem).

This experiment demonstrated loss of H3K36me3 in cells overexpressing FLAG-KDM4A WT (Figure 3.4a, c,e) when normalised against cells expressing FLAG-KDM4A MUT (Figure 3.4b, d,e) and revealed a 44 ± 2.0 % loss in KDM4A activity against this mark in hypoxia (Figure 3.4f), indicating that hypoxia affects the catalytic activity of KDM4A against both H3K9me3 and H3K36me3 to a similar degree. Only a single biological repeat of this experiment was performed, precluding statistical analysis.

The *in vitro* experiments in Chapter 2 demonstrated that the activity of KDM4A possessed a graded response to hypoxia, hence the biochemical potential for oxygen sensing. To understand whether the *in vitro* trend observed is reflective of the cellular situation, the immunofluorescence assay was used to assess KDM4A activity in HeLa at 3.0% and 5.0% O_2, thereby evaluating the response of cellular KDM4A activity to varying degrees of hypoxia. The protocol and analyses described above were used, and KDM4A activity relative to a normoxic control (activity = 1) was calculated (Figure 3.5), then averages across experiments on different days evaluated.

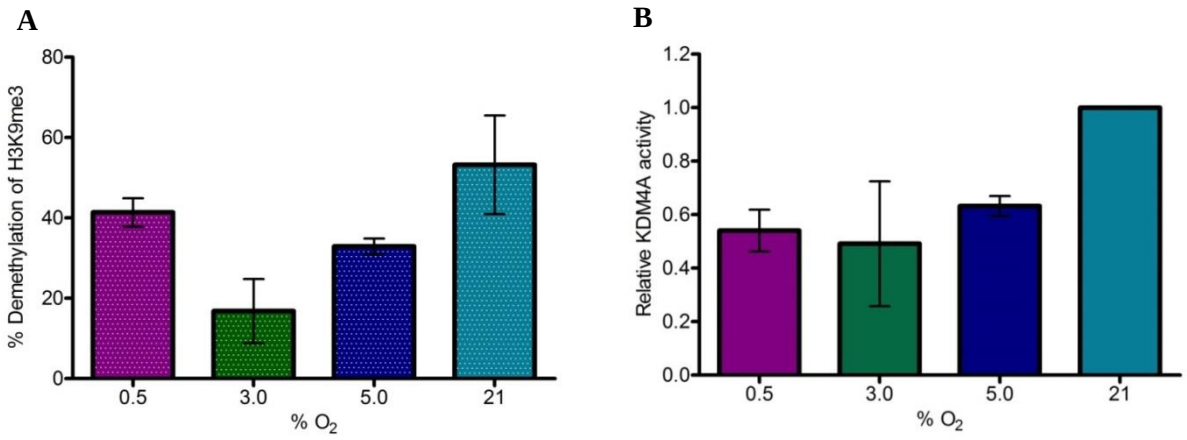

Figure 3.5 A) Average percentage demethylation of H3K9me3 and **B)** average relative activity of ectopically expressed KDM4A in HeLa cells exposed to different oxygen concentration, control = 21% O_2. Experiments in different oxygen concentrations were performed on different days. Loss of H3K9me3 levels in HeLa cells incubated in hypoxia (0.5-5.0% O_2), relative to those in KDM4A MUT-transfected cells, was compared to that in cells incubated in normoxia, and used to calculate relative activity of KDM4A. Graph was plotted using GraphPad Prism v5.04, error bars represent sd, N = 3 biological repeats for 0.5% O_2, N = 2 biological repeats for 3.0 and 5.0% O_2.

The results from these experiments in different O_2 concentrations proved inconclusive. Although a loss of KDM4A activity relative to normoxia was observed in each hypoxic condition (Figure 3.5a), no clear difference in the degree of activity loss was observed between 0.5 and 5.0% O_2. At 5.0% O_2, the average KDM4A activity was 63 ± 3.7% of the maximum activity, higher than that of 54 ± 7.8% at 0.5% O_2 (Figure 3.5a) However, at 3% O_2, the activity of the enzyme appeared to be at a minimum of 49 ± 23% compared to normoxia (Figure 3.5a). This lack of trend may indicate that cellular KDM4A activity does

not display a graded response to hypoxia within the range of O_2 concentrations tested. However, high experimental error may also be obscuring a trend, which is likely due to the experimental design. The availability of only one hypoxic workstation meant that these experiments could not be performed concurrently; hence these were independent, single point experiments, and data from different days and different O_2 concentrations could not be reliably compared, or subjected to statistical analysis.

3.2.4. Points for improvement

Further analysis highlighted a lack of reproducibility of these experiments. Plotting the raw data, as percentage demethylation of H3K9me3 in KDM4A WT-overexpressing cells compared to KDM4A-MUT transfected cells in each oxygen condition rather than relative activity compared to normoxia, shows a high degree of variability across different experiments. In particular, the degree of demethylation of H3K9me3 by KDM4A WT in normoxia across all of the individual experiments was found to vary between 34.2 and 68.2% (Figure 3.5b). Although calculation of relative KDM4A activity to an internal control in each condition may compensate for this somewhat, these inherent problems prompted efforts to understand and improve the experimental approach used. Several areas for improvement were identified in order to accurately and quantitatively assess the impact of varying oxygen concentration on cellular KDM4A activity.

The transient transfection protocol used resulted in a variable number of highly KDM4A-overexpressing cells in each experiment. Plotting the number of KDM4A-WT transfected cells used for analysis of normoxic and hypoxic KDM4A activity across the single point experiments described herein (normoxia: 21% O_2 N (biological repeats) = 7, hypoxia: 0.5% O_2 N = 3, 3.0% O_2 N = 2, 5.0% O_2 N = 2) revealed a large spread about the mean number of transfected cells, with a minimum of 24 and a maximum of 981 cells used in analysis (Figure 3.6).

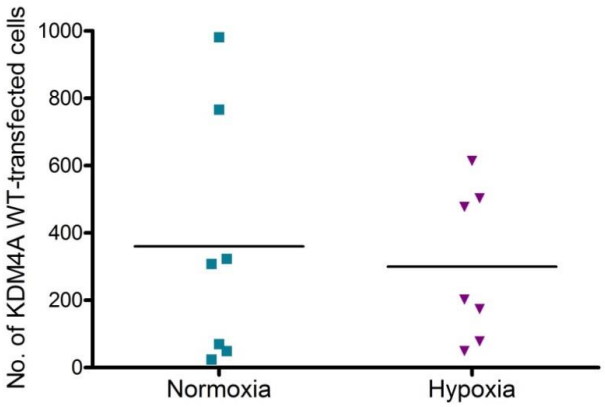

Figure 3.6. Numbers of transiently transfected HeLa cells included in the highly FLAG-KDM4A WT overexpressing population used for immunofluorescent analysis of H3K9me3 levels and KDM4A activity. Data is aggregated from N = 7 individual biological repeats, in which cells were incubated in normoxia (teal squares) = 21% O_2, and varying degrees of hypoxia (purple triangles) = 0.5% O_2 (N = 3 biological repeats), 3.0% O_2 (N = 2 biological repeats) and 5.0% O_2 (N = 2 biological repeats). Data was plotted using GraphPad Prism, black line represents the mean number of transfected cells in each case.

A further difficulty with these single-point O_2 dependence experiments may have been the transfection time used. The HeLa cells were incubated in normoxia with the transfection reagent and DNA for 24 h prior to exposure to hypoxia. During this transfection period, any ectopically expressed KDM4A WT was likely able to demethylate native H3K9me3 prior to the start of the experiment. This may have reduced the signal window in which hypoxic inhibition of KDM4A activity could be measured, thereby minimising any observable differences in KDM4A activity under the different oxygen conditions, although further experiments are required to evaluate the magnitude of this effect.

3.3. Oxygen-dependence assays in U2OS F-KDM4A cells

The challenges encountered in performing immunofluorescence experiments in transiently transfected HeLa prompted the design of an alternative cellular system for the assessment of the effect of hypoxia on the activity of KDM4A. Several areas for improvement were highlighted. Both increased numbers of overexpressing cells and consistent activity of the overexpressed enzyme in biological repeats were required to enable statistical analysis and direct comparisons to be drawn across multiple oxygen concentrations. These experimental requirements were likely to be met using a stably-overexpressing system. Moreover, a system in which cells could be incubated in the desired oxygen concentration immediately upon overexpression of KDM4A would ensure that all ectopically expressed KDM4A was exposed to hypoxia and the H3K9me3 signal window was not affected by demethylase activity during a normoxic incubation period. Moreover, analysis of multiple oxygen concentrations should be carried out on the same day, so that direct comparisons between hypoxic conditions could be made easily, using the same normoxic control experiment. To this end, multiple hypoxic workstations were also made available, thanks to the Ratcliffe Laboratory, NDM, Oxford.

3.3.1. Characterisation of the F-KDM4A U2OS cell line

A U2OS cell line that stably overexpressed doxycycline (dox)-inducible FLAG-KDM4A WT (F-KDM4A U2OS cells) had previously been designed and produced by Dr Norma Masson, (Ratcliffe Laboratory, NDM, University of Oxford) and was kindly donated for the purpose of subsequent oxygen-dependence experiments.

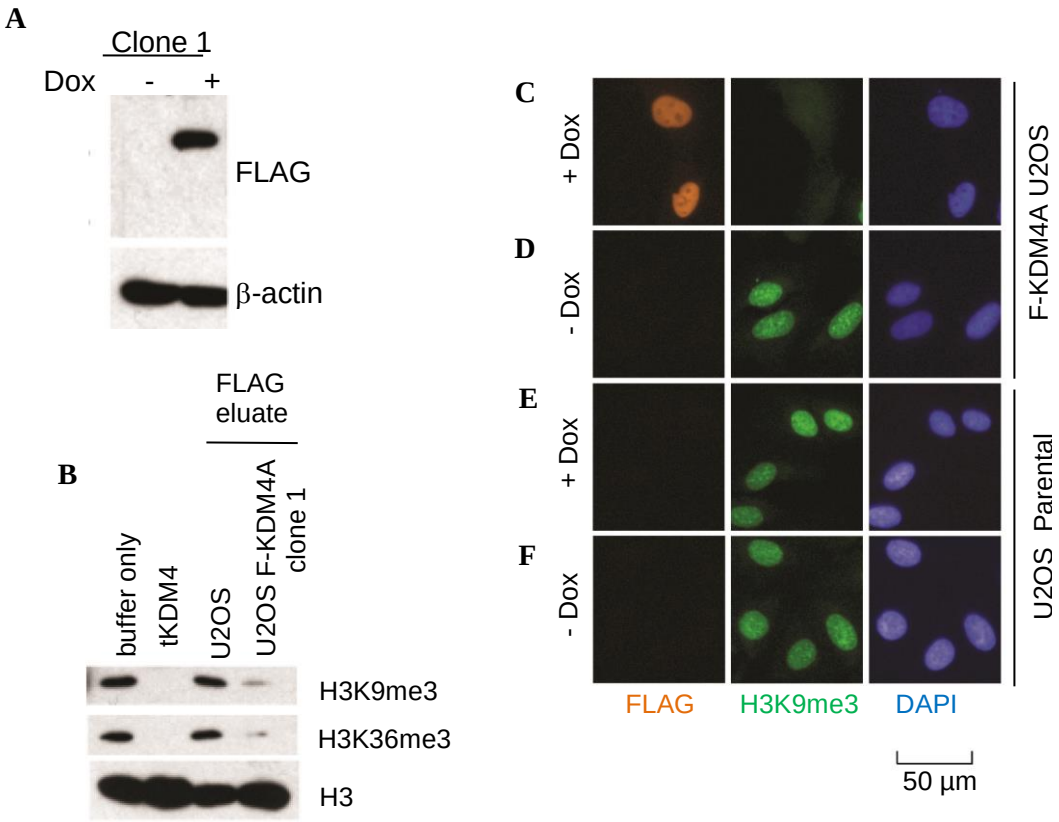

Figure 3.7 A) Western blot analysis of FLAG in cells treated ± dox (24 h) confirms that FLAG-KDM4A WT expression is dox-inducible. **B)** FLAG-KDM4A WT purified from F-KDM4A U2OS cells displays demethylase activity against H3K9me3 and H3K36me3. Parental U2OS cells (as control) or U2OS F-KDM4A cells were treated with dox for 24 h and F-KDM4A was then purified from extracts using anti-FLAG M2-Agarose beads (Sigma), followed by FLAG peptide. FLAG eluate was then incubated with purified histones (25 μg), 2OG (1 mM), L-ascorbate (2 mM) and $FeSO_4$ (50 μM). tKDM4A (10 μg) was used as a positive control. Reactions were incubated at 37 °C (16 h), then analysed *via* western blot. All data was provided by Dr Norma Masson, Ratcliffe Lab, NDM Oxford. **C-F)** Selected images from immunofluorescence analysis of **C, D)** U2OS F-KDM4A and **E, F)** U2OS Flp-in-Trex (parental) cells treated +/- dox for 24 h. Cells were fixed and stained for FLAG (orange) and H3K9me3 (green). Cells were fixed, stained and imaged simultaneously and images were processed using the same fluorescence parameters. Figures adapted with permission from Hancock *et al.*[251], Copyright (2017), American Chemical Society.

Characterisation of this cell line by Dr Masson (Figure 3.7a, b) confirmed that the F-KDM4A U2OS cells overexpressed active, FLAG-tagged KDM4A in a dox-inducible manner. Further analysis *via* immunofluorescence confirmed dox-inducible expression of FLAG-KDM4A WT in the F-KDM4A U2OS cells with concomitant loss of H3K9me3 (Figure 3.7C, D). Furthermore parental U2OS Flp-in-Trex cells (i.e. U2OS cells containing the Flp-In™ expression vector to enable generation of stably overexpressing clones, but not containing the F-KDM4A gene) demonstrated no FLAG fluorescence or subsequent changes

to H3K9me3 levels when dosed with dox for 24 h (5.0 % CO_2, 37 °C), indicating that dox does not affect endogenous H3K9me3 levels, or result in FLAG overexpression in the absence of the vector encoding FLAG-KDM4A WT.

To characterise these cells further, an immunofluorescence experiment was performed to assess the effect of the length of exposure to dox on induction of FLAG-KDM4A WT within the cells. Cells were dosed with dox at 1 $\mu g.mL^{-1}$ for 0.5, 1, 2, 4, 6 and 24 h, prior to being fixed, stained and imaged (Figure 3.8a-g) as described previously (Chapter 3.2, Chapter 7.2.6). As no U2OS cell line that stably overexpressed dox-inducible FLAG-KDM4A MUT was available, F-KDM4A U2OS cells that had not been treated with dox (uninduced cells) were used as a control. FLAG fluorescence levels in these uninduced cells was set as a baseline value and used to identify a highly FLAG-KDM4A expressing population of dox-treated (induced) cells at each dox dosing time. Only cells with FLAG fluorescence of >5-fold greater than the baseline value were included in the induced population (Figure 3.8h). The number of induced cells was then calculated for each dox dosing time tested (Figure 3.8bi).

The average H3K9me3 fluorescence in these induced cells was calculated and normalised against the average H3K9me3 fluorescence in uninduced cells, in order to calculate the percentage demethylation of H3K9me3 by overexpressed KDM4A WT (Figure 3.8j, k, Equation 3.3).

$$\%\ \text{demethylation}_{\text{H3K9me3}} = 100 \times \left(1 - \left(\frac{\text{H3K9me3 fluorescence}_{+\text{Dox}}}{\text{H3K9me3 fluorescence}_{-\text{Dox}}}\right)\right) \qquad \textbf{3.3}$$

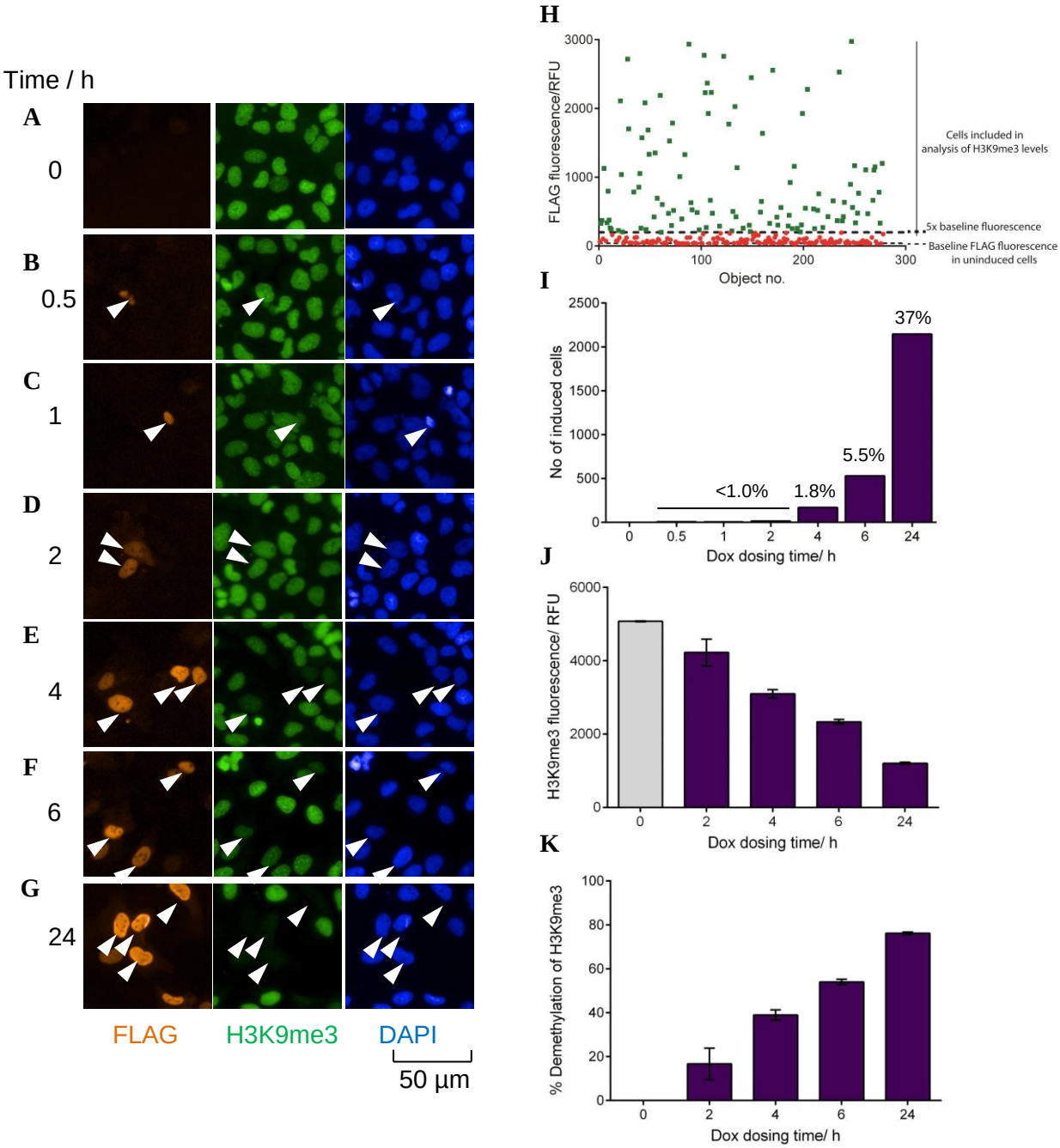

Figure 3.8.A-G). Selected images from immunofluorescence analysis of the effect of exposure time to dox on overexpression of FLAG-KDM4A WT (orange) and loss of H3K9me3 (green) in F-KDM4A U2OS cells dosed with 1 µg.mL^{-1} dox for 0-24 h. Cells were processed, imaged and analysed at the same time, using the same fluorescence intensity signal window. **H)** Scheme detailing selection of FLAG-KDM4A WT-overexpressing (induced) cells using FLAG fluorescence intensity. **I)** Number of induced cells under different dox treatment times. Numbers denote percentage induced cells in the total cell population. **J)** H3K9me3 fluorescence intensities in induced cells under the different dox dosing times. Purple bars indicate data from induced cells, grey from the entire cell population. **K)** Percentage demethylation of H3K9me3 in induced cells under the dox dosing conditions relative to those in uninduced cells. Data was plotted and analysed in GraphPad Prism v5.04, error bars represent sem.

This experiment confirmed that overexpression of KDM4A WT in the F-KDM4A U2OS cells is induced by dox in a time-dependent manner (Figure 3.8a-i). Although the overexpression of KDM4A WT within the F-KDM4A U2OS cells was heterogeneous, analysis of FLAG fluorescence revealed increased numbers of KDM4A overexpressing cells compared to those achieved in experiments using transiently transfected HeLa (Figure 3.1e, Chapter 3.2). Exposure of cells to dox for less than 2 h was insufficient time to induce enough cells for analysis, while dox dosing for 6 h or 24 h produced much greater numbers of cells overexpressing FLAG-KDM4A WT (> 500 and > 2000, respectively, Figure 3.8i). H3K9me3 levels in induced F-KDM4A U2OS cells treated with dox for 2–24 h were analysed and found to be reduced compared to those in uninduced cells (Figure 3.8j), confirming demethylase activity of the overexpressed enzyme, and the percentage demethylation of H3K9me3 was increased on increasing dox dosing time (Figure 3.8k).

Overall, evaluation of the F-KDM4A cells revealed that they comprised an improved system with which to investigate the cellular oxygen dependence of KDM4A activity compared to transiently transfected HeLa (Chapter 3.2). After 24 h, overexpression of KDM4A WT in the F-KDM4A U2OS cells resulted in demethylation of approximately 80% of native H3K9me3 (Figure 3.8k) compared to a maximum of 68% observed in transiently transfected HeLa (Figure 3.5b). Use of F-KDM4A U2OS cells therefore ensures a large signal window in which to calculate changes to KDM4A activity upon exposure to different oxygen concentrations. The induction protocol also facilitated immediate incubation of cells in the desired oxygen concentration following treatment with dox, to ensure that all ectopically expressed enzyme was exposed to hypoxia throughout the experiment. For subsequent experiments, a dox dosing time of 24 h was chosen to ensure a maximum number of induced cells. Therefore, these cells and this protocol (24 h incubation in parallel hypoxic

workstations) were taken forward for further immunofluorescence experiments to analyse the effect of varying oxygen concentration on cellular KDM4A activity.

3.3.2. Oxygen-dependence assays in F-KDM4A U2OS cells

Having verified the suitability of the F-KDM4A U2OS cells, they were used in an immunofluorescence assay to assess the oxygen dependence of cellular KDM4A activity over a physiologically relevant range of oxygen concentrations. F-KDM4A U2OS cells were treated with dox (1 $\mu g.mL^{-1}$) to induce overexpression of KDM4A WT, then immediately incubated at 0.1%, 1.0%, 5.0% and 21% O_2 for 24 h. Cells were subsequently fixed, stained and imaged as described previously (Chapter 3.2, Figure 3.9a-d). Uninduced cells (i.e. cells not treated with dox) were used as a control in each oxygen concentration. The analysis protocol used in the HeLa immunofluorescence assay (Chapter 3.2) was adapted for use with the F-KDM4A U2OS cells. The heterogeneous overexpression of KDM4A (Chapter 3.3.1) necessitated selection of a more homogeneous cell population for analysis. Therefore, FLAG fluorescence intensity of uninduced cells was used as a control to select induced cells, as described previously (Figure 3.8h). H3K9me3 fluorescence signal in these induced cells was normalised against that in uninduced control cells incubated at the same concentration of O_2, to enable calculation of percentage demethylation of H3K9me3 (Equation 3.3, Figure 3.9e), which was then used to calculate relative KDM4A activity in each O_2 concentration (Equation 3.4, Figure 3.9f).

$$\text{Relative KDM4A activity} = \left(\frac{\%\ \text{demethylation H3K9me3}_{x\%\ O_2}}{\%\ \text{demethylation H3K9me3}_{21\%\ O_2}} \right) \qquad \textbf{3.4}$$

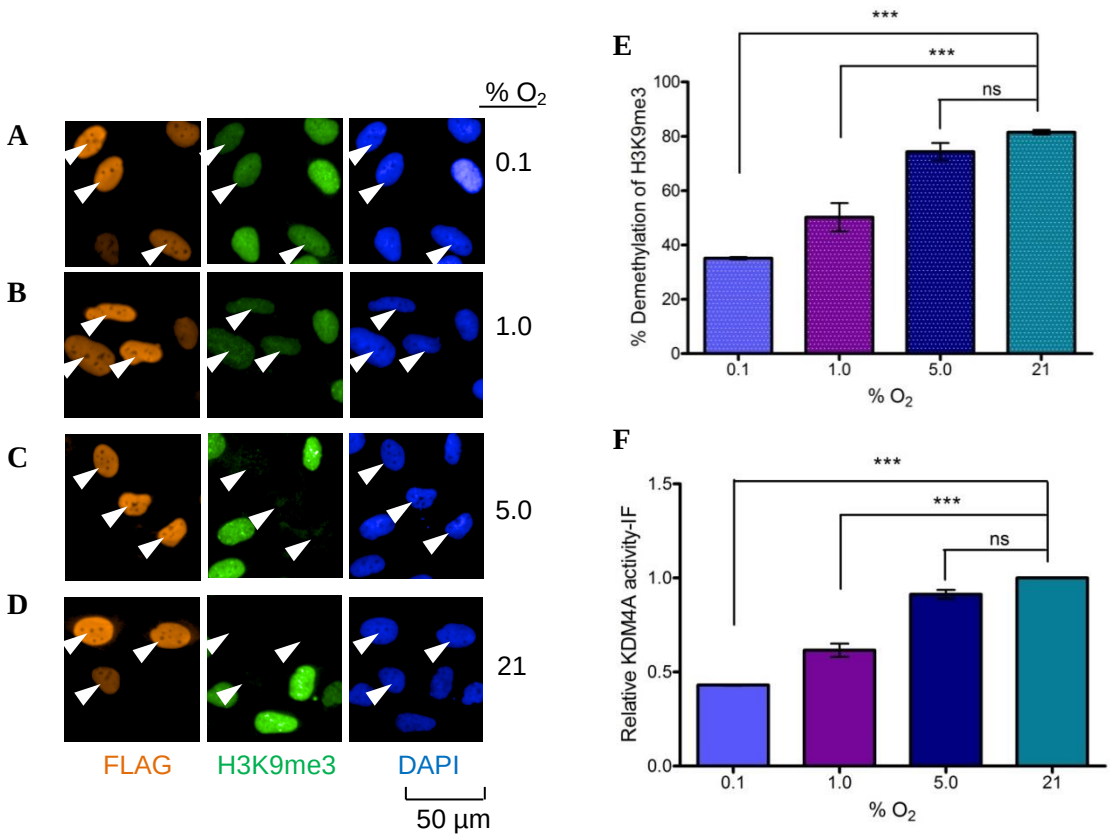

Figure 3.9. **A-D)** Selected images from immunofluorescence analysis of the response of KDM4A activity to hypoxia. F-KDM4A U2OS cells were dosed with 1 µg.mL^{-1} dox then incubated at 0.1-21% O_2 for 24 h. Cells were stained for FLAG-KDM4A WT (orange) and H3K9me3 (green). All cells were fixed and stained, and the images were processed and analysed at the same time, using the same fluorescence intensity signal window. **E)** Percentage demethylation of H3K9me3 in induced cells relative to those in uninduced cells incubated at the same O_2 concentration. **F)** Relative KDM4A demethylase activity under the different O_2 concentrations. N = 3 biological repeats, error bars represent sd. One-way ANOVA with Dunnett's multiple comparison test against the result for 21% O_2 was performed in GraphPad Prism v5.04. Figures adapted with permission from Hancock *et al.*[251], Copyright (2017), American Chemical Society.

Table 3.3 Average relative KDM4A activities in F-KDM4A U2OS cells incubated at 0.1-21% O_2, as calculated from immunofluorescence experiments. Values are given ± sd. P values were evaluated from one-way ANOVA with Dunnett's multiple comparison test against the result for 21% O_2, using GraphPad Prism v5.04.

% O_2	% loss of H3K9me3 (± sd)	Relative KDM4A activity
0.1	35 ± 0.4	0.43 ± 0.01 (P < 0.001)
1.0	50 ± 5.2	0.62 ± 0.06 (P < 0.001)
5.0	74 ± 3.2	0.91 ± 0.04
21	81 ± 0.8	1.00

The results of this experiment revealed that the cellular activity of KDM4A displays a graded response to oxygen availability (Figure 3.8) in F-KDM4A U2OS cells. At 21% O_2,

the percentage loss of H3K9me3 was 81 ± 0.8%, compared to 35 ± 0.4% at 0.1% O_2 (Figure 3.9e), corresponding to an approximately 57% loss in KDM4A activity (Figure 3.9f, Table 3.3). Overall, the data show that the cellular demethylase activity of KDM4A is decreased with decreasing oxygen availability (Figure 3.8f), in concordance with the *in vitro* oxygen dependence observed (Chapter 2.4). Moreover, analysis of the raw data showed that the percentage demethylation in each oxygen concentration was consistent across three biological repeats (Figure 3.9e), indicating that the F-KDM4A U2OS cells provide a more reproducible and therefore reliable system than the transiently transfected HeLa used for preliminary experiments (Chapter 3.2).

Western blots using the F-KDM4A U2OS cells were performed to assess the effect of KDM4A overexpression in normoxia and hypoxia on a number of endogenous trimethylated lysine histone marks, namely, the known KDM4A substrate marks H3K9me3 and H3K36me3, and non-substrate H3K4me3 and H3K27me3[113] (Chapter 7.2.7). F-KDM4A U2OS cells were treated with or without dox, as in the immunofluorescence experiments described above, and incubated at 0.1, 1.0, 5.0 and 21% O_2 for 24 h. Cells were then lysed in SDS-urea buffer (6.7 M urea, 10 mM Tris-Cl (pH 6.8), 10% glycerol, 1.0% SDS, supplemented with 1mM dithiothreitol and Complete Protease Inhibitor Mixture (Roche Applied Science). Chapter 7.2.7). Lysates were sonicated to shear genomic DNA and frozen at –80°C. Additional control samples, comprising parental U2OS Flp-in-Trex cells treated with or without dox, were incubated at 21% O_2 (Figure 3.10, 21(P)), in order to assess the effect of doxycycline on the histone marks in the absence of FLAG-KDM4A WT overexpression. A BCA assay (ThermoScientific) was used to quantify protein concentration in each sample, and 1 μg of each sample was used in each analysis (Chapter 7.2.7).

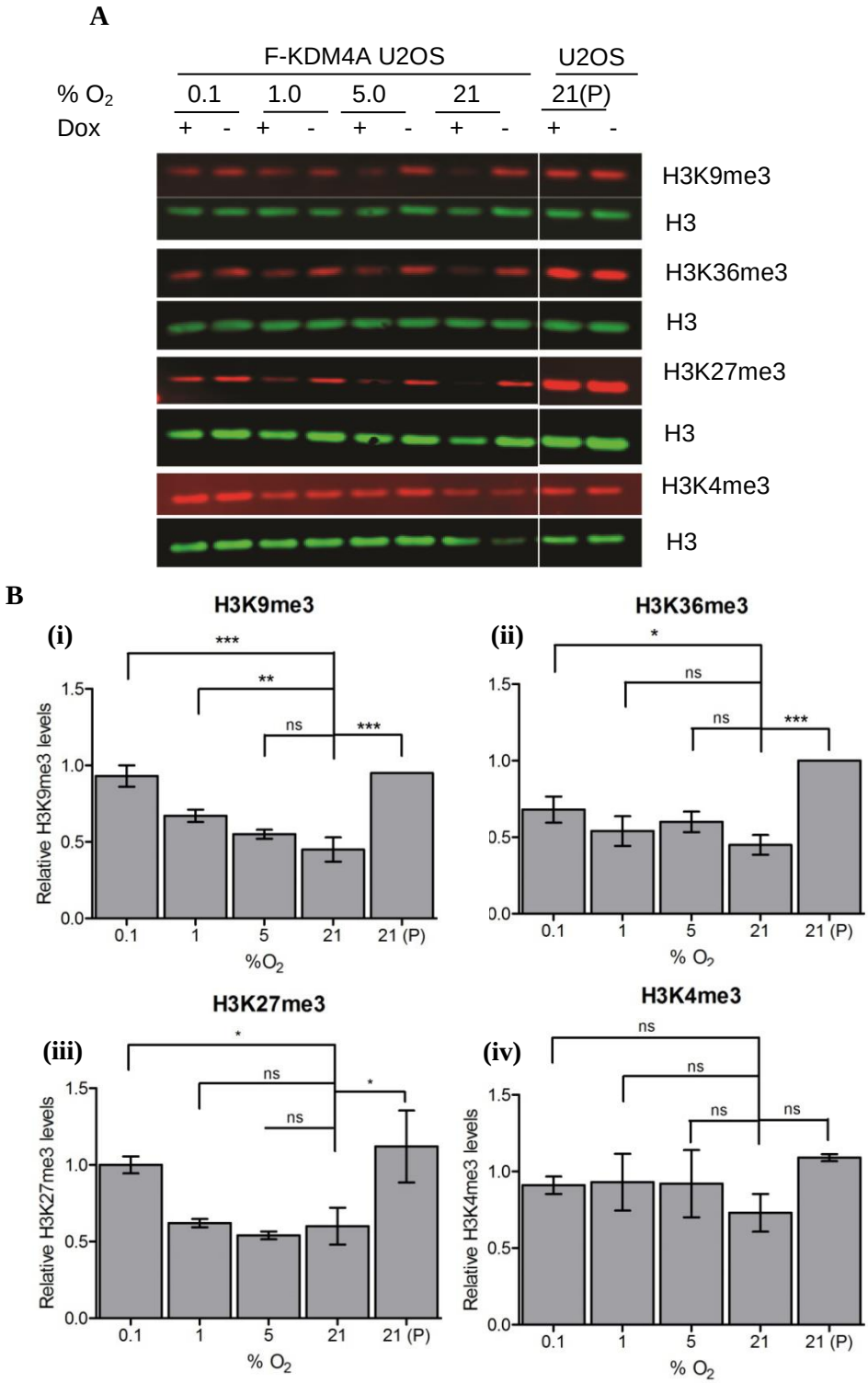

Figure 3.10 A) Representative western blots showing levels of H3K9me3, H3K36me3 & H3K27me3 histone methylation marks in induced or uninduced F-KDM4A U2OS cells incubated at 0.1-21% O_2. P indicates parental U2OS Flip-in-T-rex cells. The membrane was stained simultaneously for H3K9me3/H3K36me3/H3K27me3/H3K4me3 and H3, with methylation marks being normalised against the signal for H3. Western blots were imaged using Odyssey® CLx Fluorescent Imaging System (LI-COR) and analysed using Image Studio™ software (LI-COR). **B)** Quantification of **(i)** H3K9me3 (N = 3 biological repeats), **(ii)** H3K36me3 (N = 3 biological repeats) and **(iii)** H3K27me3 (N = 2 biological repeats) and **(iv)** H3K4me3 (N = 2 biological repeats) levels from western blots. Fluorescence intensity of trimethylated lysine marks was normalised to H3 fluorescence and then quantitated relative to those in uninduced cells incubated at the same O_2 concentration. Error bars denote sd, and two-way ANOVA with Dunnett's multiple comparison test was performed using GraphPad Prism v5.04. Figures reproduced with permission from Hancock *et al.*[251], Copyright (2017), American Chemical Society.

Multiplexed fluorescent western blots enable quantitative analysis of multiple proteins at the same time; hence samples were probed simultaneously for a methylated histone lysine mark and a histone H3 loading control, which appear at the same molecular weight. Fluorescence intensity of the methylated histone mark in question was normalised against H3 fluorescence, then normalised values from induced cells were evaluated relative to those in uninduced samples incubated at the same O_2 concentration.

Analysis of H3K9me3 levels confirmed the results of the immunofluorescence experiments; namely, overexpression of KDM4A resulted in a loss of H3K9me3 levels in normoxia, and loss of H3K9me3 was reduced in a graded manner with decreasing oxygen concentration (Figure 3.10a, b(i)). Investigation of H3K36me3 revealed a similar, although less pronounced trend to that seen for H3K9me3 (Figure 3.10a, b(ii)). Interestingly, while H3K4me3 levels were not significantly altered in the experimental conditions tested (Figure 3.10a, b(iv)), H3K27me3 levels also displayed a similar, although not statistically significant, trend to the known KDM4A-substrate marks (Figure 3.10a, b (iii)). The changes to this non-canonical KDM4A substrate may be due to catalytic activity of the overexpressed enzyme against this mark, which has been shown in an *in vitro* setting[117], although further experimental evidence is required to support this in cells. Alternatively, recent work has shown that demethylase activity and selectivity against a specific mark may be affected by nearby post-translational modifications, often due to disruption of necessary binding interactions[262,263]. Therefore, in this case hypoxically-induced changes to H3K9me3 or H3K36me3 may affect H3K27me3 levels *via* an indirect mechanism. The control experiment revealed that dox treatment of parental cells had no effect on the histone methylation marks assessed, while global levels of the methylated histone marks assessed were not altered in uninduced cells (dox -) under the O_2 concentrations tested.

Western blot analysis was also used to quantify levels of KDM4A overexpression in the samples. Samples were probed using antibodies against both FLAG and KDM4A, levels of which were normalised against a β-actin loading control (Figure 3.11a, b). HIF-1α levels were also probed using a mouse anti-human HIF-1α antibody (BD Transduction Laboratories™, Chapter 7.2.5) and normalised against a β-actin loading control, in order to confirm cellular hypoxia in the hypoxic conditions tested.

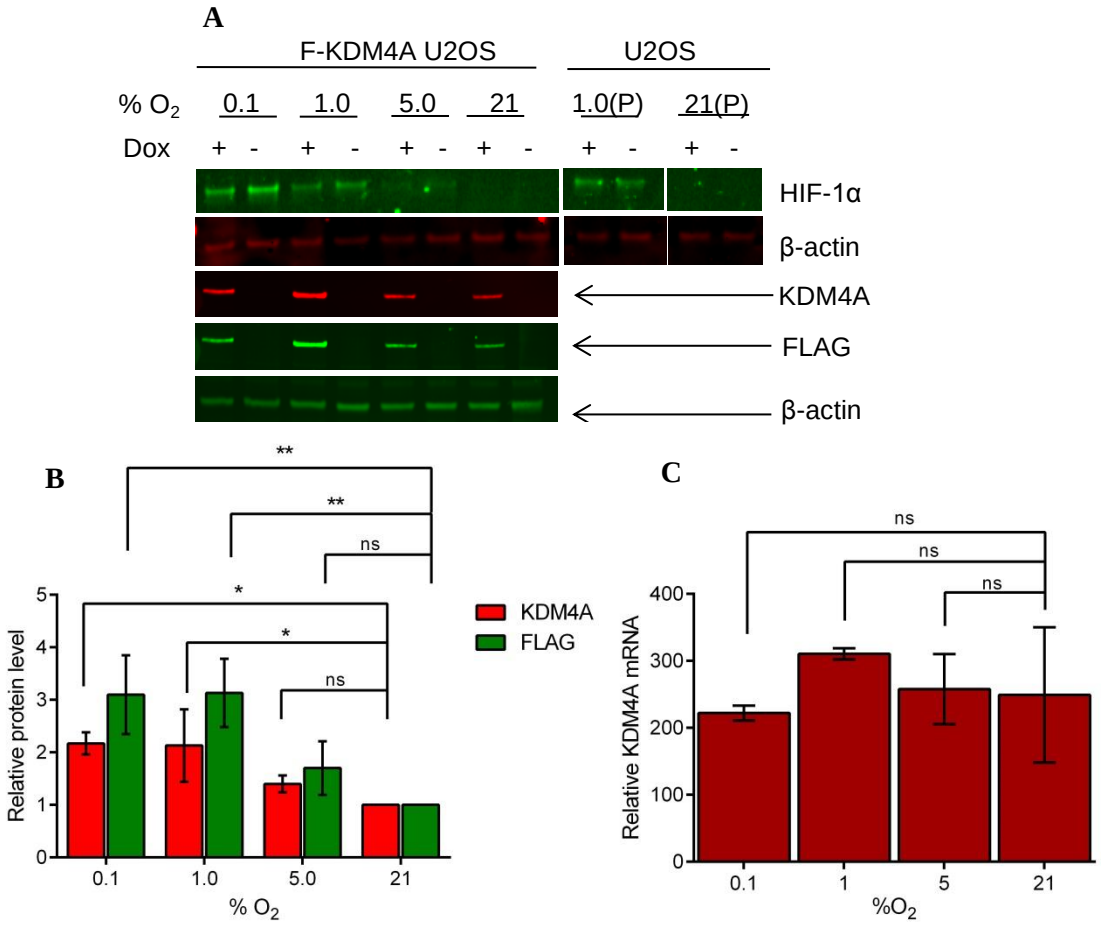

Figure 3.11 A) Representative western blots of cell lysates from induced and uninduced U2OS F-KDM4A and parental Flp-in-Trex U2OS cells (P) probed for HIF-1α, KDM4A and FLAG in cells incubated at 0.1-21 % O_2 for 24 h. β-actin was used as a loading control. Western blots were imaged using Odyssey® CLx Fluorescent Imaging System (LI-COR) and analysed using Image Studio™ software (LI-COR). Images have been cropped to show only relevant molecular weights. **B)** Quantification of FLAG-KDM4A protein from western blots. Levels of overexpressed FLAG-KDM4A were normalised relative to those in normoxic cells treated with dox. Error bars denote sd, and two-way ANOVA with Dunnett's multiple comparison test was performed using GraphPad Prism, N = 3 biological repeats. **C)** Relative KDM4A mRNA levels in U2OS F-KDM4A cells +/- dox incubated for 24 h in 0.1–21% oxygen were analysed by RT-qPCR. Data was processed using CFX Manager™ Software v3.1 (Bio-Rad) and two-way ANOVA with Dunnett's multiple comparison was performed using GraphPad Prism v5.04, N = 2 biological repeats, control = 21% O_2. Figures adapted with permission from Hancock *et al.*[251], Copyright (2017), American Chemical Society.

Consistent with previous reports, increased KDM4A protein was observed with decreasing oxygen concentration (Figure 3.11a, b), although RT-qPCR analysis revealed no significant difference in expression level at the mRNA level (Figure 3.11c). Therefore, the loss of KDM4A activity calculated from the immunofluorescence experiments described above may have been underestimated, as the immunofluorescence protocol does not take into account relative enzyme concentration across the oxygen concentrations tested (Figure 3.9). This increase in KDM4A protein is likely due to the mechanism described by Black *et al.*, in which the interaction between KDM4A and the SCF-ubiquitin ligase responsible for its degradation is reduced in hypoxia, increasing the half-life of the protein[259], although further empirical analysis to explore this phenomenon was not within the scope of this project.

3.4. The biological impact of hypoxic inhibition of KDM4A

The oxygen-dependence experiments described above demonstrated that the activity of KDM4A could be reduced in physiological hypoxia. KDM4A is an epigenetic protein involved in the activation and repression of genes, and hypoxic restriction of its activity may therefore have an effect on the expression level of the genes it is responsible for regulating. This is of particular pertinence to the involvement of KDM4A in hypoxic disease states, as described in Chapter 1.6.2, in which aberrant epigenetic regulation may contribute to dysregulation of disease-specific genes. Experiments were therefore designed to investigate the biological impact of inhibition of KDM4A activity in hypoxia.

3.4.1. The effect of hypoxia on expression of HIF target genes

A number of putative KDM4A target genes have been postulated in recent literature[142,264–268]. KDM4A was first identified as a repressor of the achaete-scute like homolog 2 (ASCL2) *via* its interaction with the NCoR corepressor[142]. Subsequent ChIP-seq experiments have

detected binding of KDM4A at the promoter region of several genes, along with changes to their expression levels upon KDM4A knockout in many cases, as summarised in Table 3.4.

Table 3.4 Putative KDM4A target genes, as identified using ChIP-based techniques in a number of cell lines.

Target gene	Cell line	Changes to gene	Method
CHD5	U2OS, IMR90		
ASCL2 *PANX2* *RHOQ*	U2OS	mRNA ↗ in KDM4A$^{-/-}$ cells	ChIP-qPCR[264]
CDC6	U2OS	no change in levels	
GP5 *PPIC*	U2OS	mRNA ↘ in KDM4A$^{-/-}$ cells	
ADAM12 *CXCL5* *JAG1*	A549	mRNA ↘ & H3K9me3 ↗ in KDM4A$^{-/-}$ cells	ChIP-Seq[265]
SOX10	NS	H3K9me3 ↘ at promoter	ChIP[266]
SNAIL2		NS	
MYOG	C2C12	NS	ChIP[267]
GPS2/PPARγ target genes	3T3-L1 (differentiated)	H3K9me3 ↗ on KDM4A knockdown	ChIP-Seq[268]

Several of these proposed target genes were chosen for RT-qPCR analysis in the U2OS F-KDM4A cell system under different oxygen concentrations. The best-validated KDM4A target gene, *ASCL2*, was selected, along with *CHD5*, *GP5*, *PPIC* and *ADAM12*. Levels of the tumour suppressor *CHD5* in U2OS cells were shown to be increased approximately 4-fold upon siRNA-induced knockout of KDM4A[264], indicating that KDM4A is a negative regulator of this gene. Further analysis of this interaction found that overexpression of KDM4A promotes cellular transformation in a CHD5 and p53-dependent mechanism[264]. The same study found that *GP5* was also repressed by KDM4A, while KDM4A knockout caused reduced expression of Peptiylprolyl Isomerase C, *PPIC*, indicating that KDM4A may also act as a transcriptional activator[264]. A different study in A549 cells found that KDM4A

directly transactivates A Disintegrin and Metalloprotease 12, *ADAM12*, a gene overexpressed in a number of human carcinomas, *via* demethylation of H3K9me3[265].

RT-qPCR analysis of these genes was undertaken using the primers reported in published literature studies (Chapter 7.2.8), the efficiency of which was evaluated using dose-response experiments (Appendix 3) according to the Pfaffl method[269]. While the primers for *ADAM12, PPIC, GP5, KDM4A, CA9* and *HIF-1α* were found to be linear and possess efficiencies of 1.8-2.2 (Appendix 3), these tests revealed that the *ASCL2* primer was not suitable for use in this system (data shown in Appendix 3). Given that this gene is repressed by KDM4A, the high levels of FLAG-KDM4A WT overexpression in the induced F-KDM4A U2OS (approximately 300-fold, compared to uninduced cells, Figure 3.11c) may repress *ASCL2* to levels below the limit of detection in this system. Further analysis using a higher primer concentration did not determine conditions that would enable analysis of *ASCL2* in these cells (Appendix 3).

F-KDM4A U2OS cells were treated with dox to induce overexpression of KDM4A WT, then incubated at 1.0 or 21% O_2 for 24 h. Uninduced cells were also exposed to the same conditions for use as a control. Total mRNA was isolated from cells using a mirVana™ mRNA isolation kit (Ambion), and genomic DNA removed using a Turbo DNA-*free*™ kit (Ambion). Reverse transcription was achieved using a High Capacity cDNA Reverse Transcription kit (Applied Biosystems). 1.6-3 ng cDNA was then submitted to RT-qPCR, using 300 nM of the relevant primer and Power SYBR® Green PCR master mix (Applied Biosystems). β-actin, the primers for which were kindly donated by Dr Mun Chiang Chan (Ratcliffe Laboratory, NDM, University of Oxford), was validated as a housekeeping gene (Appendix 3), and the ΔΔCt method[270] was used to evaluate expression levels relative to uninduced cells incubated at the same O_2 concentration.

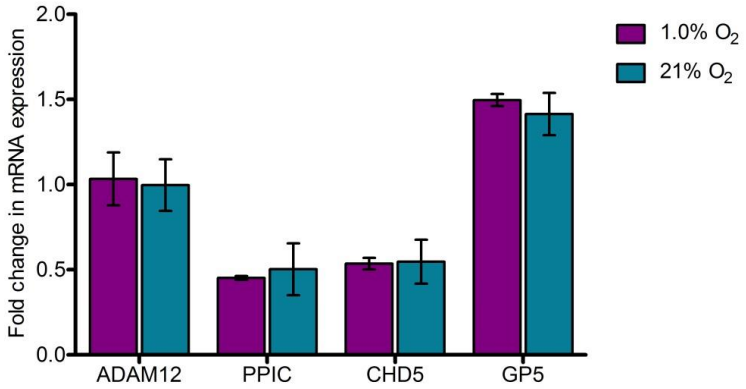

Figure 3.12 Relative mRNA expression of *ADAM12, PPIC, CHD5* and *GP5* in F-KDM4A U2OS cells treated with dox and incubated at 1.0% or 21% O_2 (24 h), as quantified by RT-qPCR. Expression levels were calculated relative to those in uninduced cells incubated at the same O_2 concentration. Data was processed using CFX Manager™ Software v3.1 (Bio-Rad). N = 3 biological repeats, error bars denote sd.

Analysis of *ADAM12, PPIC, CHD5* and *GP5* showed that, contrary to literature reports[264,265], *ADAM12* showed no change in expression, while *PPIC* was repressed due to overexpression of KDM4A and *GP5* levels were increased. *CHD5* levels were reduced, as expected[264]. In all cases, exposure to hypoxia did not appear to affect the level of repression or activation due to KDM4A overexpression (Figure 3.12). These results may indicate that the F-KDM4A U2OS overexpression system is not suitable for qPCR analysis, due to the aforementioned high levels of KDM4A overexpression, which result in approximately 50% demethylation of global H3K9me3 levels, even at 1.0% O_2 (Chapter 3.3, Table 3.3). It is therefore possible that the loss of H3K9me3 at specific genes in these cells is sufficient to influence the level of expression, even in hypoxia. Moreover, these genes have not been validated as KDM4A targets in multiple cell lines, nor has the H3K9me3 status at the promoters of *PPIC, CHD5* and *GP5* been evaluated[264], hence KDM4A may not be directly involved in their regulation *via* its catalytic activity upon this mark, and the involvement of alternative biological pathways is also possible. Further validation of KDM4A target genes using ChIP-based methods is therefore necessary, and may assist in determining the biological impact of hypoxic inhibition of KDM4A activity on epigenetic regulation of specific genes.

Despite the lack of convincing results from the investigation of KDM4A target genes in the F-KDM4A U2OS cells, further RT-qPCR analysis was carried out on a number of well-characterised HIF target genes. The interplay between the KDMs and HIF has been the subject of numerous recent studies, and direct interaction between HIF and KDM3A[210,215], KDM4C[216] and KDM6B[271] at specific HIF target genes has been observed. Therefore, the impact of KDM4A overexpression on regulation of HIF target genes in hypoxia was assessed using RT-qPCR. The expression of the carbonic anhydrase 9 gene (*CA9*) is strongly HIF-1-dependent[272]; hence *CA9* was chosen for assessment, as its strong overexpression in hypoxia would provide a large signal window within which to observe any KDM4A-dependent changes. Primers were donated by Dr Mun Chiang Chan (Ratcliffe Laboratory, NDM, University of Oxford) and tested for efficiency (Appendix 3) and *CA9* levels were assessed in samples from F-KDM4A U2OS cells treated ± dox then incubated at 0.1, 1.0, 5.0 or 21% O_2 for 24 h. Parental U2OS Flp-in-Trex cells (P) treated with and without dox were incubated at 1.0 and 21% to control for the effect of dox independently of KDM4A overexpression.

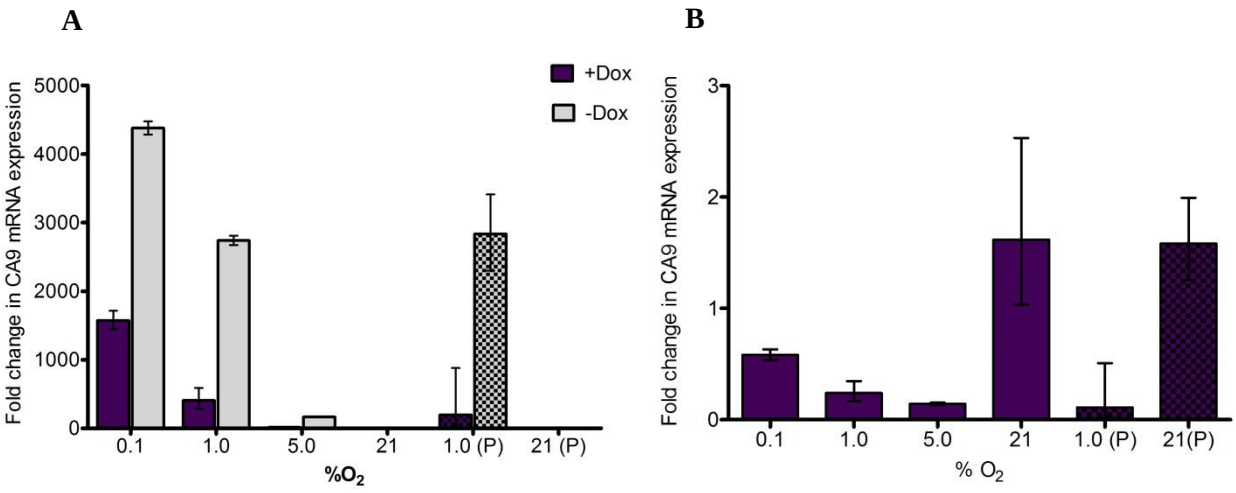

Figure 3.13. Relative mRNA expression of *CA9* in F-KDM4A U2OS cells or Flp-in-Trex U2OS cells (P, patterned) treated +/- dox and incubated at 0.1- 21% O_2 (24 h), as quantified by RT-qPCR. **A)** *CA9* levels were calculated relative to those in normoxic cells treated with the same dox conditions. **B)** Expression of *CA9* in induced cells relative to uninduced cells incubated at the same O_2 concentration. Data was processed using CFX Manager™ Software v3.1 (Bio-Rad). Error bars represent 95% confidence intervals (CI), n = 3 technical repeats.

CA9 levels in all samples were normalised against those in cells incubated in normoxia and treated with the same dox concentration (0 or 1 $\mu g.mL^{-1}$), revealing a large and oxygen-dependent increase in *CA9* expression in hypoxia (Figure 3.13a). Furthermore, in an alternative analysis, normalisation of CA9 levels in induced cells relative to those in uninduced cells incubated at the same O_2 concentration revealed an apparent dox-dependent blunting of *CA9* activation in hypoxia, the extent of which was apparently reduced in response to reduction of O_2 availability (Figure 3.13b). Initial evaluation of this might suggest that KDM4A overexpression could limit CA9 activation in hypoxia, and loss of KDM4A activity might minimise this effect under increasing levels of hypoxia. However, this dox-dependent reduction in *CA9* upregulation was also observed in the parental cells incubated at 1.0% O_2 (Figure 3.13b), suggesting that changes to the expression of *CA9* upon treatment of cells with dox are dependent on dox, rather than on KDM4A-overexpression.

This prompted analysis of *HIF-1α* levels in the samples. RT-qPCR analysis was performed to assess expression of *HIF-1α* at the transcript level in the F-KDM4A U2OS samples, and in parental samples incubated at 1.0 and 21% O_2, relative to β-actin. *HIF-1α* levels in each sample were then normalised against those in normoxic samples treated with or without dox (Figure 3.14a), or alternatively, dox treated samples were normalised against uninduced controls incubated at the same O_2 concentration (Figure 3.14b).

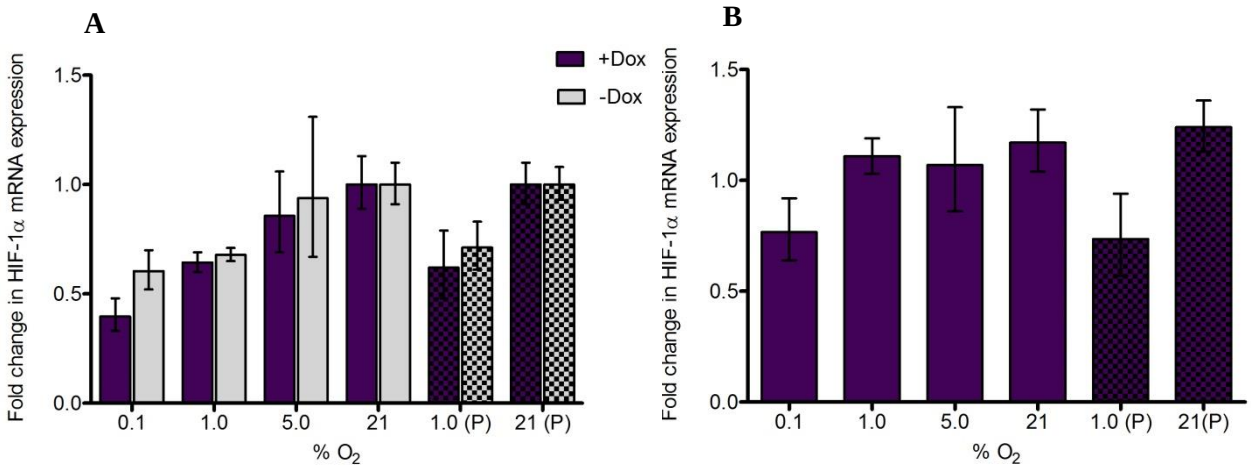

Figure 3.14. Relative mRNA expression of *HIF-1α* in F-KDM4A U2OS cells or U2OS Flp-in-Trex cells (P, patterned) treated with (purple) or without (grey) dox and incubated at 0.1- 21% O_2 (24 h), as quantified by RT-qPCR. **A)** *HIF-1α* levels were calculated relative to those in normoxic cells treated with the same dox conditions. **B)** Expression of *HIF-1α* in induced cells relative to uninduced cells incubated at the same O_2 concentration. Data was processed using CFX Manager™ Software v3.1 (Bio-Rad). Error bars denote 95% CI, n = 3 technical repeats.

This analysis revealed a graded loss of *HIF-1α* at the transcript level in hypoxia (Figure 3.14a), a phenomenon which has been reported previously and attributed to reduced mRNA stability[273]. This trend is in direct contrast to the trend observed for *CA9* (Figure 3.13a). Normalisation of *HIF-1α* levels in dox-treated cells in each O_2 concentration against untreated cells showed a small dox-dependent increase in *HIF-1α* in all samples, except F-KDM4A U2OS cells incubated at 0.1% O_2, in which dox appeared to reduce *HIF-1α* expression (Figure 3.14b). Overall, there appears to be no significant change in *HIF-1α* expression on treatment of F-KDM4A U2OS cells or parental U2OS Flp-in-Trex cells with dox under the conditions tested, hence changes in *HIF-1α* expression at the transcript level are unlikely to account for the trends in *CA9* expression described above (Figure 3.13). However, HIF is constitutively expressed, and its expression at the protein level is regulated by the activity of the HIF hydroxylases. Upregulation of the protein due to reduced proteasomal degradation is necessary in order to activate HIF target genes[157]; hence analysis at the mRNA level is only partially indicative of how HIF levels may be affected in this system. Western blots were previously performed to validate the hypoxic conditions used in

these cellular experiments and showed induction of HIF-1α protein under hypoxia (Figure 3.11a). While technical difficulties precluded numerical quantification of HIF-1α levels from western blots, visual assessment suggests that dox treatment may reduce HIF-1α induction in hypoxia relative to those in uninduced F-KDM4A U2OS cells exposed to the same O_2 concentration. This may explain the apparent blunting of *CA9* upregulation in response to dox observed in the RT-qPCR experiment (Figure 3.13), although further investigation is required to understand the mechanism behind these dox-induced changes to HIF-1α levels, and whether KDM4A plays a role in this phenomenon.

Overall, the RT-qPCR analyses described here revealed that further validation of KDM4A target genes is necessary to enable assessment of the effect of hypoxia on their expression. Moreover, an alternative cellular system is required for these analyses. The impact of dox on expression of the genes tested remains ambiguous. The very high levels of KDM4A overexpression in the F-KDM4A U2OS cells, while beneficial in assessing enzyme activity due to a large signal window with respect to measurement of the loss of global H3K9me3 levels, are counterproductive to the evaluation of the physiological effect of hypoxic restriction of KDM4A activity on downstream biological processes. The use of a cell line that constitutively overexpresses lower levels of KDM4A may be helpful in further experiments, along with KDM4A-knockout cell lines. The possible effect of KDM4A activity on the upregulation of HIF target genes must also be assessed in an alternative system and may be cell type dependent. The use of pVHL knockout RCC4 cells, in which HIF is not degraded in normoxia, may be helpful in these analyses, but was not possible within the time constraints of this project.

3.4.2. The impact of hypoxia on chromatin structure

As an alternative readout of the biological impact of hypoxic inhibition of KDM4A in cells, assessment of the effect of hypoxia on chromatin structure in KDM4A-overexpressing cells

was proposed. The KDM4A substrate mark H3K9me3 is associated with condensed, transcriptionally silent heterochromatin, and is known to facilitate recruitment of heterochromatin protein, HP1, a regulator of heterochromatin formation[274]. The demethylase activity of KDM4C against H3K9me3 was previously shown in immunofluorescence experiments to reduce nuclear levels of an HP1 isoform, HP1β, in HEK293 cells. Moreover, in RKO cells exposed to hypoxia for 6 h, levels of HP1β were increased, concomitant with an increase in H3K9me3[199]. Given the loss of KDM4A activity in hypoxia demonstrated above (Chapter 3.2, 3.3), it is possible that hypoxia could increase the association of HP1 with the chromatin, ultimately leading to the silencing of KDM4A-regulated genes. Preliminary immunofluorescence experiments were therefore designed to assess HP1β levels in KDM4A-overexpressing cells exposed to hypoxia and normoxia. In order to evaluate the impact of the catalytic activity, rather than overexpression, of KDM4A on HP1β, a KDM4A MUT control was required, necessitating the use of a transiently transfected system. U2OS cells were therefore transfected with the FLAG-KDM4A WT or FLAG-KDM4A MUT-encoding constructs used in the HeLa immunofluorescence experiments described above (Chapter 7.2) for 4 h, before incubation at 1.0 or 21% O_2 for 24 h. Cells were stained for either FLAG and HP1β, or FLAG and H3K9me3, then imaged as described previously Chapter 3.2, Chapter 7.2.6). H3K9me3 or HP1β levels were quantified in transfected cells and in a non-transfected control. As described previously, H3K9me3 levels in KDM4A WT-overexpressing cells were normalised relative to those in KDM4A MUT-transfected cells, while HP1β fluorescence was analysed relative to those in NTC cells.

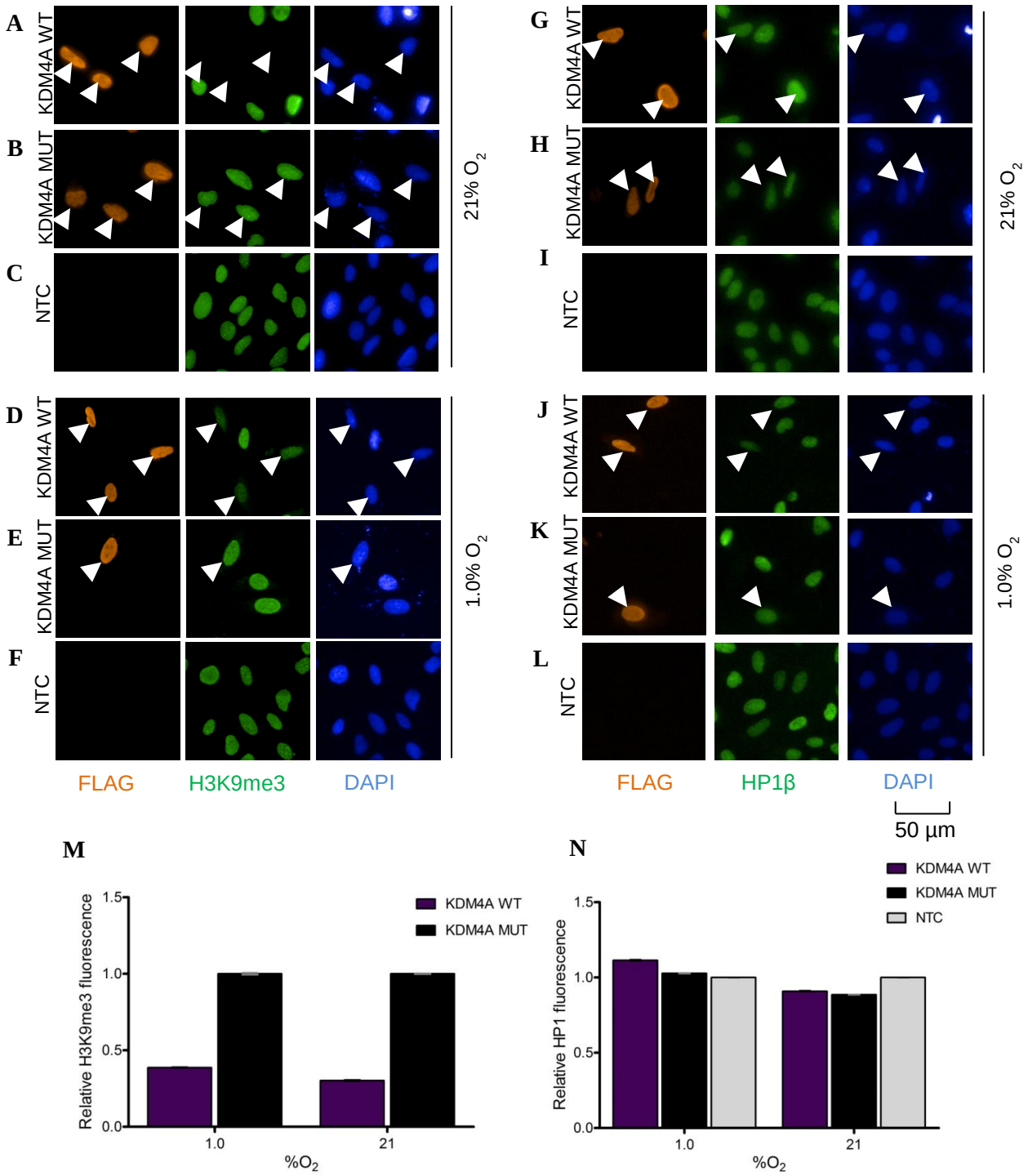

Figure 3.15. **A-L)** Selected images from immunofluorescence analysis of the response of HP1β to KDM4A overexpression in normoxia and hypoxia. U2OS cells were transfected with FLAG-KDM4A WT **(A, D, G, J)** or FLAG KDM4A MUT **(B, E H, K)** at 1.0 or 21% O_2 for 24 h. Cells were stained for FLAG (orange) and H3K9me3 (green, **A-F**) or FLAG and HP1β (green, **G-L**). FLAG fluorescence intensity was used to select transfected cells (white arrows) and levels of H3K9me3/HP1β were quantified in these cells. Images were processed and analysed at the same time, using the same fluorescence intensity signal window for each epitope. **M)** Relative fluorescence intensity of H3K9me3 in KDM4A WT-overexpressing cells, compared to KDM4A MUT-transfected cells incubated at the same O_2 concentration. **N)** Relative HP1β fluorescence in cells overexpressing KDM4A WT (purple) and KDM4A MUT (black), and non-transfected control cells (NTC, grey) under normoxia and hypoxia. n >50 cells, error bars represent sem.

In both normoxia and hypoxia, overexpression of KDM4A WT resulted in a loss of H3K9me3 levels (Figure 3.15a, d, m), as observed previously. Some reduction in H3K9me3 demethylation was observed in hypoxia, although less than had previously been seen in transiently transfected HeLa and the F-KDM4A U2OS cells (Chapter 3.2, Chapter 3.3.2), which may be due to the different cell type used. Furthermore, analysis of HP1β fluorescence indicated that there were no significant differences in the levels of HP1β upon overexpression of either KDM4A WT or KDM4A MUT compared to those in NTC cells in both normoxia and hypoxia (Figure 3.15g-l, n). These results may suggest that KDM4A activity has little effect on the association of HP1β with the chromatin, although this would be contrary to literature reports, which clearly demonstrate a link between H3K9me3 status and HP1β recruitment[199,274]. Therefore, it was likely that the experimental design and conditions required optimisation to enable proper assessment of HP1β.

In a second experiment using the same conditions, cells were pre-extracted using a cytoskeleton buffer[275] (10 mM PIPES pH 7.0, 100 mM NaCl, 3 mM $MgCl_2$, 300 mM sucrose, 0.5 % Triton-X), in an effort to ensure that only chromatin-bound HP1β was assessed. Cells were transfected, incubated at 0.1% or 21% O_2 for 24 h, then pre-extracted, before being fixed, stained and imaged as described above.

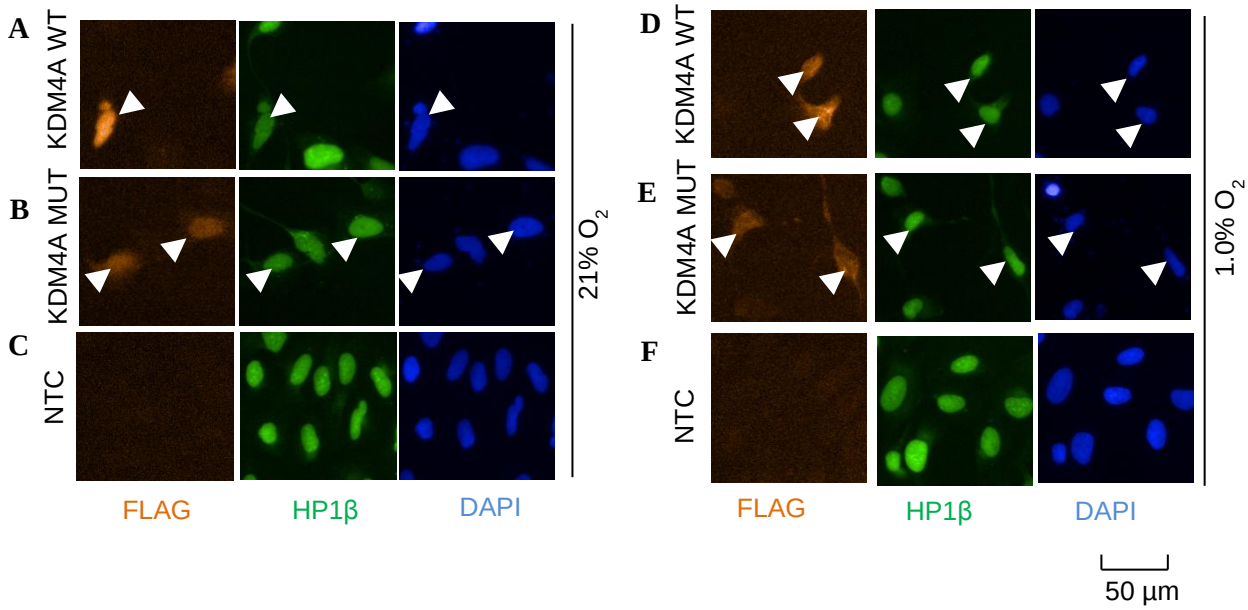

Figure 3.16.a-f. Selected images from immunofluorescence analysis of the response of HP1β to KDM4A overexpression in normoxia and hypoxia. U2OS cells were transfected with FLAG-KDM4A WT (a, d) or FLAG KDM4A MUT (b, e) at 1.0 or 21% O_2 for 24 h. Cells were pre-extracted using cytoskeleton buffer, then stained for FLAG (orange) and HP1β (green). Images were processed and analysed at the same time, using the same fluorescence intensity signal window for each fluorophore.

It was apparent from the images procured in this experiment (Figure 3.16a-f) that FLAG fluorescence was less intense and less well-defined than in previous immunofluorescence experiments using both HeLa and the F-KDM4A U2OS cells (Figure 3.2, Figure 3.7, 3.8). This is likely due to pre-extraction of the cells removing a large proportion of the ectopically expressed FLAG-KDM4A from the cell nuclei prior to staining. Insufficient FLAG fluorescence remained to enable identification of a homogeneously KDM4A-expressing population of transfected cells (Figure 3.16); hence further analysis could not be reliably performed. Upon visual assessment, it appeared that overexpression of KDM4A WT in normoxia had resulted in some loss of HP1β signal (Figure 3.16a-c); although lack of quantitative analysis across a large number of cells means that a reliable conclusion cannot be drawn from this experiment.

Optimisation of the pre-extraction protocol, along with a better means of identifying a homogenously KDM4A-overexpressing cell population following pre-extraction are necessary. Western blot experiments, which allow for fractionation of cell lysates, may be

more appropriate for these analyses. High levels of KDM4A overexpression are necessary to overcome the limitation that western blot experiments do not allow for the selection of a population of cells prior to analysis; hence the F-KDM4A U2OS cells would be preferable to the transiently transfected system. Alongside this, the engineering of a cell line stably overexpressing dox-inducible KDM4A MUT would be necessary to assess the effect of the catalytic activity, rather than just overexpression, of KDM4A in normoxia and hypoxia on HP1 recruitment.

3.5. Discussion

The work described in this chapter aimed to assess the impact of hypoxia on the cellular activity of KDM4A. Immunofluorescence experiments in transiently transfected HeLa cells (Chapter 3.2) revealed that demethylation of H3K9me3 by ectopically overexpressed KDM4A WT was diminished in cells exposed to 0.5% O_2 for 24 h. Analysis of H3K36me3 using this method showed a similar hypoxic restriction of KDM4A activity against this mark. Although these experiments successfully evaluated this trend, a more quantitative and reproducible system was sought in order to investigate varying degrees of hypoxia on cellular KDM4A.

A U2OS cell line stably-overexpressing dox-inducible full-length FLAG-KDM4A WT (F-KDM4A U2OS cells) was validated for KDM4A-WT overexpression and activity (Chapter 3.3.1). Both consistent overexpression of KDM4A WT in a large population of cells and high levels of demethylation confirmed that these cells were a suitable system for oxygen titration experiments. Exposure of induced cells to 0.1, 1.0, 5.0 and 21% O_2 revealed that the cellular activity of the ectopically expressed KDM4A against native H3K9me3 demonstrated a graded response to oxygen availability (Chapter 3.3.2). This is in concordance with the *in vitro* experiments described in Chapter 2, confirming the oxygen sensitivity of KDM4A activity and further implying that KDM4A may be capable of an oxygen sensing role in the

context of epigenetic regulation. Furthermore, the correlation between the *in vitro* and cellular oxygen sensitivities evaluated in these experiments demonstrates that biochemical analysis may be reflective of cellular trends. This was apparently also true for the HIF hydroxylases, for which cellular analyses revealed differential oxygen sensitivities[173] in line with the differences in the observed *in vitro* $K_m^{app}(O_2)$ values[171,245].

In preliminary work together with Dr Akane Kawamura, the effect of hypoxia on the cellular activity of TET1 was assessed. Levels of 5hmC in U2OS cells stably overexpressing dox-inducible TET1 catalytic domain were evaluated in cells incubated at different O_2 concentrations using immunofluorescence under similar conditions as those used in experiments with the F-KDM4A U2OS cells (24 h). Interestingly, TET1 activity also displayed a graded loss of activity with reduced oxygen availability, with an apparently increased loss of activity at 0.1 and 1.0% O_2 compared to that observed for KDM4A (Figure 3.17).

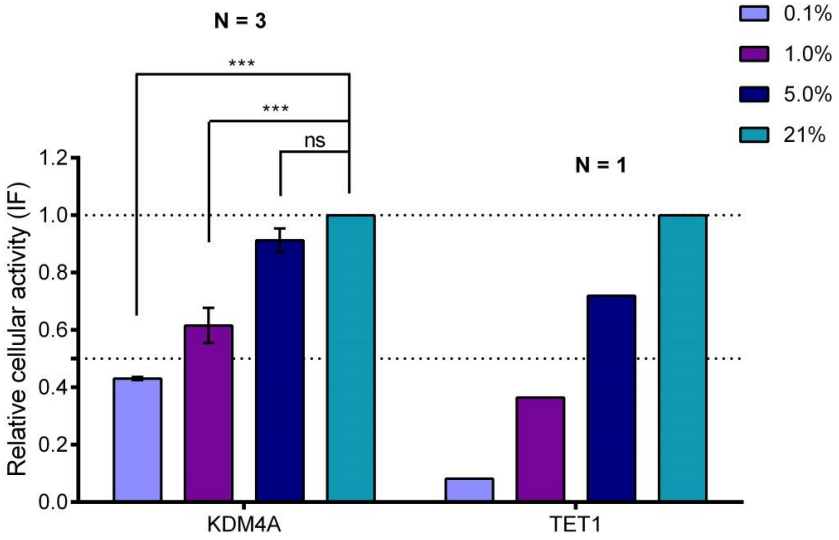

Figure 3.17. Comparison of the effect of varying degrees of hypoxia on the catalytic activity of KDM4A and TET1. Immunofluorescence experiments in U2OS cells stably overexpressing dox-inducible full-length FLAG-KDM4A WT (KDM4A) or the FLAG-tagged catalytic domain of TET1 (TET1) were used to evaluate the cellular activity of these enzymes at 0.1, 1.0, 5.0 and 21% O_2. Activities are calculated relative to the maximum activity at 21% O_2. Data was plotted and analysed using GraphPad Prism v5.04, One-way ANOVA with Dunnett's multiple comparison test was performed on KDM4A data, as described above (Figure 3.9f). Error bars (KDM4A data) represent sd, N=3 biological repeats.

This data suggests that TET1 is highly sensitive to oxygen concentrations, consistent with the recent study implicating reduced activity of the TETs in DNA hypermethylation in hypoxic tumours[257]. Taken together, these data imply that, as well as histone modifications, DNA methylation may be a further epigenetic mark that is regulated in an oxygen-dependent manner. *In vitro* evaluation of the $K_m^{app}(O_2)$ for TET1 using the MFC oxygen dependence assay (Chapter 2) would enable direct comparison between the TETs and the other 2OG oxygenases investigated using this method, and extend our understanding of the relationship between biochemical and cellular oxygen sensitivity, and differential oxygen sensitivities across the 2OG oxygenase superfamily.

Western blots confirmed the oxygen sensitivity of the canonical KDM4A substrate marks H3K9me3 and H3K36me3 to oxygen availability in cells overexpressing KDM4A WT (Chapter 3.3.2). The H3K4me3 mark, which is known not to be demethylated by KDM4A, was unaffected by varying degrees of hypoxia upon overexpression of KDM4A. However, levels of H3K27me3 did appear to be reduced on induction of KDM4A WT overexpression, with some change in severe hypoxia (0.1%). Although this may be indicative of direct action of the enzyme on this mark, evidence within the literature for this renders it more likely that aberrant methylation at H3K9me3 and H3K36me3 may impact upon the methylation status of this distal lysyl residue, *via* effects on the binding or activity of modifiers of this mark. Changes to global levels of the H3 methylation marks tested were not apparent in cells not overexpressing KDM4A, regardless of O_2 concentration. Overall, these experiments indicate that hypoxia has the potential to affect numerous histone post-translational modifications. This may have an impact upon transcriptional regulation by affecting a variety of epigenetic signals, although in an endogenous setting these changes are likely to be subtle and possibly locus-specific.

The western blots detailed in Chapter 3.3.2 also demonstrated increased KDM4A protein in hypoxia, in line with literature reports[259]. Together with the cellular activity assays, these investigations demonstrate that both KDM4A activity and protein levels can be 'tuned' in varying degrees of hypoxia, with concomitant changes to histone lysine methylation status, thereby providing a potential means of oxygen sensing at the chromatin level.

The remainder of the experiments described in this chapter were undertaken in order to understand the biological impact of hypoxic restriction of KDM4A activity (Chapter 3.4). RT-qPCR analysis of potential KDM4A target genes proved inconclusive, while investigation of the effect of KDM4A activity on the regulation of HIF target genes was also limited by the experimental system used (Chapter 3.4.1). However, exploration of alternative systems, such as RNAi knockdown experiments, the use of CRISPR/Cas9 technology to produce a KDM4A knockout cell line, or ChIP-based techniques may aid in the validation of KDM4A target genes and the effect of hypoxia on these genes.

Hypoxic inhibition of KDM4A activity is likely to result in changes to chromatin structure, *via* aberrant regulation of H3K9me3. This mark is known to recruit HP1β to the chromatin, facilitating the formation of heterochromatin and silencing of genes[274]. An immunofluorescence-based assay to assess the effect of hypoxia HP1β levels in cells overexpressing KDM4A WT and KDM4A MUT requires further optimisation (Chapter 3.4.2). The F-KDM4A U2OS cell line used in the cellular activity assays may well be of use in western blot analysis of chromatin-bound HP1β, which remains of interest for future investigation.

Chapter 4: Small molecule inhibitors of KDM4A

4.1. Introduction

Members of the 2OG oxygenase superfamily of enzymes catalyse an extensive range of reactions necessary for numerous biological functions, including fatty acid metabolism and the hypoxic response. The importance of the 2OG oxygenases in both normal homeostasis and disease has led to extensive efforts across numerous academic research groups and industry to develop selective small-molecule inhibitors of members of this enzyme family[276]. These inhibitors are of use both as chemical probes to explore the function of these enzymes[277], and as precursors to drug-like molecules for use as therapeutic agents.

4.1.1. Generic 2OG oxygenase inhibitors

A major challenge to the development of potent and selective inhibitors is the similarity of the 2OG oxygenase enzymes. The conserved active site Fe^{2+}- and 2OG- binding residues, and DSBH motif[81], as well as the adherence to a consensus mechanism, necessitate the identification of alternative structural or mechanistic features to exploit in the development of a molecule targeting a particular subfamily or individual enzyme. A number of generic, pan-2OG oxygenase inhibitors have been described within the literature, many of which chelate to the active site metal and occupy the 2OG binding site[278]. These include the *N*-oxalyl amino acid *N*-oxalylglycine[279] (**1**, NOG) and its cell-permeable methyl ester derivative dimethyoxalylglycine (**2**, DMOG)[280], 2,4-pyridinedicarboxylic acid (**3,** 2,4-PDCA)[281] and 5-carboxy-8-hydroxyquinoline (**4**, IOX1)[282], (Table 4.1).

Table 4.1 Structures and IC_{50} values for the pan-2OG oxygenase inhibitors NOG **1**, DMOG **2**, 2,4-PDCA **3**, and IOX1 **4,** against a number of 2OG oxygenases. Values in normal type were obtained using MS-based assays, in italics *via* AlphaScreen[382], and underlined using a formaldehyde release assay[252]. ND = not determined.

Compound	IC_{50} / μM	
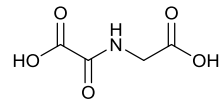 **1** NOG	PHD2	0.8[254], *10*[283]
	FIH	46[254]
	KDM4A	<u>17</u>[254]
	KDM6B	*0.3*[282]
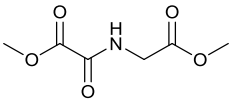 **2** DMOG	PHD2	ND
	FIH	
	KDM4A	
	KDM6B	
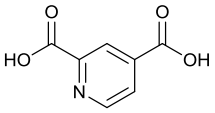 **3** 2,4-PDCA	PHD2	6[261], *28.6*[282]
	FIH	1.1[261], <1[282]
	KDM4A	0.4[261], *1.95*[282]
	KDM6B	*33*[282]
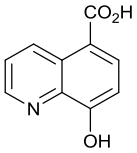 **4** IOX1	PHD2	14.3[261], *14.3*[282]
	FIH	20.5[261], 7.6[282]
	KDM4A	*0.2*[282], 1.7[261]
	KDM6B	*0.14*[282]

While these compounds are not very selective for any single enzyme or subfamily within the 2OG oxygenase superfamily, they are used extensively as tool compounds, often as hypoxia mimics due to their inhibition of the HIF hydroxylase enzymes[280] (Table 4.1). Furthermore, both crystallographic investigation of the interactions of these inhibitors with various 2OG oxygenases and *de novo* structure activity relationship (SAR) studies have enabled their derivatisation to produce more potent and selective inhibitors[278].

4.1.2. Small molecule inhibitors of JmjC-KDMs

The development of small molecule inhibitors of the JmjC-KDMs is a burgeoning clinical area, which has recently been extensively reviewed[284,285]. Although a detailed review of

these inhibitors is beyond the scope of this thesis, both general JmjC-KDM inhibitors and molecules targeting the KDM2, KDM4, KDM5, KDM6 and KDM7 families have been reported, examples of which are discussed below.

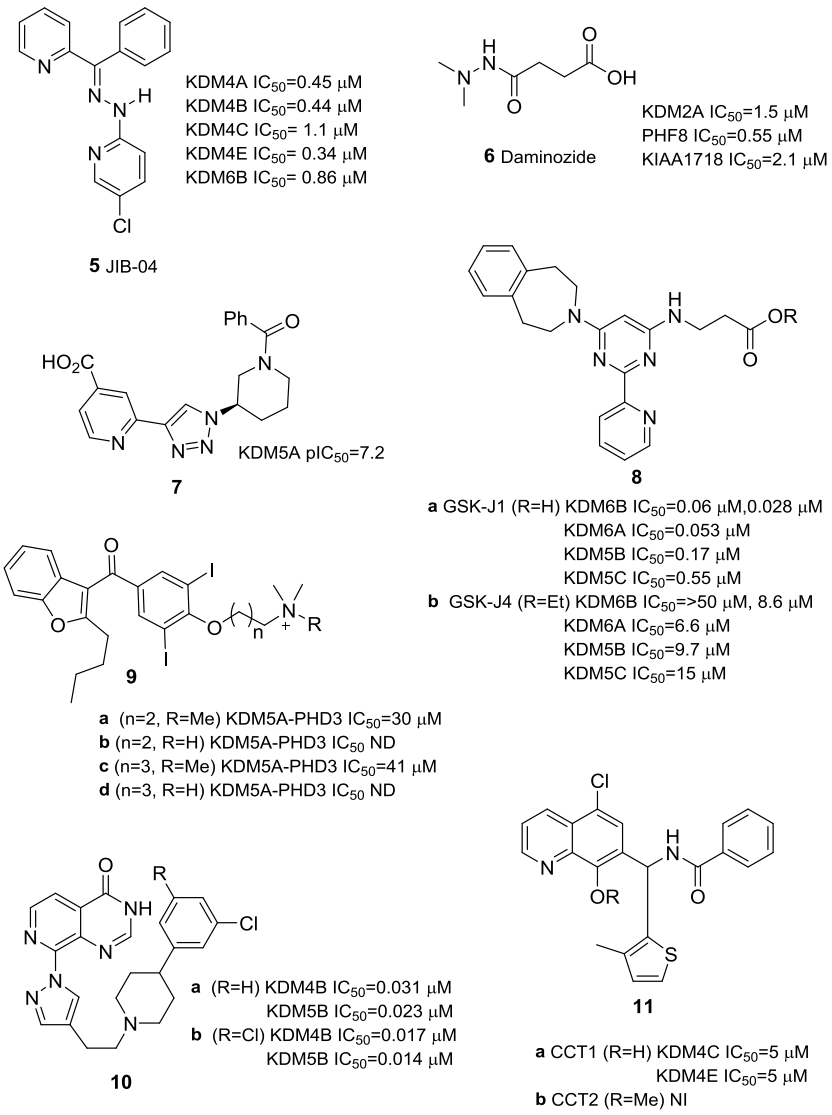

Figure 4.1 Structures and IC_{50} values for example synthetic small molecule inhibitors of the JmjC-KDMs. ND = not determined.

The generic non-2OG competitive JmjC-KDM inhibitor JIB-04 (Figure 4.1, **5**) was identified in a cell-based screen of CMV promoter-driven GFP expression and found to modulate the growth of cancer cells and tumour xenografts in mice[286]. *In vitro* assays confirmed its activity against members of the KDM4, KDM5 and KDM6 subfamilies (IC_{50} values against

KDM4 subfamily members ranging from 0.44-1.1 μM, KDM6B IC_{50} = 0.86 μM), while the TETs and the FAD-dependent demethylase KDM1A remained unaffected[286].

Subfamily-specific inhibitors include the plant-growth regulator daminozide (Figure 4.1, **6**), which inhibits the KDM2/7 subfamily members (KDM2A IC_{50} = 1.5 μM, PHF8 IC_{50} = 0.55 μM) in a 2OG-competitive manner, with approximately 100-fold selectivity over other KDMs[287]. More recently, optimisation of a novel triazolopyridine scaffold yielded a highly potent and selective (pIC_{50}=7.2) inhibitor of KDM2A[288] (Figure 4.1, **7**). As with many other JmjC-KDM inhibitors, this compound was revealed to occupy the 2OG binding site upon co-crystallisation with KDM4A[288]. A further 2OG-competitive inhibitor, the pyridyl-pyrimidine biaryl compound GSK J1 (Figure 4.1, **8a**), along with its cell permeable ester derivative GSK J4 (Figure 4.,1 **8b**), was first identified as a highly potent inhibitor of the KDM6 subfamily (KDM6B IC_{50} = 0.06 μM)[289]. However, subsequent studies by others have found this inhibitor to target KDM5 subfamily members with only approximately 5-fold less potency as against the KDM6 enzymes (KDM5 IC_{50} values ranging from 0.17- 15 μM)[290].

Recent studies on the KDM5 subfamily have targeted domains other than the catalytic JmjC domain. A number of small molecules with high binding affinity for the plant homeodomain finger 3 (PHD3) domain were found to compete for binding with an H3K4me3 peptide, leading to the development of a series of analogues with IC_{50} values of 25-40 μM against KDM5A[291] (Figure 4.1, **9a-d**).

4.1.2.1. KDM4 inhibitors

A number of KDM4 subfamily inhibitors have also recently been identified in the literature. A high-throughput screening campaign highlighted a series of 4-(pyridin-2-yl)thiazol-2-amine compounds as templates for subsequent structure-based optimisation that produced potent and cell-permeable dual inhibitors of KDM4 and KDM5 subfamily members[292]

(Figure 4.1, **10a, b**). Finally, structural insights from co-crystallisation of the broad spectrum 2OG oxygenase inhibitor IOX1 with KDM4A prompted modification of IOX1 at the C-7 position to produce the KDM4-specific inhibitor CCT1 (Figure 4.1, **11a**) and its inactive methylated counterpart CCT2[293] (Figure 4.1, **11b**). CCT1 was verified as a KDM4 inhibitor in HeLa cells transiently overexpressing KDM4A, with an EC_{50} value of 9 μM, demonstrating an approximately 10-fold increase in potency over IOX1 (EC_{50} = 86 μM). Moreover, treatment of patient-derived lung cancer cells with CCT1 reduced their viability (EC_{50}= 6 μM), while patient-matched healthy lung cells were largely unaffected[293].

4.1.3. Endogenous inhibitors of the 2OG oxygenases

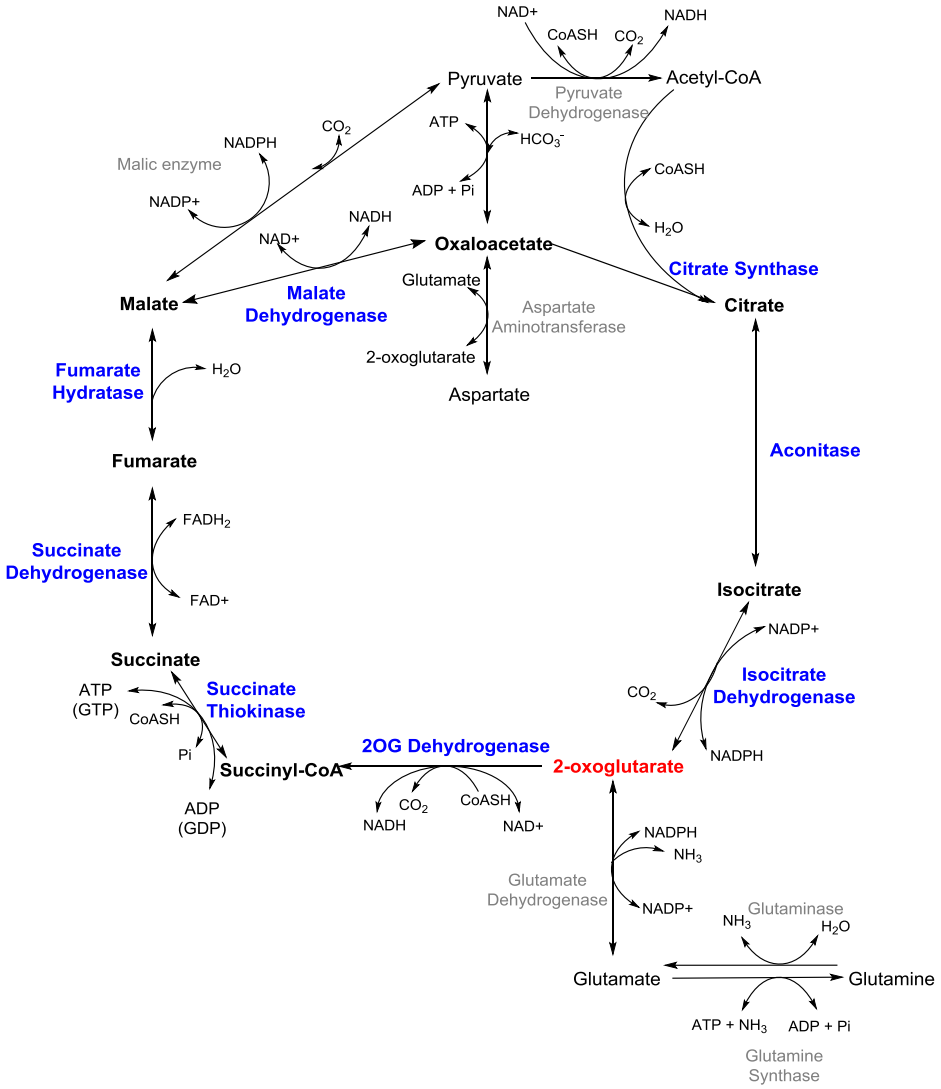

Figure 4.2 The tricarboxylic acid (TCA) cycle. TCA cycle intermediates and enzymes (blue type) are in bold, while related compounds and enzymes (grey) are in normal type. 2OG is highlighted in red.

As well as synthetic inhibitors of 2OG-oxygenases, a number of endogenous compounds have been reported to impact upon their activity. Of note are several tricarboxylic acid (TCA) cycle intermediates, of which 2OG and its oxidative product in the 2OG-oxygenase catalytic cycle, succinate, are members (Figure 4.2). Levels of TCA cycle intermediates may be drastically altered in hypoxia[294,295], hence have been extensively studied in the context of hypoxia and the HIF hydroxylases. Increased levels of succinate (Table 4.2, **12**) and fumarate (Table 4.2, **13**) in tumours carrying mutations in the genes encoding fumarate hydratase and succinate dehydrogenase (Figure 4.2) were found to result in inhibition of the

HIF hydroxylases and upregulation of HIF, potentially leading to increased tumour vascularisation and growth[296–298]. Subsequent molecular studies found fumarate and succinate to bind in the 2OG-binding site of FIH[294] and assessed the inhibitory concentrations of a number of TCA cycle intermediates for the HIF hydroxylases (Table 4.2). Moreover, studies on KDM4E also found succinate and fumarate to be inhibitory at 320 and 2300 μM, respectively[252] (Table 4.2).

Table 4.2 Structures and IC_{50} values for the TCA cycle intermediates succinate **12**, fumarate **13**, isocitrate **14**, and *(R)*-2HG **15** and *(S)*-2HG **16** against a number of 2OG oxygenases. Values in normal type were obtained using MS-based assays, in italics *via* radioactive 2OG-turnover assays[294,299] and underlined using a formaldehyde release assay[252]. # the compound of interest was preincubated with the enzyme for 1 h prior to the enzymatic reaction. NI= non-inhibitory, ND= not determined.

Compound	**IC_{50} /μM**				
	PHD2	**FIH**	**KDM5B**	**KDM4A**	**KDM4E**
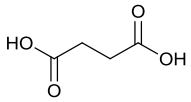 **12** succinate	*19*[#], *>10000*[294] *510*[299]	*NI*[294] *>10000*[299]	ND	ND	<u>320</u>[252]
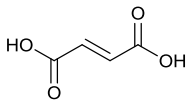 **13** fumarate	*3*[#], *220*[294] *80*[299]	*NI*[294] *>10000*[299]	ND	ND	<u>2300</u>[252]
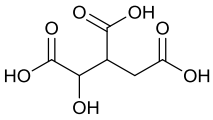 **14** isocitrate	*41*[#], *>10000*[294]	*NI*[294]	ND	ND	ND
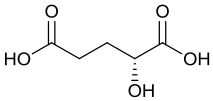 **15** *(R)*-2HG	7300[254]	1500[254]	K_i= 10870[300]	<u>24</u>[254]	ND
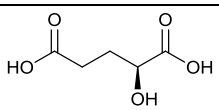 **16** *(S)*-2HG	K_i= 1150[301] 419[254]	189[254]	K_i= 628[300]	<u>26</u>[254]	NM

The isocitrate dehydrogenases (IDHs, Figure 4.2) are also subject to gain-of-function mutations in cancers, resulting in either conversion of 2OG to *(R)*-2-hydroxyglutarate (2HG,

Table 4.2, **15**) or reduced conversion of isocitrate (Table 4.2, **14**) to 2OG[254]. Increased levels of the *(S)*-2HG enantiomer (Table 4.2, **16**) may also be produced. There is conflicting evidence as to whether 2HG production upregulates HIF *via* HIF hydroxylase inhibition[300,302–304]. Indeed, Koivunen *et al.* reported that *(R)*-2HG activates the PHDs by substituting for 2OG, thereby reducing HIF levels in IDH-mutant human astrocyte cells[301]. Further analysis of this showed that the presence of reducing agents, such as L-ascorbate and glutathione, can cause the non-enzymatic oxidation of *(R)*-2HG to 2OG, thereby producing sufficient 2OG for the catalytic activity of the 2OG oxygenases[305]. Despite the controversy surrounding the 2HGs and the HIF hydroxylases, there is general consensus that both *(R)*- and *(S)*-2HG inhibit numerous other 2OG oxygenases in a 2OG-competitive manner, including the TET enzymes[300,301,306], the collagen prolyl hydroxylases[301,304] and the KDMs[254,300,301,307], for several of which *in vitro* IC_{50} values have been determined (Table 4.2).

Notably, the study by Chowdhury *et al.* found that IC_{50} values for isolated KDM4A were 24 and 26 μM for *(R)*- and *(S)*-2HG, respectively, the lowest of the enzymes tested[254]. Subsequent investigation in cells overexpressing KDM4A found dose-dependent inhibition of H3K9me3 demethylation by both enantiomers at 5 and 10 mM[254]. Given that 2HG levels have been shown to reach millimolar concentrations in IDH mutant gliomas[305,308], these results indicate that changes to cellular 2HG concentrations may have a functionally relevant effect on KDM activity and subsequent epigenetic regulation in disease states. Moreover, concentrations of *(S)*-2HG were found to be increased in hypoxia *via* conversion of 2OG by lactate dehydrogenase A (LDHA)[309], prompting the question as to how hypoxic changes to TCA cycle intermediates may affect epigenetic regulation by the KDMs.

4.1.4. Chapter aims

The work described in Chapter 3 revealed that the cellular activity of ectopically expressed KDM4A was reduced in conditions of low oxygen. Although immunofluorescence and western blot experiments (Chapter 3) suggested that this restriction of KDM4A activity was mainly due to lack of oxygen availability, cellular hypoxia is a complex phenomenon, which impacts upon cellular homeostasis in a number of ways. As well as the upregulation of HIF target genes[149], hypoxia also alters the cellular concentration of TCA cycle intermediates[295,309] and reactive oxygen species (ROS, Chapter 5). Therefore, the aim of the experiments described in this chapter was to utilise small molecule inhibitors of the 2OG oxygenases, both synthetic and endogenous, to assess the contribution of changes to the TCA cycle in hypoxia to the observed hypoxic inhibition of cellular KDM4A activity. In order to do so, both cellular and *in vitro* dose-response assays using IOX1 and various cell permeable TCA cycle intermediate derivatives were performed. Overall, these experiments aimed to understand further the extent to which KDM4A is sensitive to oxygen concentration, and how hypoxia-induced changes in cells other than reduced oxygen availability may contribute to altered KDM4A activity, hence histone lysine methylation status and subsequent epigenetic regulation, in hypoxic disease states.

F-KDM4A U2OS cells used in immunofluorescence experiments with IOX1 (Chapter 4.2) were produced and kindly donated by Dr Norma Masson (Ratcliffe Laboratory, NDM, University of Oxford). Dimethyl (R)- and (S)-2HG were synthesised by Pauline Lang during her time as a visiting student in the Schofield Laboratory.

4.2. Hypoxic inhibition of KDM4A: contribution of TCA cycle intermediates

While IOX1 (Table 4.1, **4**) is not a KDM4A-specific inhibitor[282], its status as a 2OG-competitive inhibitor is useful in the context of evaluating the impact of potential changes to the tricarboxylic acid cycle in hypoxia, including alterations in 2OG levels, on the activity of KDM4A. Overall, this analysis was aimed to aid in understanding how factors other than reduced oxygen availability may contribute to the hypoxic inhibition of KDM4A observed in cells (Chapter 3).

To this end, an immunofluorescence experiment in the F-KDM4A U2OS cells used in the analysis of cellular KDM4A activity in hypoxia (Chapter 3.3) was designed to assess the inhibitory effect of IOX1 in normoxia and hypoxia. F-KDM4A U2OS cells were treated with dox, to induce overexpression of *N*-terminally FLAG-tagged KDM4A WT (KDM4A WT), and varying concentrations of IOX1, and then incubated at 1.0 or 21% O_2 for 24 h. Uninduced control cells were also treated with the same IOX1 concentrations and incubated in each condition. After 24 h, cells were fixed and stained for FLAG and H3K9me3 (Chapter 7.2.5), then imaged using an Operetta® high content imaging system (PerkinElmer) and analysed using Harmony™ software (PerkinElmer). Quantification of the percentage H3K9me3 fluorescence in KDM4A-WT overexpressing cells relative to levels in uninduced cells was performed for each concentration of IOX1 investigated in normoxia and hypoxia, and a dose-response curve (relative H3K9me3 vs log[IOX1]) was plotted and used to evaluate the EC_{50} value of IOX1 for KDM4A in each condition (Figure 4.3a).

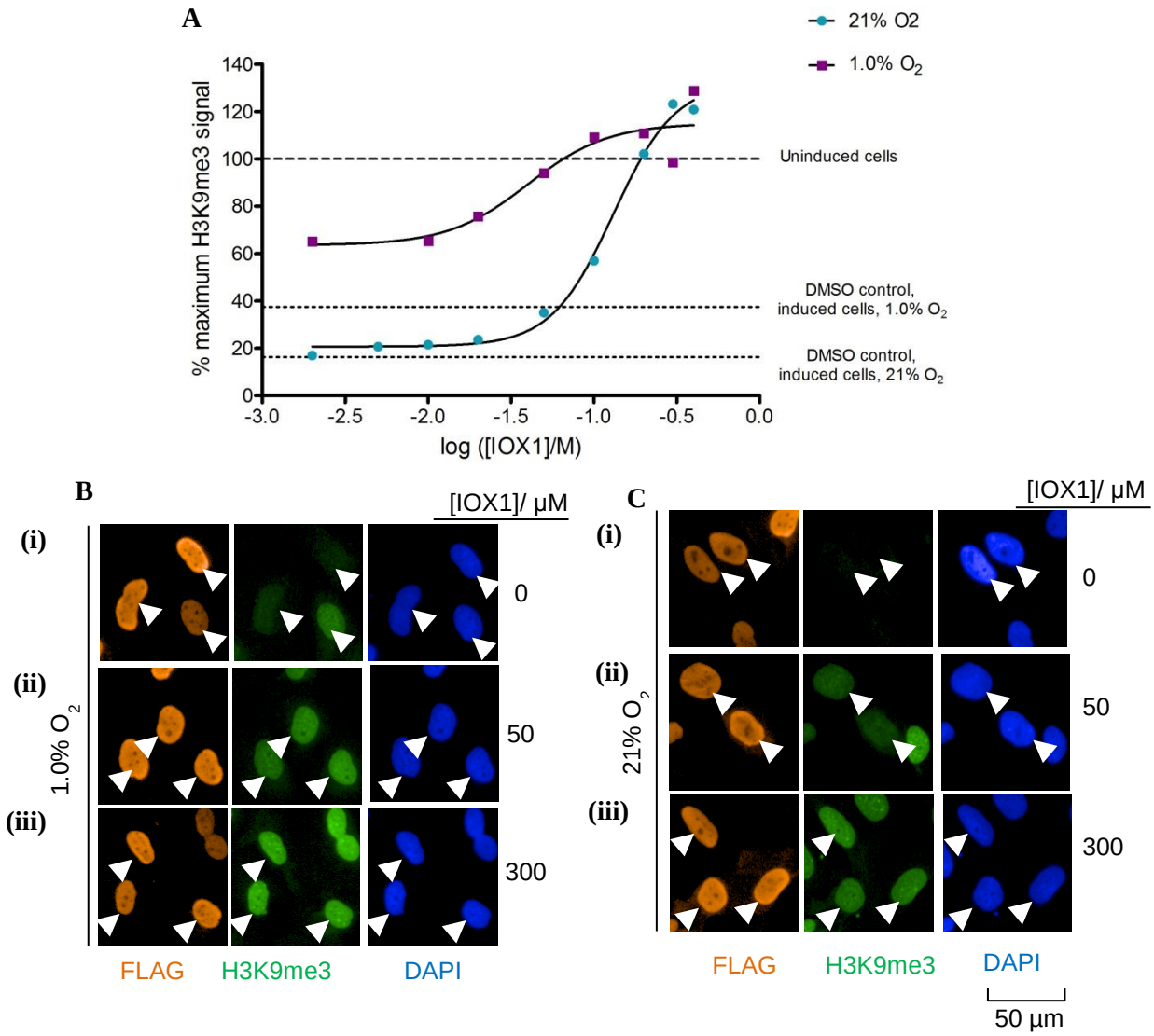

Figure 4.3 A) Dose-response curves for the effect of increasing concentrations of IOX1 on loss of H3K9me3 fluorescence in F-KDM4A U2OS cells overexpressing KDM4A WT and incubated in 21% O_2 (teal circles) and 1.0% O_2 (purple squares). Immunofluorescence analysis was used to evaluate H3K9me3 levels in dox-induced cells, which were normalised relative to those in uninduced cells dosed with the same IOX1 concentration and incubated at the same percentage O_2. % Maximum H3K9me3 fluorescence was plotted against log([IOX1]/M) and fitted to a log[inhibitor] vs response (variable slope) non-linear regression model using GraphPad Prism, v5.04. Error bars (not visible) denote sem, n > 900 cells per point. **B, C)** Representative images from the immunofluorescence analysis of F-KDM4A U2OS cells, dosed with dox and **(i)** 0 μM, **(ii)** 50 μM and **(iii)** 300 μM and incubated at **B)** 1.0% O_2 and **C)** 21% O_2. Cells highly overexpressing FLAG-KDM4A (orange, marked with arrows) were chosen for analysis of H3K9me3 (green) levels. Cells were fixed, stained and imaged at the same time, and images were processed using the same fluorescence parameters.

Table 4.3 Cellular E_{50} values for IOX1 against overexpressed KDM4A WT in F-KDM4A U2OS cells incubated in 1.0 and 21% O_2 for 24 h. Data were fitted to a dose-response non-linear regression model (variable slope) using GraphPad Prism v5.04.

% O_2	EC_{50}(IOX1)/ μM	95% CI/ μM
1.0	39.9	9.59–166
21	131	103–167

As expected, the minimum H3K9me3 levels in KDM4A WT-overexpressing cells incubated in hypoxia were higher than in normoxic cells, indicating reduced KDM4A demethylase activity, as evaluated previously (Chapter 3.3.1). Interestingly, the EC_{50}(IOX1) values for KDM4A demonstrated a clear shift from 131 μM (95% CI = 103–167 μM) in normoxia to 39.9 μM (95% CI= 9.6–166 μM) in hypoxia (Table 4.3). The increased potency of KDM4A in hypoxia is possibly due to reduced competition from endogenous 2OG levels, which have previously been reported to be decreased in hypoxic cells and reduced by up to 90% in ischaemic rat hearts[295,310]. Therefore, *in vitro* inhibition studies were mounted to probe this phenomenon further.

Inhibition of recombinant tKDM4A by IOX1 in the presence of low (10 μM) and high concentrations (100 μM) of 2OG was assessed in both normoxia (21% O_2) and hypoxia (1.0% O_2) using a MALDI-TOF MS assay (Chapter 2.2.1). The low 2OG concentration used was less than the K_m^{app}(2OG) of 26 ± 7 μM evaluated using the same MALDI-TOF MS assay (Chapter 2.3), to enable IOX1 to compete for the binding site easily. These analyses were aimed to evaluate the hypothesis that lack of 2OG in hypoxic cells was responsible for the reduced potency of IOX1, due to decreased competition for the 2OG binding site.

Table 4.4 Conditions used in *in vitro* MALDI-TOF MS-based experiments designed to evaluate IC_{50} values for IOX1 against tKDM4A in 1.0 and 21% O_2.

Reaction component	Final concentration/ μM
tKDM4A	1
Fe^{2+}	10
L-ascorbate	100
2OG	10 or 100
$H3_{1-15}$K9me3 peptide	100

The conditions used for these experiments are detailed in Table 4.4. Hypoxic (1.0 % O_2) experiments were undertaken in an Invivo$_2$ 500 hypoxic workstation using solutions that had been pre-equilibrated at 1.0% O_2 for 24 h to make stock solutions of Fe^{2+}, 2OG, L-ascorbate and $H3_{1-15}$K9me3 peptide. tKDM4A (1 µM) was added to a master mix of $H3_{1-15}$K9me3 peptide (100 µM), 2OG (10 or 100 µM), L-ascorbate (100 µM), Fe^{2+} (10 µM) and IOX1 (varying concentrations) to initiate the demethylase reaction, which was incubated for 5 min, a time point chosen to ensure that the reaction was assessed during its linear range (Chapter 2.3), at 37 °C. Reactions were then quenched with MeOH, and the extent of demethylation of the $H3_{1-15}$K9me3 peptide was assessed using MALDI-TOF MS (Chapter 7.1.5).

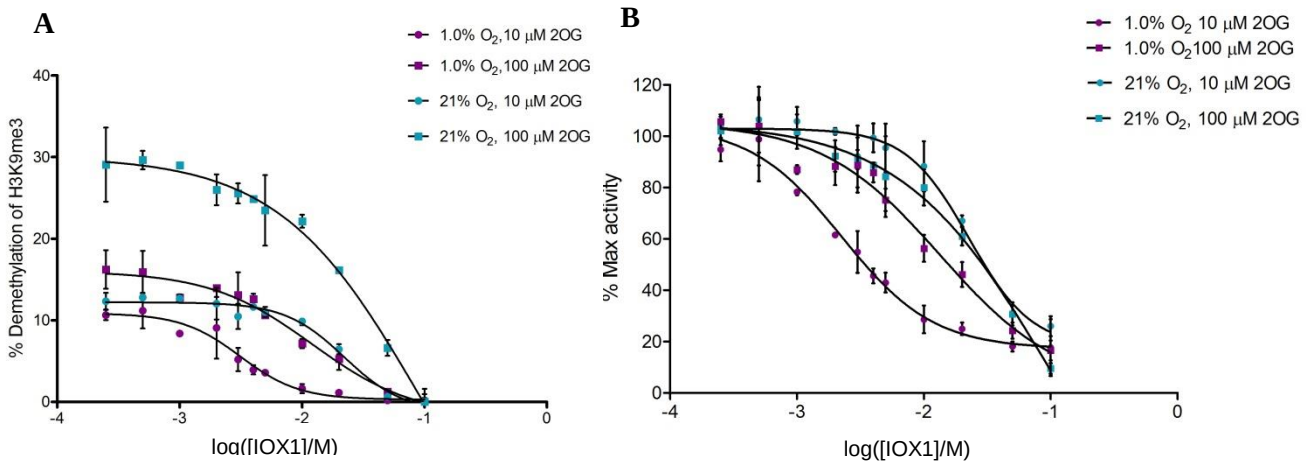

Figure 4.4 Dose-response curves for the effect of increasing concentrations of IOX1 on the activity of tKDM4A against an $H3_{1-15}$K9me3 peptide, under conditions of 1.0% O_2 (purple) and 21% O_2 (teal) in the presence of 10 µM (circles) or 100 µM (squares) 2OG. **A)** Percentage demethylation of $H3_{1-15}$K9me3 was evaluated using MALDI-TOF MS plotted against log([IOX1]. **B)** Data was transformed by normalising the percentage demethylation of $H3_{1-15}$K9me3 against that in a control experiment dosed with 1.0% DMSO under the same O_2 and 2OG concentrations. Data was fitted to a log[inhibitor] vs response (variable slope) non-linear regression using GraphPad Prism, v5.04. Error bars denote sd, n=3 technical repeats.

Table 4.5 *In vitro* IC_{50} values for IOX1 against recombinant tKDM4A WT in 1.0% and 21% O_2 under conditions of low (10 µM) and high (100 µM) 2OG, as evaluated using a MALDI-TOF MS assay. Data were fitted to a log[inhibitor] vs response (variable slope) non-linear regression model using GraphPad Prism v5.04. K_m^{app}(2OG) = 23 ± 7 µM, K_m^{app}($H3_{1-15}$H3K9me3)= 25 ± 3 µM (Chapter 2.3).

% O_2	[2OG]/ µM	IC_{50}(IOX1)/ µM	95% CI/ µM
1.0	10	2.6	1.59–3.21
	100	13.5	5.36–34.1
21	10	22.6	15.0–34.2
	100	94.6	10.2–879

The results of these experiments revealed that the IC_{50} values of IOX1 under normoxia, were 22.6 µM in the presence of 10 µM 2OG, and approximately 4 x higher at 94.6 µM with 100 µM 2OG (Figure 4.4, Table 4.5). This confirms that IOX1 inhibition is dependent on the concentration of 2OG, as expected from the 2OG competitive binding of IOX1 observed in crystallographic studies[261]. This trend was also observable in 1.0% O_2: the IC_{50} of IOX1 was 2.6 µM with 10 µM 2OG, increasing to 13.5 µM in the presence of saturating conditions of 100 µM 2OG (Table 4.5). Interestingly, under each 2OG concentration tested *in vitro*, the IC_{50} values in hypoxia were lower than the values evaluated in normoxia, mirroring the trend observed in the cellular experiments (Figure 4.3).

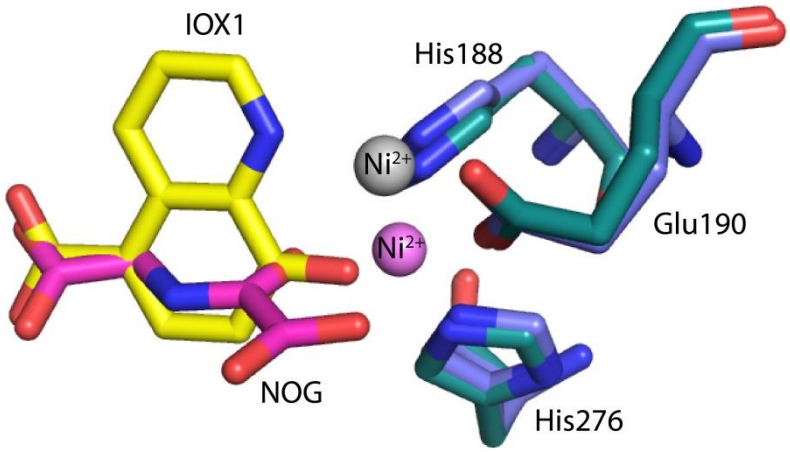

Figure 4.5 View from the crystal structure of IOX1 (yellow) bound in the active site of KDM4A (blue residues, PDB ID 3NJY) overlaid with that of NOG (pink) bound to KDM4A (teal residues, PDB ID 2OQ6). Binding of IOX1 to KDM4A causes a translocation of the bound metal (Ni^{2+}, grey) from its usual position when 2OG/NOG is bound (Ni^{2+}, pink). IOX1 binds in a position such that it occupies both the 2OG and putative O_2 binding sites.

Overall, these results suggest that, both oxygen availability and 2OG concentration have an impact on the inhibitory potency of IOX1. At 1.0% O_2 KDM4A is not saturated with respect to oxygen (Chapter 2.4), therefore the rate of reaction is limited, which may contribute to the increased inhibition by IOX1 observed. Furthermore, inspection of the crystal structure of KDM4A bound to IOX1 reveals that, as well as mimicking the bidentate metal chelation of the metal centre by NOG, which is thought to bind in the same manner as 2OG[145], IOX1 may

also compete for binding in the O_2 binding site (Figure 4.5). Furthermore, binding of IOX1 to KDM4A also appears to result in translocation of the metal centre when compared to its position when NOG is present[282] (Figure 4.5). Kinetic analysis has confirmed that IOX1 is a mixed-mode inhibitor, both competing for the 2OG-binding site and disrupting the binding of prime substrate, as well as displaying tight-binding inhibitory behaviour[261]. As binding of prime substrate is thought to be necessary to induce O_2 binding during 2OG oxygenase-catalysed reactions, disruption of peptide binding may also affect the binding of O_2. Taken together, both the limited rate of reaction of KDM4A in hypoxia and the mixed-mode inhibitory behaviour of IOX1 may explain the additive effects of lack of oxygen and reduced 2OG availability in decreasing the inhibitory concentration of IOX1 in hypoxia.

While these experiments provide some evidence that 2OG availability may play a role in limiting KDM4A activity in hypoxia in cells, further experiments were undertaken to confirm this and investigate the impact of other TCA cycle intermediates and 2OG-mimetic inhibitors on KDM4A activity. The compounds selected for investigation were the cell-permeable TCA-cycle ester derivatives dimethyl (dm) 2OG (**17**), dm succinate (**18**), dm *(S)*-2HG (**19**), dm *(R)*-2HG (**20**), *n*-octyl *(S)*-2HG (**21**) and *n*-octyl *(R)*-2HG (**22**) (Figure 4.6). IOX1 was also tested to validate the transient transfection system used.

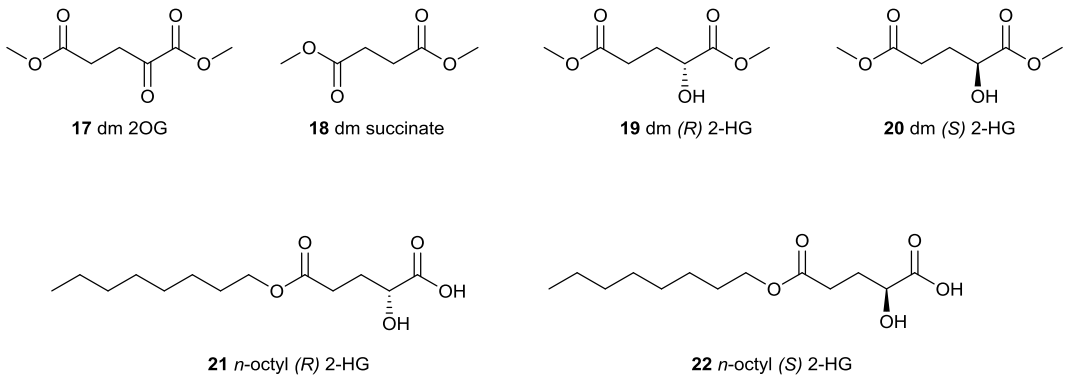

Figure 4.6 Structures of the ester derivatives of the TCA cycle intermediates tested in cellular dose-response experiments.

Primary experiments in F-KDM4A U2OS cells showed no dose response for any of the compounds tested (data not shown), likely because of the very high levels of KDM4A WT overexpression in these cells resulting in an increased inhibitory concentration of the compound. Therefore, transiently transfected U2OS cells were used in an attempt to achieve 'dosable' levels of KDM4A overexpression, and to provide a catalytically-inactive KDM4A control to minimise the potential confounding effect of dox-induction. U2OS cells were transiently transfected with pcDNA3 encoding FLAG-KDM4A WT or FLAG-KDM4A MUT using FuGENE® HD and a 4 h transfection time (Chapter 3. 2.2, Chapter 7.2.2). After 4 h, cell media was changed to DMEM containing the relevant dose of the compound of interest and 1.0% DMSO. The 2HG esters (Figure 4.6, **19, 20, 21, 22**) were also dissolved in HEPES pH 7.0, in order to maintain the pH of the cell media, hence in experiments using these compounds, all cell media contained 0.5 mM HEPES pH 7.0. Cells were then incubated at 21% O_2 or 1.0% O_2 for 24 h, then fixed, stained for FLAG and H3K9me3, and imaged as described previously (Chapter 3, Chapter 7.2.6). H3K9me3 fluorescence levels in KDM4A-overexpressing cells were measured and plotted as a function of the log of the concentration of the compound of interest (Figure 4.7, Figure 4.8, Figure 4.9). As an indicator of the maximum possible KDM4A activity, H3K9me3 fluorescence in DMSO-control treated KDM4A WT-transfected cells was also evaluated, levels above which in compound-treated cells would indicate inhibition of KDM4A activity. H3K9me3 levels in untreated KDM4A MUT-transfected cells were also calculated and used as a baseline to detect endogenous effects of the compounds, observable as H3K9me3 fluorescence above this level.

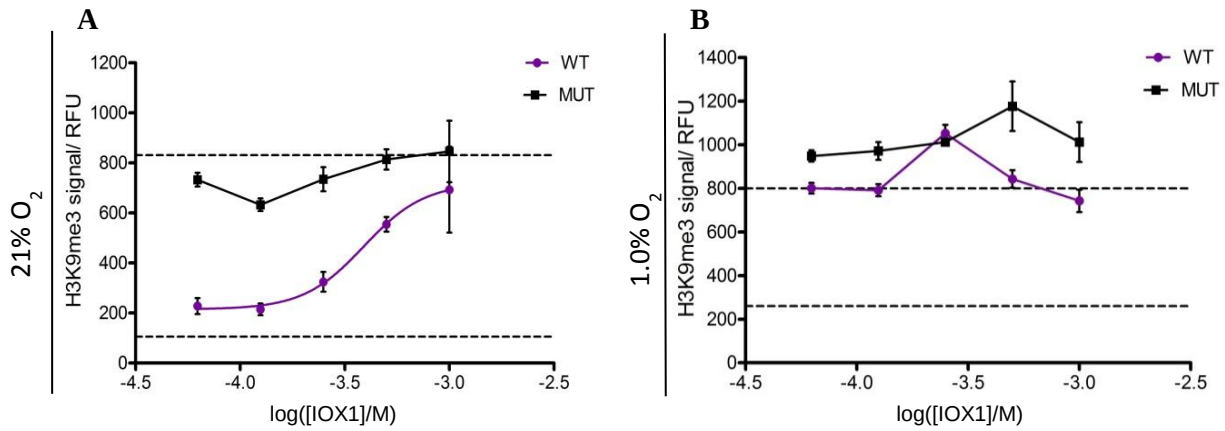

Figure 4.7 Dose response curves for IOX1 in U2OS cells transiently overexpressing KDM4A WT (purple squares) or KDM4A MUT (black squares) and incubated in **A)** 21% O_2 or **B)** 1.0% O_2 for 24 h. Immunofluorescence was used to evaluate H3K9me3 fluorescence, which was then plotted against log[IOX1]. EC_{50} values were calculated using a log[inhibitor] vs response (variable slope) non-linear regression model in GraphPad Prism v5.04. Baseline fluorescence in untreated KDM4A WT cells is represented by the lower dashed line, while H3K9me3 fluorescence in untreated KDM4A MUT cells is plotted as the upper dashed line. Error bars represent s.e.m, n > 50 cells.

The results of the experiments with IOX1 showed a similar trend to that observed in the F-KDM4A U2OS cells (Figure 4.3), namely that IOX1 demonstrates increased inhibition of KDM4A in hypoxia (Figure 4.7b). A dose-response curve was generated in normoxia (Figure 4.6a), and yielded an EC_{50} value of 391 μM (95% CI = 137–1110 μM), which, although higher than that obtained in normoxic F-KDM4A U2OS cells (Table 4.3), is apparently less inhibitory than in cells incubated at 1.0% O_2, for which an IC_{50} value could not be evaluated (Figure 4.7b). Indeed, in hypoxia, each concentration of IOX1 tested proved inhibitory, increasing the measured H3K9me3 fluorescence in KDM4A WT-transfected cells to levels approximately equal to those in KDM4A MUT-transfected cells (Figure 4.7b). Therefore, lower concentrations of IOX1 should be tested in this system to evaluate the EC_{50} in hypoxia. However, this experiment demonstrated that the transiently transfected system was suitable for use in evaluating the inhibitory effect of the compounds of interest.

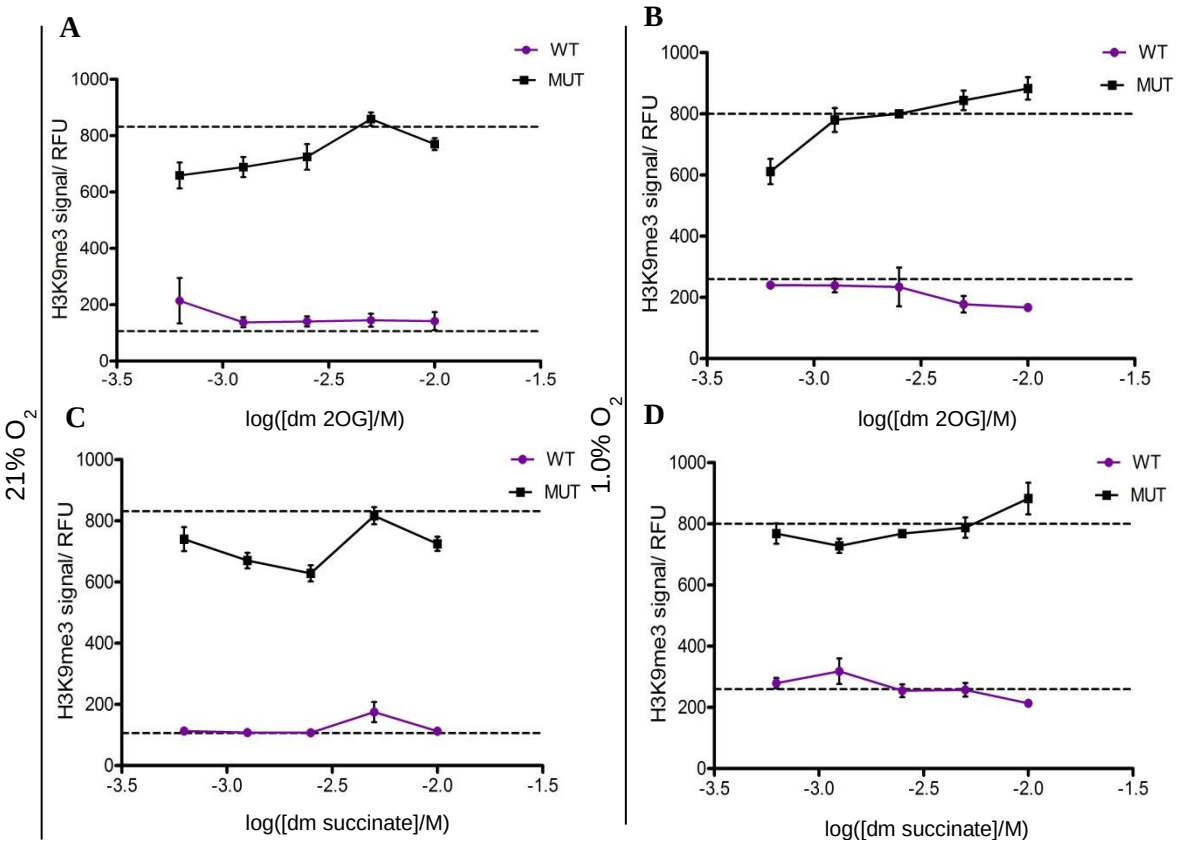

Figure 4.8 Dose response curves for **A, B)** dm 2OG and **C, D)** dm succinate in U2OS cells transiently overexpressing KDM4A WT (purple squares) or KDM4A MUT (black squares) and incubated in **A, C)** 21% O_2 or **B, D)** 1.0% O_2 for 24 h. Immunofluorescence-evaluated H3K9me3 fluorescence was plotted against log[inhibitor/ M] using GraphPad Prism v5.04. Baseline fluorescence in untreated KDM4A WT cells is represented by the lower dashed line, while H3K9me3 fluorescence in untreated KDM4A MUT cells is plotted as the upper dashed line on each graph. Error bars represent s.e.m, n >10 cells in each case.

KDM4A WT-transfected cells dosed with dm 2OG (Figure 4.6, **17**) showed a negligible increase in H3K9me3 fluorescence in normoxia, and an increased loss of H3K9me3 levels in hypoxia at concentrations above 2.5 mM, although a general, dose-dependent increase in H3K9me3 fluorescence in KDM4A MUT-transfected cells. (Figure 4.8a, b). This suggests increased activity of KDM4A WT on dosing with dm 2OG in hypoxia, indicating that 2OG availability may limit cellular KDM4A activity under conditions of low oxygen. Conversely, dosing cells overexpressing both KDM4A WT and KDM4A MUT with dm succinate (Figure 4.6, **18**) resulted in no significant changes to H3K9me3 levels compared to baseline levels in both normoxia and hypoxia (Figure 4.8c, d).

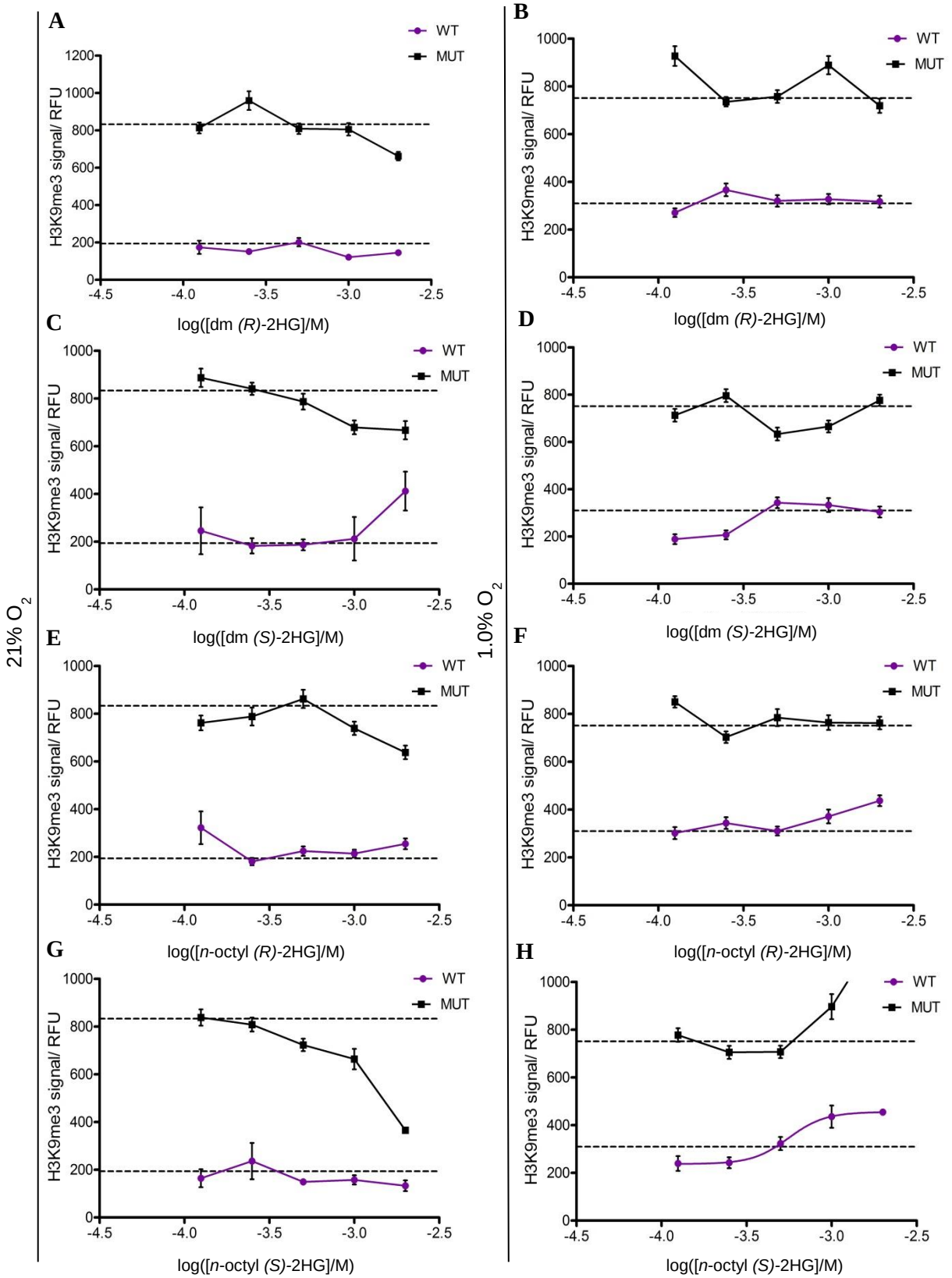

Figure 4.9 Dose response curves for **A, B)** dm *(R)*-2HG **C, D)** dm *(S)*-2HG, **E, F)** *n*-octyl *(R)*-2HG and **G, H)** *n*-octyl *(S)*-2HG in U2OS cells transiently overexpressing KDM4A WT (purple squares) or KDM4A MUT (black squares) and incubated in **A, C, E, G)** 21% O_2 or **B, D, F, H)** 1.0% O_2 for 24 h. Immunofluorescence was used to evaluate H3K9me3 fluorescence, which was then plotted against log([inhibitor/M]) using GraphPad Prism v5.04. Baseline fluorescence in untreated KDM4A WT cells is represented by the lower dashed line, while H3K9me3 fluorescence in untreated KDM4A MUT cells is plotted as the upper dashed line in each graph. Error bars represent s.e.m, n>10 cells in each case. Data for *n*-octyl *(S)*-2HG in hypoxic KDM4A WT-transfected cells, **H)** was fitted to a dose response (variable slope) linear regression model using GraphPad Prism v5.04.

All four 2HG compounds tested (dm *(R)*-2HG, dm *(S)*-2HG, *n*-octyl *(R)*-2HG and *n*-octyl *(S)*-2HG) resulted in only minimal changes to H3K9me3 fluorescence in cells overexpressing KDM4A WT in normoxia (Figure 4.9a, c, e, g), with the exception of dm *(S)*-2HG, which was inhibitory at the maximum concentration (2mM, Figure 4.9c). However, although, dm *(S)*-2HG and dm *(R)*-2HG were also not inhibitory in KDM4A WT-transfected cells incubated at 1.0% O_2 (Figure 4.9b, d), their *n*-octyl ester counterparts did result in some inhibition of KDM4A WT at concentrations greater than 0.5 mM (Figure 4.9f, h), suggesting increased cell permeability conferred by the *n*-octyl group[311]. Indeed, the data from cells dosed with *n*-octyl *(S)*-2HG and incubated at 1.0% O_2 was able to be fitted to a dose-response curve using GraphPad Prism, producing an EC_{50} value of 558 μM (95% CI= 435–732 μM), in concordance with previous reports that hypoxic increases to *(S)*-2HG concentrations resulted in altered H3K9 methylation[309]. However, an increased number of data points is necessary to improve the fit of the dose-response model and improve the accuracy of the EC_{50} value obtained. Furthermore, H3K9me3 levels in KDM4A MUT-transfected cells incubated in hypoxia also show an increase at high concentrations of *n*-octyl *(S)*-2HG, suggesting an endogenous effect of the compound on the H3K9me3 mark. Interestingly, in normoxia, all four 2HG compounds tested appear to result in loss of H3K9me3 fluorescence in KDM4A MUT-overexpressing cell when dosed at high concentrations (Figure 4.9a, c, e, g), again indicating possible endogenous effects of these compounds. However, similar changes were not apparent in hypoxia (Figure 4.9b, d, f, h). Further investigation is therefore necessary to verify these changes and understand the mechanisms behind them.

Overall, the results obtained (Figure 4.9) indicate that the cellular inhibitory concentrations of the 2HGs against KDM4A WT are likely to be in the hundred μM- mM range, as was previously reported in cellular experiments using HeLa cells ectopically expressing

KDM4A[254]. In certain cancer cell lines, mutation to IDH enzymes has been shown to increase *(R)*-2HG levels to up to 10 mM[308], a concentration which is likely to inhibit KDM activity, thereby leading to changes to histone lysine methylation, which has also been previously reported[307].

4.3. Small molecule 2OG oxygenase inhibitors in cardiac hypertrophy

The previously reported involvement of KDM4A in cardiac hypertrophy (CH)[239] raises the question as to whether KDM4A could be a therapeutic target in this disease state. CH is a marker of heart failure[312] (HF), a condition affecting over 500,000 people in the UK[313]. Current treatment strategies for HF include the use of pharmacological agents aimed at preventing hypertension, a major determinant of HF, including angiotensin converting enzyme inhibitors (ACEis), angiotensin receptor blockers (ARBs) and β-blockers[314]. Recent additions to the therapeutic arsenal against HF also include inhibitors against neprilysin, the enzyme responsible for cleavage of the natriuretic peptides, which stimulate vasodilation and natriuresis[315]. Moreover, a novel inhibitor, LCZ696, combining ARB and neprilysin inhibitor moieties was found to possess increased efficacy over ACEi treatment in HF patients[316], hence therapeutic strategies mimicking this mode of action have been recommended by the European Society of Cardiology[314].

Despite these therapeutic advances, further understanding and better preventative strategies against HF are required[317]. CH is both symptomatic of and a risk factor for HF, in particular HF with preserved ejection fraction[318], a disease with increasing prevalence and morbidity and mortality rates[317], therapies targeting CH in combination with current pharmacological strategies have been proposed[319]. Increased understanding of the molecular pathways underlying CH has revealed a multitude of redundant signalling pathways, highlighting the need for therapeutic agents that are able to target several pathways at once, or so-called ‘distal nodes’ at which pathways converge[319]. Epigenetic targets may present such a strategy

due to their potential impact on the transcription of numerous genes[320]. Indeed, histone acetylation has previously been explored in the context of CH, revealing inhibition of HDACs to blunt the hypertrophic response, encompassing both cell growth and expression of hypertrophy-related genes, to various stimuli[321–324], as well as reversing established hypertrophy in a mouse model[324]. Further exploration of epigenetic pathways may therefore be of significance to furthering understanding of the mechanisms underlying CH and alternative preventative strategies.

The work discussed throughout Chapters 2 and 3 of this thesis highlights the potential pathological effects of the hypoxic inhibition of KDM4A, *via* which hypermethylation of histone lysine residues is likely to lead to an altered epigenetic signature. Conversely, the reported involvement of KDM4A in CH[239,325] comprises its increased expression and catalytic activity against H3K9me3 at the *FHL1* promoter to induce overexpression of the cardiac stress sensor FHL1[239]. However, in both cases, altered KDM4A activity may ultimately lead to aberrant expression of disease-related genes. In the case of CH, pharmacological inhibition of KDM4A in order to prevent its activity at the *FHL1* promoter is of potential therapeutic benefit. Therefore, investigations were mounted to validate KDM4A as a therapeutic target in CH, as well as exploring the role of various other 2OG oxygenases in this disease state *via* the use of a panel of inhibitors. This was work undertaken as a collaborative project with Dr Tim McKinsey (University of Colorado, Denver).

The McKinsey Laboratory has developed a high-throughput, phenotypic cell-based assay in neonatal rat ventricular myocytes (NRVMs) for the investigation of the biological pathways involved in the development of CH[326]. Dosing of the NRVMs with phenylephrine (PE), a known agonist of CH, induces a hypertrophic response, which can be measured using cell-based imaging techniques and RT-qPCR analysis of known CH biomarkers, including Atrial

Natriuretic Factor (ANF, Figure 4.10). Addition of compounds with known targets to the cells +/- PE can inform on the pathways involved in the development of, or protection against, CH.

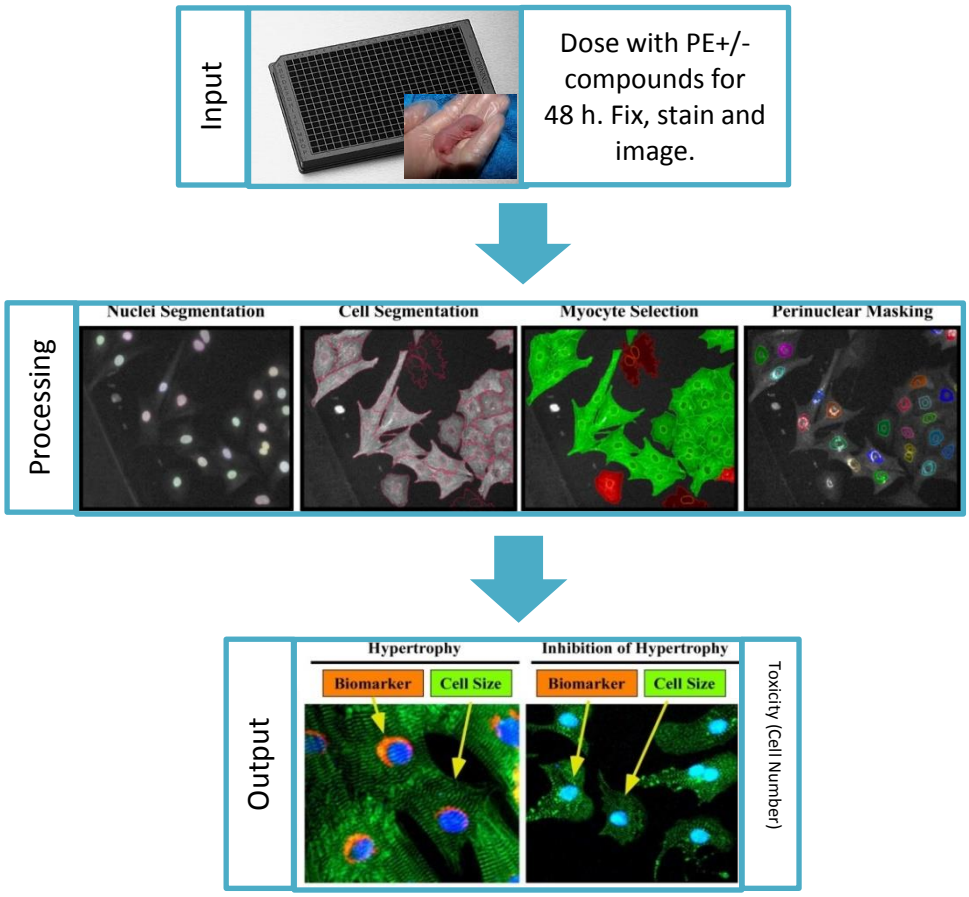

Figure 4.10 Workflow of the cellular cardiac hypertrophy assay developed by the McKinsey Lab, University of Colorado, Denver. Neonatal rat ventricular myocytes were treated with PE and compounds of interest, and then stained for α-actinin (green) and the hypertrophic biomarker ANF (orange). Cell nuclei were stained using Hoescht dye (blue). Cells were imaged and analysed using an Operetta® high content imaging system and analysed using Harmony™ software (PerkinElmer). Figures adapted from Reid *et al.*[326] with permission from the authors.

Compounds of interest are added to the NRVMs in the presence and absence of PE. After 48 h dosing, cells are fixed, stained and imaged using an Operetta® high content imaging system (PerkinElmer). Images are then analysed using software that has been programmed to identify cardiomyocytes and the perinuclear envelope therein; following which measurement of cell area and ANF-staining in the perinuclear envelope facilitates quantification of the

hypertrophic response[326]. RT-qPCR measurement of *ANF* gene expression is also used to validate the phenotypic assay results.

A number of 2OG oxygenase inhibitors were screened by Matthew Stratton, McKinsey Laboratory, University of Colorado, Denver. This inhibitor panel comprised both the pan-2OG oxygenase inhibitors DMOG[280] and IOX1[282] **4, (**Table 4.1), the generic JmjC-KDM JIB-04[286] (Figure 4.1, **5**) and inhibitors that have been reported as specific to a particular subfamily or individual enzyme, including CCT1 and CCT2[293] (Figure 4.1, **11a, 11b**). While a complete set of results from this screen is pending at the time of writing, preliminary RT-qPCR analyses of *ANF* expression with the KDM4-subfamily inhibitor CCT1 and its inactive counterpart CCT2 have been performed.

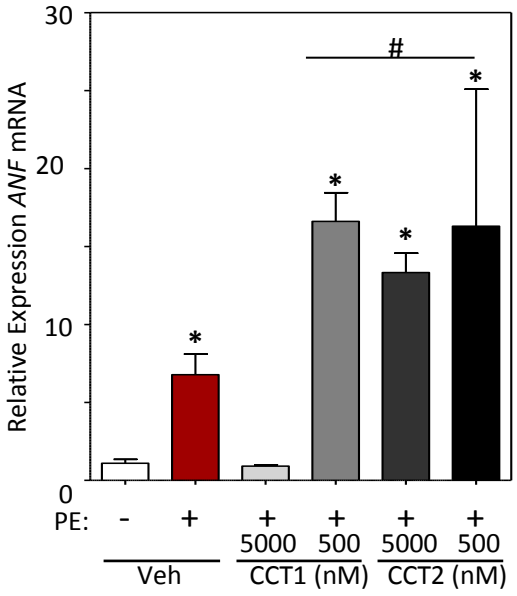

Figure 4.11 Results of the RT-qPCR analysis of *ANF* expression in NRVMs dosed with phenylephrine (PE) ± 500 or 5000 nM CCT1 and CCT2. Figure produced by Dr Tim McKinsey, University of Colorado, Denver.

Dosing of NRVMs with 5 µM CCT1/CCT2 ± PE showed that the PE-induced upregulation of *ANF* was almost completely abrogated by CCT1, while CCT2 showed an increase in ANF expression. However, at a concentration of 500 nM, both CCT1 and CCT2 appeared to increase *ANF* expression above the level induced by PE, indicating a pro-hypertrophic mode

of action (Figure 4.11). The differences observed at different dosing concentrations are likely due to off-target effects of CCT1 and CCT2 at the lower concentration tested, promoting *ANF* upregulation. However, at higher concentrations when KDM4 demethylases are likely inhibited[293], *ANF* upregulation is also inhibited. These results suggest that inhibition of KDM4 demethylases may protect against CH, although further testing in the phenotypic imaging assay (Figure 4.10) is required to confirm this, along with knock-out experiments to verify that the abrogation of ANF upregulation occurs *via* inhibition of KDM4A by CCT1. The results from the full panel of 2OG oxygenase inhibitors submitted to this screen will be informative in evaluating the specificity of the response of CCT1 in the ANF expression assay. Orthogonal assays, such as ChIP of KDM4A and H3K9me3 at the *ANF* and *FHL1* promoters to assess the mode by which KDM4A may promote hypertrophic gene expression in the NRVMs, would also be informative in validating KDM4A as a therapeutic target in CH. Moreover, the potential off-target effects of CCT1 at low concentrations would need to be addressed in order to progress with a drug-discovery programme targeting KDM4A, necessitating the development of more potent and specific KDM4A inhibitors.

4.4. Discussion

The experiments described in this chapter used small-molecule inhibitors of KDM4A to investigate the contribution of factors other than direct lack of oxygen availability on the catalytic activity of KDM4A in hypoxia. The pan-2OG oxygenase, 2OG-mimetic inhibitor IOX1 (Table 4.1, **4**) and dm 2OG (Figure 4.6, **17**) were used to assess the effect of potential changes to 2OG availability in hypoxia[295] on KDM4A activity, while a number of TCA cycle intermediate derivatives, in particular *(R)*- and *(S)*-2HG were also tested, to evaluate the effect of perturbations of the TCA cycle in hypoxia[295,309].

IOX1 was found to possess increased potency against KDM4A in cells incubated at 1.0% O_2 compared to those incubated at 21% O_2, indicating possible reduced competition for the

2OG or O_2 binding sites in hypoxia (Figure 4.5). However, further investigation of the inhibition of isolated tKDM4A by IOX1 under different O_2 and 2OG concentrations found that reduced O_2 availability increased the IC_{50} value obtained for IOX1 with KDM4A, independently of 2OG concentration. It is possible that this is because IOX1 is a mixed-mode 2OG oxygenase inhibitor, which binds in both the 2OG- and substrate binding sites of KDM4A, disrupting O_2 binding and resulting in reduced competition for the KDM4A active site in hypoxia. Moreover, a reduced rate of demethylation by KDM4A under non-saturating O_2 conditions is also likely to contribute to increased inhibition by IOX1 in hypoxia.

Subsequent evaluation of the effect of the cell permeable dimethyl ester derivative of 2OG, dm 2OG (Figure 4.6, **17**), demonstrated a small increase in demethylation of H3K9me3 by overexpressed KDM4A WT in U2OS cells incubated in 1.0% O_2 (Figure 4.8b), indicating that reduced 2OG concentrations may well limit KDM4A activity in hypoxia. The K_m^{app}(2OG) value evaluated for tKDM4A (Chapter 2.3) is relatively low at 26.7 μM, while the $K_m^{app}(O_2)$ of 173 ± 23 μM is high compared to that of other 2OG oxygenases (Chapter 2.1, Chapter 2.4). Taken together, these *in vitro* values suggest that reduced O_2 availability is likely to affect KDM4A activity more profoundly than reduction in 2OG levels. However, the cellular results indicate that reduction in 2OG concentration may contribute to the loss of KDM4A activity in hypoxic cells observed in Chapter 3, resulting in an increase in global H3K9me3 levels, which may result in aberrant gene expression in hypoxia.

Investigation of a number of additional cell permeable ester derivatives of TCA cycle intermediates shown to inhibit several 2OG oxygenases (Table 4.2), revealed that succinate (Figure 4.8c, d) and both *(R)*- and *(S)*-enantiomers of 2HG (Figure 4.9a-h) are not potent inhibitors of KDM4A. However, a small increase in the inhibition of KDM4A WT in hypoxia by the *n*-octyl esters of the 2HGs tested suggests that reduced 2OG concentrations, hence reduced competition for the 2OG-binding site, under conditions of low oxygen may

increase the susceptibility of KDM4A to inhibition by 2OG-competitive inhibitors in hypoxia, as observed with IOX1 (Figure 4.3). This inhibition may contribute to the loss of KDM4A catalytic activity observed in hypoxic cells (Chapter 3.2, 3.3), although the high concentrations necessary to inhibit KDM4A activity suggest this contribution to be minimal. Further investigation *via* metabolomics would enable the relative levels of 2OG and other TCA cycle intermediates to be assessed in normoxia and hypoxia, thereby further increasing understanding of how these may change in hypoxia and ultimately affect the activity of the 2OG oxygenases.

The observed differential inhibition of KDM4A in hypoxia by 2OG-mimetic inhibitors may be of therapeutic benefit. The increased potency of inhibitors under conditions of low oxygen may be exploited in targeting KDM4A in hypoxic disease states, such as cancer and cardiovascular disease, in which KDM4A activity results in pathophysiological consequences[239,327]. However, this differential inhibition may only apply to 2OG-mimetic inhibitors, many of which target numerous 2OG oxygenases. Further study and development of KDM4-subfamily specific inhibitors (e.g. CCT1, Figure 4.1, **11a**) is necessary to ascertain the feasibility and utility of KDM4A-specific inhibition in disease states.

Investigation of the inhibition of KDM4A in a cellular model of CH (Dr Tim McKinsey, University of Colorado, Denver, Chapter 4.3), produced promising preliminary results. RT-qPCR analysis of expression of *ANF*, a biomarker of CH[230,231] upon dosing of cells with phenylephrine, a known hypertrophic agonist, in conjunction with CCT1 and CCT2 (Figure 4.1, **11a** and **11b**, respectively) showed that CCT1 blunted the hypertrophic response at 5 μM, while CCT2 had minimal effects (Figure 4.11), suggesting that targeting KDM4A in CH may be of therapeutic benefit. However, dosing at 500 nM produced an increased hypertrophic response (Figure 4.11), indicating off-target effects. The development of more potent and specific KDM4A inhibitors, along with further cellular investigation, would aid in

understanding the mode of action of CCT1 in this case, and in validating KDM4A as a therapeutic target in CH. However, these early results suggest that modulation of KDM activity may be of therapeutic benefit in this disease state, in which KDM4A has been shown to contribute to the aberrant expression of disease-related genes *via* its catalytic demethylase activity[239]. Numerous studies have revealed altered histone post-translational modifications in cardiovascular disease states including cardiac hypertrophy, cardiomyopathy and heart failure[233–238] (Chapter 1.6); hence intervention at the epigenetic level may present a promising therapeutic strategy in multiple indications, and the continued advancement of small-molecule inhibitors of the KDMs could ultimately add to the clinical arsenal against these diseases.

Chapter 5: The effect of reactive oxygen species on the activity of KDM4A

5.1. Introduction

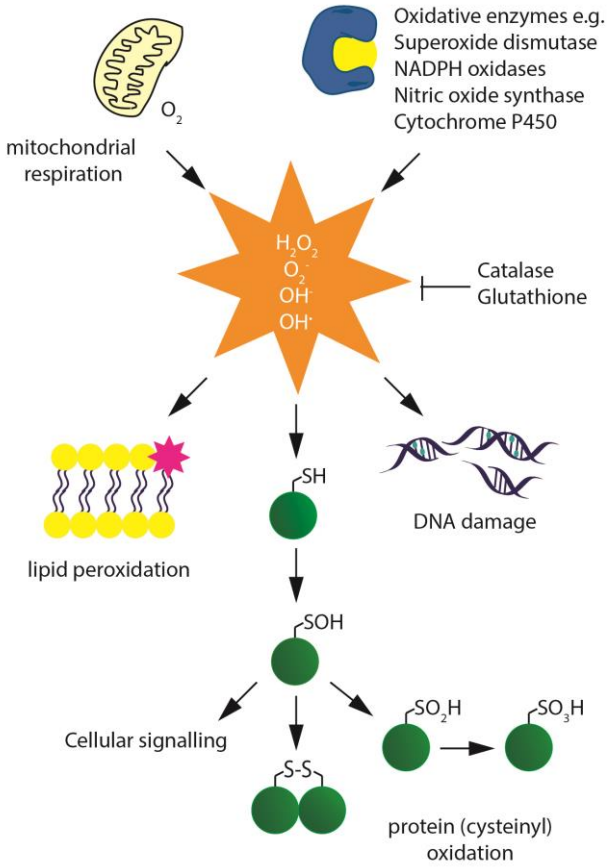

Figure 5.1 Biological sources and consequences of ROS production.

Reactive oxygen species (ROS) are highly reactive small molecules that may be generated during the course of many cellular processes. Mitochondrial respiration involves the two-electron reduction of molecular oxygen to produce water, but can also result in the one-electron reduction of oxygen to produce a superoxide radical anion, which is a precursor of hydrogen peroxide *via* dismutation by superoxide dismutase[328–331]. The reactions of several enzymes including NADPH oxidases, nitric oxide synthase and cytochrome P450

enzymes[332–334] also result in the production of ROS, as do many cellular stresses. One such stress is hypoxia, during which increased production of ROS by the mitochondria has been observed in mammalian cell cultures[335]. However, further study demonstrated that isolated mitochondria exposed to hypoxia did not increase their ROS output, suggesting that factors external to the mitochondria, such as activation of NADPH oxidase and synthesis of NO, trigger increased ROS production in hypoxia[336,337]. Elevated ROS levels are thought to contribute to the cellular response to hypoxia, *via* activation of signalling cascades that both stabilise HIF and reduce oxygen demand[338–340].

ROS also participate in other cellular signalling pathways, such as autophagy[341,342] and kinase signalling[338,343], often *via* oxidation of lipids or redox-sensitive amino acid residues in proteins, resulting in changes to protein stability, localisation, activity and interactions, and presenting numerous methods of signal transduction[333]. One such amino acid is cysteine, the thiol group of which may be oxidised to sulfenic acid, which may then form a disulfide bridge with other cysteine residues, or be further oxidised to sulfinic or sulfonic acids (Figure 5.1), depending on its protein environment, pK_a, solvent exposure and accessibility to ROS[343]. While this is often a mechanism of cellular signalling, the propensity of ROS to react with cysteinyl residues and other redox-sensitive chemical moieties can also be damaging to cells. The presence of antioxidant systems such as glutathione and catalase is designed to scavenge and neutralise ROS, but under certain conditions, excess ROS, particularly H_2O_2, which is readily able to diffuse across intra-cellular membranes, may escape reduction and exert pathological effects. Non-specific oxidation of cysteine can result in the misfolding[344] or aggregation of proteins due to processes including the formation of disulfide bridges, while methionine may also be oxidised[345], but a major mechanism of ROS-mediated cell damage is the oxidation of iron, which resides either in labile intracellular pools, or in iron-sulfur (Fe-S) clusters[345,346]. These clusters are comprised of sulfide-linked

Fe ions in various oxidation states and are found in a wide range of metalloproteins. Both superoxide, O_2^-, and H_2O_2 can release Fe^{2+} from these clusters, which is itself damaging[346]. Furthermore, reaction of H_2O_2 with Fe^{2+} *via* the Fenton reaction (Equation 5.1), results in the production of a highly reactive hydroxyl radical, which may proceed in further harmful oxidative reactions with proteins and lipids and DNA[343].

$$Fe^{2+} + H_2O_2 \rightarrow Fe^{3+} + OH^- + OH\bullet \qquad \textbf{5.1}$$

The deleterious effects of ROS have been linked to the development of cancer *via* DNA damage leading to mutagenesis and chromosomal instability, and aberrant signal transduction[347,348]. Oxidative stress has also been implicated in the pathophysiology of neurodegenerative diseases such as Parkinson's disease and Alzheimer's disease[344]. Moreover, it is of particular note to this thesis that there is substantial evidence for the involvement of ROS in cardiovascular disease states including ischaemia-reperfusion injury[349–351], atherosclerosis[352], heart failure[353,354], and cardiac hypertrophy[355–358]. The role of ROS in the development of these diseases has largely been attributed to dysregulation of ROS-dependent signalling pathways resulting in, amongst other pathological changes, metabolic dysfunction, vascular remodelling and the induction of cellular apoptosis[349,351,353,359,360]. Whilst many of these pathological mechanisms are well understood, therapeutic strategies for the prevention of ROS-induced cardiovascular disease are limited[351], with minimal success of antioxidant therapy[349,350,358,360] and pre- or post-conditioning strategies involving brief cycles of ischaemia-reperfusion prior to an ischaemic insult[361,362] in the clinic. Therefore, further exploration into the deleterious effects of ROS is required to enable the discovery of "druggable targets" in this context[350,363].

Recent studies have begun to ascertain the effect of ROS on epigenetic factors. ROS-mediated activation of the MAPK pathway has been shown to have an impact on chromatin remodelling *via* changes to H3 phosphorylation[364] and histone acetylation[365,366]. ROS also

affect DNA methylation status in a number of ways. Firstly, oxidative stress-induced DNA damage has been proposed to affect DNA methyltransferase (DNMT) activity, as the damaged DNA is no longer a viable substrate for these enzymes, leading to DNA hypomethylation[367]. Furthermore, ROS have been shown to reduce cellular levels of the universal methyl donor *S*-adenosylmethionine (SAM), which is a co-factor in the reaction of the DNMT enzymes, hence resulting in reduced DNMT activity under oxidative stress[368]. Interestingly, TET1-mediated DNA demethylation was shown to be protective against H_2O_2-induced death of mouse cerebellar granule cells[369]. Moreover, H_2O_2 treatment of human embryonic carcinoma cells induced DNA damage and increased binding of the DNA-methyltransferase DNMT1 to the chromatin, which subsequently lead to an increase in chromatin bound levels of the deacetylase SIRT1 and members of the Polycomb repressor (PcG) complex at CpG-islands, with ultimate gene silencing and concomitant changes to histone methylation status at the affected gene promoters[370]. Global histone lysine methylation levels, particularly at H3K9, H3K4 and H3K27, and DNA methylation levels were found to be increased in BEAS-2B cells following exposure to H_2O_2[371]. Pre-treatment of cells with ascorbate was found to somewhat ameliorate changes to histone lysine methylation status, hence Niu *et al.* proposed that this increase in histone methylation was due to oxidation of the Fe^{2+} co-factor to Fe^{3+} resulting in reduced demethylase activity of the JmjC-KDMs. Indeed, use of a cell-free system with increased levels of Fe^{2+} and ascorbate appeared to increase demethylation of H3K4, providing evidence to support this hypothesis[371]. However, the direct effect of H_2O_2 on the activity of individual KDMs remains to be investigated.

In a similar experiment, the effect of ROS on the related 2OG oxygenases PHD2 & FIH was investigated. U2OS cells stably overexpressing HIF were dosed with 10 μM *tert*-butyl hydroperoxide over 3 h and demonstrated inhibition of asparaginyl hydroxylation by FIH,

whereas PHD2-catalysed prolyl hydroxylation was only modestly inhibited[372]. This may relate to their hypoxia sensitivities; FIH activity is maintained at lower concentrations of oxygen than PHD2 activity, both in cells and *in vitro*[173], indicating that the hypoxia-derived increase in ROS may provide a mode of HIF regulation that is distinct from reduction in oxygen availability. Depletion of chelatable Fe^{2+} by treatment of cells with iron chelators ablated inhibition of FIH by peroxide, suggesting that this inhibition may be, at least in part, due to oxidation of Fe^{2+} *via* Fenton chemistry (Equation 5.1)[372]. However, further work is required to fully understand the effect of peroxide on FIH and the differential effect on the HIF hydroxylase enzymes. Previous work in the group (Dr Lars Hillringhaus, unpublished data) evaluated the *in vitro* sensitivity of FIH and PHD2 to H_2O_2, and found that preincubation of the enzymes with H_2O_2 inhibited the activity of FIH, but not PHD2, producing IC_{50} values of 161 ± 1.4 μM and > 10 mM, respectively. This is in accordance with the cellular experiments described above, and again demonstrates differential H_2O_2 sensitivity across the 2OG oxygenase enzymes.

5.1.1. Chapter aims

The work described in Chapter 3 of this thesis demonstrated that KDM4A activity is attenuated in hypoxia. While *in vitro* experiments (Chapter 2) revealed that the activity of the isolated enzyme is highly sensitive to oxygen availability, cellular hypoxia does not purely constitute reduced oxygen tension, but also changes to the TCA cycle (Chapters 3 & 4) and increased ROS production, as discussed above. Given the recent literature demonstrating changes to histone methylation under oxidative stress, and the results of prior investigation of the effect of ROS on the HIF hydroxylases, thorough investigation of the impact of ROS, in the form of H_2O_2, on the demethylase activity of KDM4A was undertaken, in order to ascertain whether ROS may contribute to hypoxic loss of KDM4A activity in cells.

Preliminary experiments to determine the sensitivity of tKDM4A towards peroxide (Chapter 5.2) were carried out with Ms Monica Esteban, a summer student under my supervision. In vitro inhibition experiments using PHD2 and FIH were performed by Dr Lars Hillringhaus (a former member of the Schofield Laboratory, University of Oxford). The iron quantification assay (Chapter 5.3.2) was performed according to a protocol provided by Dr Mark White (Chapter 7.1.2). Recombinant PHD2 and FIH for use in the stability experiments (Chapter 5.3.5) were kindly provided by Dr Tom McAllister and Dr Adam Hardy (Kawamura/Schofield Groups, University of Oxford). The F-KDM4A U2OS cells used in cellular experiments were produced and kindly donated by Dr Norma Masson (Ratcliffe Laboratory, NDM, University of Oxford).

5.2. Preliminary work & assay development

In an initial assessment of ROS on KDM4A, assays were developed (in conjunction with Monica Esteban) to investigate the effect of hydrogen peroxide on both the stability and activity of the enzyme. As hydrogen peroxide could impact on KDM4A *via* both oxidation of the enzyme itself and oxidation of the Fe^{2+} co-factor, both reducing the available Fe^{2+} and producing the hydroxyl radical $OH^{\bullet}$, it was important to configure assays to be able to explore these factors. Furthermore, the presence of the reducing agent L-ascorbate in *in vitro* assays of 2OG oxygenases has been postulated to ameliorate the effects of reactive oxygen species or oxidation of Fe^{2+},[371], hence was a further factor for investigation.

5.2.1. Inhibition of tKDM4A by H_2O_2

Preliminary experiments were conducted with recombinant tKDM4A, prepared according to the standard protocol (Chapter 7.1.2). A MALDI-TOF activity assay was developed to enable a dose-response curve for H_2O_2 to be generated in two different contexts; the first in which KDM4A was introduced to a master mix of reaction components [$H3_{1\text{-}15}$K9me3

peptide substrate, (100 μM), Fe^{2+} (10 μM), 2OG (100 μM) and L-ascorbate (100 μM)] containing H_2O_2, and the second in which tKDM4A, 2OG and L-ascorbate were preincubated with H_2O_2 prior to initiation of the reaction with Fe^{2+} and $H3_{1-15}K9me3$ peptide substrate (Chapter 7.1.5). The percentage maximum activity was plotted against concentration of H_2O_2 in order to calculate the IC_{50} value.

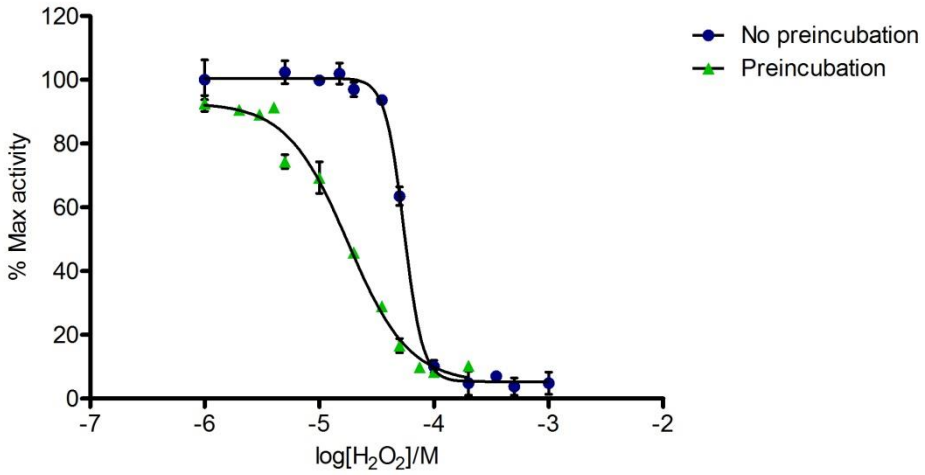

Figure 5.2 IC_{50} curves for tKDM4A with peroxide under different conditions. tKDM4A was preincubated at 37 °C with H_2O_2 (green triangles) or added to a reaction mix containing H_2O_2 (blue circles). The IC_{50}s of H_2O_2 for tKDM4A were revealed to be 16.9 μM (95% CI = 12.6–22.6 μM) and 54.7 μM (95% CI = 52.6–57.0 μM), respectively. Data was plotted, fitted and analysed using GraphPad Prism v5.04. N = 3 biological repeats, error bars denote sd.

Preincubation of the enzyme with H_2O_2 produced an IC_{50} of 16.9 μM (95% CI = 12.6–22.6 μM), compared to an IC_{50} value of 54.7 μM (95% CI = 52.6–57.0 μM) when the enzyme was introduced to the reaction mix containing H_2O_2. These differences suggest alternative mechanisms of inhibition under the two different reaction conditions. Direct addition of H_2O_2 to the enzyme proved more inhibitory, suggesting oxidative damage to the enzyme. Conversely, the introduction of peroxide to the reaction mix containing Fe^{2+} likely results in oxidation of the iron *via* Fenton chemistry (equation 5.1), depleting H_2O_2 concentration before the addition of enzyme, thereby ameliorating the effects of peroxide on the enzyme itself.

5.2.2. The effect of H_2O_2 on the stability and oligomerisation of tKDM4A

The effect of H_2O_2 on the stability of tKDM4A was then assessed using SDS-PAGE. The enzyme was incubated with H_2O_2 under different conditions (Table 5.1) for 30 min at 37°C, with total reaction volume of 10 µL. The reaction was quenched with 2 x SDS loading buffer (Chapter 7.1.3) without the addition of a reducing agent to ensure that any oxidation of the protein by H_2O_2 was not reversed.

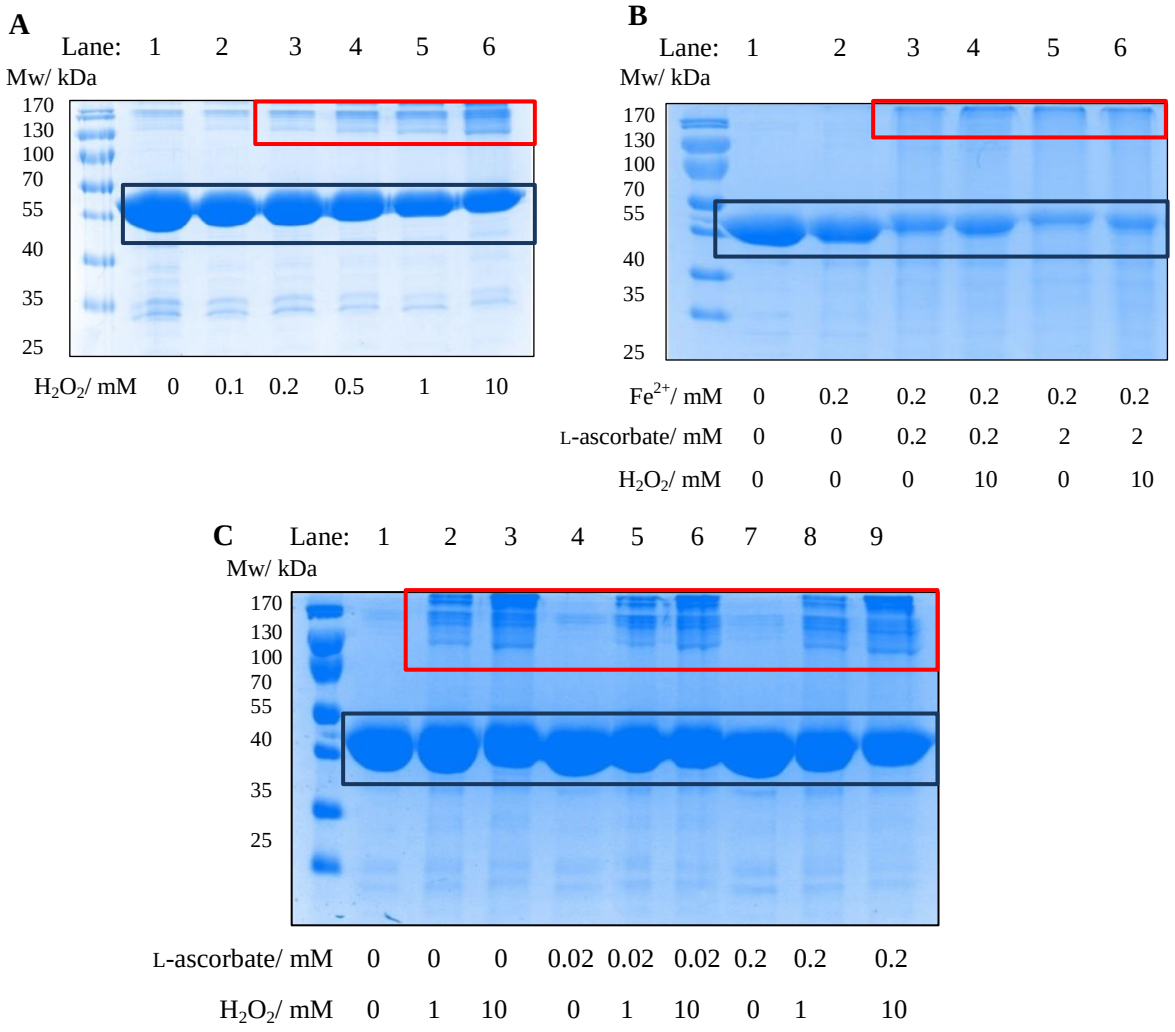

Figure 5.3 SDS-PAGE gels reveal that addition of H_2O_2 and/or a mixture of Fe^{2+} and L-ascorbate is damaging to tKDM4A, causing aggregation of the protein. Bands highlighted in dark blue correspond to intact tKDM4A, while bands highlighted in red are tKDM4A aggregates or precipitates. In each case, lane 1 was loaded with a pre-stained molecular weight ladder. **A)** Increasing concentrations of H_2O_2 cause an apparently-dose dependent aggregation of tKDM4A. **B)** Addition of both Fe^{2+} and L-ascorbate at equimolar concentrations (10 x enzyme concentration) induces aggregation of tKDM4A, while further addition of peroxide does not appear to have an additive effect. Addition of Fe^{2+}alone produced no perceptible effect on the enzyme. **C)** The addition of L-ascorbate to tKDM4A does not appear to be protective against damage induced by H_2O_2.

First, 0.1-10 mM H_2O_2 was titrated against 10 µg tKDM4A (at a concentration of 20 µM) and incubated for 30 min, to assess whether there was a dose-dependent effect on the enzyme's structural integrity. It was found that H_2O_2 concentrations above 0.5 mM (Figure 5.3a, lanes 4-7) led to aggregation of the protein, with an apparent increase in aggregation observed at higher concentrations. Due to the possibility of Fenton reactions occurring, and to the proposed protective role of ascorbate, Fe^{2+} and L-ascorbate were also incubated with the protein, in the presence and absence of H_2O_2, and the effect on tKDM4A stability was also evaluated using SDS-PAGE. In standard MALDI-TOF activity assay conditions, Fe^{2+} is present at 10 x the enzyme concentration, with L-ascorbate present at 100 x [tKDM4A]. In the stability assays, the ratio of enzyme:Fe^{2+} was maintained at 1:10, whilst L-ascorbate was added stoichiometrically, or in 10- or 100-fold excess of the protein (20 µM, 200 µM or 2 mM, respectively). The addition of Fe^{2+} alone (i.e. no H_2O_2 was present, Figure 5.3b, lane 3) did not cause any demonstrable aggregation of tKDM4A, but aggregation was induced, rather than protected against, by the further addition of either 200 µM or 2 mM L-ascorbate (Figure 5.3b, lanes 4 and 6). This may be due to a previously described oxidative reaction of Fe^{2+} and L-ascorbate in solutions containing molecular oxygen, potentially giving rise to Fe^{3+}-L-ascorbate complexes and other reactive oxygen species, including H_2O_2[373], which could then oxidise redox-sensitive amino acid residues within the protein. In concordance with this, L-ascorbate did not appear to protect tKDM4A against H_2O_2-induced aggregation (Figure 5.3c, lanes 5-10).

These preliminary results indicated that tKDM4A is sensitive to H_2O_2, which exerts adverse effects on both its activity and stability. However, the effect of the presence of an unknown concentration of Fe^{2+} in the enzyme stock remained a confounding factor in inhibition assays, due to the possibility of Fenton chemistry under both sets of conditions. Therefore, the preparation of apo-tKDM4A (i.e. tKDM4A containing no active site metal) was deemed

necessary for full evaluation of the effects of oxidation by both H_2O_2 and Fe^{2+} on the enzyme.

5.3. Apo-tKDM4A

The preliminary peroxide inhibition data (Chapter 5.2) was generated using a preparation of tKDM4A that likely co-purified with residual iron[110] (Figure 5.5). Whilst the differences in peroxide IC_{50} obtained under the different reaction conditions were striking, it is possible that residual iron present in the enzyme stock may have confounded the results due to a dual mechanism of action taking place during the preincubation; both oxidation of the enzyme and oxidation of Fe^{2+}. This metal oxidation could have a number of effects, either blunting the oxidation of the enzyme *via* competitive reaction with H_2O_2, or production of other ROS that also exert an effect on the tKDM4A. Therefore, investigation of the effect of ROS on the apo-enzyme was necessary.

5.3.1. Development of a method to produce apo-tKDM4A

It was first necessary to develop and optimise a protocol for the production of apo-tKDM4A. Initial experiments followed a procedure developed in the lab for the production of apo-PHD2[85,374]. After metal-ion affinity FPLC purification of tKDM4A from *E. Coli* lysate on a His-Trap column (Chapter 7.1.2), selected fractions were pooled and incubated overnight with 100 mM EDTA at 4°C, with a final protein concentration of 1 $mg.mL^{-1}$[185]. However, this was found to cause significant precipitation of the enzyme, with insufficient soluble protein remaining to submit to further purification *via* gel filtration FPLC. The soluble protein was concentrated and desalted using a PD10 column to remove residual EDTA, and was stored for further analysis of purity and activity.

The protocol was adapted to use 1 mM EDTA in the incubation step, which was intended as a less harsh alternative. However, enzyme precipitation still occurred and resulted in

insufficient protein for further purification *via* size exclusion chromatography (Chapter 7.1.2). SDS-PAGE analysis revealed the presence of apparent aggregation products following both protocols (Figure 5.4, lanes 2 & 3), confirming the detrimental effect of direct EDTA-treatment on tKDM4A stability.

As direct addition of EDTA to tKDM4A during purification was found to result in protein precipitation, dialysis of previously purified tKDM4A against EDTA was attempted. tKDM4A at a concentration of 9.3 $mg.mL^{-1}$ was dialysed against 10 mM EDTA in dialysis buffer (50 mM HEPES pH 7.5, 500 mM NaCl) for 16 h at 4 °C, followed by dialysis for a further 16 h against dialysis buffer containing approximately 2 $mg.mL^{-1}$ chelex, to ensure against the presence of any metal ions. This gentler method did not cause visible precipitation or aggregation of the protein (Figure 5.4, lane 4), and tKDM4A at a concentration of 5.8 $mg.mL^{-1}$ was recovered and flash-frozen in liquid N_2 and stored at –80 °C for use in experiments.

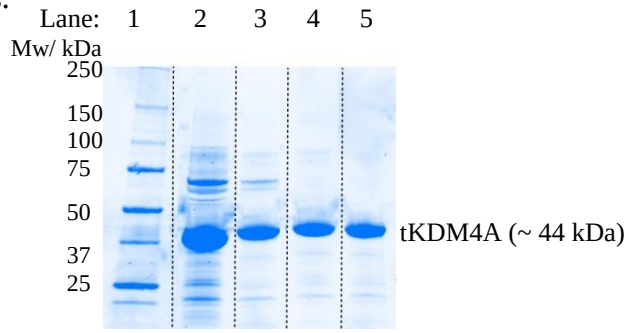

Figure 5.4 SDS-PAGE gel to assess the integrity of different preparations of tKDM4A upon treatment to remove co-purified Fe^{2+}. Lane 1: Molecular weight ladder. Lane 2: tKDM4A treated overnight with 100 mM EDTA. Lane 3: tKDM4A treated overnight with 1 mM EDTA. Lane 4: EDTA-dialysed tKDM4A. Lane 5: untreated tKDM4A. Only relevant lanes from SDS-PAGE gel analysis are shown: dotted lines show where image has been cropped to remove blank lanes.

5.3.2. Iron quantification

To verify that EDTA treatment had removed all residual iron from the enzyme, an iron quantification assay using bathophenanthroline disulfonic acid and potassium metabisulfite was performed. This is a colourimetric assay requiring the use of a standard curve of

preparations of $FeSO_4$ in order to quantify Fe^{2+} in unknown samples (Chapter 7.1.2), and was carried out on 100 μM samples from an untreated tKDM4A preparation, EDTA-incubated tKDM4A (1 mM EDTA, Figure 5.4 lane 3) and EDTA-dialysed tKDM4A (Figure 5.4 lane 4). The results demonstrated clear differences in the iron content of the preparations and confirmed the lack of Fe^{2+} in EDTA-dialysed tKDM4A, while direct incubation of tKDM4A removed only approximately 78% of co-purified iron (Figure 5.5).

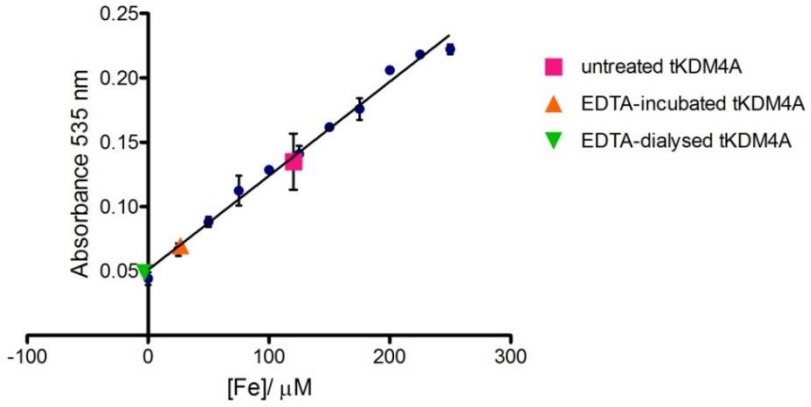

Figure 5.5 An Fe^{2+} occupancy test on protein samples from three preparations of tKDM4A revealed residual co-purified Fe^{2+} in both untreated and EDTA-incubated samples, while dialysis of previously purified tKDM4A against EDTA removed all discernible Fe^{2+}. n = 3 technical repeats, error bars denote sd.

Having successfully produced apo-tKDM4A, its activity then needed to be assessed to ensure its viability in inhibition assays. The extent of demethylation of an $H3_{1\text{-}15}K9me3$ peptide (Chapter 2.2, Chapter 7.1.4) after 5 min by both the EDTA-incubated (1 mM) and EDTA-dialysed tKDM4A preparations under standard conditions (Chapter 2.2, Chapter 7.1.5), but with both 10 μM and 50 μM Fe^{2+}, was evaluated using a standard MALDI-TOF activity assay (Chapter 2.2), in order to compare their activity.

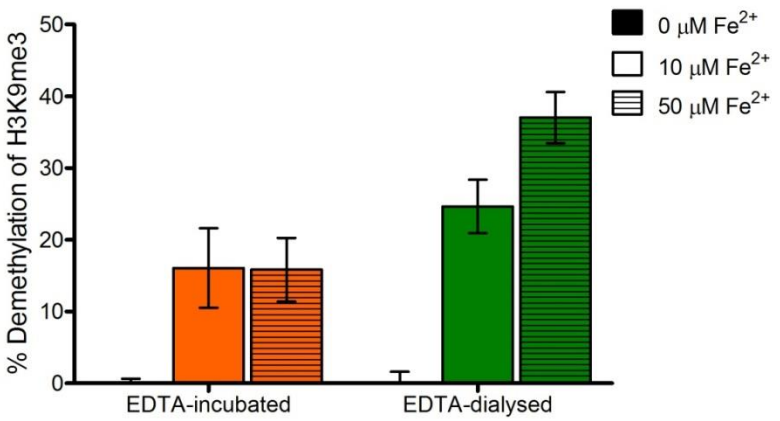

Figure 5.6 A standard MALDI-TOF MS assay was used to assess the activity of the EDTA-incubated tKDM4A (orange) and the EDTA-dialysed tKDM4A (green) preparations with 0 μM (black bars, not seen) 10 μM (plain bars) and 50 μM (striped bars) Fe^{2+}. n = 3 technical repeats, error bars represent sd.

The results of this assay revealed that, under the same standard conditions, the EDTA-dialysed tKDM4A displayed increased demethylase activity compared to that of EDTA-incubated enzyme (Figure 5.6). The reasons for this may be two-fold; firstly, the more gentle dialysis method resulted in less precipitation of the enzyme, hence there is likely more correctly folded, active enzyme present in the dialysed tKDM4A preparation than in the EDTA-incubated preparation, and secondly, EDTA treatment removes both co-purified Fe^{2+} and other residual metal ions that may be bound to the active site. Ni^{2+} is known to leach from the HisTrap column during enzyme purification, and is able to bind to the tKDM4A active site[145], hence competes with Fe^{2+}. As EDTA-dialysis was more efficient in removing Fe^{2+} from tKDM4A, it may be that it also removed residual Ni^{2+}, therefore increasing its activity. The addition of 50 μM Fe^{2+} (Figure 5.6, striped bars) also increased the activity of the EDTA-dialysed tKDM4A preparation compared to 10 μM Fe^{2+} (Figure 5.6, plain bars), likely due to increased Fe^{2+} occupancy of the tKDM4A active site. However, to maintain consistency with previous experiments, 10 μM Fe^{2+} was used in all subsequent experiments. Finally, the omission of Fe^{2+} (Figure 5.6, black bars) from these experiments resulted in a lack of activity of both enzyme preparations, confirming the need for the addition of exogenous Fe^{2+} in subsequent experiments.

5.3.3. The effect of H_2O_2 on the activity of apo-tKDM4A

The successfully purified and active apo-tKDM4A was submitted to the previously developed inhibition and stability assays with H_2O_2 (Chapter 5.2). Interestingly, addition of H_2O_2 to the reaction mix prior to initiation of the reaction with apo-tKDM4A produced an IC_{50} value of 54.5 μM (95% CI = 48.7–61.1 μM, Figure 5.7), which corresponds to the value obtained with the non-apo tKDM4A preparation (95% CI = 52.6–57.0 μM, Figure 5.2). That the absence of Fe^{2+} in the enzyme added to initiate the reaction had no impact on the inhibitory concentration of H_2O_2 suggests that oxidation, and therefore depletion, of Fe^{2+} in the reaction mix prior to the enzymatic reaction is the most likely mode of loss of tKDM4A activity under these conditions.

The protocol for the assessment of the effect of direct addition of H_2O_2 to tKDM4A prior to enzymatic reaction was altered slightly in light of the results from preliminary experiments (Chapter 5.2). The presence of L-ascorbate in the stability assays was shown to have no protective effect against H_2O_2-induced aggregation of tKDM4A (Figure 5.2c), but this had not been confirmed in activity assays. Therefore, H_2O_2 was added directly to either tKDM4A alone, or to a mixture of tKDM4A and L-ascorbate (100 μM), before addition to the reaction mix of $H3_{1-15}$K9me3 peptide substrate (100 μM), Fe^{2+} (10 μM) and 2OG (100 μM). L-ascorbate (100 μM) was present in the reaction mix if not added to the enzyme: H_2O_2 mix.

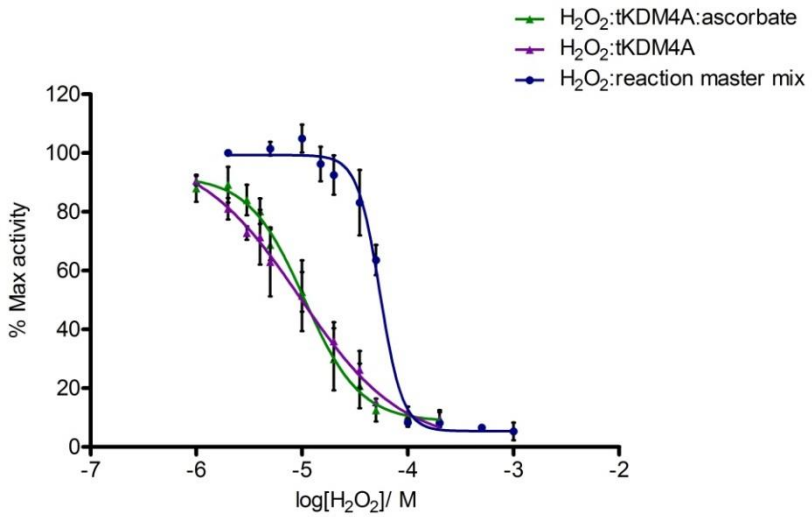

Figure 5.7 IC_{50} curves for apo-tKDM4A with peroxide under different conditions. Apo-tKDM4A was preincubated with H_2O_2 in the presence (green triangles, N = 3 biological repeats) or absence (purple triangles, N = 3 biological repeats) of L-ascorbate, or added to a reaction mix containing H_2O_2 (blue circles, n = 3 technical repeats). The IC_{50}s of peroxide for tKDM4A were revealed to be 10.5 μM (95% CI = 8.7–12.6 μM), 9.5 μM (95% CI = 6.4–14.1 μM) and 54.5 μM (95% CI = 48.7–61.1 μM), respectively. Data was plotted, fitted and analysed using GraphPad Prism v5.04, error bars denote sd.

The results of these experiments produced IC_{50} values for H_2O_2 of 10.5 μM (95% CI = 8.7–12.6 μM) with L-ascorbate added to the enzyme:H_2O_2 mix and 9.5 μM (95% CI = 6.4–14.1 μM) when L-ascorbate was added to the reaction master mix and not the enzyme:H_2O_2 mix (Figure 5.7). The lack of significant difference in these IC_{50} values indicates that the presence of L-ascorbate does not confer significant protection against the damaging effects of direct addition of H_2O_2 to tKDM4A, and is concordant with the preliminary stability assay results (Figure 5.3c). However, the IC_{50} value obtained on adding peroxide to the non-apo enzyme of 16.9 μM is somewhat higher than the values obtained with apo-tKDM4A, and although under slightly different conditions, suggests that the presence of Fe^{2+}, or other metal ions or reaction components, blunts the direct oxidation of the enzyme by H_2O_2. This may be *via* oxidation of the free Fe^{2+} in the solution, which occurs at a faster rate than the reaction of H_2O_2 with cysteinyl residues in proteins[345], reducing the amount of available H_2O_2. Fe^{2+} oxidation also produces ROS, including the hydroxyl radical *via* Fenton chemistry (equation 5.1) which could also react with tKDM4A, although $OH^{\bullet}$ exists only

transiently, as it reacts with diffusion-limited rates[345]. Given the complexity of the possible redox reactions that may occur in these assays, kinetic and dynamic analyses need to be performed to understand this phenomenon fully.

5.3.4. The effect of H_2O_2 on the stability of apo-tKDM4A

Having confirmed the inhibitory effect of H_2O_2 on apo-tKDM4A, SDS-PAGE assays were performed to assess the effect of the addition of H_2O_2, Fe^{2+} and L-ascorbate on the stability of the apo-enzyme. The results from preliminary experiments with non-apo tKDM4A (Chapter 5.1) indicated that the addition of either H_2O_2 or a mixture of Fe^{2+} and L-ascorbate resulted in aggregation of tKDM4A, whilst L-ascorbate, despite its nature as a reducing agent, did not protect against the effects of H_2O_2. The stability assays on apo-tKDM4A were designed to mimic the conditions of activity assays, using 25 µM apo-tKDM4A, 10-fold excess of Fe^{2+} (250 µM) and 100-fold excess of L-ascorbate (2.5 mM). 10 mM H_2O_2 was used, as this concentration was found to inhibit tKDM4A completely, as well as PHD2 and FIH, as discussed previously (Chapter 5.1). This would therefore enable comparison with PHD2 and FIH in further experiments. In inhibition experiments, it had been found that H_2O_2 was less inhibitory when added to a mixture containing Fe^{2+} prior to the addition of tKDM4A (Chapter 5.3.3), which may be due to oxidation of Fe^{2+} reducing the concentration of H_2O_2 available to then react with the enzyme. In an attempt to address this, for one sample, H_2O_2 and Fe^{2+} were mixed before being added to the apo-tKDM4A. Reactions were set up under the relevant conditions (Figure 5.8), with a total reaction volume of 10 µL, and incubated at 37°C for 30 min. Reactions were then quenched with an equal volume of 2 x non-reducing SDS-PAGE loading buffer and analysed *via* SDS-PAGE (Figure 5.8).

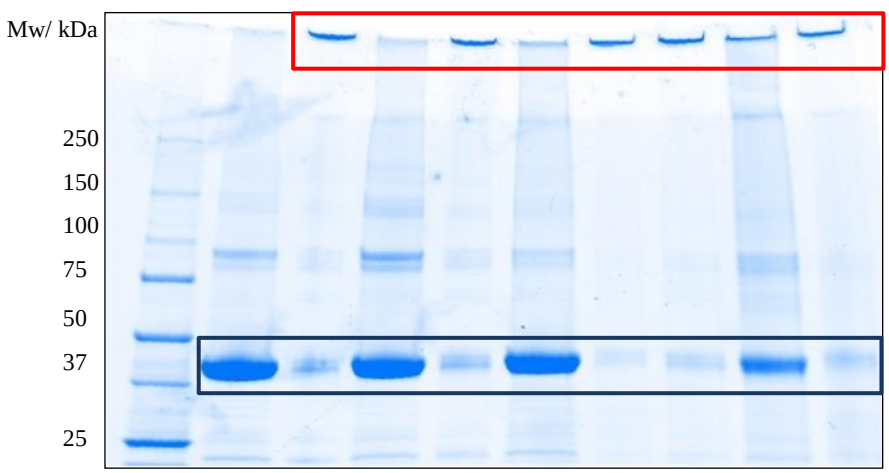

Lane	2	3	4	5	6	7	8*	9	10
Apo-tKDM4A (25 μM)	+	+	+	+	+	+	+	+	+
L-ascorbate (2.5 mM)	-	-	+	+	-	-	-	+	+
Fe^{2+} (0.25 mM)	-	-	-	-	+	+	+	+	+
H_2O_2 (10 mM)	-	+	-	+	-	+	+	-	+

Figure 5.8 SDS-PAGE analysis of the effect of H_2O_2, either alone or in combination with Fe^{2+} and L-ascorbate on apo-tKDM4A. Bands highlighted in dark blue correspond to intact apo-tKDM4A, while bands highlighted in red are apo-tKDM4A aggregates or precipitates. Lane 1 was loaded with a pre-stained molecular weight ladder. *For the sample in lane 8, Fe^{2+} and H_2O_2 were mixed together before addition to apo-tKDM4A. In all other lanes, reagents were added sequentially in the order: L-ascorbate, Fe^{2+} and H_2O_2.

The results of this experiment were in concordance with those observed in preliminary experiments (Chapter 5.2.2), namely, that peroxide caused aggregation of apo-tKDM4A, either when added to the protein alone or in the presence of Fe^{2+} and/or L-ascorbate (Figure 5.8, lanes 3, 5, 7, 8 & 10). Indeed, in experiments with apo-tKDM4A, any tKDM4A aggregates formed were unable to move through the gel at all, indicating that oxidation, leading to precipitation of the protein, had likely occurred. The addition of Fe^{2+} with or without L-ascorbate, also caused aggregation of apo-tKDM4A (Figure 5.8, lanes 6 & 9), with some evidence of slight aggregation on the addition of L-ascorbate alone (Figure 5.8, lane 4). Hence, apo-tKDM4A is sensitive to the presence of oxidising agents, either when added directly or when generated *in situ* by the reaction of Fe^{2+} with L-ascorbate[373]. As previously observed (Figure 5.3c), the addition of L-ascorbate is not protective against oxidation of

tKDM4A by H_2O_2. Interestingly, addition of H_2O_2 to Fe^{2+} before incubation with the protein produced no discernible change in protein aggregation, in contrast to the inhibition assays (Chapter 5.3.3), where addition of H_2O_2 to a reaction mix containing Fe^{2+} prior to addition of apo-tKDM4A lead to an increased inhibitory concentration of peroxide when compared to direct addition of H_2O_2 to the enzyme. However, the concentration of H_2O_2 used in these SDS-PAGE assays is much higher than the IC_{50} values obtained for H_2O_2 in the inhibition assays (Chapter 5.3.3), and much higher than the concentration of Fe^{2+} used. Therefore, the depletion of H_2O_2 *via* reaction with Fe^{2+} or other reaction components is likely to be minimal, leaving sufficient residual H_2O_2 to cause oxidative damage to the protein.

5.3.5. Comparison with other 2OG oxygenases

The *in vitro* experiments described above revealed KDM4A to be highly sensitive to inhibition by H_2O_2 compared to previously assessed 2OG oxygenases. Both FIH and PHD2 possess higher IC_{50} values for H_2O_2 (161 ± 1.4 μM and >10 mM, respectively, Dr Lars Hillringhaus, Chapter 5.1), indicating differential sensitivity towards H_2O_2 across the 2OG oxygenase superfamily. The experiments described above also revealed tKDM4A to be susceptible to oxidative damage by H_2O_2 (Figure 5.3, Figure 5.8). Therefore, it was of interest to assess whether the trends observed in the IC_{50} values for the three enzymes persisted in differences in their susceptibilities to oxidative damage by H_2O_2. SDS-PAGE was used to assess the effect of H_2O_2 on recombinant truncated PHD2 (~28 kDa, provided by Dr Tom McAllister), truncated FIH (~40 kDa, provided by Dr Adam Hardy) and tKDM4A (~44 kDa), as well as recombinant human TET1 (80 kDa, Epigentek). The recombinant enzymes were incubated ± 10 mM H_2O_2, a concentration chosen as it was known to inhibit tKDM4A and FIH, but not PHD2, for 5 min, before analysis *via* SDS-PAGE as previously (Chapter 5.2.2, Chapter 5.3.4).

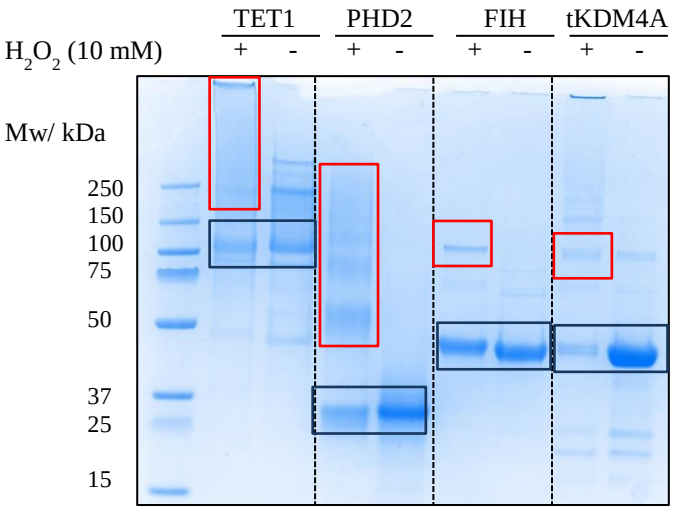

Figure 5.9 SDS-PAGE analysis of the effect of 10 mM H_2O_2 on TET1, PHD2, FIH and apo-tKDM4A. Bands highlighted in dark blue correspond to intact proteins at the expected molecular weight, while bands highlighted in red are apparent aggregates or precipitates. Lane 1 was loaded with a pre-stained molecular weight ladder.

The results of this experiment revealed that H_2O_2 treatment resulted in aggregation or oxidation of tKDM4A, as expected, as well as damage to TET1, as evidenced by bands or indistinct 'smearing' of higher molecular weights upon treatment with H_2O_2 (highlighted in red, Figure 5.9). Interestingly, in contrast to the trend in their *in vitro* sensitivities, PHD2 incurred significant damage upon treatment with 10 mM H_2O_2, a concentration known not to inhibit the catalytic activity of the enzyme under the reported conditions (Dr Lars Hillringhaus, unpublished data), while FIH displayed only minimal damage (Figure 5.9) despite inhibition at a lower concentration of 161 μM. These results indicate that the mechanism of inhibition by H_2O_2 may be different across these enzymes. In the case of tKDM4A, oxidative damage to the enzyme is likely to impact its activity significantly, whereas PHD2 may retain activity even upon aggregation or oxidation. Further exploration is necessary in order to determine the factors contributing to the differential sensitivity of the 2OG oxygenases surveyed towards H_2O_2. Proteomic analysis of the samples analysed *via* SDS-PAGE would aid in identifying any reactive amino acid residues within the enzymes that are susceptible to oxidation by H_2O_2, and may contribute towards the different sensitivities observed.

5.4. The effect of H_2O_2 on KDM4A activity in cells

The *in vitro* experiments described above revealed the inhibitory and damaging effect of H_2O_2 on tKDM4A. It was therefore of interest to correlate the *in vitro* sensitivity of KDM4A to ROS with the effect of H_2O_2 on KDM4A activity in cells. The work described in previous chapters on the effect of hypoxia on KDM4A activity has demonstrated that biochemical analysis of the factors affecting enzyme activity can be informative in understanding the impact of environmental changes (i.e. hypoxia) on the activity and function of enzymes in a cellular context (Chapters 2 and 3). Therefore, correlation of the effect of peroxide on tKDM4A *in vitro* with that on demethylation of native methylated histone substrate by full length KDM4A in cells was proposed to provide an insight into whether the production of ROS in hypoxia[336,337] might contribute to hypoxic inhibition of cellular KDM4A activity, as discussed previously (Chapter 5.1, Chapter 3). The aim of the work described in this section was to adapt the immunofluorescence assay used in cellular hypoxia experiments (Chapter 3) for use in testing the effect of peroxide on the cellular activity of KDM4A.

5.4.1. Measurement of H_2O_2 concentrations

Previously published reports of assays to assess the effect of ROS on the cellular activity of the HIF hydroxylases employed repeated addition of *tert*-butyl hydroperoxide to the cell media at 25 min intervals[372]. However, this study did not investigate the dose-dependence of the effect. To enable accurate determination of a cellular EC_{50} of H_2O_2 for KDM4A, it was necessary to evaluate the concentration and dosing interval necessary to maintain a consistent H_2O_2 in cell culture throughout the experiment. To this end, the persistence of H_2O_2 in a variety of buffers was assessed using a peroxide-detecting assay, involving the use of the peroxidase reagent Ampliflu™ Red.

5.4.1.1. Principles of the Ampliflu™ Red assay

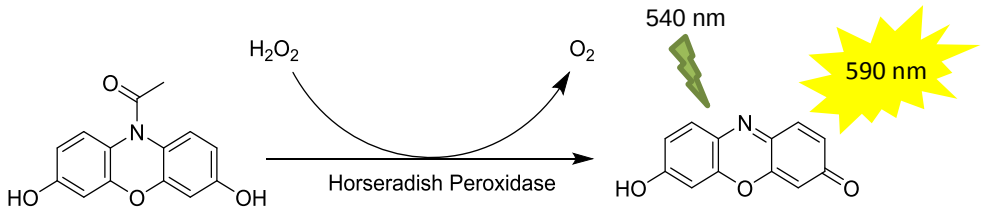

Ampliflu™ Red
(10-acetyl-3,7-dihydroxyphenoxazine)

Resorufin
(10-acetyl-3,7-dihydroxyphenoxazine)

Figure 5.10 Principles of the Ampliflu™ Red assay. Ampliflu™ Red reacts in a 1:1 stoichiometry with H_2O_2 in the presence of horseradish peroxidase to produce the fluorescent oxidation product resorufin.

The Ampliflu™ Red assay exploits the oxidase activity of horseradish peroxidase (HRP) in order to detect peroxide or peroxidase activity. Ampliflu™ Red (10-acetyl-3,7-dihydroxyphenoxazine) reacts with H_2O_2 in a 1:1 stoichiometry in the presence of HRP to produce the fluorescent oxidation product resorufin (7-Hydroxy-3*H*-phenoxazin-3-one) (Figure 5.10). The excitation maximum of resorufin is 571 nm, with an emission maximum at 585 nm, which allows detection by either fluorescent or spectrophotometric methods[375]. However, the close proximity of these wavelengths necessitated the use of a 540/590 nm fluorescence module available for use in a PHERAstar FS microplate reader (BMG Labtech). Preparation of standard concentrations of H_2O_2 allows the production of a standard curve, which may then be used to calculate H_2O_2 concentration in samples of interest.

5.4.1.2. Evaluation of H_2O_2 concentrations in assay buffers

Initial experiments aimed to assess how long 10 µM H_2O_2 would persist in a number of buffers and cell culture media: PBS, HEPES pH 7.5, DMEM (no phenol red, Sigma) and Opti-MEM™ (Gibco™). 10 µM H_2O_2 was added to the relevant buffer 180, 60, 30, 20 or 10 min prior to the addition of Ampliflu™ Red and HRP at a final concentration 50 µM and 0.1 $U.mL^{-1}$, respectively. The fluorescence of the samples was measured and correlated to H_2O_2 concentration, using a standard curve (Figure 5.11a).

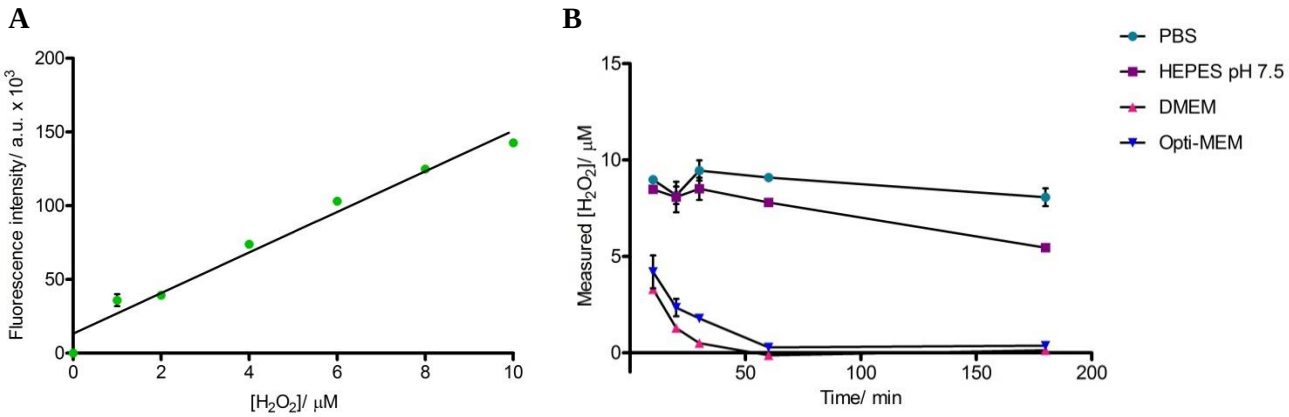

Figure 5.11 A) Standard curve produced using known concentrations of H_2O_2 in the Ampliflu™ Red assay, from which to calculate the concentration of H_2O_2 in experimental samples. **B)** Graph showing measured concentration of H_2O_2 in PBS (teal circles), HEPES pH7.5 (purple squares), DMEM (pink triangles) and OptiMEM™ (blue triangles) 10, 20, 30, 60 and 180 min after dosing with 10 µM H_2O_2. Graphs were plotted in GraphPad Prism v5.04, error bars denote sd, n = 2 technical repeats.

The results from this experiment revealed that H_2O_2 concentrations in PBS were maintained at approximately 9 µM over the 3 hour timecourse (Figure 5.10b). The measured H_2O_2 concentration in the HEPES pH 7.5 remained at approximately 8 µM for up to 1 h, but a reduction in concentration at 3 h was seen (Figure 5.10b). This indicates that, as in the *in vitro* experiments performed to determine the effect of H_2O_2 on tKDM4A were carried out in HEPES pH 7.5 for 5 min (Chapter 5.2, 5.3), the concentration of H_2O_2 added is likely to have been maintained throughout the course of these experiments. However, the Ampliflu™ Red assay revealed that the concentration of H_2O_2 in both DMEM and OptiMEM™ was significantly depleted compared to PBS at all time points (Figure 5.11b).

As the planned cell-based experiments were necessarily to be carried out in cell culture medium (OptiMEM™ or DMEM) for cell viability, further exploration of conditions for optimal H_2O_2 dosing was necessary. OptiMEM™ was chosen due to the slightly increased persistence of H_2O_2, as measured previously (Figure 5.11b). To evaluate whether higher concentrations of H_2O_2 could be maintained within the media, the addition of bolus doses of 10 µM or 20 µM H_2O_2 at regular intervals over an hour was investigated (Figure 5.12). H_2O_2 at the required concentration was added to 50 µL OptiMEM at 10, 20, 30 and 60 minute intervals over a total period of 1 h, after which the Ampliflu™ Red assay was used to evaluate the concentration of H_2O_2 in each sample using a standard curve, as described previously (Figure 5.11a).

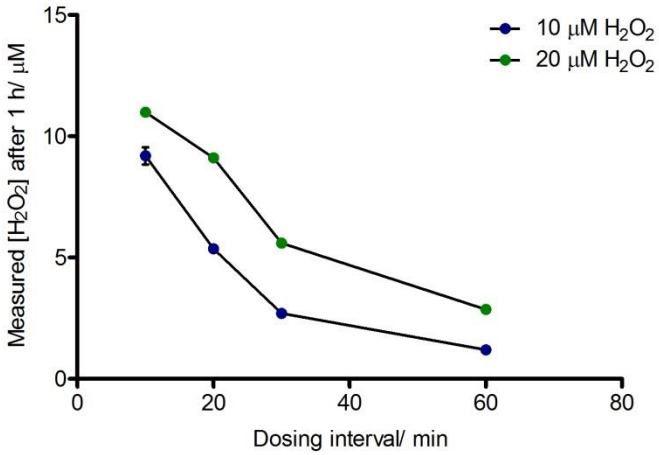

Figure 5.12 Graph showing concentration of H_2O_2 measured using the Ampliflu™ Red assay on samples of OptiMEM was dosed with bolus addition of 10 µM (dark blue circles) or 20 µM (green circles) H_2O_2 at regular intervals of 10, 20, 30 and 60 min for a total time of 60 min before measurement of H_2O_2 concentration. Graphs were plotted in GraphPad Prism v5.04, error bars denote sd, n = 2 technical repeats.

The measured concentration of H_2O_2 in the media was increased upon repeated addition of both H_2O_2 concentrations tested compared to single doses, as measured previously (Figure 5.11b). Dosing intervals of 10 min resulted in a final concentration of approximately 9 µM when dosing with10 µM H_2O_2, and 11 µM H_2O_2 upon addition of 20 µM H_2O_2, while longer dosing intervals resulted in reduced final concentrations of H_2O_2 (Figure 5.12). This study

indicated that repeat dosing of a higher concentration would be necessary to maintain the required concentration of H_2O_2 in cell-culture media. These data were subsequently taken forward into the design of an immunofluorescence experiment to ascertain the effect of H_2O_2 on the cellular activity of KDM4A.

5.4.2. Design of an immunofluorescence assay to determine the effect of H_2O_2 on KDM4A activity in cells

Having determined the *in vitro* sensitivity of tKDM4A towards H_2O_2 (Chapter 5.2, 5.3), and the conditions necessary to maintain a stable concentration of H_2O_2 in cell culture media (Chapter 5.5.1), preliminary experiments were performed in order to optimise the immunofluorescence assay used to evaluate the cellular activity of KDM4A in hypoxia (Chapter 3, Chapter 7.2.6) for use with H_2O_2. An initial dosing concentration of 10 μM H_2O_2 was chosen, so that changes to histone methylation could be observed while minimising cell death.

The doxycycline-inducible stably-overexpressing U2OS FLAG-KDM4A cell line was investigated, as in previous experiments (Chapter 3, Chapter 4) this had shown a high level of FLAG-KDM4A overexpression and good signal window in which to assess changes to the level of demethylation of H3K9me3 by overexpressed enzyme. In previous cellular inhibition assays (Chapter 4), the inhibitor being tested was added to the cells concomitantly with doxycycline, to ensure that all overexpressed KDM4A was exposed to the inhibitor in question, as well as maintaining KDM4A levels throughout the experiment. However, as H_2O_2 is highly reactive, it is possible that it may react with doxycycline, thereby reducing concentrations of both H_2O_2 and doxycycline present in the cell culture media. Therefore, to avoid problems arising from this, it was decided to first induce overexpression of KDM4A with DMEM containing doxycycline (1 μg.mL^{-1}) for 4 h, then remove the induction media and dose with 10 μM H_2O_2 in OptiMEM™ at regular intervals, replacing the

OptiMEM™:H_2O_2 mix each time. Although the AmpliFlu™ Red assays (Chapter 5.5.1) had indicated that the optimal dosing window would be 10 min, the practicality of using this window with cells was of concern. Frequent removal of the cells from the incubator in order to dose them was likely to cause perturbations in temperature and CO_2 concentration, which may affect the results of the experiment. Therefore, a dosing interval of 30 min was chosen as a compromise. The total dosing time of 3 h was chosen based on previous studies in the literature, in order to minimise the potential cytotoxic effects of H_2O_2. Uninduced cells not overexpressing FLAG-KDM4A were also dosed with H_2O_2 and used as a control. After 3 h of dosing, cells were fixed, permeabilised and stained for FLAG and H3K9me3 (Figure 5.13 a-c), as described previously (Chapter 3.2, 7.2.6). Imaging and quantification of H3K9me3 levels was carried out using an Operetta High Contents Imager (Perkin Elmer) with Harmony® software.

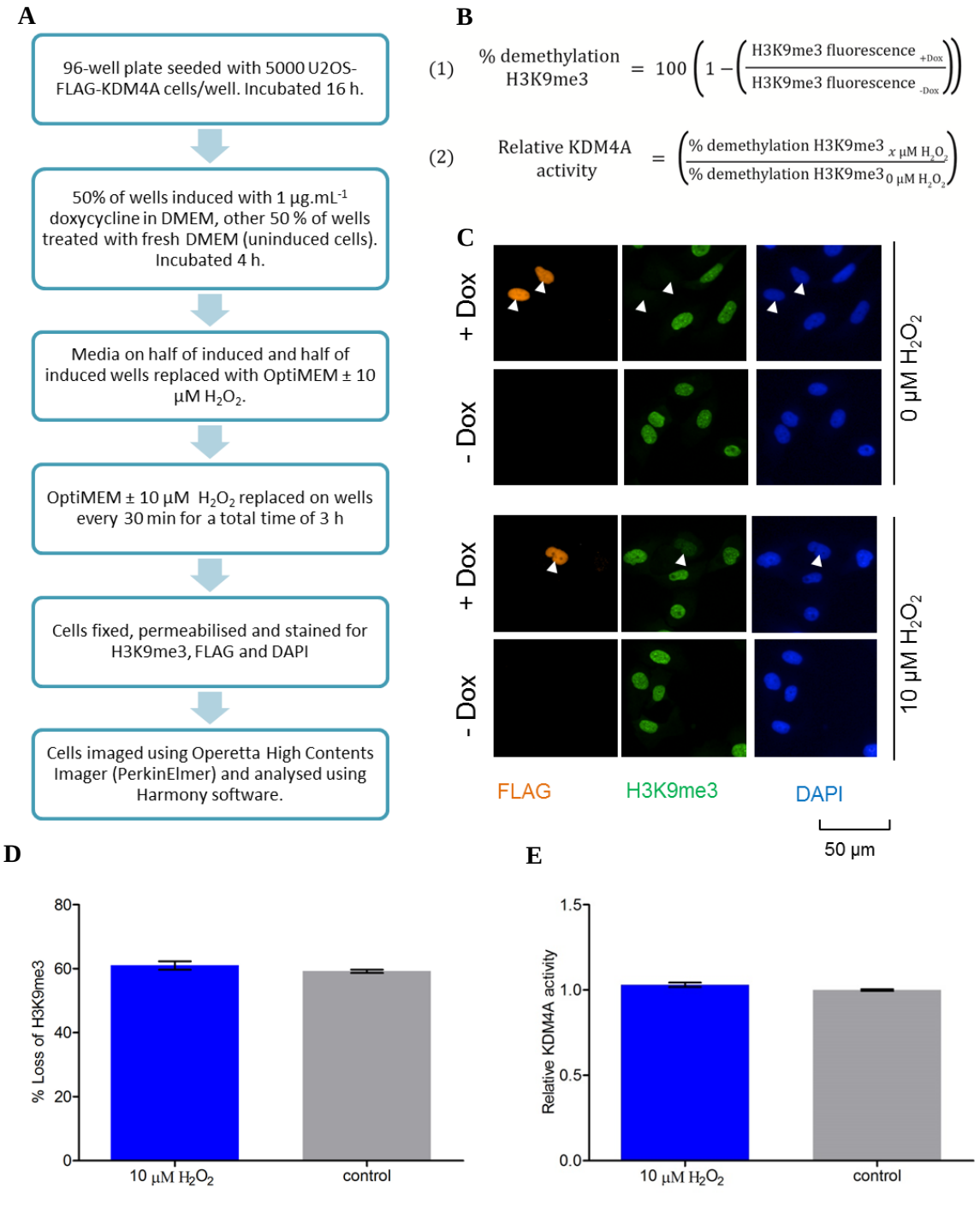

Figure 5.13 Preliminary design and testing of a cell-based immunofluorescence assay to assess the effect of H_2O_2 on KDM4A. **A)** Workflow of experiment. **B)** Equations used to calculate % demethylation of H3K9me3 in FLAG-KDM4A overexpressing cells, and relative activity of KDM4A. **C)** Selected images from the preliminary immunofluorescence experiment. U2OS FLAG-KDM4A cells were induced to overexpress FLAG-KDM4A (+Dox, orange) and dosed with 10 µM H_2O_2 at 30 min intervals for 3 h. H3K9me3 signal (green) in induced cells (indicated by arrows) was normalised against signal in uninduced cells (-Dox) and correlated to enzyme activity. Images were processed and analysed at the same time using the same fluorescence intensity signal window. **D)** Graph showing percentage demethylation of H3K9me3 in cells overexpressing FLAG-KDM4A when dosed with 10 µM H_2O_2 (blue) or left untreated (grey). Error bars denote standard error, n > 40. **E)** Graph showing relative KDM4A activity in cells dosed with 10 µM H_2O_2 (blue) or left untreated (grey). Error bars denote sem, n > 40 cells per treatment.

On analysis of this experiment, it was clear that 4 h doxycycline exposure was insufficient time to produce high levels of FLAG-KDM4A overexpression in the cells (Figure 5.13c). Fewer than 50 overexpressing cells were identified upon imaging 3 triplicate doxycycline-induced wells. However, subsequent analysis of H3K9me3 levels was carried out to determine factors to optimise further. Levels of H3K9me3 in cells overexpressing FLAG-KDM4A were normalised against those in uninduced cells treated in the same manner, then correlated to KDM4A activity (Figure 5.13a, b). Interestingly, the raw data indicated an approximately 60% loss of H3K9me3 signal on overexpression of FLAG-KDM4A in both cells dosed with H_2O_2 and the control cells, corresponding to only a minor (3%) increase in relative KDM4A activity upon dosing the cells with 10 µM H_2O_2.

Given the low level of induction after 4 h doxycycline treatment, it was decided that in subsequent experiments, doxycycline would be used throughout H_2O_2 dosing in an attempt to achieve increased overexpression of FLAG-KDM4A. Cells were induced with 1 µg.mL^{-1} doxycycline in OptiMEM™ and incubated for 4 h. Moreover, as dosing with 10 µM H_2O_2 produced very little effect on the KDM4A activity (Figure 5.13), the H_2O_2 concentration used was increased. Bolus addition of 20 µM H_2O_2 was performed at 30 min intervals over 4 h, with no replacement of media, in an attempt to increase the exposure of the cells to H_2O_2 (Figure 5.14a). After 4 h, cells were fixed, processed and analysed using the procedure described above and in Chapter 7.2.6 (Figure 5.14a-c).

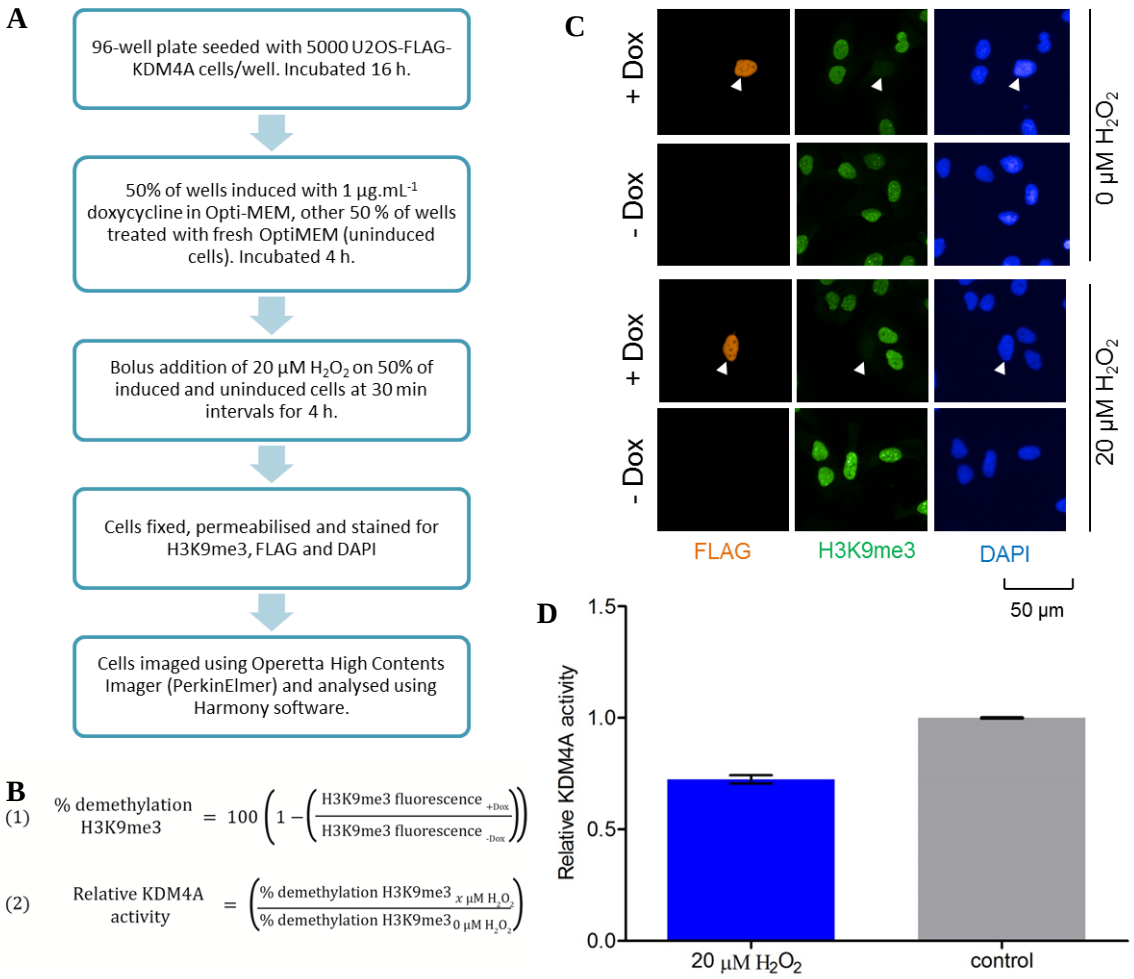

Figure 5.14 Further optimisation of a cell-based immunofluorescence assay to assess the effect of H_2O_2 on KDM4A. **A)** Workflow of experiment. **B)** Equations used to calculate % demethylation of H3K9me3 in FLAG-KDM4A overexpressing cells, and relative activity of KDM4A. **C)** Selected images from the preliminary immunofluorescence experiment. U2OS FLAG-KDM4A cells were induced to overexpress FLAG-KDM4A (+Dox, orange) and dosed with bolus addition of 20 µM H_2O_2 30 min intervals for 4 h. H3K9me3 signal (green) in induced cells (indicated by arrows) was normalised against signal in uninduced cells (-Dox) and correlated to enzyme activity Images were processed and analysed at the same time, using the same fluorescence intensity signal window. **D)** Graph showing relative KDM4A activity in cells dosed with 20 µM H_2O_2 (blue) or left untreated (grey). Error bars denote sem, n > 40 cells per treatment.

The results demonstrated that, despite the longer exposure to doxycycline, the number of FLAG-KDM4A overexpressing cells was still low (<60 per condition). However, the increased concentration of H_2O_2 and dosing time compared to the first immunofluorescence experiment (Figure 5.13) did result in observable changes to the extent of H3K9me3 demethylation in the KDM4A-overexpressing cells. KDM4A activity in cells dosed with H_2O_2 was reduced to approximately 72% of that in untreated control cells (Figure 5.14d), in

concordance with the *in vitro* experiments, in which a loss of KDM4A activity was seen on exposure to H_2O_2 (Chapter 5.2, 5.3).

The preliminary attempts at design of a cellular immunofluorescence assay to assess the effect of H_2O_2 on the activity of KDM4A indicate that further optimisation is required. A longer doxycycline induction time in conjunction with H_2O_2 treatment produced a more significant effect on KDM4A activity (Figure 5.14d), which was in concurrence with *in vitro* experiments, so these conditions should be taken forward for further optimisation. However, in both experiments, fewer than 60 cells were induced to overexpress KDM4A. Therefore, efforts should be focussed on increasing overexpression of KDM4A, potentially using transient transfection rather than doxycycline-inducible cells. Cells tolerated 20 μM H_2O_2 dosing over 4 h, so a longer dosing time and increased H_2O_2 concentrations can be tested, in order to produce a dose-response curve for the effect of H_2O_2 on cellular KDM4A activity.

While the proposed experiments will be possible from a practical perspective, care must still be taken in the interpretation of the results. Exogenous addition of H_2O_2 may not result in an increase in the cellular concentration of ROS, but instigate a cellular signalling cascade. Moreover, should the H_2O_2 permeate the cells, it is still possible that it may not interact directly with the overexpressed KDM4A, but that disruption of alternative biological pathways may indirectly affect its activity. The use of a more cell-permeable peroxide source such as *tert*-butyl hydroperoxide, would potentially aid in elucidating the mechanism by which H_2O_2 affects cellular KDM4A activity. Furthermore, a recent study reported the development of a method to measure intracellular H_2O_2 concentration[376], which may also aid in understanding how exogenous H_2O_2 exerts the effects observed above. However, the *in vitro* experiments described above demonstrate that H_2O_2 does have a direct effect on the enzyme, suggesting that high concentrations of H_2O_2 in cells are also likely to directly impact upon KDM4A activity.

5.5. Discussion

The work described in this chapter details the development of *in vitro* assays to evaluate the effect of H_2O_2 on the activity and stability of isolated tKDM4A. This revealed that KDM4A activity is highly sensitive to H_2O_2 concentration with IC_{50} values ranging between 9.5 μM (95% CI = 6.4–14.1 μM) and 54.7 μM (95% CI = 52.6–57.0 μM) under the conditions tested (Chapter 5.2.1, 5.3.3). Furthermore, SDS-PAGE assays demonstrated that addition of H_2O_2 to the enzyme, as well as both Fe^{2+} and L-ascorbate, induces aggregation of tKDM4A (Chapter 5.2.2, 5.3.4), indicating that both direct oxidation of the enzyme and Fenton chemistry resulting in oxidation of Fe^{2+} contributes to inhibition of the enzyme.

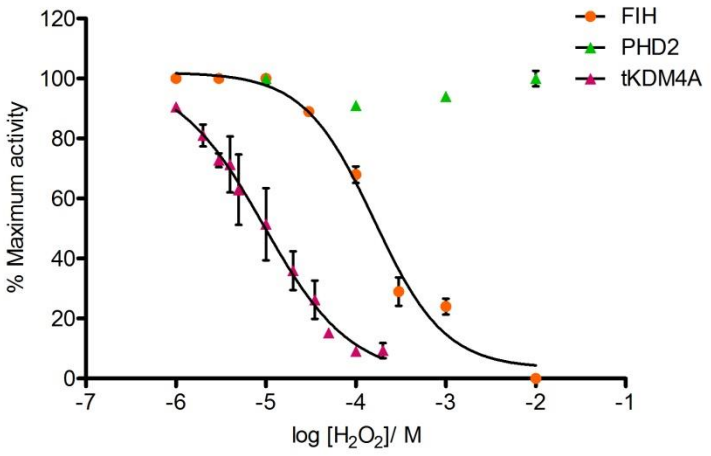

Enzyme	IC_{50}
PHD2	>10 mM
FIH	161 ± 1.4 μM
tKDM4A	9.5 μM (95% CI = 6.4–14.1 μM)

Figure 5.15 Dose response experiments revealed differential sensitivity of three different 2OG oxygenase enzymes towards H_2O_2. Preincubation of PHD2 (green triangles, n = 3 technical repeats), FIH (orange circles, n = 3 technical repeats) or tKDM4A (pink triangles, N = 3 biological repeats) with different concentrations of H_2O_2 produced IC_{50} values of >10 mM, 161 ± 1.4 μM and 9.5 ± 1.3 μM, respectively. Experiments using PHD2 and FIH were performed by Dr Lars Hillringhaus. Data was plotted, fitted and analysed using GraphPad Prism, error bars denote sd.

The *in vitro* assays described in this chapter (Chapter 5.3.3) revealed tKDM4A to be highly sensitive towards H_2O_2 compared to the HIF hydroxylase enzymes PHD2 and FIH when investigated under similar conditions (Dr Lars Hilliringhaus, Figure 5.15). Preincubation of FIH and PHD2 with H_2O_2 before reaction with peptide substrate produced IC_{50} values for

H_2O_2 of 161 ± 1.4 μM and >10 mM, respectively, compared to a value of 9.5 μM (95% CI = 6.4–14.1 μM) for tKDM4A (Chapter 5.3.3).

Analysis of the effects of H_2O_2 on the stability of tKDM4A, PHD2 and FIH revealed aggregation or oxidation of both tKDM4A and PHD2 upon incubation with 10 mM H_2O_2, while FIH incurred only minimal damage (Figure 5.9). These results are in contrast to the inhibition studies described above, *via* which FIH was found to be more sensitive than PHD2, indicating that the mechanisms of inhibition by H_2O_2, may be different for each of the enzymes studied. These mechanisms may include oxidation of highly reactive residues within the protein, or oxidation of the active site Fe^{2+}. Further investigation of PHD2 and FIH using the methods described above for tKDM4A could help to elucidate these differences, while proteomic analysis is hoped to highlight the presence of specific reactive residues that may underpin the susceptibility of these enzymes to inhibition by H_2O_2. However, care must be taken in the interpretation of these results, as the concentrations of H_2O_2 used in the stability assays was very high (0.1- 10 mM) and unlikely to be reflective of the biological situation.

The high sensitivity of PHD2 activity towards oxygen availability is proposed to underpin its role as an oxygen sensor[85], hence the comparatively high sensitivity of KDM4A towards ROS suggests that the KDMs may possess the potential to act as sensors of oxidative stress in the context of epigenetic regulation. Under hypoxic conditions, increased production of ROS may contribute to the loss of activity of KDM4A in cellular hypoxia, as investigated in Chapter 3, which could then affect the expression of KDM4A-regulated genes. The cellular assay to investigate the effect of H_2O_2 on KDM4A activity in cells requires further optimisation (Chapter 5.5), but remains an interesting avenue for further study, in order to fully understand the mechanisms by which hypoxia may exert an effect on epigenetic regulation.

Chapter 6: Summary and Conclusions

The JmjC-KDMs are enzymes involved in epigenetic regulation *via* the removal of methyl groups from methylated lysyl residues within the *N*-terminal histone tails. The human epigenetic response is highly complex, and regulates transcription in response to multiple environmental stimuli. The KDMs belong to the 2OG oxygenase superfamily, hence are related to the cellular oxygen sensing HIF hydroxylases, and possess an absolute requirement for molecular oxygen for their catalytic activity. Therefore, one possible stimulus that may affect epigenetic regulation is altered oxygen availability. Indeed, several studies have demonstrated aberrant histone lysine methylation and changes to KDM expression levels in hypoxia[250]. A recent study highlighted that the KDM4 subfamily member KDM4E demonstrates a graded response to oxygen concentration[191], providing a starting point for the project discussed herein.

The aim of the work described in this thesis was to evaluate the effect of hypoxia on the model JmjC-KDM, KDM4A, in both biochemical and cellular contexts. Experiments described in Chapter 2 optimised a MALDI-TOF MS assay for the determination of the $K_m^{app}(O_2)$ for isolated KDM4A, producing a value of 173 ± 23 μM (Chapter 2.4). The oxygen sensing HIF hydroxylases PHD2 and FIH, have also been evaluated using this method, revealing $K_m^{app}(O_2)$ values of > 450 μM and 100 ± 10 μM, respectively[171,245]. Moreover, using alternative methods, several other 2OG oxygenases, including C-P4H and mPAHX have been found to have significantly lower $K_m^{app}(O_2)$ values[167,169] (Chapter 2.1). Therefore, from a biochemical perspective, KDM4A appears to be highly sensitive to oxygen availability in comparison to related enzymes, with an oxygen dependence

approaching that of the cellular oxygen sensor PHD2, hence KDM4A possesses the biochemical potential to act as an oxygen sensor in the context of epigenetic regulation.

Along with studies on the isolated enzymes, the response of PHD2 and FIH to changes in oxygen concentration has been evaluated in cells. It has been reported that PHD2 activity is abrogated at concentrations below 1.0% O_2 in cells, while FIH maintains activity[173]. This indicates that the *in vitro* $K_m^{app}(O_2)$ values evaluated for these enzymes are reflective of their relative oxygen sensitivities in cells. Therefore, the effect of hypoxia on the cellular activity of KDM4A was investigated, in order to confirm whether the oxygen sensitivity of the enzyme was also apparent in a biological context. Chapter 3 describes immunofluorescence and western blot analysis of the effect of hypoxia on the catalytic activity of ectopically expressed KDM4A against native H3K9me3 in HeLa and U2OS cells. These studies confirmed that loss of H3K9me3 due to KDM4A activity was reduced under conditions of low oxygen (Chapter 3.2). Furthermore, a graded response of KDM4A activity to oxygen concentrations between 0.1 and 21% O_2 was observed (Chapter 3.3.2). These results were in accordance with the *in vitro* $K_m^{app}(O_2)$ value obtained, further confirming the oxygen sensitivity of KDM4A. Moreover, the agreement between the cellular and biochemical studies demonstrates the utility of *in vitro* analyses in understanding and comparing the factors affecting enzymatic activity.

The biochemical and cellular oxygen sensitivity of KDM4A revealed in these investigations suggest the potential for KDM4A to act as an oxygen sensor in the context of epigenetic regulation: in response to cellular hypoxia, KDM4A activity is hindered, resulting in increased levels of histone lysine methylation and changes to gene expression. Therefore, attempts were made to evaluate the impact of restricted KDM4A activity on the expression of putative KDM4A target genes, using the cellular system employed in the immunofluorescence experiments. RT-qPCR analysis of reported KDM4A target genes

ADAM12, *PPIC* and *CHD5*[264,265] demonstrated no differences to their expression in KDM4A-overexpressing cells incubated in either 1.0% or 21% O_2 (Chapter 3.4.1). While this may indicate that hypoxic loss of KDM4A activity has little impact on downstream transcriptional regulation, the system used in this investigation must be optimised. ChIP-qPCR or ChIP-seq experiments would further validate KDM4A target genes and enable their expression to be evaluated at an endogenous level, mitigating any potential effect that high levels of KDM4A overexpression may have. Moreover, the hypoxically upregulated expression of the HIF target gene CA9 appeared to be blunted by dox (Chapter 3.4.1), which was used to conditionally overexpress KDM4A in the U2OS cells used, hence endogenous studies would also alleviate the possible effect of dox on KDM4A target genes.

In a further attempt to evaluate the biological impact of KDM4A inhibition by hypoxia, immunofluorescence experiments were used to investigate potential changes to chromatin structure. H3K9me3 is associated with closed, transcriptionally repressed heterochromatin, and facilitates the binding of heterochromatin binding protein, HP1β[274]. Therefore, loss of H3K9me3 catalysed by KDM4A would be expected to reduce levels of chromatin-associated HP1β, and reduced KDM4A activity would result in an increase of HP1β. Preliminary experiments revealed no changes to HP1β levels in KDM4A-overexpressing cells in either hypoxia or normoxia (Chapter 3.4.2). However, these experiments were performed on intact cells, hence may be examining total HP1β, rather than the chromatin bound fraction. Further optimisation of the experimental approach, including the use of western blot analysis of fractionated cells, would ensure that only chromatin bound HP1β were evaluated, and enable conclusive examination of the effect of hypoxic inhibition of KDM4A on chromatin structure.

Despite the fact that the investigations into the biological impact of hypoxic inhibition of KDM4A proved challenging and require refinement, the work described in Chapters 2 and 3

confirms that KDM4A is sensitive to loss of oxygen availability, with a reduced capacity to demethylate histone lysine residues under hypoxia. This suggests that changes to oxygen availability are likely to impact on epigenetic regulation, presenting an alternative or complementary biological pathway to the HIF system by which hypoxia may have an impact on gene expression. The extent to which KDM4A is unique among the KDMs in its ability to 'sense' oxygen remains to be determined, and the application of the methods described in these chapters to other KDM family members would further our understanding of the full impact of hypoxia on histone lysine methylation.

Subsequent chapters of this thesis address further exploration of the mechanism of loss of KDM4A activity in hypoxia. While the *in vitro* experiments demonstrated that reduced oxygen concentrations alone result in inhibition of KDM4A, cellular hypoxia does not only constitute lack of oxygen availability in isolation; the hypoxic response activates hundreds of genes with roles in diverse biological processes[148], many of which may also impact on KDM4A activity. These include changes to metabolism in the form of altered concentrations of TCA cycle intermediates[295], as discussed in Chapter 4, and possible increased production of reactive oxygen species[335], which was addressed in Chapter 5.

Chapter 4 details experimental approaches to investigation of changes to TCA cycle intermediates, utilising small molecule inhibitors of the 2OG oxygenases. Cell-permeable ester derivatives of 2OG, succinate and 2HG were tested in cellular immunofluorescence assays to assess the effect of changes to their concentrations on the activity of ectopically expressed KDM4A against H3K9me3. Dose-response experiments using dimethyl and *n*-octyl esters of *(S)*- and *(R)*-2HGs, which have previously been shown to inhibit a number of 2OG oxygenases[254,299,300,306], revealed that these compounds are only minimally inhibitory against KDM4A. *n*-octyl *(S)*-2HG possessed an EC_{50} value of 558 μM in 1.0% O_2, while the remaining compounds could not be adequately fitted to a non-linear regression model of

inhibition (Chapter 4.2). This suggests that cellular levels of 2HG must be increased to millimolar levels in order to inhibit KDM4A. The concentration of 2HG is known to reach these levels in certain cancers encoding mutations in *IDH*[308], and increased levels of *(S)*-2HG that have been reported to be sufficient to impact upon histone lysine methylation are proposed to result from the conversion of 2OG by LDHA in hypoxia[309]. Conversely, high concentrations of dimethyl 2OG appeared to somewhat increase the loss of H3K9me3 in cells incubated in hypoxia (Chapter 4.2), indicating augmented activity of KDM4A. This suggests that reduced 2OG levels in hypoxia, as a result of its conversion by LDHA to *(S)*-2HG[309] or reduced conversion of isocitrate[254], are also likely to impact upon KDM4A activity.

The 2OG-competitive inhibitor IOX1[282] was also used to investigate the possibility that reduced concentrations of 2OG may contribute to the loss of KDM4A activity in hypoxia. The cellular EC_{50} value of IOX1 was found to be increased from 39.9 μM in normoxia to 131 μM in 1.0% O_2 (Chapter 4.2) implying decreased competition with IOX1 for the 2OG binding site. Subsequent *in vitro* inhibition studies with recombinant KDM4A confirmed that reduced 2OG concentrations increase the inhibitory potency of IOX1. However, in the presence of the same 2OG concentration, the IC_{50} value of IOX1 was still reduced in hypoxia, indicating that O_2 concentration also has an impact on its inhibitory potency (Chapter 4.2). Inspection of the crystal structure of IOX1 bound to KDM4A (Chapter 4.2) reveals that IOX1 binds in both the 2OG and O_2 binding sites[282], hence reduced competition for the O_2 binding site, as well as a decreased rate of reaction under non-saturating O_2 conditions, may also increase the ability of IOX1 to inhibit KDM4A activity.

The increased susceptibility of KDM4A to inhibitors may be of therapeutic benefit. While hypoxic inhibition of KDM4A may have pathophysiological consequences due to aberrant epigenetic regulation, increased expression and locus-specific activity of KDM4A has been

implicated in a number of disease states. Notably, overexpression of KDM4A exacerbates cardiac hypertrophy, with increased expression of the stress sensor FHL1 linked to activity of KDM4A activity at the *FHL1* promoter[239]. Therefore, KDM4A may present a therapeutic target in cardiac hypertrophy. To this end, the KDM4-subfamily inhibitor CCT1[293] (**11a**, Chapter 4.1) was submitted to a phenotype-based assay cardiac hypertrophy[326] (in collaboration with Matthew Stratton, and Dr Tim McKinsey, University of Colorado, Denver). At a concentration of 5 μM, CCT1 ameliorated phenylephrine induced overexpression of *ANF*, apparently validating the involvement of KDM4A in cardiac hypertrophy. However, at a lower concentration of CCT1 (500 nM), *ANF* expression was increased above a control (Chapter 4.3). This suggests potential off-target effects of CCT1. The implications of the results of this experiment are two-fold. Firstly, further validation of KDM4A as a therapeutic target is necessary, and may encompass cell-based imaging techniques (on-going, in collaboration with the McKinsey Laboratory, University of Colorado, Denver) and knockout studies. Secondly, the development of KDM4A-specific inhibitors would provide further means for elucidating its role in disease states, as well as a basis from which to develop drugs to target the enzyme.

In vitro exploration of the effect of H_2O_2 on recombinant KDM4A revealed an IC_{50} value for H_2O_2 of 9.5 μM (95% CI = 6.4–14.1 μM, Chapter 5.3.3) upon preincubation with the enzyme. Similar studies of FIH and PHD2 found them to possess IC_{50} values for H_2O_2 of 161 μM and > 10 mM, respectively (Chapter 5.5, Dr Lars Hillringhaus), indicating that KDM4A is potentially highly sensitive to reactive oxygen species compared to these other 2OG oxygenases. Further study *via* SDS-PAGE found that exposure of KDM4A to high concentrations of H_2O_2 is likely to result in oxidative damage to the enzyme (Chapter 5.3.5). Surprisingly, given its resistance to inhibition by H_2O_2, PHD2 also demonstrated aggregation upon incubation with 10 mM H_2O_2 (Chapter 5.3.5). Further investigation of these effects

using proteomic analysis is necessary to elucidate the mechanism of inhibition of these enzymes by H_2O_2, which may include oxidation of reactive amino acid residues within the protein[343]. Cellular immunofluorescence experiments found dosing of U2OS cells overexpressing KDM4A with 20 μM H_2O_2 to result in loss of catalytic activity of KDM4A against native H3K9me3 (Chapter 5.4), in concordance with the *in vitro* studies. Taken together, the results of the experiments undertaken with H_2O_2 demonstrate that the production of reactive oxygen species in hypoxia may contribute to hypoxic inhibition of KDM4A in cells.

Overall, the work described in this thesis has revealed the catalytic activity of KDM4A to be sensitive to limiting oxygen concentrations, both *in vitro* and in cells. Further exploration has revealed factors that may contribute to cellular inhibition of KDM4A in hypoxia, including the production of reactive oxygen species and changes to the levels of TCA cycle intermediates. While the biological impact of hypoxic restriction of KDM4A activity on downstream transcriptional processes remains to be determined, the implications of the results described herein are likely to influence the expression of genes, which may have pathological consequences in hypoxic disease states, including cancer and cardiovascular conditions.

Chapter 7: Materials and Methods

7.1. Materials and methods relating to *in vitro* experiments

All reagents used were from Sigma, unless otherwise stated. The water used was from a Millipore Milli-Q system with a 0.22 µm filter. All biological procedures employed standard sterile technique, and equipment and media were sterilised by autoclaving at 121 °C (20 min). Other heat-sensitive solutions were sterilised using a 0.22 µm filter. The pH of all buffers used was measured using Hanna Instruments HI 9321 microprocessor pH meter fitted with a 5 mm diameter electrode, and adjusted using stock solutions of NaOH or concentrated HCl.

7.1.1. Production of recombinant protein

Bacterial growth medium: 2 Tryptone/Yeast (2TY, Table 7.1) bacterial growth medium was prepared and autoclaved by Mr H. M. Jubier. Kanamycin and ampicillin were used at a final concentration of 0.03 $mg.mL^{-1}$ and 0.1 $mg.mL^{-1}$, respectively. Isopropyl β-D-1-thiogalactopyranoside (IPTG, Apollo Scientific) and antibiotics were filter-sterilised prior to use with a Minisart 0.45 µM syringe filter.

Table 7.1 Recipes for bacterial growth media (SOC = Super Optimal broth with Catabolite Repression).

	2TY medium (per 1 L)	SOC Medium (per 100 mL)	Agar (per 1 L)
Tryptone (OXOID)	16.0 g	2.0 g	10.0 g
Yeast extract	10.0 g	0.5 g	5.0 g
NaCl	5.0 g	0.058 g	10.0 g
KCl	---	0.019 g	---
NaOH (1 M)	---	0.4 mL	---
Agar (Fisher)			20.0 g

Plasmids:

Table 7.2 Plasmids used for the expression of KDM4A in *E. coli* and mammalian cell culture. pcDNA3-*N*-Flag-LIC constructs were originally supplied by Dr Rob Klose (Department of Biochemistry, University of Oxford) and were kindly donated by Dr Louise Walport (Schofield Laboratory).

Protein	Vector	Tag	Resistance
N-His_6-$KDM4A_{1-359}$ (tKDM4A)	pNIC28-BSA4	*N*-His_6	Kanamycin
Full length *N*-FLAG-KDM4A WT or *N*-FLAG-KDM4A MUT	pcDNA3-*N*-Flag-LIC	FLAG	Ampicillin

DNA concentration was measured using a NanoDrop ND-1000 UV/Vis spectrophotometer (Thermo Scientific), measuring the absorbance at 260 nm.

Transformation: Competent cells (35 µL) and DNA (100 µg) were mixed and incubated on ice for 20 min. The mixture was then heat shocked at 42 °C (45 s) and left on ice for a further 2 min. Cells were gently resuspended in SOC medium (200 µL) and then incubated in a waterbath (Grant) at 37 °C for 45 min. Cells (100 µL) were spread on an agar plate, left to dry and incubated at 37 °C (20 h). Plates were stored at 4 ºC.

Plasmid purification: The plasmid was transformed into *E. coli* XL10 Gold cells (Stratagene). 10 mL 2TY medium containing the appropriate antibiotic was inoculated with single colony from the transformation and incubated overnight (37 ºC, 220 rpm shaking, 20 h). Plasmid DNA purification was achieved using a Fermentas GeneJET™ Maxiprep kit, according to the manufacturer's protocol.

Large scale protein expression: The plasmid was transformed into *E. coli* BL21 (DE3) cells. A single transformed colony was used to inoculate 100 mL 2TY medium containing the appropriate antibiotic and grown overnight (37 ºC, 220 rpm shaking, 20 h). 12 x 600 mL flasks of 2TY medium containing the appropriate antibiotic were each inoculated using 7.5 mL overnight culture, and incubated at 37 °C, 220 rpm. $O.D._{600\ nm}$ was measured using a Novaspec® II spectrophotometer (Pharmacia), with untreated medium used as a reference

and cells were grown until $O.D._{600\ nm}$ = 0.6-0.8. IPTG (0.5 mM) was then used to induce each flask, and cells were incubated at 18 ºC (20 h, 220 rpm), before harvesting *via* centrifugation (Beckmann Avanti™ J-26S XP centrifuge, 10153 x *g*, 8 min). Harvested cell pellets were frozen at –80 °C.

7.1.2. Purification of recombinant protein:

FPLC buffers: Buffers for purification were prepared according to the recipes in Table 7.3, and were filtered using 0.22 µm filters and de-gassed before use.

Table 7.3 Buffers used in FPLC purification of recombinant tKDM4A.

	Immobilized Metal Affinity Chromatography			**Size exclusion chromatography**
	Binding buffer (A)	**Wash buffer (B)**	**Elution Buffer (C)**	**Buffer D**
2-[4-(2-hydroxyethyl)piperazin-1-yl]ethanesulfonic acid (HEPES) pH 7.5	10 mM	10 mM	10 mM	10 mM
NaCl	500 mM	500 mM	500 mM	500 mM
glycerol	5.0% (v/v)	5.0% (v/v)	5.0% (v/v)	5.0% (v/v)
imidazole	10 mM	30 mM	500 mM	---

Cell lysate preparation: Cells were resuspended in Buffer A (100 mL) containing 0.1 M phenylmethylsulfonyl fluoride (PMSF) and 1 mg DNAase1 *via* gentle stirring at 4 °C. Once resuspended, cells were lysed *via* sonication using a SONICS VibraCell 150 sonicator at 60% amplitude for 12 x 30 s bursts, with 30 s breaks in between. Lysed cells were centrifuged (Beckmann Avanti™ J-25 centrifuge, 31554 x *g*, 20 min; 69673 x *g*, 20 min) and the supernatant was collected and filtered through a 0.45 µm syringe filter (Minisart).

Protein purification: An ÄKTA FPLC system (GE Healthcare) was used for protein purification. *Immobilized Metal Affinity Chromatography (IMAC):* A 5 mL HisTrap fast flow column was charged with 50 mM $NiSO_4$ and pre-equilibrated with Buffer A, before loading with cell lysate (1 $mL.min^{-1}$). Buffer B was used to wash the column until the UV

trace returned to baseline. Protein was eluted using a gradient of 0-100% Buffer C over 75 mL, then 25 mL at 100% B, in 5 mL fractions. SDS-PAGE analysis and inspection of the UV trace determined the fractions (high protein:impurity ratios) to be pooled. *Size Exclusion Chromatography:* A Superdex S200 300 mL column (GE Healthcare) was pre-equilibrated with Buffer D. Protein from IMAC was concentrated to 2.0 mL and loaded onto the column with a flow rate of 2 $mL.min^{-1}$. Protein was eluted in Buffer D using automated UV Fractionation over 360 mL in 5 mL fractions. Protein fractions to be pooled and concentrated for use as enzyme stock were selected *via* analysis of the UV trace and SDS-PAGE (see below). Selected fractions were concentrated and aliquoted into 5–100 µL volumes, before being flash-frozen in liquid nitrogen and stored at –80 °C.

A NanoDrop ND-1000 UV/Vis spectrophotometer (Thermo Scientific) was used to determine protein concentration. 1.8 µL of protein sample was loaded, and absorbance at 280 nm was measured. The extinction coefficient, ε, was calculated using the ProtParam tool on the ExPASY Proteomics Server (www.expasy.org). ε(tKDM4A) = 75,300 $M^{-1}.cm^{-1}$.

Production of Apo-protein: 500 µL tKDM4A stock (294 µM) that had been previously purified *via* FPLC (see above) was introduced into a 3.5 kDa molecular weight cut-off dialysis cassette (Slide-a-Lyzer, Thermo Scientific) and incubated in dialysis buffer (50 mM HEPES pH 7.5, 500 mM NaCl) supplemented with 10 mM EDTA (700 mL) with gentle stirring at 4 °C. Dialysis buffer containing EDTA was replaced after 4 h, then a further 4 h, then incubated for a further 16 h overnight. The cassette was then transferred to fresh dialysis buffer without EDTA, supplemented with 2 $mg.mL^{-1}$ Chelex (700 mL) and dialysed for a further 24 h (4 °C, gentle stirring), with the buffer being replaced after 4 and 8 h. Enzyme stock was removed from the cassette, aliquoted into 5–100 µL volumes, flash frozen in liquid nitrogen and stored at –80 °C.

Iron occupancy assay: $FeSO_4$ was dissolved at concentrations of 0–250 μM in 0.5 M HCl for use as standard solutions. Protein samples for assessment were diluted in varying concentrations of HCl to give a final protein concentration of 100 μM in 0.5 M HCl. Samples were then heated at 80 °C for 10 min, then centrifuged to precipitate protein (Sigma 1-14 microfuge, 12470 x *g*, 5 min, 21° C) and the supernatant collected for analysis. Standard solutions and samples (20 μL of each) were then mixed with saturated ammonium acetate (20 μL), sodium metabisulfite (100 mM, 5 μL), bathophenanthroline disulfonic acid (100 mM, 1 μL) and H_2O (54 μL). Samples were incubated for 10 min, then 3 x 30 μL of each sample and standard were transferred into a clear bottomed, black 96-well half area microplate (Greiner Bio-One) and the absorbance at 535 nm measured using a PHERAstar FS microplate reader (BMG Labtech). The concentration of Fe^{2+} in protein samples was then interpolated using the standard curve.

7.1.3. SDS-PAGE analysis

Table 7.4 Recipes used for the production and running of polyacrylamide gels. *Note: β-mercaptoethanol was omitted in stability assays of the effect of H_2O_2 on tKDM4A, Chapter 5).

	SDS-PAGE separating gel buffer	**SDS-PAGE stacking gel buffer**	**1 x SDS-PAGE running buffer**	**2x protein loading buffer**
Tris-HCl pH 8.8	750 mM	---	25 mM	---
Tris-HCl pH 6.8	---	250 mM	---	50 mM
SDS	0.2% (w/v)	0.2% (w/v)	1.0% (w/v)	2.0% (w/v)
glycine	---	---	192 mM	---
glycerol	---	---	---	12% (v/v)
Bromophenol blue	---	---	---	0.2% (w/v)
β-mercaptoethanol*	---	---	---	5.0% (v/v)

Gels (per gel):

Table 7.5 Composition of polyacrylamide gels.

	Separating gel 15%	**Stacking gel 15%**
30% acrylamide	2.5 mL	300 µL
Milli-Q H_2O	---	700 µL
SDS-PAGE separating buffer	2.5 mL	---
SDS-PAGE stacking buffer	---	1 mL
Tetramethylethylenediamine (TEMED)	10 µL	5 µL
25% Ammonium persulfate (APS)	25 µL	10 µL

3.5 mL of separating gel and 1 mL of stacking gel were used per gel. APS and TEMED were added to gels immediately before pouring.

Staining and destaining gels:

Table 7.6 Composition of gel stain and destain solutions.

	Gel stain	**Gel destain**
Acetic acid	10% (w/v)	10% (w/v)
Methanol	30% (w/v)	30% (w/v)
Coomassie Brilliant Blue ®	0.25% (w/v)	---

Samples for SDS-PAGE analysis were mixed in a 1:1 ratio with 2 x SDS loading buffer and heated to 100 °C for 5 min before loading. A PageRuler^{TM} Thermo Scientific Molecular weight marker was used on all gels. Gels were run at 180 V for 50 min using a Bio-Rad Mini-PROTEAN II system, stained for 20 min using gel stain solution (Table 7.6) and then incubated in destain solution (Table 7.6) overnight. Gels were imaged using a ChemiDoc MP system (Bio-Rad).

7.1.4. Synthesis and purification of histone fragment peptides

Synthesis of the histone H3 peptide fragments $H3_{7\text{-}14}$K9me3 (ARKme3STGGK) and $H3_{1\text{-}15}$K9me3 (ARTKQTARKme3STGGKA) was carried out according to the methods detailed below. Both peptides were synthesised with *C*-terminal amide moieties.

Solid phase peptide synthesis: Peptides were synthesised using Fluorenylmethyloxycarbonyl (Fmoc) rink amide MBHA resin (0.05 mol, CS Bio) on a Liberty Blue™ automated microwave peptide synthesiser (CEM). N^{α}-Fmoc-protected amino acids (Polymer labs, 1 mmol per residue) in dimethylformamide (DMF, 5 mL per equivalent), except trimethyllysine (GL BioChem, China, 0.6 mmol in 3 mL DMF) and were activated using diisopropylcarbodiimide (DIC) and hydroxybenzotriazole (HOBt) at a ratio of 1:1 in DMF. A solution of trifluoroacetic acid (TFA, 92.5%), triisopropylsilane (2.5%), 1, 3-dimethoxybenzene (2.5%) and water (2.5%), was used to cleave the peptides from the resin. Peptides were then lyophilised and purified (see below).

Peptide purification: Peptides dissolved in water and up to 30% acetonitrile were purified *via* High Performance Liquid Chromatography (HPLC) using a Dionex UltiMate 3000 system and a VYDAC© Protein and Peptide C18 silica column (Grace Division Discovery Sciences™). $H3_{7\text{-}14}$K9me3 purification used a gradient of 0–20% acetonitrile over 20 min, while $H3_{1–15}$K9me3 used a gradient of 0-40% acetonitrile over 60 min. Peptide fractions of sufficient purity for use were identified using the UV trace (220 nm) and MALDI analysis. Peptide purity (Appendix 1) was assessed using High Performance Liquid Chromatography/ Liquid-Chromatography-Mass Spectrometry (HPLC/LC-MS) on an Agilent Technologies 1200 series HPLC/LC-MS system attached to an Agilent Technologies 6120 quadrupole mass spectrometer. Peptides were analysed using a Grace Vydac 218TP 50 mm x 4.6 mm

C^{18} column and the solvent conditions used in Table 7.7. Data was analysed using Agilent Chemstation software.

Table 7.7 Conditions used in the HPLC/LC-MS analysis of peptide purity. Solvent A is H_2O with 0.1% TFA. Solvent B is acetonitrile with 0.1% TFA.

Time/ min	Solvent A/ %	Solvent B/%
0.00	98.0	2.0
0.50	98.0	2.0
5.00	50.0	50.0
7.50	15.0	85.0
8.50	0.0	100.0
9.25	98.0	2.0
10.00	98.0	2.0

7.1.5. *In vitro* kinetic and inhibition assays

Assays were performed in 50 mM HEPES pH 7.5 unless otherwise stated. Di-ammonium iron(II) sulphate hexahydrate, $(NH_4)_2SO_4$ $FeSO_4.6H_2O$, was used as the source of Fe^{2+} in all experiments. This was dissolved in 20 mM HCl at a concentration of 100 mM, before dilution in Milli-Q water to the desired concentration.

Demethylation assay to assess enzyme activity: Reaction components were made up as follows, unless otherwise stated:

Table 7.8 General conditions used in *in vitro* demethylation assays.

	Stock concentration/ mM	Final concentration/ µM
Enzyme	0.05	1
Peptide	1.0	100
2OG	10	100
L-ascorbate	10	100
Fe^{2+}	1.0	10

A master mix containing buffer, peptide substrate, 2OG, L-ascorbate and Fe^{2+}were mixed and incubated at 37 °C for 2 min. The reaction was initiated by the addition of enzyme and at requisite time points, 5 µL reaction mixture was taken and quenched with an equal volume of methanol. Samples were stored at –20 °C until needed for MALDI analysis. All reactions were performed in triplicate unless otherwise stated.

Oxygen dependence assay: Final concentrations of reagents used were as follows:

Table 7.9 Conditions used in oxygen dependence assays.

Reaction component	**Concentration in $K_m^{app}(O_2)$ determination/ µM**
tKDM4A	1
Fe^{2+}	10
L-ascorbate	100
2OG	100
$H3_{7\text{-}14}$K9me3 Peptide	100
$H3_{1\text{-}15}$K9me3 Peptide	200

Enzyme stock from purification (Chapter 7.1.2) was thawed, aliquoted into 2 µL volumes, flash frozen in liquid nitrogen and stored at –80 °C until required. Aliquots were then thawed, diluted to 50 µM and used for three subsequent reactions (triplicate points) as required. Diluted peptide (96 µL) was sealed in a glass vial (Hichrom Ltd.), the lid of which was also sealed with Parafilm M ®. A 21 gauge needle was used to introduce the gas mixture composed of the desired percentage O_2 and N_2 from Mass Flow Controller (Brooks Instruments) into the vial, with a second 21 gauge needle used to maintain atmospheric pressure. A single vial containing peptide was equilibrated in this manner at 37 °C for 10 min. The needles were then removed from the vial and gas-tight Hamilton syringes were used to add minimal volumes of L-ascorbate, 2OG and Fe^{2+} sequentially, before the reaction was initiated *via* the addition of enzyme. The contents of the vial were mixed *via* gentle tapping for 10 s and then returned to incubate at 37 °C for 5 min. 100 µL methanol was

added to the vial to quench the reaction, 50 µL of which was taken into an eppendorf, flash frozen in liquid nitrogen, and stored at –20 °C until required for MALDI analysis. All points were assayed in triplicate.

***In vitro* IOX1 inhibition assays:** Assays used either 10 or 100 µM 2OG, as stated. For hypoxic experiments, buffer and water were equilibrated for 24 h in an Invivo$_2$ 500 hypoxic workstation set to 1.0% O_2, before being used to make stock solutions. Hypoxic assays were carried out in the hypoxic workstation.

Varied concentrations of IOX1^{282} (1 µL, to give a final concentration of 1.0% DMSO) were added to the reaction master mix of Fe^{2+}, L-ascorbate, 2OG and buffer (8 µL per reaction) immediately prior to initiation of the reaction by the addition of 1 µL enzyme (10 µM stock solution). Reactions were quenched with an equal volume of methanol after 5 min prior to MALDI analysis.

Peroxide inhibition assays: H_2O_2 was diluted in water to 10 x the final concentration required. All incubations and reactions were carried out at 37 °C and reaction components were used at the final concentrations detailed in Table 7.9, unless otherwise stated. Reactions were quenched after 5 min with an equal volume of methanol and frozen at –20 °C prior to MALDI analysis.

Preincubation of enzyme with H_2O_2: Varied concentrations of H_2O_2 (1 µL of 10 x stock) were added to 1.4 µM tKDM4A and buffer ± L-ascorbate (100 µM) to give a final volume of 8 µL per reaction. After 5 min, 2 µL of a master mix of peptide, 2OG, Fe^{2+} and L-ascorbate, if not mixed with the enzyme initially, was added to the tKDM4A:H_2O_2 mix to initiate the reaction.

Addition of H_2O_2 to reaction master mix: A master mix of peptide, buffer, 2OG and L-ascorbate (8 µL per reaction) was incubated at 37 °C, before the addition of varied concentrations of H_2O_2 (1 µL). Enzyme (1 µL) was added to each reaction immediately, to initiate the reaction.

SDS-PAGE analysis of the structural effect of H_2O_2: Recombinant enzyme (20 µM) was incubated with varied concentrations of Fe^{2+}, L-ascorbate and H_2O_2 (Chapter 5.2.2, Chapter 5.3.4) in a final volume of 25 µL at 37 °C for 30 min. Reactions were then quenched with an equal volume of 2 x protein loading buffer without the addition of β-mercaptoethanol (Table 7.4) and analysed *via* SDS-PAGE (Chapter 7.1.3).

Measurement of H_2O_2 concentration using an AmpliFlu™ Red assay: 50 µL of sample or H_2O_2 standard was dispensed into each well of a clear bottomed, black 96-well half area microplate (Greiner Bio-One) and treated as described (Chapter 5.4.1). After the relevant time period, 50 µL of a master mix containing AmpliFlu™ Red (100 µM) and Horseradish Peroxidase (0.2 $U.mL^{-1}$) was added to each well and incubated at room temperature (rt) for 30 min. Fluorescence was then measured using a 540/590 nm fluorescence module in a PHERAstar FS microplate reader, and the concentration of H_2O_2 in samples calculated using the standard curve[375].

MALDI analysis of peptide samples: 1 µL of α-cyano-4-hydroxycinnamic acid (CHCA MALDI matrix) and 1 µL of sample were added to each of a 96-spot MALDI plate. Samples were analysed in positive reflectron mode, flight tube voltage 12000 V, reflectron voltage 5200 V. Spectra were processed using MASSLYNX 4.0 (Waters), and the following parameters: background subtraction polynomial order 3, below curve (%) 10, tolerance 0.010; smooth window (channels) ± 3, number of smooths 5, Savitzky Golay method. The percentage of demethylated peptide was calculated using the following formula:

$$\%\ demethylated\ peptide\ = \frac{P_2}{P_1+P_2+P_3} + \frac{P_3}{P_1+P_2+P_3} \times 100 \qquad \textbf{7.1}$$

where:

P_1 = intensity of the peak of the trimethylated peptide substrate

P_2 = intensity of the monodemethylated peptide peak (M_w = M_w(peptide) - 14)

P_3 = intensity of the didemethylated peptide peak (M_w = M_w(peptide) - 28).

7.2. Materials and protocols relating to experiments in mammalian cells

All cell culture procedures were carried out using sterile technique in a laminar flowhood. All pipette tips and microfuge tubes used were sterile cell culture grade. Where sterile consumables could not be obtained, plasticware was autoclaved (20 min, 121 °C) before use. All equipment and consumables were sprayed with 70% ethanol before being introduced into the flowhood. Phosphate buffered saline (PBS pH 7.2, Life Technologies) was used in all wash steps in cell culture experiments, unless otherwise stated. All mammalian cells were incubated at 5.0% CO_2, 37 °C and grown until 70–80% confluent in T25 cell culture flasks, after which they were passaged or used in experiments.

7.2.1. Provenance and maintenance of mammalian cell lines

HeLa and U2OS cells were obtained from ATCC and maintained in Dulbecco's Modified Eagle Medium (DMEM) supplemented with 10% foetal bovine serum (FBS) and 1.0% L-glutamine. Penicillin G (50 IU.mL^{-1}): streptomycin (50 μg.mL^{-1}) (Pen:Strep, Invitrogen), was also added to growth medium for U2OS cells.

U2OS cells stably overexpressing dox-inducible FLAG-tagged KDM4A (F-KDM4A U2OS cells) were produced and kindly donated by Dr Norma Masson (Ratcliffe Laboratory, NDM, University of Oxford). U2OS cells stably overexpressing the catalytic domain of human

TET1 were produced by Dr Akane Kawamura. Cells were maintained in selection medium (DMEM supplemented with Tet system-approved FBS, (10%, Clontech), Pen:Strep (Invitrogen) L-glutamine (1.0%), hygromycin B (150 μg.mL^{-1}; Roche Applied Science) and blasticidin S (5 μg.mL^{-1}, Invitrogen)) and which was also used throughout all experimental procedures.

7.2.2. General cell culture procedures

Passaging cells: For a 1:10 split, medium was aspirated from the cells, which were then washed with 5 mL PBS. Cells were detached from the flask *via* the addition of 0.5 mL Trypsin-EDTA (0.25%), followed by incubation at 5.0% CO_2, 37 °C for 3–5 min. Cells were then gently resuspended in fresh growth medium (5.5 mL), before 0.6 mL were transferred to a clean flask containing 5.4 mL fresh growth medium.

Seeding 96-well plates: Medium was aspirated from confluent cells in a T75 flask, which were then washed (10 mL PBS) and detached using 0.25% Trypsin-EDTA solution (1 mL, see above for procedure). Cells were gently resuspended in 11 mL fresh medium and transferred to a sterile falcon tube. To count cell number, 10 μL cell suspension was mixed with an equal volume of 0.4% Trypan Blue (Life Technologies). 10 μL of the cell:Trypan Blue mix was introduced to the chamber of a dual chamber slide (Bio-Rad) and cells were counted using a TC20™ Automated Cell Counter (Bio-Rad). Cells were then diluted with fresh medium to give 8 x 10^4 HeLa cells.mL^{-1}, 5 x 10^4 F-KDM4A U2OS cells.mL^{-1} or 5.5 x 10^4 U2OS cells.mL^{-1}. Cell suspension (100 μL of HeLa or F-KDM4A U2OS cell suspensions or 90 μL of U2OS cell suspension) was dispensed per well of a 96-well Cell Carrier™, black, clear bottom TC treated plate (PerkinElmer) and 100 μL PBS was added to surrounding wells. Cells were incubated overnight (5.0% CO_2, 37 °C, 16 h).

Transient transfection: *Experiments in HeLa:* FuGENE® HD transfection reagent (Promega) was mixed with DNA stock solution at a ratio of 1:3 in OptiMEM minimal medium (Life Technologies) to give a final DNA concentration of 0.02 μg/μL. Medium on cells in the 96 well plates was replaced with 100 μL fresh media and the DNA-FuGENE® solution (5 μL) added to each appropriate well and mixed thoroughly. Cells were then incubated (5.0% CO_2, 37 °C).

Experiments in U2OS cells: U2OS cells were plated in 90 μL per well if transfected using Lipofectamine® 3000 reagent (Thermo Fisher Scientific) according to the manufacturer's protocol. Briefly, for each well to be transfected, 0.1 μg DNA was mixed with 5 μL Gibco® OptiMEM™ (Thermo Fisher Scientific) and 0.15 μL P3000 reagent. 0.15 μL Lipofectamine 3000 and 5 μL OptiMEM™ per well were mixed in a separate tube, then plasmid P3000 solution and the Lipofectamine® 3000 solution were mixed gently and incubated at rt for 5min. 10 μL of the plasmid:Lipofectamine mix was added to each well and incubated for 4 h (37 °C, 5.0% CO_2) prior to further experimental manipulation.

7.2.3. Hypoxic treatment of cells

HeLa cells: Prior to hypoxic incubation, HeLa cells were transfected with DNA encoding FLAG-KDM4A WT or FLAG KDM4A MUT using the FuGENE® HD transfection reagent (see protocol above) for 4 or 24 h, as stated, before medium containing the transfection reagent was replaced.

F-KDM4A U2OS cells: Growth medium on F-KDM4A U2OS cell was replaced with fresh media with or without dox (1 $\mu g.mL^{-1}$) before being immediately incubated at the required percentage O_2.

Cells treated as above were incubated in Invivo$_2$ 400 hypoxic workstations set to 0.1%, 0.5%, 3.0%, 5.0% or 21% O_2, (5.0% CO_2, 37 °C) for 24 h. Dissolved oxygen concentration in the medium above the cells was measured at regular intervals using an OxyLite Dissolved Oxygen Monitor with a bare fibre sensor (Oxford Optronix. See Appendix 2 for O_2 measurements).

7.2.4. Dosing of cells with small molecules:

U2OS cells: Following 4 h transient transfection, the growth medium on U2OS cells was replaced with medium containing the compound(s) of interest supplemented with 1.0% DMSO. Medium containing dm *(S)*-2HG, dm *(R)*-2HG, n-octyl *(S)*-2HG and n-octyl *(R)*-2HG was also supplemented with 0.5 mM HEPES pH 7.0 to avoid an increase in pH. *F-KDM4A U2OS cells:* After plating, medium on cells was replaced with medium containing IOX1 at varied concentrations and 1.0% DMSO, ± 1 μg.mL^{-1} dox. Both types of cells were incubated at either 1.0% or 21% O_2 (5.0% CO_2, 37 °C) for 24 h.

Peroxide inhibition experiments: *Experiment 1:* F-KDM4A U2OS cells were treated with DMEM ± dox (1 μg.mL^{-1}) and incubated for 4 h. The growth medium was replaced with OptiMEM™ ± 10 μM H_2O_2 every 30 min for a total time of 3 h. *Experiment 2:* F-KDM4A U2OS cells were treated with OptiMEM™ ± dox (1 μg.mL^{-1}) and incubated for 4 h. 2 μL H_2O_2 (1 mM) to give a final concentration of 20 μM, was added to relevant wells every 30 min, for a total dosing time of 4 h.

7.2.5. Antibodies used in immunofluorescence and western blot experiments

Primary and secondary antibodies used in immunofluorescence (IF) and western blot (WB) experiments are detailed in the table below.

Table 7.10 Antibodies used in immunofluorescence (IF) and western blot (WB) experiments.

	Experiment	Epitope	Conjugate	Host species	Source & catalogue no	Dilution
Primary antibodies	IF, WB	H3K9me3	---	Rabbit	Abcam, ab8898	1:1000
	IF, WB	H3K36me3	---	Rabbit	Abcam, ab9050	1:500
	IF, WB	FLAG	---	Mouse M2	Sigma, F1804	1:1000
	IF	5hmC	---	Rabbit	Active Motif 39769	1:500
	IF	HP1β	--	Rabbit	Abcam Ab10478	1:200
	WB	KDM4A	---	Rabbit	Bethyl Laboratories, A300-861A	1:1000
	WB	H3K4me3	---	Rabbit	Diagenode, C15410003-50	1:500
	WB	H3K27me3	---	Rabbit	Millipore, 07-449	1:500
	WB	H3	---	Mouse	Abcam, ab10799	1:1000
	WB	HIF-1α (human)	---	Mouse	BD Transduction Laboratories,	1:1000*
	WB	β-actin	---	Chicken	Abcam, ab13822	1:500
Secondary antibodies	IF	Rabbit IgG (H+L)	Alexa Fluor® 488	Goat	Life Technologies, A11034	1:500
	IF	Mouse IgG (H+L)	Alexa Fluor® 594	Goat	Life Technologies, A11032	1:500
	WB	Rabbit IgG (H+L)	Dylight 680	Goat	Life Technologies, 35568	1:10,000
	WB	Mouse IgG (H+L)	Dylight 800	Goat	Life Technologies, 35521	1:10,000
	WB	Chicken IgY (H+L)	Dylight 680	Goat	Thermo Fisher Scientific, SA5-10074	1:10,000

Antibodies for IF were diluted in blocking solution (3.0% FBS in PBS). Antibodies for WB were diluted in 3% SEA BLOCK (Thermo Scientific) in PBS + 0.1% Tween-20 (PBS-T),

with the exception of HIF-1α antibody, which was diluted in 5.0% (w/v) milk solution in PBS-T.

7.2.6. Immunofluorescence experiments

After treatment of cells in the relevant experimental conditions (see above) for the appropriate time, all immunofluorescence plates in a single experiment were processed concurrently. Plates were removed from the hypoxic workstations or incubator, and the medium aspirated. Cells were washed once then fixed and treated with antibodies according to the protocols below. All wash steps use 1 x PBS, and 50 µL of all solutions was used per well.

H3K9me3 fixing: Cells were incubated in 4% paraformaldehyde in PBS (50 µL/well) for 20 min rt then washed once.

H3K36me3 fixing: Cells were incubated in ice cold methanol for 4.5 min at –20 ºC then washed once.

TET1 overexpressing cells: After fixing and permeabilisation (see below), cells were washed with PBS and incubated in 2N HCl (30 min). HCl was removed by aspiration and well neutralised using 100 mM Tris-HCl pH 8.0 (15 min). After washing, the standard protocol for blocking and staining (see below) was subsequently followed.

After fixing, cells were treated with 0.5% Triton-X in PBS at rt for 6 min to permeabilise cell membranes, then washed once. Cells were blocked in 3.0% FBS in PBS for 60 min at rt. Blocking solution was aspirated from cells prior to the addition of primary antibodies (anti-FLAG and anti-histone lysine mark, Table 7.10) and incubation at rt overnight (16 h). After 3 x 5 min washes, fluorescently conjugated secondary antibodies (Table 7.10) were added to

cells and plates were incubated in the dark for 1 h at rt. Following a further 3 x 5 min washes, cell nuclei were stained using 4',6-diamidino-2-phenylindole (DAPI, 1:8000 in PBS, 3 min, rt, dark). DAPI was removed prior to 3 further 5 min washes, after which cells were imaged and analysed using an Operetta® High Content Imaging Microscope (PerkinElmer). In general, 3 wells of a 96 well plate were used per experimental condition, and 9 fields per well were imaged at 20 x magnification. Transfected or induced cells were selected using the FLAG fluorescence as described in Chapter 3, and H3K9me3 levels in the selected cells were calculated and averaged. Calculation of percentage demethylation of H3K9me3 and KDM4A activity were performed as described using equations 3.1-3.4. Standard error of the mean (sem) was calculated for the total sample population selected in individual experiments, while standard deviation (sd) was used to determine error between biological repeats.

7.2.7. Western blot experiments

Preparation of cell lysates: F-KDM4A U2OS cells were plated in 12-well clear TC-treated plates (Costar®, Corning) and incubated for 16 h (5.0% CO_2, 37 °C). Cells were then treated ± dox (1 μg.mL^{-1}), and incubated in hypoxic conditions (Chapter 7.2.3) for 24 h and remained in the hypoxic workstations during processing. Cells were washed in 1 x PBS, which had been incubated in the hypoxic workstation for 24 h, then scraped in SDS-Urea buffer (6.7 M urea, 10 mM Tris-Cl pH 6.8, 10% glycerol (w/v), and 1.0% SDS (w/v) supplemented with 1 mM dithiothreitol and Complete Protease Inhibitor Mixture (Roche Applied Science), 60 μL/well). Lysates were collected into a clean, sterile 1.6 mL microfuge tube and removed from the hypoxic workstations. Lysates were then sonicated using a Bandelin Sonoplus HD270 system, with a MS73 microtip (3 mm diameter, 10% amplitude, 3

x 10 s bursts with 10 s pauses) to shear genomic DNA. Lysates were aliquoted into 10 µL volumes and stored at –80 °C.

Protein concentration was assessed in samples using a Pierce Bicinchoninic Acid (BCA) Protein Assay Kit (Thermo Fisher Scientific), according to the microplate procedure in the manufacturer's protocol[377]. Standard samples were made by diluting bovine serum albumin (BSA, Thermo Fisher Scientific) in SDS-Urea buffer.

*Western blotting***:** Samples were prepared for loading in NuPAGE® LDS Sample Buffer (4 x, Life Technologies), supplemented with 100 µM dithiothreitol (DTT) and 1 µg protein sample was loaded per lane of a NuPAGE® Novex® Bis-Tris Precast gel (4-12%, 1 mm, 15 well, Thermo Fisher Scientific). Gels were run using a XCell SureLock™ Mini-Cell electrophoresis system (Thermo Fisher Scientific) and NuPAGE® MES SDS Running Buffer (20 x, Thermo Fisher Scientific) at 180 V for 40 min.

Proteins were transferred onto nitrocellulose membranes (0.45 µm pore size, Invitrogen) using wet transfer in an XCell SureLock™ Mini-Cell electrophoresis system with the XCell II Blot Module, at 30V, 4 ºC for 1 hr in transfer buffer (25 mM Tris base, 192 mM glycine, 10% methanol).

Membranes were blocked overnight at rt in 50% SEA BLOCK (Thermo Fisher Scientific) in PBS. Blocking solution was removed and membranes were incubated with primary antibodies (Table 7.10) for 1 h at rt with gentle shaking. After 3 x 5 min washes with PBS-T secondary antibodies (Table 7.10) were added and the membrane covered and incubated at rt for 1 h with gentle shaking. Following 3 further washes, the membrane was imaged on an Odyssey® CLx Infrared Imaging System (Licor) and analysed using Image Studio™ software.

Western blot analyses: Fluorescence signal of bands identified using Image Studio™ software was divided by the band surface area to give fluorescence intensity. Fluorescence intensity of methylated histone marks was normalised against that of H3 imaged on the same western blot, while fluorescence intensity of KDM4A and HIF was normalised relative to simultaneously imaged β-actin. Relative levels of each mark of interest in the samples tested were then calculated as described (Chapter 3.3.2).

7.2.8. RT-qPCR experiments

All experiments with RNA used DEPC-treated water and RNAse-free certified plasticware. Before work with isolated RNA, all laboratory benches and equipment were treated with RNase*Zap*® (Ambion™). Before work with cDNA, laboratory benches and pipettes were cleaned using Distel High Level Laboratory Disinfectant (Tristel) to remove all traces of DNA and RNA.

Isolation of mRNA: Following treatment of the cells under hypoxic conditions (see above), plates were removed from hypoxic workstations and total RNA isolated and purified using a mirVana miRNA isolation kit (Life Technologies) according to the manufacturer's protocol[378]. DNA was then removed from samples using a Turbo DNA-*free*™ kit (Invitrogen). RNA integrity, purity and concentration was assessed using a NanoDrop ND-1000 UV/Vis spectrophotometer, measuring the absorbance at 230, 260 and 280 nm. Samples with an A_{260}:A_{280} ratio of 1.8–2.2 were deemed of sufficient purity for use in RT-qPCR analysis. RNA was stored at –80 °C.

Reverse transcription to produce cDNA libraries: 500 ng of each RNA sample was reverse transcribed using a High-Capacity cDNA Reverse Transcription kit (Applied Biosystems) on

a DNA Engine Tetrad® 2 Peltier thermal cycler (Bio-Rad), using the conditions in Table 7.11 and according to the manufacturer's protocol[379].

Table 7.11 Thermal cycling conditions used in reverse transcription of cDNA.

Step	**1**	**2**	**3**	**4**
Temperature/ °C	25	37	85	10
Time/ min	10	120	5	∞

RT-qPCR primers: RT-qPCR primer sequences were derived from the primary literature (Table 7.12). Primers were ordered from Sigma.

Table 7.12 Oligonucleotide primer sets used in RT-qPCR analyses. Fwd: forward sequence (5'–3'), Rev: reverse sequence (3'–5'). * Primers were kindly donated by Dr Mun Chiang Chan, Ratcliffe Laboratory, NDM, University of Oxford.

Target	**Oligonucleotide Primer Sequence**	**Reference**
ADAM12	Fwd: CACCATTGAAAAACTAAGGTGTGTG Rev: GAGCCTGACAGGGTTGGAAG	380
ASCL2 set A	Fwd: GAAGGAGGGCGTGAGAAAG Rev: GCGGCTGGTTTTTAAATGTATAG	264
ASCL2 set B	Fwd: AGCCCGGCTCCCCGCGTTCCGCCTACT Rev: TAGCCCCCTAACCAGCTGGAGAAGTCG	142
β-actin	Fwd: GCTGTGCTACGTCGCCCTG Rev: GGAGGAGCTGGAAGCAGCC	*
CA9	Fwd: AAATCGCTGAGGAAGGCTCAGA Rev: CAGGGCGGTGTAGTCAGAGA	*
CHD5	Fwd: AGGATTACCACACGCTGACC Rev: GGTTCTTCTTGGCAATGAGTG	264
GP5	Fwd: ACTGCCACGCCTTCCTTT Rev: GCCTGTGAGAATGAAGAGCA	264
HIF1α	Fwd: GTCGGACAGCCTCACCAAACAGAGC Rev: GTTAACTTGATCCAAAGCTCTGAG	*
KDM4A	Fwd: GCCGCTAGAAGTTTCAGTGAG Rev: GCGTCCCTTGGACTTCTTATT	264
PPIC	Fwd: GGATTTCATGATTCAAGGAGGT Rev: TCTCACCATAGATGCTCACACC	264

The linearity and efficiency of primers were validated using a dilution series of input cDNA (Appendix 3), according to the method described by Pfaffl[269]. Briefly a dilution series of cDNA was tested against 300 nM primers using the protocol below. Ct values were then plotted against log[cDNA], then the slope of the resultant line of best fit used to calculate efficiency and the valid Ct range of each primer set (Appendix 3).

RT-qPCR analysis: RT-qPCR analysis reactions were set up in 20 µL volumes in a white skirted 96-well Hard-Shell ® PCR plates (thin walled, Bio-Rad) as follows.

Table 7.13 Reaction conditions used in RT-qPCR analyses.

Component	Stock concentration	Volume per reaction/ µL
cDNA	0.78125 ng.µL^{-1}	2
Forward + reverse primer mix	2 µM each	3
Power SYBR® Green Master Mix (Applied Biosystems)	--	10
H_2O	--	5

Reactions were carried out in a CFX1000™ Thermal Cycler with a CFX96™ Real-Time System (Bio-Rad) using the following thermal cycling conditions.

Table 7.14 Thermal cycling conditions used in RT-qPCR analyses.

Step	Activation	PCR (40 cycles)	
		Denature	Anneal/Extend
Temperature/ °C	95	95	60
Time	10 min	15 s	1 min

Data was collected and processed using CFX Manager™ Software v3.1 (Bio-Rad) and analysed using β-actin as a housekeeping gene, according to the ΔCt method[270]. 95% confidence intervals (CI) were calculated for technical repeats using the method described in the Applied Biosystems manual, page 56–59[270].

Chapter 8: References

(1) Crick, F. (1970) Central dogma of molecular biology. *Nature 227*, 561–3.

(2) Waddington, C. H. (2012) The epigenotype. 1942. *Int. J. Epidemiol. 41*, 10–3.

(3) Waddington, C. (1957) The Strategy of the Genes. George Allen & Unwin Ltd.

(4) Riggs, A., Martienssen, R., and Russo, V. (1996) Introduction, in *Epigenetic Mechanisms of Gene Regulation*. Cold Spring Harbour Monograph Archive.

(5) Bird, A. (2007) Perceptions of epigenetics. *Nature 447*, 396–398.

(6) Berger, S. L., Kouzarides, T., Shiekhattar, R., and Shilatifard, A. (2009) An operational definition of epigenetics. *Genes Dev 23*, 781–783.

(7) Bheda, P., and Schneider, R. (2014) Epigenetics reloaded: the single-cell revolution. *Trends Cell Biol. 24*, 712–723.

(8) Gill, M. E., Erkek, S., and Peters, A. H. (2012) Parental epigenetic control of embryogenesis: a balance between inheritance and reprogramming? *Curr. Opin. Cell Biol. 24*, 387–396.

(9) Kamakaka, R. T., and Biggins, S. (2005) Histone variants: deviants? *Genes Dev. 19*, 295–310.

(10) Luger, K., Mäder, A. W., Richmond, R. K., Sargent, D. F., and Richmond, T. J. (1997) Crystal structure of the nucleosome core particle at 2.8 A resolution. *Nature 389*, 251–60.

(11) Arents, G., Burlingame, R. W., Wang, B. C., Love, W. E., and Moudrianakis, E. N. (1991) The nucleosomal core histone octamer at 3.1 A resolution: a tripartite protein assembly and a left-handed superhelix. *Proc. Natl. Acad. Sci. U. S. A. 88*, 10148–52.

(12) Pan, C., and Fan, Y. (2016) Role of H1 linker histones in mammalian development and stem cell differentiation. *Biochim. Biophys. Acta - Gene Regul. Mech. 1859*, 496–509.

(13) Gao, M., Nadaud, P. S., Bernier, M. W., North, J. A., Hammel, P. C., Poirier, M. G., and Jaroniec, C. P. (2013) Histone H3 and H4 N-terminal tails in nucleosome arrays at cellular concentrations probed by magic angle spinning NMR spectroscopy. *J. Am. Chem. Soc. 135*, 15278–81.

(14) Saikusa, K., Fuchigami, S., Takahashi, K., Asano, Y., Nagadoi, A., Tachiwana, H., Kurumizaka, H., Ikeguchi, M., Nishimura, Y., and Akashi, S. (2013) Gas-phase structure of the histone multimers characterized by ion mobility mass spectrometry and molecular dynamics simulation. *Anal. Chem. 85*, 4165–71.

(15) Iwasaki, W., Miya, Y., Horikoshi, N., Osakabe, A., Taguchi, H., Tachiwana, H., Shibata, T., Kagawa, W., and Kurumizaka, H. (2013) Contribution of histone N-terminal tails to the structure and stability of nucleosomes. *FEBS Open Bio 3*, 363–9.

(16) Talbert, P. B., and Henikoff, S. (2010) Histone variants--ancient wrap artists of the epigenome. *Nat. Rev. Mol. Cell Biol. 11*, 264–75.

(17) Ismail, I. H., and Hendzel, M. J. (2008) The gamma-H2A.X: is it just a surrogate marker of double-strand breaks or much more? *Environ. Mol. Mutagen. 49*, 73–82.

(18) Witt, O., Albig, W., and Doenecke, D. (1996) Testis-specific expression of a novel

human H3 histone gene. *Exp. Cell Res. 229*, 301–6.

(19) Palmer, D. K., O'Day, K., Trong, H. L., Charbonneau, H., and Margolis, R. L. (1991) Purification of the centromere-specific protein CENP-A and demonstration that it is a distinctive histone. *Proc. Natl. Acad. Sci. U. S. A. 88*, 3734–8.

(20) Park, Y.-J., and Luger, K. (2008) Histone chaperones in nucleosome eviction and histone exchange. *Curr. Opin. Struct. Biol. 18*, 282–9.

(21) Zlatanova, J., Bishop, T. C., Victor, J.-M., Jackson, V., and van Holde, K. (2009) The Nucleosome Family: Dynamic and Growing. *Structure 17*, 160–171.

(22) Felsenfeld, G., and Groudine, M. (2003) Controlling the double helix. *Nature 421*, 448–453.

(23) Woodcock, C. L., and Ghosh, R. P. (2010) Chromatin higher-order structure and dynamics. *Cold Spring Harb. Perspect. Biol. 2*, a000596.

(24) Chuang, J. C., and Jones, P. A. (2007) Epigenetics and microRNAs. *Pediatr. Res. 61*, 24R–29R.

(25) Becker, P. B., and Hörz, W. (2002) ATP-Dependent Nucleosome Remodeling. *Annu. Rev. Biochem. 71*, 247–273.

(26) Bird, A. P. CpG-rich islands and the function of DNA methylation. *Nature 321*, 209–13.

(27) Edwards, C. A., and Ferguson-Smith, A. C. (2007) Mechanisms regulating imprinted genes in clusters. *Curr. Opin. Cell Biol. 19*, 281–289.

(28) Kelsey, G., and Feil, R. (2013) New insights into establishment and maintenance of DNA methylation imprints in mammals. *Philos. Trans. R. Soc. Lond. B. Biol. Sci. 368*, 20110336.

(29) Gartler, S. M., and Riggs, A. D. (1983) Mammalian X-chromosome inactivation. *Annu. Rev. Genet. 17*, 155–90.

(30) Heard, E., Clerc, P., and Avner, P. (1997) X-chromosome inactivation in mammals. *Annu. Rev. Genet. 31*, 571–610.

(31) Watt, F., and Molloy, P. L. (1988) Cytosine methylation prevents binding to DNA of a HeLa cell transcription factor required for optimal expression of the adenovirus major late promoter. *Genes Dev. 2*, 1136–43.

(32) Boyes, J., and Bird, A. (1991) DNA methylation inhibits transcription indirectly via a methyl-CpG binding protein. *Cell 64*, 1123–34.

(33) Klose, R. J., and Bird, A. P. (2006) Genomic DNA methylation: the mark and its mediators. *Trends Biochem. Sci. 31*, 89–97.

(34) Smith, Z. D., Chan, M. M., Mikkelsen, T. S., Gu, H., Gnirke, A., Regev, A., and Meissner, A. (2012) A unique regulatory phase of DNA methylation in the early mammalian embryo. *Nature 484*, 339–44.

(35) Okano, M., Bell, D. W., Haber, D. A., and Li, E. (1999) DNA methyltransferases Dnmt3a and Dnmt3b are essential for de novo methylation and mammalian development. *Cell 99*, 247–57.

(36) Law, J. A., and Jacobsen, S. E. (2010) Establishing, maintaining and modifying DNA methylation patterns in plants and animals. *Nat. Rev. Genet. 11*, 204–20.

(37) Zhu, J.-K. (2009) Active DNA demethylation mediated by DNA glycosylases. *Annu.*

Rev. Genet. 43, 143–66.

(38) Tahiliani, M., Koh, K. P., Shen, Y., Pastor, W. A., Bandukwala, H., Brudno, Y., Agarwal, S., Iyer, L. M., Liu, D. R., Aravind, L., and Rao, A. (2009) Conversion of 5-methylcytosine to 5-hydroxymethylcytosine in mammalian DNA by MLL partner TET1. *Science 324*, 930–5.

(39) Ito, S., Shen, L., Dai, Q., Wu, S. C., Collins, L. B., Swenberg, J. A., He, C., and Zhang, Y. (2011) Tet proteins can convert 5-methylcytosine to 5-formylcytosine and 5-carboxylcytosine. *Science 333*, 1300–3.

(40) He, Y.-F., Li, B.-Z., Li, Z., Liu, P., Wang, Y., Tang, Q., Ding, J., Jia, Y., Chen, Z., Li, L., Sun, Y., Li, X., Dai, Q., Song, C.-X., Zhang, K., He, C., and Xu, G.-L. (2011) Tet-mediated formation of 5-carboxylcytosine and its excision by TDG in mammalian DNA. *Science 333*, 1303–7.

(41) Sancar, A., Lindsey-Boltz, L. A., Unsal-Kaçmaz, K., and Linn, S. (2004) Molecular mechanisms of mammalian DNA repair and the DNA damage checkpoints. *Annu. Rev. Biochem. 73*, 39–85.

(42) Morgan, H. D., Dean, W., Coker, H. A., Reik, W., and Petersen-Mahrt, S. K. (2004) Activation-induced cytidine deaminase deaminates 5-methylcytosine in DNA and is expressed in pluripotent tissues: implications for epigenetic reprogramming. *J. Biol. Chem. 279*, 52353–60.

(43) Nabel, C. S., Jia, H., Ye, Y., Shen, L., Goldschmidt, H. L., Stivers, J. T., Zhang, Y., and Kohli, R. M. (2012) AID/APOBEC deaminases disfavor modified cytosines implicated in DNA demethylation. *Nat. Chem. Biol. 8*, 751–8.

(44) Straussman, R., Nejman, D., Roberts, D., Steinfeld, I., Blum, B., Benvenisty, N., Simon, I., Yakhini, Z., and Cedar, H. (2009) Developmental programming of CpG island methylation profiles in the human genome. *Nat. Struct. Mol. Biol. 16*, 564–571.

(45) Illingworth, R. S., and Bird, A. P. (2009) CpG islands – "A rough guide." *FEBS Lett. 583*, 1713–1720.

(46) Kouzarides, T. (2007) Chromatin modifications and their function. *Cell 128*, 693–705.

(47) Strahl, B. D., and Allis, C. D. (2000) The language of covalent histone modifications. *Nature 403*, 41–5.

(48) Lee, J.-S., Smith, E., and Shilatifard, A. (2010) The Language of Histone Crosstalk. *Cell 142*, 682–685.

(49) Zhang, T., Cooper, S., and Brockdorff, N. (2015) The interplay of histone modifications - writers that read. *EMBO Rep. 16*, 1467–81.

(50) Tan, M., Luo, H., Lee, S., Jin, F., Yang, J. S., Montellier, E., Buchou, T., Cheng, Z., Rousseaux, S., Rajagopal, N., Lu, Z., Ye, Z., Zhu, Q., Wysocka, J., Ye, Y., Khochbin, S., Ren, B., and Zhao, Y. (2011) Identification of 67 Histone Marks and Histone Lysine Crotonylation as a New Type of Histone Modification. *Cell 146*, 1016–1028.

(51) Xie, Z., Dai, J., Dai, L., Tan, M., Cheng, Z., Wu, Y., Boeke, J. D., and Zhao, Y. (2012) Lysine succinylation and lysine malonylation in histones. *Mol. Cell. Proteomics 11*, 100–7.

(52) Xu, Y.-M., Du, J.-Y., and Lau, A. T. Y. (2014) Posttranslational modifications of human histone H3: an update. *Proteomics 14*, 2047–60.

(53) Hebbes, T. R., Thorne, A. W., and Crane-Robinson, C. (1988) A direct link between

core histone acetylation and transcriptionally active chromatin. *EMBO J. 7*, 1395–402.

(54) Yang, X.-J., and Seto, E. (2007) HATs and HDACs: from structure, function and regulation to novel strategies for therapy and prevention. *Oncogene 26*, 5310–5318.

(55) Hong, L., Schroth, G. P., Matthews, H. R., Yau, P., and Bradbury, E. M. (1993) Studies of the DNA binding properties of histone H4 amino terminus. Thermal denaturation studies reveal that acetylation markedly reduces the binding constant of the H4 "tail" to DNA. *J. Biol. Chem. 268*, 305–14.

(56) Lee, D. Y., Hayes, J. J., Pruss, D., and Wolffe, A. P. (1993) A positive role for histone acetylation in transcription factor access to nucleosomal DNA. *Cell 72*, 73–84.

(57) Vettese-Dadey, M., Grant, P. A., Hebbes, T. R., Crane- Robinson, C., Allis, C. D., and Workman, J. L. (1996) Acetylation of histone H4 plays a primary role in enhancing transcription factor binding to nucleosomal DNA in vitro. *EMBO J. 15*, 2508–18.

(58) Foster, E. R., and Downs, J. A. (2005) Histone H2A phosphorylation in DNA double-strand break repair. *FEBS J. 272*, 3231–40.

(59) Rossetto, D., Avvakumov, N., and Côté, J. (2012) Histone phosphorylation: a chromatin modification involved in diverse nuclear events. *Epigenetics 7*, 1098–108.

(60) Wei, Y., Mizzen, C. A., Cook, R. G., Gorovsky, M. A., and Allis, C. D. (1998) Phosphorylation of histone H3 at serine 10 is correlated with chromosome condensation during mitosis and meiosis in Tetrahymena. *Proc. Natl. Acad. Sci. U. S. A. 95*, 7480–4.

(61) Di Lorenzo, A., and Bedford, M. T. (2011) Histone arginine methylation. *FEBS Lett. 585*, 2024–31.

(62) Cuthbert, G. L., Daujat, S., Snowden, A. W., Erdjument-Bromage, H., Hagiwara, T., Yamada, M., Schneider, R., Gregory, P. D., Tempst, P., Bannister, A. J., and Kouzarides, T. (2004) Histone deimination antagonizes arginine methylation. *Cell 118*, 545–53.

(63) Black, J. C., Van Rechem, C., and Whetstine, J. R. (2012) Histone Lysine Methylation Dynamics: Establishment, Regulation, and Biological Impact. *Mol. Cell 48*, 491–507.

(64) Bannister, A. J., and Kouzarides, T. (2003) Histone Methylation: Recognizing the Methyl Mark. *Methods Enzymol. 376*, 269–288.

(65) Barski, A., Cuddapah, S., Cui, K., Roh, T.-Y., Schones, D. E., Wang, Z., Wei, G., Chepelev, I., and Zhao, K. (2007) High-resolution profiling of histone methylations in the human genome. *Cell 129*, 823–37.

(66) Santos-Rosa, H., Schneider, R., Bannister, A. J., Sherriff, J., Bernstein, B. E., Emre, N. C. T., Schreiber, S. L., Mellor, J., and Kouzarides, T. (2002) Active genes are tri-methylated at K4 of histone H3. *Nature 419*, 407–11.

(67) Schneider, R., Bannister, A. J., Myers, F. A., Thorne, A. W., Crane-Robinson, C., and Kouzarides, T. (2004) Histone H3 lysine 4 methylation patterns in higher eukaryotic genes. *Nat. Cell Biol. 6*, 73–7.

(68) Jenuwein, T. (2001) Re-SET-ting heterochromatin by histone methyltransferases. *Trends Cell Biol. 11*, 266–273.

(69) Rea, S., Eisenhaber, F., O'Carroll, D., Strahl, B. D., Sun, Z. W., Schmid, M., Opravil, S., Mechtler, K., Ponting, C. P., Allis, C. D., and Jenuwein, T. (2000) Regulation of chromatin structure by site-specific histone H3 methyltransferases. *Nature 406*, 593–9.

(70) Tachibana, M., Sugimoto, K., Fukushima, T., and Shinkai, Y. (2001) Set domain-containing protein, G9a, is a novel lysine-preferring mammalian histone methyltransferase with hyperactivity and specific selectivity to lysines 9 and 27 of histone H3. *J. Biol. Chem. 276*, 25309–17.

(71) Patel, A., Dharmarajan, V., Vought, V. E., and Cosgrove, M. S. (2009) On the mechanism of multiple lysine methylation by the human mixed lineage leukemia protein-1 (MLL1) core complex. *J. Biol. Chem. 284*, 24242–56.

(72) Boriack-Sjodin, P. A., and Swinger, K. K. (2016) Protein Methyltransferases: A Distinct, Diverse, and Dynamic Family of Enzymes. *Biochemistry 55*, 1557–1569.

(73) Zhang, X., Wen, H., and Shi, X. (2012) Lysine methylation: beyond histones. *Acta Biochim. Biophys. Sin. (Shanghai). 44*, 14–27.

(74) Shi, Y., Lan, F., Matson, C., Mulligan, P., Whetstine, J. R., Cole, P. A., and Casero, R. A. (2004) Histone demethylation mediated by the nuclear amine oxidase homolog LSD1. *Cell 119*, 941–953.

(75) Scrutton, N. S., Edmondson, D. E., Mattevi, A., *et al*. (2004) Chemical aspects of amine oxidation by flavoprotein enzymes. *Nat. Prod. Rep. 21*, 722.

(76) Karytinos, A., Forneris, F., Profumo, A., Ciossani, G., Battaglioli, E., Binda, C., and Mattevi, A. (2009) A novel mammalian flavin-dependent histone demethylase. *J. Biol. Chem. 284*, 17775–82.

(77) Nguyen, A. T., and Zhang, Y. (2011) The diverse functions of Dot1 and H3K79 methylation. *Genes Dev. 25*, 1345–58.

(78) Clifton, I. J., McDonough, M. A., Ehrismann, D., Kershaw, N. J., Granatino, N., and Schofield, C. J. (2006) Structural studies on 2-oxoglutarate oxygenases and related double-stranded beta-helix fold proteins. *J. Inorg. Biochem. 100*, 644–69.

(79) McDonough, M. A., Loenarz, C., Chowdhury, R., Clifton, I. J., and Schofield, C. J. (2010) Structural studies on human 2-oxoglutarate dependent oxygenases. *Curr. Opin. Struct. Biol. 20*, 659–72.

(80) Martinez, S., and Hausinger, R. P. (2015) Catalytic Mechanisms of Fe(II)- and 2-Oxoglutarate-dependent Oxygenases. *J. Biol. Chem. 290*, 20702–11.

(81) Roach, P. L., Clifton, I. J., Fülöp, V., Harlos, K., Barton, G. J., Hajdu, J., Andersson, I., Schofield, C. J., and Baldwin, J. E. (1995) Crystal structure of isopenicillin N synthase is the first from a new structural family of enzymes. *Nature 375*, 700–704.

(82) Valegård, K., van Scheltinga, A. C., Lloyd, M. D., Hara, T., Ramaswamy, S., Perrakis, A., Thompson, A., Lee, H. J., Baldwin, J. E., Schofield, C. J., Hajdu, J., and Andersson, I. (1998) Structure of a cephalosporin synthase. *Nature 394*, 805–9.

(83) Zhou, J., Gunsior, M., Bachmann, B. O., Townsend, C. A., and Solomon, E. I. (1998) Substrate Binding to the α-Ketoglutarate-Dependent Non-Heme Iron Enzyme Clavaminate Synthase 2: Coupling Mechanism of Oxidative Decarboxylation and Hydroxylation. *J. Am. Chem. Soc. 120*, 13539–13540.

(84) Zhang, Z., Ren, J., Stammers, D. K., Baldwin, J. E., Harlos, K., and Schofield, C. J. (2000) Structural origins of the selectivity of the trifunctional oxygenase clavaminic acid synthase. *Nat. Struct. Biol. 7*, 127–33.

(85) Flashman, E., Hoffart, L. M., Hamed, R. B., Bollinger Jr., J. M., Krebs, C., and

Schofield, C. J. (2010) Evidence for the slow reaction of hypoxia-inducible factor prolyl hydroxylase 2 with oxygen. *FEBS J 277*, 4089–4099.

(86) Welford, R. W. D., Kirkpatrick, J. M., McNeill, L. A., Puri, M., Oldham, N. J., and Schofield, C. J. (2005) Incorporation of oxygen into the succinate co-product of iron(II) and 2-oxoglutarate dependent oxygenases from bacteria, plants and humans. *FEBS Lett. 579*, 5170–4.

(87) Price, J. C., Barr, E. W., Tirupati, B., Bollinger, J. M., and Krebs, C. (2003) The first direct characterization of a high-valent iron intermediate in the reaction of an alpha-ketoglutarate-dependent dioxygenase: a high-spin FeIV complex in taurine/alpha-ketoglutarate dioxygenase (TauD) from Escherichia coli. *Biochemistry 42*, 7497–508.

(88) Hoffart, L. M., Barr, E. W., Guyer, R. B., Bollinger, J. M., and Krebs, C. (2006) Direct spectroscopic detection of a C-H-cleaving high-spin Fe(IV) complex in a prolyl-4-hydroxylase. *Proc. Natl. Acad. Sci. U. S. A. 103*, 14738–43.

(89) De Jong, L., Albracht, S. P. J., and Kemp, A. (1982) Prolyl 4-hydroxylase activity in relation to the oxidation state of enzyme-bound iron: The role of ascorbate in peptidyl proline hydroxylation. *Biochim. Biophys. Acta - Protein Struct. Mol. Enzymol. 704*, 326–332.

(90) Knowles, H. J., Raval, R. R., Harris, A. L., and Ratcliffe, P. J. (2003) Effect of Ascorbate on the Activity of Hypoxia-inducible Factor in Cancer Cells. *Cancer Res. 63*.

(91) Flashman, E., Davies, S. L., Yeoh, K. K., and Schofield, C. J. (2010) Investigating the dependence of the hypoxia-inducible factor hydroxylases (factor inhibiting HIF and prolyl hydroxylase domain 2) on ascorbate and other reducing agents. *Biochem. J. 427*.

(92) Takeuchi, T., Yamazaki, Y., Katoh-Fukui, Y., Tsuchiya, R., Kondo, S., Motoyama, J., and Higashinakagawa, T. (1995) Gene trap capture of a novel mouse gene, jumonji, required for neural tube formation. *Genes Dev. 9*, 1211–22.

(93) Yamane, K., Toumazou, C., Tsukada, Y., Erdjument-Bromage, H., Tempst, P., Wong, J., and Zhang, Y. (2006) JHDM2A, a JmjC-containing H3K9 demethylase, facilitates transcription activation by androgen receptor. *Cell 125*, 483–95.

(94) Cockman, M. E., Webb, J. D., and Ratcliffe, P. J. (2009) FIH-dependent asparaginyl hydroxylation of ankyrin repeat domain-containing proteins. *Ann. N. Y. Acad. Sci. 1177*, 9–18.

(95) Ge, W., Wolf, A., Feng, T., Ho, C., Sekirnik, R., Zayer, A., Granatino, N., Cockman, M. E., Loenarz, C., Loik, N. D., Hardy, A. P., Claridge, T. D. W., Hamed, R. B., Chowdhury, R., Gong, L., Robinson, C. V, Trudgian, D. C., Jiang, M., Mackeen, M. M., McCullagh, J. S., Gordiyenko, Y., Thalhammer, A., Yamamoto, A., Yang, M., Liu-Yi, P., Zhang, Z., Schmidt-Zachmann, M., Kessler, B. M., Ratcliffe, P. J., Preston, G. M., Coleman, M. L., and Schofield, C. J. (2012) Oxygenase-catalyzed ribosome hydroxylation occurs in prokaryotes and humans. *Nat. Chem. Biol. 8*, 960–2.

(96) Youn, M.-Y., Yokoyama, A., Fujiyama-Nakamura, S., Ohtake, F., Minehata, K., Yasuda, H., Suzuki, T., Kato, S., and Imai, Y. (2012) JMJD5, a Jumonji C (JmjC) domain-containing protein, negatively regulates osteoclastogenesis by facilitating NFATc1 protein degradation. *J. Biol. Chem. 287*, 12994–3004.

(97) Del Rizzo, P. A., Krishnan, S., and Trievel, R. C. (2012) Crystal structure and functional analysis of JMJD5 indicate an alternate specificity and function. *Mol. Cell. Biol. 32*, 4044–52.

(98) Webby, C. J., Wolf, A., Gromak, N., Dreger, M., Kramer, H., Kessler, B., Nielsen, M. L., Schmitz, C., Butler, D. S., Yates, J. R., Delahunty, C. M., Hahn, P., Lengeling, A., Mann, M., Proudfoot, N. J., Schofield, C. J., and Böttger, A. (2009) Jmjd6 catalyses lysyl-hydroxylation of U2AF65, a protein associated with RNA splicing. *Science 325*, 90–3.

(99) Sinha, K. M., Yasuda, H., Coombes, M. M., Dent, S. Y. R., and de Crombrugghe, B. (2010) Regulation of the osteoblast-specific transcription factor Osterix by NO66, a Jumonji family histone demethylase. *EMBO J. 29*, 68–79.

(100) Lu, Y., Chang, Q., Zhang, Y., Beezhold, K., Rojanasakul, Y., Zhao, H., Castranova, V., Shi, X., and Chen, F. (2009) Lung cancer-associated JmjC domain protein mdig suppresses formation of tri-methyl lysine 9 of histone H3. *Cell Cycle 8*, 2101–9.

(101) Hsia, D. A., Tepper, C. G., Pochampalli, M. R., Hsia, E. Y. C., Izumiya, C., Huerta, S. B., Wright, M. E., Chen, H.-W., Kung, H.-J., and Izumiya, Y. (2010) KDM8, a H3K36me2 histone demethylase that acts in the cyclin A1 coding region to regulate cancer cell proliferation. *Proc. Natl. Acad. Sci. U. S. A. 107*, 9671–6.

(102) Chang, B., Chen, Y., Zhao, Y., and Bruick, R. K. (2007) JMJD6 is a histone arginine demethylase. *Science 318*, 444–7.

(103) Tsukada, Y., Fang, J., Erdjument-Bromage, H., Warren, M. E., Borchers, C. H., Tempst, P., and Zhang, Y. (2005) Histone demethylation by a family of JmjC domain-containing proteins. *Nature 439*, 811–816.

(104) Tzatsos, A., Pfau, R., Kampranis, S. C., and Tsichlis, P. N. (2009) Ndy1/KDM2B immortalizes mouse embryonic fibroblasts by repressing the Ink4a/Arf locus. *Proc. Natl. Acad. Sci. 106*, 2641–2646.

(105) Loh, Y.-H., Zhang, W., Chen, X., George, J., and Ng, H.-H. (2007) Jmjd1a and Jmjd2c histone H3 Lys 9 demethylases regulate self-renewal in embryonic stem cells. *Genes Dev. 21*, 2545–57.

(106) Yamane, K., Toumazou, C., Tsukada, Y., Erdjument-Bromage, H., Tempst, P., Wong, J., and Zhang, Y. (2006) JHDM2A, a JmjC-containing H3K9 demethylase, facilitates transcription activation by androgen receptor. *Cell 125*, 483–495.

(107) Kim, J.-Y., Kim, K.-B., Eom, G. H., Choe, N., Kee, H. J., Son, H.-J., Oh, S.-T., Kim, D.-W., Pak, J. H., Baek, H. J., Kook, H., Hahn, Y., Kook, H., Chakravarti, D., and Seo, S.-B. (2012) KDM3B Is the H3K9 Demethylase Involved in Transcriptional Activation of lmo2 in Leukemia. *Mol. Cell. Biol. 32*, 2917–2933.

(108) Kim, S.-M., Kim, J.-Y., Choe, N.-W., Cho, I.-H., Kim, J.-R., Kim, D.-W., Seol, J.-E., Lee, S. E., Kook, H., Nam, K.-I., Kook, H., Bhak, Y.-Y., and Seo, S.-B. (2010) Regulation of mouse steroidogenesis by WHISTLE and JMJD1C through histone methylation balance. *Nucleic Acids Res. 38*, 6389–403.

(109) Liu, L., Kim, H., Casta, A., Kobayashi, Y., Shapiro, L. S., and Christiano, A. M. (2014) Hairless is a histone H3K9 demethylase. *FASEB J. 28*, 1534–1542.

(110) Klose, R. J., Yamane, K., Bae, Y., Zhang, D., Erdjument-Bromage, H., Tempst, P., Wong, J., and Zhang, Y. (2006) The transcriptional repressor JHDM3A demethylates trimethyl histone H3 lysine 9 and lysine 36. *Nature 442*, 312–6.

(111) Fodor, B. D., Kubicek, S., Yonezawa, M., O'Sullivan, R. J., Sengupta, R., Perez-Burgos, L., Opravil, S., Mechtler, K., Schotta, G., and Jenuwein, T. (2006) Jmjd2b antagonizes H3K9 trimethylation at pericentric heterochromatin in mammalian cells. *Genes*

Dev. 20, 1557–62.

(112) Cloos, P. A. C., Christensen, J., Agger, K., Maiolica, A., Rappsilber, J., Antal, T., Hansen, K. H., and Helin, K. (2006) The putative oncogene GASC1 demethylates tri- and dimethylated lysine 9 on histone H3. *Nature 442*, 307–11.

(113) Whetstine, J. R., Nottke, A., Lan, F., Huarte, M., Smolikov, S., Chen, Z., Spooner, E., Li, E., Zhang, G., Colaiacovo, M., and Shi, Y. (2006) Reversal of histone lysine trimethylation by the JMJD2 family of histone demethylases. *Cell 125*, 467–81.

(114) Chen, Z., Zang, J., Whetstine, J., Hong, X., Davrazou, F., Kutateladze, T. G., Simpson, M., Mao, Q., Pan, C.-H., Dai, S., Hagman, J., Hansen, K., Shi, Y., and Zhang, G. (2006) Structural insights into histone demethylation by JMJD2 family members. *Cell 125*, 691–702.

(115) Shin, S., and Janknecht, R. (2007) Diversity within the JMJD2 histone demethylase family. *Biochem. Biophys. Res. Commun. 353*, 973–977.

(116) Trojer, P., Zhang, J., Yonezawa, M., Schmidt, A., Zheng, H., Jenuwein, T., and Reinberg, D. (2009) Dynamic Histone H1 Isotype 4 Methylation and Demethylation by Histone Lysine Methyltransferase G9a/KMT1C and the Jumonji Domain-containing JMJD2/KDM4 Proteins. *J. Biol. Chem. 284*, 8395–405.

(117) Williams, S. T., Walport, L. J., Hopkinson, R. J., Madden, S. K., Chowdhury, R., Schofield, C. J., and Kawamura, A. (2015) Studies on the catalytic domains of multiple JmjC oxygenases using peptide substrates. *Epigenetics 9*, 1596–1603.

(118) Christensen, J., Agger, K., Cloos, P. A. C., Pasini, D., Rose, S., Sennels, L., Rappsilber, J., Hansen, K. H., Salcini, A. E., and Helin, K. (2007) RBP2 Belongs to a Family of Demethylases, Specific for Tri-and Dimethylated Lysine 4 on Histone 3. *Cell 128*, 1063–1076.

(119) Iwase, S., Lan, F., Bayliss, P., de la Torre-Ubieta, L., Huarte, M., Qi, H. H., Whetstine, J. R., Bonni, A., Roberts, T. M., and Shi, Y. (2007) The X-linked mental retardation gene SMCX/JARID1C defines a family of histone H3 lysine 4 demethylases. *Cell 128*, 1077–88.

(120) Eissenberg, J. C., Lee, M. G., Schneider, J., Ilvarsonn, A., Shiekhattar, R., and Shilatifard, A. (2007) The trithorax-group gene in Drosophila little imaginal discs encodes a trimethylated histone H3 Lys4 demethylase. *Nat. Struct. Mol. Biol. 14*, 344–346.

(121) Lee, M. G., Norman, J., Shilatifard, A., and Shiekhattar, R. (2007) Physical and Functional Association of a Trimethyl H3K4 Demethylase and Ring6a/MBLR, a Polycomb-like Protein. *Cell 128*, 877–887.

(122) Blair, L. P., Cao, J., Zou, M. R., Sayegh, J., and Yan, Q. (2011) Epigenetic Regulation by Lysine Demethylase 5 (KDM5) Enzymes in Cancer. *Cancers (Basel). 3*, 1383–404.

(123) Agger, K., Cloos, P. A. C., Christensen, J., Pasini, D., Rose, S., Rappsilber, J., Issaeva, I., Canaani, E., Salcini, A. E., and Helin, K. (2007) UTX and JMJD3 are histone H3K27 demethylases involved in HOX gene regulation and development. *Nature 449*, 731–4.

(124) De Santa, F., Totaro, M. G., Prosperini, E., Notarbartolo, S., Testa, G., and Natoli, G. (2007) The histone H3 lysine-27 demethylase Jmjd3 links inflammation to inhibition of polycomb-mediated gene silencing. *Cell 130*, 1083–94.

(125) Lan, F., Bayliss, P. E., Rinn, J. L., Whetstine, J. R., Wang, J. K., Chen, S., Iwase, S., Alpatov, R., Issaeva, I., Canaani, E., Roberts, T. M., Chang, H. Y., and Shi, Y. (2007) A histone H3 lysine 27 demethylase regulates animal posterior development. *Nature 449*, 689–

694.

(126) Lee, M. G., Villa, R., Trojer, P., Norman, J., Yan, K.-P., Reinberg, D., Di Croce, L., and Shiekhattar, R. (2007) Demethylation of H3K27 regulates polycomb recruitment and H2A ubiquitination. *Science 318*, 447–50.

(127) Hong, S., Cho, Y.-W., Yu, L.-R., Yu, H., Veenstra, T. D., and Ge, K. (2007) Identification of JmjC domain-containing UTX and JMJD3 as histone H3 lysine 27 demethylases. *Proc. Natl. Acad. Sci. 104*, 18439–18444.

(128) Walport, L. J., Hopkinson, R. J., Vollmar, M., Madden, S. K., Gileadi, C., Oppermann, U., Schofield, C. J., and Johansson, C. (2014) Human UTY(KDM6C) is a male-specific Nε-methyl lysyl demethylase. *J. Biol. Chem. 289*, 18302–13.

(129) Loenarz, C., Ge, W., Coleman, M. L., Rose, N. R., Cooper, C. D. O., Klose, R. J., Ratcliffe, P. J., and Schofield, C. J. (2010) PHF8, a gene associated with cleft lip/palate and mental retardation, encodes for an Nepsilon-dimethyl lysine demethylase. *Hum. Mol. Genet. 19*, 217–22.

(130) Huang, C., Xiang, Y., Wang, Y., Li, X., Xu, L., Zhu, Z., Zhang, T., Zhu, Q., Zhang, K., Jing, N., and Chen, C. D. (2010) Dual-specificity histone demethylase KIAA1718 (KDM7A) regulates neural differentiation through FGF4. *Cell Res. 20*, 154–65.

(131) Yokoyama, A., Okuno, Y., Chikanishi, T., Hashiba, W., Sekine, H., Fujiki, R., and Kato, S. (2010) KIAA1718 is a histone demethylase that erases repressive histone methyl marks. *Genes to Cells 15*, no-no.

(132) Wen, H., Li, J., Song, T., Lu, M., Kan, P.-Y., Lee, M. G., Sha, B., and Shi, X. (2010) Recognition of histone H3K4 trimethylation by the plant homeodomain of PHF2 modulates histone demethylation. *J. Biol. Chem. 285*, 9322–6.

(133) Horton, J. R., Upadhyay, A. K., Qi, H. H., Zhang, X., Shi, Y., and Cheng, X. (2010) Enzymatic and structural insights for substrate specificity of a family of jumonji histone lysine demethylases. *Nat. Struct. Mol. Biol. 17*, 38–43.

(134) Tu, S., Teng, Y.-C., Yuan, C., Wu, Y.-T., Chan, M.-Y., Cheng, A.-N., Lin, P.-H., Juan, L.-J., and Tsai, M.-D. (2008) The ARID domain of the H3K4 demethylase RBP2 binds to a DNA CCGCCC motif. *Nat. Struct. Mol. Biol. 15*, 419–421.

(135) Yao, W., Peng, Y., and Lin, D. (2010) The flexible loop L1 of the H3K4 demethylase JARID1B ARID domain has a crucial role in DNA-binding activity. *Biochem. Biophys. Res. Commun. 396*, 323–8.

(136) Yi, C., Jia, G., Hou, G., Dai, Q., Zhang, W., Zheng, G., Jian, X., Yang, C.-G., Cui, Q., and He, C. (2010) Iron-catalysed oxidation intermediates captured in a DNA repair dioxygenase. *Nature 468*, 330–3.

(137) Huang, Y., Fang, J., Bedford, M. T., Zhang, Y., and Xu, R.-M. (2006) Recognition of histone H3 lysine-4 methylation by the double tudor domain of JMJD2A. *Science 312*, 748–51.

(138) Lee, J., Thompson, J. R., Botuyan, M. V., and Mer, G. (2008) Distinct binding modes specify the recognition of methylated histones H3K4 and H4K20 by JMJD2A-tudor. *Nat. Struct. Mol. Biol. 15*, 109–11.

(139) Shin, S., and Janknecht, R. (2007) Activation of androgen receptor by histone demethylases JMJD2A and JMJD2D. *Biochem. Biophys. Res. Commun. 359*, 742–6.

(140) Wissmann, M., Yin, N., Müller, J. M., Greschik, H., Fodor, B. D., Jenuwein, T., Vogler, C., Schneider, R., Günther, T., Buettner, R., Metzger, E., and Schüle, R. (2007) Cooperative demethylation by JMJD2C and LSD1 promotes androgen receptor-dependent gene expression. *Nat. Cell Biol. 9*, 347–53.

(141) Shi, L., Sun, L., Li, Q., Liang, J., Yu, W., Yi, X., Yang, X., Li, Y., Han, X., Zhang, Y., Xuan, C., Yao, Z., and Shang, Y. (2011) Histone demethylase JMJD2B coordinates H3K4/H3K9 methylation and promotes hormonally responsive breast carcinogenesis. *Proc. Natl. Acad. Sci. U. S. A. 108*, 7541–6.

(142) Zhang, D., Yoon, H.-G., and Wong, J. (2005) JMJD2A is a novel N-CoR-interacting protein and is involved in repression of the human transcription factor achaete scute-like homologue 2 (ASCL2/Hash2). *Mol. Cell. Biol. 25*, 6404–14.

(143) Gray, S. G., Iglesias, A. H., Lizcano, F., Villanueva, R., Camelo, S., Jingu, H., Teh, B. T., Koibuchi, N., Chin, W. W., Kokkotou, E., and Dangond, F. (2005) Functional characterization of JMJD2A, a histone deacetylase- and retinoblastoma-binding protein. *J. Biol. Chem. 280*, 28507–18.

(144) Hillringhaus, L., Yue, W. W., Rose, N. R., Ng, S. S., Gileadi, C., Loenarz, C., Bello, S. H., Bray, J. E., Schofield, C. J., and Oppermann, U. (2011) Structural and evolutionary basis for the dual substrate selectivity of human KDM4 histone demethylase family. *J Biol Chem 286*, 41616–41625.

(145) Ng, S. S., Kavanagh, K. L., McDonough, M. A., Butler, D., Pilka, E. S., Lienard, B. M., Bray, J. E., Savitsky, P., Gileadi, O., von Delft, F., Rose, N. R., Offer, J., Scheinost, J. C., Borowski, T., Sundstrom, M., Schofield, C. J., and Oppermann, U. (2007) Crystal structures of histone demethylase JMJD2A reveal basis for substrate specificity. *Nature 448*, 87–91.

(146) Wang, G. L., Jiang, B. H., Rue, E. A., and Semenza, G. L. (1995) Hypoxia-inducible factor 1 is a basic-helix-loop-helix-PAS heterodimer regulated by cellular O2 tension. *Proc. Natl. Acad. Sci. U. S. A. 92*, 5510–4.

(147) Kaelin, W. G., and Ratcliffe, P. J. (2008) Oxygen sensing by metazoans: the central role of the HIF hydroxylase pathway. *Mol. Cell 30*, 393–402.

(148) Schödel, J., Mole, D. R., and Ratcliffe, P. J. (2013) Pan-genomic binding of hypoxia-inducible transcription factors. *Biol. Chem. 394*, 507–17.

(149) Schofield, C. J., and Ratcliffe, P. J. (2004) Oxygen sensing by HIF hydroxylases. *Nat. Rev. Mol. Cell Biol. 5*, 343–54.

(150) Ratcliffe, P. J. (2007) HIF-1 and HIF-2: working alone or together in hypoxia? *J. Clin. Invest. 117*, 862–5.

(151) Wilkins, S. E., Abboud, M. I., Hancock, R. L., and Schofield, C. J. (2016) Targeting Protein-Protein Interactions in the HIF System. *ChemMedChem 11*, 773–86.

(152) Keith, B., Johnson, R. S., and Simon, M. C. (2011) HIF1α and HIF2α: sibling rivalry in hypoxic tumour growth and progression. *Nat. Rev. Cancer 12*, 9–22.

(153) Loboda, A., Jozkowicz, A., and Dulak, J. (2010) HIF-1 and HIF-2 transcription factors--similar but not identical. *Mol. Cells 29*, 435–42.

(154) Ravenna, L., Salvatori, L., and Russo, M. A. (2016) HIF3α: the little we know. *FEBS J. 283*, 993–1003.

(155) Duan, C. (2016) Hypoxia-inducible factor 3 biology: complexities and emerging themes. *Am. J. Physiol. Cell Physiol. 310*, C260-9.

(156) Masson, N., Willam, C., Maxwell, P. H., Pugh, C. W., and Ratcliffe, P. J. (2001) Independent function of two destruction domains in hypoxia-inducible factor-alpha chains activated by prolyl hydroxylation. *EMBO J. 20*, 5197–206.

(157) Ratcliffe, P. J., Maxwell, P. H., Wiesener, M. S., Chang, G.-W., Clifford, S. C., Vaux, E. C., Cockman, M. E., Wykoff, C. C., Pugh, C. W., and Maher, E. R. (1999) The tumour suppressor protein VHL targets hypoxia-inducible factors foroxygen-dependent proteolysis. *Nature 399*, 271–275.

(158) Cockman, M. E., Masson, N., Mole, D. R., Jaakkola, P., Chang, G. W., Clifford, S. C., Maher, E. R., Pugh, C. W., Ratcliffe, P. J., and Maxwell, P. H. (2000) Hypoxia inducible factor-alpha binding and ubiquitylation by the von Hippel-Lindau tumor suppressor protein. *J. Biol. Chem. 275*, 25733–41.

(159) Jaakkola, P., Mole, D. R., Tian, Y. M., Wilson, M. I., Gielbert, J., Gaskell, S. J., von Kriegsheim, A., Hebestreit, H. F., Mukherji, M., Schofield, C. J., Maxwell, P. H., Pugh, C. W., and Ratcliffe, P. J. (2001) Targeting of HIF-alpha to the von Hippel-Lindau ubiquitylation complex by O2-regulated prolyl hydroxylation. *Science 292*, 468–72.

(160) Berra, E., Benizri, E., Ginouvès, A., Volmat, V., Roux, D., and Pouysségur, J. (2003) HIF prolyl-hydroxylase 2 is the key oxygen sensor setting low steady-state levels of HIF-1alpha in normoxia. *EMBO J. 22*, 4082–90.

(161) McNeill, L. A., Hewitson, K. S., Claridge, T. D., Seibel, J. F., Horsfall, L. E., and Schofield, C. J. (2002) Hypoxia-inducible factor asparaginyl hydroxylase (FIH-1) catalyses hydroxylation at the beta-carbon of asparagine-803. *Biochem. J. 367*, 571–5.

(162) Lando, D., Peet, D. J., Whelan, D. A., Gorman, J. J., and Whitelaw, M. L. (2002) Asparagine hydroxylation of the HIF transactivation domain a hypoxic switch. *Science 295*, 858–61.

(163) Ogryzko, V. V, Schiltz, R. L., Russanova, V., Howard, B. H., and Nakatani, Y. (1996) The transcriptional coactivators p300 and CBP are histone acetyltransferases. *Cell 87*, 953–9.

(164) Arany, Z., Huang, L. E., Eckner, R., Bhattacharya, S., Jiang, C., Goldberg, M. A., Bunn, H. F., and Livingston, D. M. (1996) An essential role for p300/CBP in the cellular response to hypoxia. *Proc. Natl. Acad. Sci. U. S. A. 93*, 12969–73.

(165) Bruick, R. K., and McKnight, S. L. (2001) A conserved family of prolyl-4-hydroxylases that modify HIF. *Science 294*, 1337–40.

(166) Myllyharju, J. (2013) Prolyl 4-hydroxylases, master regulators of the hypoxia response. *Acta Physiol. (Oxf). 208*, 148–65.

(167) Hirsilä, M., Koivunen, P., Günzler, V., Kivirikko, K. I., and Myllyharju, J. (2003) Characterization of the human prolyl 4-hydroxylases that modify the hypoxia-inducible factor. *J. Biol. Chem. 278*, 30772–80.

(168) Koivunen, P., Hirsilä, M., Günzler, V., Kivirikko, K. I., and Myllyharju, J. (2004) Catalytic properties of the asparaginyl hydroxylase (FIH) in the oxygen sensing pathway are distinct from those of its prolyl 4-hydroxylases. *J. Biol. Chem. 279*, 9899–904.

(169) Ehrismann, D., Flashman, E., Genn, D. N., Mathioudakis, N., Hewitson, K. S., Ratcliffe, P. J., and Schofield, C. J. (2007) Studies on the activity of the hypoxia-inducible-

factor hydroxylases using an oxygen consumption assay. *Biochem. J. 401*, 227–34.

(170) Dao, J. H., Kurzeja, R. J. M., Morachis, J. M., Veith, H., Lewis, J., Yu, V., Tegley, C. M., and Tagari, P. (2009) Kinetic characterization and identification of a novel inhibitor of hypoxia-inducible factor prolyl hydroxylase 2 using a time-resolved fluorescence resonance energy transfer-based assay technology. *Anal. Biochem. 384*, 213–23.

(171) Tarhonskaya, H., Chowdhury, R., Leung, I. K. H., Loik, N. D., McCullagh, J. S. O., Claridge, T. D. W., Schofield, C. J., and Flashman, E. (2014) Investigating the contribution of the active site environment to the slow reaction of hypoxia-inducible factor prolyl hydroxylase domain 2 with oxygen. *Biochem. J. 463*, 363–72.

(172) Ryle, M. J., Padmakumar, R., and Hausinger, R. P. (1999) Stopped-flow kinetic analysis of Escherichia coli taurine/alpha-ketoglutarate dioxygenase: interactions with alpha-ketoglutarate, taurine, and oxygen. *Biochemistry 38*, 15278–86.

(173) Tian, Y.-M., Yeoh, K. K., Lee, M. K., Eriksson, T., Kessler, B. M., Kramer, H. B., Edelmann, M. J., Willam, C., Pugh, C. W., Schofield, C. J., and Ratcliffe, P. J. (2011) Differential sensitivity of hypoxia inducible factor hydroxylation sites to hypoxia and hydroxylase inhibitors. *J. Biol. Chem. 286*, 13041–51.

(174) Shahrzad, S., Bertrand, K., Minhas, K., and Coomber, B. L. Induction of DNA hypomethylation by tumor hypoxia. *Epigenetics 2*, 119–25.

(175) Hattori, M., Yokoyama, Y., Hattori, T., Motegi, S.-I., Amano, H., Hatada, I., and Ishikawa, O. (2015) Global DNA hypomethylation and hypoxia-induced expression of the ten eleven translocation (TET) family, TET1, in scleroderma fibroblasts. *Exp. Dermatol. 24*, 841–6.

(176) Watson, J. A., Watson, C. J., McCrohan, A.-M., Woodfine, K., Tosetto, M., McDaid, J., Gallagher, E., Betts, D., Baugh, J., O'Sullivan, J., Murrell, A., Watson, R. W. G., and McCann, A. (2009) Generation of an epigenetic signature by chronic hypoxia in prostate cells. *Hum. Mol. Genet. 18*, 3594–604.

(177) Watson, C. J., Collier, P., Tea, I., Neary, R., Watson, J. A., Robinson, C., Phelan, D., Ledwidge, M. T., McDonald, K. M., McCann, A., Sharaf, O., and Baugh, J. A. (2014) Hypoxia-induced epigenetic modifications are associated with cardiac tissue fibrosis and the development of a myofibroblast-like phenotype. *Hum. Mol. Genet. 23*, 2176–88.

(178) Hartley, I., Elkhoury, F. F., Heon Shin, J., Xie, B., Gu, X., Gao, Y., Zhou, D., and Haddad, G. G. (2013) Long-lasting changes in DNA methylation following short-term hypoxic exposure in primary hippocampal neuronal cultures. *PLoS One 8*, e77859.

(179) Okami, J., Simeone, D. M., and Logsdon, C. D. (2004) Silencing of the Hypoxia-Inducible Cell Death Protein BNIP3 in Pancreatic Cancer. *Cancer Res. 64*.

(180) Murai, M., Toyota, M., Suzuki, H., Satoh, A., Sasaki, Y., Akino, K., Ueno, M., Takahashi, F., Kusano, M., Mita, H., Yanagihara, K., Endo, T., Hinoda, Y., Tokino, T., and Imai, K. (2005) Aberrant Methylation and Silencing of the BNIP3 Gene in Colorectal and Gastric Cancer. *Clin. Cancer Res. 11*.

(181) Ramjiawan, A., Bagchi, R. A., Blant, A., Albak, L., Cavasin, M. A., Horn, T. R., McKinsey, T. A., and Czubryt, M. P. (2013) Roles of histone deacetylation and AMP kinase in regulation of cardiomyocyte PGC-1α gene expression in hypoxia. *Am. J. Physiol. Cell Physiol. 304*, C1064-72.

(182) Safronova, O., Pluemsampant, S., Nakahama, K., and Morita, I. (2009) Regulation of

chemokine gene expression by hypoxia via cooperative activation of NF-κB and histone deacetylase. *Int. J. Biochem. Cell Biol. 41*, 2270–2280.

(183) Kato, H., Tamamizu-Kato, S., and Shibasaki, F. (2004) Histone deacetylase 7 associates with hypoxia-inducible factor 1alpha and increases transcriptional activity. *J. Biol. Chem. 279*, 41966–74.

(184) Fath, D. M., Kong, X., Liang, D., Lin, Z., Chou, A., Jiang, Y., Fang, J., Caro, J., and Sang, N. (2006) Histone deacetylase inhibitors repress the transactivation potential of hypoxia-inducible factors independently of direct acetylation of HIF-alpha. *J. Biol. Chem. 281*, 13612–9.

(185) Pluemsampant, S., Safronova, O. S., Nakahama, K., and Morita, I. (2008) Protein kinase CK2 is a key activator of histone deacetylase in hypoxia-associated tumors. *Int. J. Cancer 122*, 333–341.

(186) Kim, M. S., Kwon, H. J., Lee, Y. M., Baek, J. H., Jang, J.-E., Lee, S.-W., Moon, E.-J., Kim, H.-S., Lee, S.-K., Chung, H. Y., Kim, C. W., and Kim, K.-W. (2001) Histone deacetylases induce angiogenesis by negative regulation of tumor suppressor genes. *Nat. Med. 7*, 437–443.

(187) Geng, H., Harvey, C. T., Pittsenbarger, J., Liu, Q., Beer, T. M., Xue, C., and Qian, D. Z. (2011) HDAC4 protein regulates HIF1α protein lysine acetylation and cancer cell response to hypoxia. *J. Biol. Chem. 286*, 38095–102.

(188) Melvin, A., and Rocha, S. (2012) Chromatin as an oxygen sensor and active player in the hypoxia response. *Cell. Signal. 24*, 35–43.

(189) Perez-Perri, J. I., Acevedo, J. M., and Wappner, P. (2011) Epigenetics: new questions on the response to hypoxia. *Int J Mol Sci 12*, 4705–4721.

(190) Cascella, B., and Mirica, L. M. (2012) Kinetic analysis of iron-dependent histone demethylases: α-ketoglutarate substrate inhibition and potential relevance to the regulation of histone demethylation in cancer cells. *Biochemistry 51*, 8699–701.

(191) Sanchez-Fernandez, E. M., Tarhonskaya, H., Al-Qahtani, K., Hopkinson, R. J., McCullagh, J. S., Schofield, C. J., and Flashman, E. (2013) Investigations on the oxygen dependence of a 2-oxoglutarate histone demethylase. *Biochem J 449*, 491–496.

(192) Costa, M., Davidson, T. L., Chen, H., Ke, Q., Zhang, P., Yan, Y., Huang, C., and Kluz, T. (2005) Nickel carcinogenesis: epigenetics and hypoxia signaling. *Mutat. Res. 592*, 79–88.

(193) Islam, K. N., and Mendelson, C. R. (2006) Permissive effects of oxygen on cyclic AMP and interleukin-1 stimulation of surfactant protein A gene expression are mediated by epigenetic mechanisms. *Mol. Cell. Biol. 26*, 2901–12.

(194) Chen, H., Yan, Y., Davidson, T. L., Shinkai, Y., and Costa, M. (2006) Hypoxic stress induces dimethylated histone H3 lysine 9 through histone methyltransferase G9a in mammalian cells. *Cancer Res. 66*, 9009–16.

(195) Johnson, A. B., Denko, N., and Barton, M. C. (2008) Hypoxia induces a novel signature of chromatin modifications and global repression of transcription. *Mutat. Res. 640*, 174–9.

(196) Xia, X., Lemieux, M. E., Li, W., Carroll, J. S., Brown, M., Liu, X. S., and Kung, A. L. (2009) Integrative analysis of HIF binding and transactivation reveals its role in maintaining histone methylation homeostasis. *Proc. Natl. Acad. Sci. U. S. A. 106*, 4260–5.

(197) Zhou, X., Sun, H., Chen, H., Zavadil, J., Kluz, T., Arita, A., and Costa, M. (2010) Hypoxia induces trimethylated H3 lysine 4 by inhibition of JARID1A demethylase. *Cancer Res. 70*, 4214–21.

(198) Tausendschön, M., Dehne, N., and Brüne, B. (2011) Hypoxia causes epigenetic gene regulation in macrophages by attenuating Jumonji histone demethylase activity. *Cytokine 53*, 256–62.

(199) Olcina, M. M., Foskolou, I. P., Anbalagan, S., Senra, J. M., Pires, I. M., Jiang, Y., Ryan, A. J., and Hammond, E. M. (2013) Replication stress and chromatin context link ATM activation to a role in DNA replication. *Mol. Cell 52*, 758–66.

(200) Osumek, J. E., Revesz, A., Morton, J. S., Davidge, S. T., and Hardy, D. B. (2014) Enhanced trimethylation of histone h3 mediates impaired expression of hepatic glucose 6-phosphatase expression in offspring from rat dams exposed to hypoxia during pregnancy. *Reprod. Sci. 21*, 112–21.

(201) Chang, S., Park, B., Choi, K., Moon, Y., Lee, H.-Y., and Park, H. (2016) Hypoxic reprograming of H3K27me3 and H3K4me3 at the INK4A locus. *FEBS Lett.*

(202) Olcina, M. M., Leszczynska, K. B., Senra, J. M., Isa, N. F., Harada, H., and Hammond, E. M. (2016) H3K9me3 facilitates hypoxia-induced p53-dependent apoptosis through repression of APAK. *Oncogene 35*, 793–9.

(203) Lu, Y., Chu, A., Turker, M. S., and Glazer, P. M. (2011) Hypoxia-induced epigenetic regulation and silencing of the BRCA1 promoter. *Mol. Cell. Biol. 31*, 3339–50.

(204) Ueda, J., Ho, J. C., Lee, K. L., Kitajima, S., Yang, H., Sun, W., Fukuhara, N., Zaiden, N., Chan, S. L., Tachibana, M., Shinkai, Y., Kato, H., and Poellinger, L. (2014) The hypoxia-inducible epigenetic regulators Jmjd1a and G9a provide a mechanistic link between angiogenesis and tumor growth. *Mol. Cell. Biol. 34*, 3702–20.

(205) Benlhabib, H., and Mendelson, C. R. (2011) Epigenetic regulation of surfactant protein A gene (SP-A) expression in fetal lung reveals a critical role for Suv39h methyltransferases during development and hypoxia. *Mol. Cell. Biol. 31*, 1949–58.

(206) Beyer, S., Kristensen, M. M., Jensen, K. S., Johansen, J. V., and Staller, P. (2008) The histone demethylases JMJD1A and JMJD2B are transcriptional targets of hypoxia-inducible factor HIF. *J. Biol. Chem. 283*, 36542–52.

(207) Wellmann, S., Bettkober, M., Zelmer, A., Seeger, K., Faigle, M., Eltzschig, H. K., and Bührer, C. (2008) Hypoxia upregulates the histone demethylase JMJD1A via HIF-1. *Biochem. Biophys. Res. Commun. 372*, 892–7.

(208) Pollard, P. J., Loenarz, C., Mole, D. R., McDonough, M. A., Gleadle, J. M., Schofield, C. J., and Ratcliffe, P. J. (2008) Regulation of Jumonji-domain-containing histone demethylases by hypoxia-inducible factor (HIF)-1alpha. *Biochem J 416*, 387–394.

(209) Yang, J., Ledaki, I., Turley, H., Gatter, K. C., Montero, J.-C. M., Li, J.-L., and Harris, A. L. (2009) Role of hypoxia-inducible factors in epigenetic regulation via histone demethylases. *Ann. N. Y. Acad. Sci. 1177*, 185–97.

(210) Krieg, A. J., Rankin, E. B., Chan, D., Razorenova, O., Fernandez, S., and Giaccia, A. J. (2010) Regulation of the histone demethylase JMJD1A by hypoxia-inducible factor 1 alpha enhances hypoxic gene expression and tumor growth. *Mol. Cell. Biol. 30*, 344–53.

(211) Fu, L., Chen, L., Yang, J., Ye, T., Chen, Y., and Fang, J. (2012) HIF-1α-induced histone demethylase JMJD2B contributes to the malignant phenotype of colorectal cancer

cells via an epigenetic mechanism. *Carcinogenesis 33*, 1664–73.

(212) Lee, H.-Y., Choi, K., Oh, H., Park, Y.-K., and Park, H. (2014) HIF-1-dependent induction of Jumonji domain-containing protein (JMJD) 3 under hypoxic conditions. *Mol. Cells 37*, 43–50.

(213) Guo, X., Tian, Z., Wang, X., Pan, S., Huang, W., Shen, Y., Gui, Y., Duan, X., and Cai, Z. (2014) Regulation of histone demethylase KDM6B by hypoxia-inducible factor-2α. *Acta Biochim. Biophys. Sin. (Shanghai).*

(214) Lee, H. Y., Yang, E. G., and Park, H. (2013) Hypoxia enhances the expression of prostate-specific antigen by modifying the quantity and catalytic activity of Jumonji C domain-containing histone demethylases. *Carcinogenesis 34*, 2706–2715.

(215) Mimura, I., Nangaku, M., Kanki, Y., Tsutsumi, S., Inoue, T., Kohro, T., Yamamoto, S., Fujita, T., Shimamura, T., Suehiro, J., Taguchi, A., Kobayashi, M., Tanimura, K., Inagaki, T., Tanaka, T., Hamakubo, T., Sakai, J., Aburatani, H., Kodama, T., and Wada, Y. (2012) Dynamic change of chromatin conformation in response to hypoxia enhances the expression of GLUT3 (SLC2A3) by cooperative interaction of hypoxia-inducible factor 1 and KDM3A. *Mol. Cell. Biol. 32*, 3018–32.

(216) Luo, W., Chang, R., Zhong, J., Pandey, A., and Semenza, G. L. (2012) Histone demethylase JMJD2C is a coactivator for hypoxia-inducible factor 1 that is required for breast cancer progression. *Proc. Natl. Acad. Sci. U. S. A. 109*, E3367-76.

(217) Brown, J. M., and Giaccia, A. J. (1998) The unique physiology of solid tumors: opportunities (and problems) for cancer therapy. *Cancer Res. 58*, 1408–16.

(218) Ramachandran, S., Ient, J., Göttgens, E.-L., Krieg, A. J., and Hammond, E. M. (2015) Epigenetic Therapy for Solid Tumors: Highlighting the Impact of Tumor Hypoxia. *Genes (Basel). 6*, 935–56.

(219) Hammond, E. M., Asselin, M.-C., Forster, D., O'Connor, J. P. B., Senra, J. M., and Williams, K. J. (2014) The Meaning, Measurement and Modification of Hypoxia in the Laboratory and the Clinic. *Clin. Oncol. 26*, 277–288.

(220) Ostadal, B., Ostadalova, I., and Dhalla, N. S. (1999) Development of Cardiac Sensitivity to Oxygen Deficiency: Comparative and Ontogenetic Aspects. *Physiol Rev 79*, 635–659.

(221) Hultén, L. M., and Levin, M. (2009) The role of hypoxia in atherosclerosis. *Curr. Opin. Lipidol. 20*, 409–14.

(222) Essop, M. F. (2007) Cardiac metabolic adaptations in response to chronic hypoxia. *J. Physiol. 584*, 715–26.

(223) Krishnan, J., Suter, M., Windak, R., Krebs, T., Felley, A., Montessuit, C., Tokarska-Schlattner, M., Aasum, E., Bogdanova, A., Perriard, E., Perriard, J.-C., Larsen, T., Pedrazzini, T., and Krek, W. (2009) Activation of a HIF1α-PPARγ Axis Underlies the Integration of Glycolytic and Lipid Anabolic Pathways in Pathologic Cardiac Hypertrophy. *Cell Metab. 9*, 512–524.

(224) Handley, M. G., Medina, R. A., Nagel, E., Blower, P. J., and Southworth, R. (2011) PET imaging of cardiac hypoxia: opportunities and challenges. *J. Mol. Cell. Cardiol. 51*, 640–50.

(225) Dawson, M. A., and Kouzarides, T. (2012) Cancer epigenetics: from mechanism to therapy. *Cell 150*, 12–27.

(226) Greer, E. L., and Shi, Y. (2012) Histone methylation: a dynamic mark in health, disease and inheritance. *Nat. Rev. Genet. 13*, 343–57.

(227) Højfeldt, J. W., Agger, K., and Helin, K. (2013) Histone lysine demethylases as targets for anticancer therapy. *Nat. Rev. Drug Discov. 12*, 917–30.

(228) Papait, R., and Condorelli, G. (2010) Epigenetics in heart failure. *Ann. N. Y. Acad. Sci. 1188*, 159–64.

(229) Duygu, B., Poels, E. M., and da Costa Martins, P. A. (2013) Genetics and epigenetics of arrhythmia and heart failure. *Front. Genet. 4*, 219.

(230) Razeghi, P., Young, M. E., Alcorn, J. L., Moravec, C. S., Frazier, O. H., and Taegtmeyer, H. (2001) Metabolic Gene Expression in Fetal and Failing Human Heart. *Circulation 104*, 2923–2931.

(231) Taegtmeyer, H., Sen, S., and Vela, D. (2010) Return to the fetal gene program: A suggested metabolic link to gene expression in the heart.

(232) Rajabi, M., Kassiotis, C., Razeghi, P., and Taegtmeyer, H. (2007) Return to the fetal gene program protects the stressed heart: a strong hypothesis. *Heart Fail. Rev. 12*, 331–43.

(233) Gaikwad, A. B., Sayyed, S. G., Lichtnekert, J., Tikoo, K., and Anders, H.-J. (2010) Renal failure increases cardiac histone h3 acetylation, dimethylation, and phosphorylation and the induction of cardiomyopathy-related genes in type 2 diabetes. *Am. J. Pathol. 176*, 1079–83.

(234) Movassagh, M., Choy, M., Knowles, D. A., Simeoni, I., Penkett, C., Goddard, M., and Foo, S. (2013) Europe PMC Funders Group Distinct Epigenomic Features in End-Stage Failing Human Hearts *124*, 2411–2422.

(235) Hohl, M., Wagner, M., Reil, J.-C., Müller, S.-A., Tauchnitz, M., Zimmer, A. M., Lehmann, L. H., Thiel, G., Böhm, M., Backs, J., and Maack, C. (2013) HDAC4 controls histone methylation in response to elevated cardiac load. *J. Clin. Invest. 123*, 1359–70.

(236) Kaneda, R., Takada, S., Yamashita, Y., Choi, Y. L., Nonaka-Sarukawa, M., Soda, M., Misawa, Y., Isomura, T., Shimada, K., and Mano, H. (2009) Genome-wide histone methylation profile for heart failure. *Genes Cells 14*, 69–77.

(237) Papait, R., Cattaneo, P., Kunderfranco, P., Greco, C., Carullo, P., Guffanti, A., Vigano, V., Stirparo, G. G., Latronico, M. V, Hasenfuss, G., Chen, J., and Condorelli, G. (2013) Genome-wide analysis of histone marks identifying an epigenetic signature of promoters and enhancers underlying cardiac hypertrophy. *Proc Natl Acad Sci U S A 110*, 20164–20169.

(238) Stein, A. B., Jones, T. A., Herron, T. J., Patel, S. R., Day, S. M., Noujaim, S. F., Milstein, M. L., Klos, M., Furspan, P. B., Jalife, J., and Dressler, G. R. (2011) Loss of H3K4 methylation destabilizes gene expression patterns and physiological functions in adult murine cardiomyocytes. *J Clin Invest 121*, 2641–2650.

(239) Zhang, Q. J., Chen, H. Z., Wang, L., Liu, D. P., Hill, J. A., and Liu, Z. P. (2011) The histone trimethyllysine demethylase JMJD2A promotes cardiac hypertrophy in response to hypertrophic stimuli in mice. *J Clin Invest 121*, 2447–2456.

(240) Michaelis, L., Menten, M. L., Johnson, K. A., and Goody, R. S. (2011) The original Michaelis constant: translation of the 1913 Michaelis-Menten paper. *Biochemistry 50*, 8264–9.

(241) Cornish-Bowden, A. (2013) The origins of enzyme kinetics. *FEBS Lett. 587*, 2725–

2730.

(242) Johnson, K. A. (2013) A century of enzyme kinetic analysis, 1913 to 2013. *FEBS Lett. 587*, 2753–2766.

(243) Briggs, G. E., and Haldane, J. B. (1925) A Note on the Kinetics of Enzyme Action. *Biochem. J. 19*, 338–9.

(244) GenScript. (2016) apparent Km.

(245) Tarhonskaya, H., Hardy, A. P., Howe, E. A., Loik, N. D., Kramer, H. B., McCullagh, J. S. O., Schofield, C. J., and Flashman, E. (2015) Kinetic Investigations of the Role of Factor Inhibiting Hypoxia-inducible Factor (FIH) as an Oxygen Sensor. *J. Biol. Chem. 290*, 19726–42.

(246) Labbé, R. M., Holowatyj, A., and Yang, Z.-Q. (2013) Histone lysine demethylase (KDM) subfamily 4: structures, functions and therapeutic potential. *Am. J. Transl. Res. 6*, 1–15.

(247) Berry, W. L., and Janknecht, R. (2013) KDM4/JMJD2 histone demethylases: epigenetic regulators in cancer cells. *Cancer Res. 73*, 2936–42.

(248) Shmakova, A., Batie, M., Druker, J., and Rocha, S. (2014) Chromatin and oxygen sensing in the context of JmjC histone demethylases. *Biochem. J. 462*, 385–95.

(249) Hausinger, R. P. FeII/alpha-ketoglutarate-dependent hydroxylases and related enzymes. *Crit. Rev. Biochem. Mol. Biol. 39*, 21–68.

(250) Hancock, R. L., Dunne, K., Walport, L. J., Flashman, E., and Kawamura, A. (2015) Epigenetic regulation by histone demethylases in hypoxia. *Epigenomics 7*, 791–811.

(251) Hancock, R. L., Masson, N., Dunne, K., Flashman, E., and Kawamura, A. (2017) The activity of JmjC histone lysine demethylase KDM4A is highly sensitive to oxygen concentrations. *ACS Chem. Biol.* acschembio.6b00958.

(252) Rose, N. R., Woon, E. C., Kingham, G. L., King, O. N., Mecinovic, J., Clifton, I. J., Ng, S. S., Talib-Hardy, J., Oppermann, U., McDonough, M. A., and Schofield, C. J. (2010) Selective inhibitors of the JMJD2 histone demethylases: combined nondenaturing mass spectrometric screening and crystallographic approaches. *J Med Chem 53*, 1810–1818.

(253) Rose, N. R. (2009) Structural, Mechanistic and Inhibition Studies on the Histone Lysine Demethylases. *DPhil Thesis University*.

(254) Chowdhury, R., Yeoh, K. K., Tian, Y.-M., Hillringhaus, L., Bagg, E. A., Rose, N. R., Leung, I. K. H., Li, X. S., Woon, E. C. Y., Yang, M., McDonough, M. A., King, O. N., Clifton, I. J., Klose, R. J., Claridge, T. D. W., Ratcliffe, P. J., Schofield, C. J., and Kawamura, A. (2011) The oncometabolite 2-hydroxyglutarate inhibits histone lysine demethylases. *EMBO Rep. 12*, 463–9.

(255) Battino, R., Rettich, T. R., and Tominaga, T. (1983) The Solubility of Oxygen and Ozone in Liquids. *J. Phys. Chem. Ref. Data 12*, 163.

(256) Cortopassi, W. A., Simion, R., Honsby, C. E., França, T. C. C., and Paton, R. S. (2015) Dioxygen Binding in the Active Site of Histone Demethylase JMJD2A and the Role of the Protein Environment. *Chem. - A Eur. J. 21*, 18983–18992.

(257) Thienpont, B., Steinbacher, J., Zhao, H., D'Anna, F., Kuchnio, A., Ploumakis, A., Ghesquière, B., Van Dyck, L., Boeckx, B., Schoonjans, L., Hermans, E., Amant, F., Kristensen, V. N., Koh, K. P., Mazzone, M., Coleman, M. L., Carell, T., Carmeliet, P., and

Lambrechts, D. (2016) Tumour hypoxia causes DNA hypermethylation by reducing TET activity. *Nature 537*, 63–68.

(258) Black, J. C., Manning, A. L., Van Rechem, C., Kim, J., Ladd, B., Cho, J., Pineda, C. M., Murphy, N., Daniels, D. L., Montagna, C., Lewis, P. W., Glass, K., Allis, C. D., Dyson, N. J., Getz, G., and Whetstine, J. R. (2013) KDM4A lysine demethylase induces site-specific copy gain and rereplication of regions amplified in tumors. *Cell 154*, 541–55.

(259) Black, J. C., Atabakhsh, E., Kim, J., Biette, K. M., Van Rechem, C., Ladd, B., Burrowes, P. D., Donado, C., Mattoo, H., Kleinstiver, B. P., Song, B., Andriani, G., Joung, J. K., Iliopoulos, O., Montagna, C., Pillai, S., Getz, G., and Whetstine, J. R. (2015) Hypoxia drives transient site-specific copy gain and drug-resistant gene expression. *Genes Dev. 29*, 1018–31.

(260) Van Rechem, C., Black, J. C., Abbas, T., Allen, A., Rinehart, C. A., Yuan, G.-C., Dutta, A., and Whetstine, J. R. (2011) The SKP1-Cul1-F-box and leucine-rich repeat protein 4 (SCF-FbxL4) ubiquitin ligase regulates lysine demethylase 4A (KDM4A)/Jumonji domain-containing 2A (JMJD2A) protein. *J. Biol. Chem. 286*, 30462–70.

(261) King, O. N. F., Li, X. S., Sakurai, M., Kawamura, A., Rose, N. R., Ng, S. S., Quinn, A. M., Rai, G., Mott, B. T., Beswick, P., Klose, R. J., Oppermann, U., Jadhav, A., Heightman, T. D., Maloney, D. J., Schofield, C. J., and Simeonov, A. (2010) Quantitative high-throughput screening identifies 8-hydroxyquinolines as cell-active histone demethylase inhibitors. *PLoS One 5*, e15535.

(262) Lohse, B., Helgstrand, C., Kristensen, J. B. L., Leurs, U., Cloos, P. A. C., Kristensen, J. L., and Clausen, R. P. (2013) Posttranslational modifications of the histone 3 tail and their impact on the activity of histone lysine demethylases in vitro. *PLoS One 8*, e67653.

(263) Pack, L. R., Yamamoto, K. R., and Fujimori, D. G. (2016) Opposing Chromatin Signals Direct and Regulate the Activity of Lysine Demethylase 4C (KDM4C). *J. Biol. Chem. 291*, 6060–70.

(264) Mallette, F. A., and Richard, S. (2012) JMJD2A promotes cellular transformation by blocking cellular senescence through transcriptional repression of the tumor suppressor CHD5. *Cell Rep. 2*, 1233–43.

(265) Kogure, M., Takawa, M., Cho, H.-S., Toyokawa, G., Hayashi, K., Tsunoda, T., Kobayashi, T., Daigo, Y., Sugiyama, M., Atomi, Y., Nakamura, Y., and Hamamoto, R. (2013) Deregulation of the histone demethylase JMJD2A is involved in human carcinogenesis through regulation of the G(1)/S transition. *Cancer Lett. 336*, 76–84.

(266) Strobl-Mazzulla, P. H., Sauka-Spengler, T., and Bronner-Fraser, M. (2010) Histone demethylase JmjD2A regulates neural crest specification. *Dev. Cell 19*, 460–8.

(267) Verrier, L., Escaffit, F., Chailleux, C., Trouche, D., and Vandromme, M. (2011) A new isoform of the histone demethylase JMJD2A/KDM4A is required for skeletal muscle differentiation. *PLoS Genet. 7*, e1001390.

(268) Cardamone, M. D., Tanasa, B., Chan, M., Cederquist, C. T., Andricovich, J., Rosenfeld, M. G., and Perissi, V. (2014) GPS2/KDM4A pioneering activity regulates promoter-specific recruitment of PPARγ. *Cell Rep. 8*, 163–76.

(269) Pfaffl, M. W. (2001) A new mathematical model for relative quantification in real-time RT-PCR. *Nucleic Acids Res. 29*, e45.

(270) ABI. (2008) Guide to Performing Relative Quantitation of Gene Expression Using

Real-Time Quantitative PCR. Applied Biosystems, Foster City CA.

(271) Guo, X., Tian, Z., Wang, X., Pan, S., Huang, W., Shen, Y., Gui, Y., Duan, X., and Cai, Z. (2014) Regulation of histone demethylase KDM6B by hypoxia-inducible factor-2α. *Acta Biochim. Biophys. Sin. (Shanghai).* gmu122-.

(272) Wykoff, C. C., Beasley, N. J. P., Watson, P. H., Turner, K. J., Pastorek, J., Sibtain, A., Wilson, G. D., Turley, H., Talks, K. L., Maxwell, P. H., Pugh, C. W., Ratcliffe, P. J., and Harris, A. L. (2000) Hypoxia-inducible Expression of Tumor-associated Carbonic Anhydrases. *Cancer Res. 60*.

(273) Uchida, T., Rossignol, F., Matthay, M. A., Mounier, R., Couette, S., Clottes, E., and Clerici, C. (2004) Prolonged hypoxia differentially regulates hypoxia-inducible factor (HIF)-1alpha and HIF-2alpha expression in lung epithelial cells: implication of natural antisense HIF-1alpha. *J. Biol. Chem. 279*, 14871–8.

(274) Nielsen, P. R., Nietlispach, D., Mott, H. R., Callaghan, J., Bannister, A., Kouzarides, T., Murzin, A. G., Murzina, N. V., and Laue, E. D. (2002) Structure of the HP1 chromodomain bound to histone H3 methylated at lysine 9. *Nature 416*, 103–107.

(275) Serrano, A., Rodríguez-Corsino, M., and Losada, A. (2009) Heterochromatin protein 1 (HP1) proteins do not drive pericentromeric cohesin enrichment in human cells. *PLoS One 4*, e5118.

(276) Brown, P. J., and Müller, S. (2015) Open access chemical probes for epigenetic targets. *Future Med. Chem. 7*, 1901–17.

(277) Arrowsmith, C. H., Audia, J. E., Austin, C., Baell, J., Bennett, J., Blagg, J., Bountra, C., Brennan, P. E., Brown, P. J., Bunnage, M. E., Buser-Doepner, C., Campbell, R. M., Carter, A. J., Cohen, P., Copeland, R. A., Cravatt, B., Dahlin, J. L., Dhanak, D., Edwards, A. M., Frederiksen, M., Frye, S. V, Gray, N., Grimshaw, C. E., Hepworth, D., Howe, T., Huber, K. V. M., Jin, J., Knapp, S., Kotz, J. D., Kruger, R. G., Lowe, D., Mader, M. M., Marsden, B., Mueller-Fahrnow, A., Müller, S., O'Hagan, R. C., Overington, J. P., Owen, D. R., Rosenberg, S. H., Roth, B., Roth, B., Ross, R., Schapira, M., Schreiber, S. L., Shoichet, B., Sundström, M., Superti-Furga, G., Taunton, J., Toledo-Sherman, L., Walpole, C., Walters, M. A., Willson, T. M., Workman, P., Young, R. N., and Zuercher, W. J. (2015) The promise and peril of chemical probes. *Nat. Chem. Biol. 11*, 536–41.

(278) Rose, N. R., McDonough, M. A., King, O. N. F., Kawamura, A., and Schofield, C. J. (2011) Inhibition of 2-oxoglutarate dependent oxygenases. *Chem. Soc. Rev. 40*, 4364–97.

(279) Elkins, J. M., Hewitson, K. S., McNeill, L. A., Seibel, J. F., Schlemminger, I., Pugh, C. W., Ratcliffe, P. J., and Schofield, C. J. (2003) Structure of Factor-inhibiting Hypoxia-inducible Factor (HIF) Reveals Mechanism of Oxidative Modification of HIF-1. *J. Biol. Chem. 278*, 1802–1806.

(280) Mole, D. R., Schlemminger, I., McNeill, L. A., Hewitson, K. S., Pugh, C. W., Ratcliffe, P. J., and Schofield, C. J. (2003) 2-Oxoglutarate analogue inhibitors of hif prolyl hydroxylase. *Bioorg. Med. Chem. Lett.*

(281) Conejo-Garcia, A., McDonough, M. A., Loenarz, C., McNeill, L. A., Hewitson, K. S., Ge, W., Liénard, B. M., Schofield, C. J., and Clifton, I. J. (2010) Structural basis for binding of cyclic 2-oxoglutarate analogues to factor-inhibiting hypoxia-inducible factor. *Bioorg. Med. Chem. Lett. 20*, 6125–6128.

(282) Hopkinson, R. J., Tumber, A., Yapp, C., Chowdhury, R., Aik, W., Che, K. H., Li, X. S., Kristensen, J. B. L., King, O. N. F., Chan, M. C., Yeoh, K. K., Choi, H., Walport, L. J.,

Thinnes, C. C., Bush, J. T., Lejeune, C., Rydzik, A. M., Rose, N. R., Bagg, E. A., McDonough, M. A., Krojer, T. J., Yue, W. W., Ng, S. S., Olsen, L., Brennan, P. E., Oppermann, U., Muller, S., Klose, R. J., Ratcliffe, P. J., Schofield, C. J., and Kawamura, A. (2013) 5-Carboxy-8-hydroxyquinoline is a broad spectrum 2-oxoglutarate oxygenase inhibitor which causes iron translocation. *Chem. Sci. 4*, 3110–3117.

(283) Chowdhury, R., Candela-Lena, J. I., Chan, M. C., Greenald, D. J., Yeoh, K. K., Tian, Y.-M., McDonough, M. A., Tumber, A., Rose, N. R., Conejo-Garcia, A., Demetriades, M., Mathavan, S., Kawamura, A., Lee, M. K., van Eeden, F., Pugh, C. W., Ratcliffe, P. J., and Schofield, C. J. (2013) Selective Small Molecule Probes for the Hypoxia Inducible Factor (HIF) Prolyl Hydroxylases. *ACS Chem. Biol. 8*, 1488–1496.

(284) Thinnes, C. C., England, K. S., Kawamura, A., Chowdhury, R., Schofield, C. J., and Hopkinson, R. J. (2014) Targeting histone lysine demethylases - Progress, challenges, and the future. *Biochim. Biophys. Acta 1839*, 1416–1432.

(285) McAllister, T. E., England, K. S., Hopkinson, R. J., Brennan, P. E., Kawamura, A., and Schofield, C. J. (2016) Recent Progress in Histone Demethylase Inhibitors. *J. Med. Chem. 59*, 1308–1329.

(286) Wang, L., Chang, J., Varghese, D., Dellinger, M., Kumar, S., Best, A. M., Ruiz, J., Bruick, R., Peña-Llopis, S., Xu, J., Babinski, D. J., Frantz, D. E., Brekken, R. A., Quinn, A. M., Simeonov, A., Easmon, J., and Martinez, E. D. (2013) A small molecule modulates Jumonji histone demethylase activity and selectively inhibits cancer growth. *Nat. Commun. 4*, 2035.

(287) Rose, N. R., Woon, E. C. Y., Tumber, A., Walport, L. J., Chowdhury, R., Li, X. S., King, O. N. F., Lejeune, C., Ng, S. S., Krojer, T., Chan, M. C., Rydzik, A. M., Hopkinson, R. J., Che, K. H., Daniel, M., Strain-Damerell, C., Gileadi, C., Kochan, G., Leung, I. K. H., Dunford, J., Yeoh, K. K., Ratcliffe, P. J., Burgess-Brown, N., von Delft, F., Muller, S., Marsden, B., Brennan, P. E., McDonough, M. A., Oppermann, U., Klose, R. J., Schofield, C. J., and Kawamura, A. (2012) Plant growth regulator daminozide is a selective inhibitor of human KDM2/7 histone demethylases. *J. Med. Chem. 55*, 6639–43.

(288) England, K. S., Tumber, A., Krojer, T., Scozzafava, G., Ng, S. S., Daniel, M., Szykowska, A., Che, K., von Delft, F., Burgess-Brown, N. A., Kawamura, A., Schofield, C. J., and Brennan, P. E. (2014) Optimisation of a triazolopyridine based histone demethylase inhibitor yields a potent and selective KDM2A (FBXL11) inhibitor. *Medchemcomm 5*, 1879–1886.

(289) Kruidenier, L., Chung, C., Cheng, Z., Liddle, J., Che, K., Joberty, G., Bantscheff, M., Bountra, C., Bridges, A., Diallo, H., Eberhard, D., Hutchinson, S., Jones, E., Katso, R., Leveridge, M., Mander, P. K., Mosley, J., Ramirez-Molina, C., Rowland, P., Schofield, C. J., Sheppard, R. J., Smith, J. E., Swales, C., Tanner, R., Thomas, P., Tumber, A., Drewes, G., Oppermann, U., Patel, D. J., Lee, K., and Wilson, D. M. (2012) A selective jumonji H3K27 demethylase inhibitor modulates the proinflammatory macrophage response. *Nature 488*, 404–8.

(290) Heinemann, B., Nielsen, J. M., Hudlebusch, H. R., Lees, M. J., Larsen, D. V., Boesen, T., Labelle, M., Gerlach, L.-O., Birk, P., and Helin, K. (2014) Inhibition of demethylases by GSK-J1/J4. *Nature 514*, E1-2.

(291) Wagner, E. K., Nath, N., Flemming, R., Feltenberger, J. B., and Denu, J. M. (2012) Identification and characterization of small molecule inhibitors of a plant homeodomain finger. *Biochemistry 51*, 8293–306.

(292) Bavetsias, V., Lanigan, R. M., Ruda, G. F., Atrash, B., McLaughlin, M. G., Tumber, A., Mok, N. Y., Le Bihan, Y.-V., Dempster, S., Boxall, K. J., Jeganathan, F., Hatch, S. B., Savitsky, P., Velupillai, S., Krojer, T., England, K. S., Sejberg, J., Thai, C., Donovan, A., Pal, A., Scozzafava, G., Bennett, J. M., Kawamura, A., Johansson, C., Szykowska, A., Gileadi, C., Burgess-Brown, N. A., von Delft, F., Oppermann, U., Walters, Z., Shipley, J., Raynaud, F. I., Westaway, S. M., Prinjha, R. K., Fedorov, O., Burke, R., Schofield, C. J., Westwood, I. M., Bountra, C., Müller, S., van Montfort, R. L. M., Brennan, P. E., and Blagg, J. (2016) 8-Substituted Pyrido[3,4-d]pyrimidin-4(3H)-one Derivatives As Potent, Cell Permeable, KDM4 (JMJD2) and KDM5 (JARID1) Histone Lysine Demethylase Inhibitors. *J. Med. Chem. 59*, 1388–409.

(293) Thinnes, C. C., Tumber, A., Yapp, C., Scozzafava, G., Yeh, T., Chan, M. C., Tran, T. A., Hsu, K., Tarhonskaya, H., Walport, L. J., Wilkins, S. E., Martinez, E. D., Müller, S., Pugh, C. W., Ratcliffe, P. J., Brennan, P. E., Kawamura, A., and Schofield, C. J. (2015) Betti reaction enables efficient synthesis of 8-hydroxyquinoline inhibitors of 2-oxoglutarate oxygenases. *Chem. Commun. (Camb). 51*, 15458–61.

(294) Hewitson, K. S., Lienard, B. M. R., McDonough, M. A., Clifton, I. J., Butler, D., Soares, A. S., Oldham, N. J., McNeill, L. A., and Schofield, C. J. (2007) Structural and Mechanistic Studies on the Inhibition of the Hypoxia-inducible Transcription Factor Hydroxylases by Tricarboxylic Acid Cycle Intermediates. *J. Biol. Chem. 282*, 3293–3301.

(295) Chinopoulos, C. (2013) Which way does the citric acid cycle turn during hypoxia? The critical role of α-ketoglutarate dehydrogenase complex. *J. Neurosci. Res. 91*, 1030–1043.

(296) Isaacs, J. S., Jung, Y. J., Mole, D. R., Lee, S., Torres-Cabala, C., Chung, Y.-L., Merino, M., Trepel, J., Zbar, B., Toro, J., Ratcliffe, P. J., Linehan, W. M., and Neckers, L. (2005) HIF overexpression correlates with biallelic loss of fumarate hydratase in renal cancer: Novel role of fumarate in regulation of HIF stability. *Cancer Cell 8*, 143–153.

(297) Pollard, P. J., Brière, J. J., Alam, N. A., Barwell, J., Barclay, E., Wortham, N. C., Hunt, T., Mitchell, M., Olpin, S., Moat, S. J., Hargreaves, I. P., Heales, S. J., Chung, Y. L., Griffiths, J. R., Dalgleish, A., McGrath, J. A., Gleeson, M. J., Hodgson, S. V, Poulsom, R., Rustin, P., and Tomlinson, I. P. M. (2005) Accumulation of Krebs cycle intermediates and over-expression of HIF1alpha in tumours which result from germline FH and SDH mutations. *Hum. Mol. Genet. 14*, 2231–9.

(298) Selak, M. A., Armour, S. M., MacKenzie, E. D., Boulahbel, H., Watson, D. G., Mansfield, K. D., Pan, Y., Simon, M. C., Thompson, C. B., and Gottlieb, E. (2005) Succinate links TCA cycle dysfunction to oncogenesis by inhibiting HIF-α prolyl hydroxylase. *Cancer Cell 7*, 77–85.

(299) Koivunen, P., Hirsila, M., Remes, A. M., Hassinen, I. E., Kivirikko, K. I., and Myllyharju, J. (2007) Inhibition of Hypoxia-inducible Factor (HIF) Hydroxylases by Citric Acid Cycle Intermediates: POSSIBLE LINKS BETWEEN CELL METABOLISM AND STABILIZATION OF HIF. *J. Biol. Chem. 282*, 4524–4532.

(300) Xu, W., Yang, H., Liu, Y., Yang, Y., Wang, P., Kim, S.-H., Ito, S., Yang, C., Wang, P., Xiao, M.-T., Liu, L., Jiang, W., Liu, J., Zhang, J., Wang, B., Frye, S., Zhang, Y., Xu, Y., Lei, Q., Guan, K.-L., Zhao, S., and Xiong, Y. (2011) Oncometabolite 2-hydroxyglutarate is a competitive inhibitor of α-ketoglutarate-dependent dioxygenases. *Cancer Cell 19*, 17–30.

(301) Koivunen, P., Lee, S., Duncan, C. G., Lopez, G., Lu, G., Ramkissoon, S., Losman, J. A., Joensuu, P., Bergmann, U., Gross, S., Travins, J., Weiss, S., Looper, R., Ligon, K. L., Verhaak, R. G. W., Yan, H., Kaelin, W. G., and Jr. (2012) Transformation by the (R)-

enantiomer of 2-hydroxyglutarate linked to EGLN activation. *Nature 483*, 484–8.

(302) Williams, S. C., Karajannis, M. A., Chiriboga, L., Golfinos, J. G., von Deimling, A., and Zagzag, D. (2011) R132H-mutation of isocitrate dehydrogenase-1 is not sufficient for HIF-1α upregulation in adult glioma. *Acta Neuropathol. 121*, 279–81.

(303) Zhao, S., Lin, Y., Xu, W., Jiang, W., Zha, Z., Wang, P., Yu, W., Li, Z., Gong, L., Peng, Y., Ding, J., Lei, Q., Guan, K.-L., and Xiong, Y. (2009) Glioma-Derived Mutations in IDH1 Dominantly Inhibit IDH1 Catalytic Activity and Induce HIF-1α. *Science (80-.). 324*.

(304) Sasaki, M., Knobbe, C. B., Itsumi, M., Elia, A. J., Harris, I. S., Chio, I. I. C., Cairns, R. A., McCracken, S., Wakeham, A., Haight, J., Ten, A. Y., Snow, B., Ueda, T., Inoue, S., Yamamoto, K., Ko, M., Rao, A., Yen, K. E., Su, S. M., and Mak, T. W. (2012) D-2-hydroxyglutarate produced by mutant IDH1 perturbs collagen maturation and basement membrane function. *Genes Dev. 26*, 2038–49.

(305) Tarhonskaya, H., Rydzik, A. M., Leung, I. K. H., Loik, N. D., Chan, M. C., Kawamura, A., McCullagh, J. S. O., Claridge, T. D. W., Flashman, E., and Schofield, C. J. (2014) Non-enzymatic chemistry enables 2-hydroxyglutarate-mediated activation of 2-oxoglutarate oxygenases. *Nat. Commun. 5*, 3423.

(306) Figueroa, M. E., Abdel-Wahab, O., Lu, C., Ward, P. S., Patel, J., Shih, A., Li, Y., Bhagwat, N., Vasanthakumar, A., Fernandez, H. F., Tallman, M. S., Sun, Z., Wolniak, K., Peeters, J. K., Liu, W., Choe, S. E., Fantin, V. R., Paietta, E., Löwenberg, B., Licht, J. D., Godley, L. A., Delwel, R., Valk, P. J. M., Thompson, C. B., Levine, R. L., and Melnick, A. (2010) Leukemic IDH1 and IDH2 mutations result in a hypermethylation phenotype, disrupt TET2 function, and impair hematopoietic differentiation. *Cancer Cell 18*, 553–67.

(307) Lu, C., Ward, P. S., Kapoor, G. S., Rohle, D., Turcan, S., Abdel-Wahab, O., Edwards, C. R., Khanin, R., Figueroa, M. E., Melnick, A., Wellen, K. E., O'Rourke, D. M., Berger, S. L., Chan, T. A., Levine, R. L., Mellinghoff, I. K., and Thompson, C. B. (2012) IDH mutation impairs histone demethylation and results in a block to cell differentiation. *Nature 483*, 474–478.

(308) Dang, L., White, D. W., Gross, S., Bennett, B. D., Bittinger, M. A., Driggers, E. M., Fantin, V. R., Jang, H. G., Jin, S., Keenan, M. C., Marks, K. M., Prins, R. M., Ward, P. S., Yen, K. E., Liau, L. M., Rabinowitz, J. D., Cantley, L. C., Thompson, C. B., Vander Heiden, M. G., and Su, S. M. (2009) Cancer-associated IDH1 mutations produce 2-hydroxyglutarate. *Nature 462*, 739–44.

(309) Intlekofer, A. M., Dematteo, R. G., Venneti, S., Finley, L. W. S., Lu, C., Judkins, A. R., Rustenburg, A. S., Grinaway, P. B., Chodera, J. D., Cross, J. R., and Thompson, C. B. (2015) Hypoxia Induces Production of L-2-Hydroxyglutarate. *Cell Metab. 22*, 304–11.

(310) Williamson, J. R., Ford, C., Illingworth, J., and Safer, B. (1976) Coordination of citric acid cycle activity with electron transport flux. *Circ. Res. 38*, I39-51.

(311) Schiller, R., Scozzafava, G., Tumber, A., Wickens, J. R., Bush, J. T., Rai, G., Lejeune, C., Choi, H., Yeh, T.-L., Chan, M. C., Mott, B. T., McCullagh, J. S. O., Maloney, D. J., Schofield, C. J., and Kawamura, A. (2014) A Cell-Permeable Ester Derivative of the JmjC Histone Demethylase Inhibitor IOX1. *ChemMedChem 9*, 566–571.

(312) Hill, J. A., and Olson, E. N. (2008) Cardiac Plasticity. *N. Engl. J. Med. 358*, 1370–1380.

(313) (2016) CVD Statistics- BHF UK Factsheet.

(314) Ponikowski, P., Voors, A. A., Anker, S. D., Bueno, H., Cleland, J. G. F., Coats, A. J. S., Falk, V., González-Juanatey, J. R., Harjola, V.-P., Jankowska, E. A., Jessup, M., Linde, C., Nihoyannopoulos, P., Parissis, J. T., Pieske, B., Riley, J. P., Rosano, G. M. C., Ruilope, L. M., Ruschitzka, F., Rutten, F. H., and van der Meer, P. (2016) 2016 ESC Guidelines for the diagnosis and treatment of acute and chronic heart failure. *Eur. J. Heart Fail. 18*, 891–975.

(315) Jhund, P. S., and McMurray, J. J. V. (2016) The neprilysin pathway in heart failure: a review and guide on the use of sacubitril/valsartan. *Heart 102*, 1342–7.

(316) McMurray, J. J. V, Packer, M., Desai, A. S., Gong, J., Lefkowitz, M. P., Rizkala, A. R., Rouleau, J. L., Shi, V. C., Solomon, S. D., Swedberg, K., Zile, M. R., and PARADIGM-HF Investigators and Committees. (2014) Angiotensin-neprilysin inhibition versus enalapril in heart failure. *N. Engl. J. Med. 371*, 993–1004.

(317) Sharma, K., and Kass, D. A. (2014) Heart failure with preserved ejection fraction: mechanisms, clinical features, and therapies. *Circ. Res. 115*, 79–96.

(318) Klapholz, M., Maurer, M., Lowe, A. M., Messineo, F., Meisner, J. S., Mitchell, J., Kalman, J., Phillips, R. A., Steingart, R., Brown, E. J., Berkowitz, R., Moskowitz, R., Soni, A., Mancini, D., Bijou, R., Sehhat, K., Varshneya, N., Kukin, M., Katz, S. D., Sleeper, L. A., Le Jemtel, T. H., and New York Heart Failure Consortium. (2004) Hospitalization for heart failure in the presence of a normal left ventricular ejection fraction. *J. Am. Coll. Cardiol. 43*, 1432–1438.

(319) McKinsey, T. A., and Kass, D. A. (2007) Small-molecule therapies for cardiac hypertrophy: moving beneath the cell surface. *Nat. Rev. Drug Discov. 6*, 617–635.

(320) McKinsey, T. A., and Olson, E. N. (2005) Toward transcriptional therapies for the failing heart: chemical screens to modulate genes. *J. Clin. Invest. 115*, 538–546.

(321) Antos, C. L., McKinsey, T. A., Dreitz, M., Hollingsworth, L. M., Zhang, C.-L., Schreiber, K., Rindt, H., Gorczynski, R. J., and Olson, E. N. (2003) Dose-dependent Blockade to Cardiomyocyte Hypertrophy by Histone Deacetylase Inhibitors. *J. Biol. Chem. 278*, 28930–28937.

(322) Kong, Y., Tannous, P., Lu, G., Berenji, K., Rothermel, B. A., Olson, E. N., and Hill, J. A. (2006) Suppression of class I and II histone deacetylases blunts pressure-overload cardiac hypertrophy. *Circulation 113*, 2579–88.

(323) Kook, H., Lepore, J. J., Gitler, A. D., Lu, M. M., Wing-Man Yung, W., Mackay, J., Zhou, R., Ferrari, V., Gruber, P., and Epstein, J. A. (2003) Cardiac hypertrophy and histone deacetylase–dependent transcriptional repression mediated by the atypical homeodomain protein Hop. *J. Clin. Invest. 112*, 863–871.

(324) Kee, H. J., Sohn, I. S., Nam, K. Il, Park, J. E., Qian, Y. R., Yin, Z., Ahn, Y., Jeong, M. H., Bang, Y.-J., Kim, N., Kim, J.-K., Kim, K. K., Epstein, J. A., and Kook, H. (2005) Inhibition of Histone Deacetylation Blocks Cardiac Hypertrophy Induced by Angiotensin II Infusion and Aortic Banding. *Circulation 113*, 51–59.

(325) Rosales, W., Carulla, J., García, J., Vargas, D., Lizcano, F., Rosales, W., Carulla, J., Garcia, J., Vargas, D., Lizcano, F., Vargas, D., and Lizcano, F. (2016) Role of Histone Demethylases in Cardiomyocytes Induced to Hypertrophy. *Biomed Res. Int. 2016*, 1–7.

(326) Reid, B. G., Stratton, M. S., Bowers, S., Cavasin, M. A., Demos-Davies, K. M., Susano, I., and McKinsey, T. A. (2016) Discovery of novel small molecule inhibitors of cardiac hypertrophy using high throughput, high content imaging. *J. Mol. Cell. Cardiol. 97*,

106–13.

(327) Berry, W. L., and Janknecht, R. (2013) KDM4/JMJD2 histone demethylases: epigenetic regulators in cancer cells. *Cancer Res. 73*, 2936–42.

(328) Boveris, A., Oshino, N., and Chance, B. (1972) The cellular production of hydrogen peroxide. *Biochem. J. 128*, 617–30.

(329) Boveris, A., and Chance, B. (1973) The mitochondrial generation of hydrogen peroxide. General properties and effect of hyperbaric oxygen. *Biochem. J. 134*, 707–16.

(330) Loschen, G., Azzi, A., Richter, C., and Flohé, L. (1974) Superoxide radicals as precursors of mitochondrial hydrogen peroxide. *FEBS Lett. 42*, 68–72.

(331) Murphy, M. P. (2009) How mitochondria produce reactive oxygen species. *Biochem. J. 417*, 1–13.

(332) Kietzmann, T., and Görlach, A. (2005) Reactive oxygen species in the control of hypoxia-inducible factor-mediated gene expression. *Semin. Cell Dev. Biol. 16*, 474–486.

(333) Holmström, K. M., and Finkel, T. (2014) Cellular mechanisms and physiological consequences of redox-dependent signalling. *Nat. Rev. Mol. Cell Biol. 15*, 411–21.

(334) Waypa, G. B., Smith, K. A., and Schumacker, P. T. (2016) O2 sensing, mitochondria and ROS signaling: The fog is lifting. *Mol. Aspects Med. 47*, 76–89.

(335) Chandel, N. S., Maltepe, E., Goldwasser, E., Mathieu, C. E., Simon, M. C., and Schumacker, P. T. (1998) Mitochondrial reactive oxygen species trigger hypoxia-induced transcription. *Proc. Natl. Acad. Sci. U. S. A. 95*, 11715–20.

(336) Hoffman, D. L., Salter, J. D., and Brookes, P. S. (2007) Response of mitochondrial reactive oxygen species generation to steady-state oxygen tension: implications for hypoxic cell signaling. *Am. J. Physiol. Heart Circ. Physiol. 292*, H101-8.

(337) Zorov, D. B., Juhaszova, M., and Sollott, S. J. (2014) Mitochondrial reactive oxygen species (ROS) and ROS-induced ROS release. *Physiol. Rev. 94*, 909–50.

(338) Sena, L. A., and Chandel, N. S. (2012) Physiological roles of mitochondrial reactive oxygen species. *Mol. Cell 48*, 158–67.

(339) Bell, E. L., Emerling, B. M., and Chandel, N. S. (2005) Mitochondrial regulation of oxygen sensing. *Mitochondrion 5*, 322–332.

(340) Chandel, N. S. (2010) Mitochondrial regulation of oxygen sensing. *Adv. Exp. Med. Biol. 661*, 339–54.

(341) Giordano, F. J. (2005) Oxygen, oxidative stress, hypoxia, and heart failure. *J. Clin. Invest. 115*, 500–8.

(342) Lee, J., Giordano, S., and Zhang, J. (2012) Autophagy, mitochondria and oxidative stress: cross-talk and redox signalling. *Biochem. J. 441*, 523–40.

(343) D'Autréaux, B., and Toledano, M. B. (2007) ROS as signalling molecules: mechanisms that generate specificity in ROS homeostasis. *Nat. Rev. Mol. Cell Biol. 8*, 813–824.

(344) Di Meo, S., Reed, T. T., Venditti, P., and Victor, V. M. (2016) Role of ROS and RNS Sources in Physiological and Pathological Conditions. *Oxid. Med. Cell. Longev. 2016*, 1245049.

(345) Imlay, J. A. (2003) Pathways of Oxidative Damage. *Annu. Rev. Microbiol. 57*, 395–

418.

(346) Dixon, S. J., and Stockwell, B. R. (2013) The role of iron and reactive oxygen species in cell death. *Nat. Chem. Biol. 10*, 9–17.

(347) Waris, G., and Ahsan, H. (2006) Reactive oxygen species: role in the development of cancer and various chronic conditions. *J. Carcinog. 5*, 14.

(348) Dawane, J. S., and Pandit, V. A. (2012) Understanding redox homeostasis and its role in cancer. *J. Clin. Diagn. Res. 6*, 1796–802.

(349) Kurian, G. A., Rajagopal, R., Vedantham, S., and Rajesh, M. (2016) The Role of Oxidative Stress in Myocardial Ischemia and Reperfusion Injury and Remodeling: Revisited. *Oxid. Med. Cell. Longev. 2016*, 1656450.

(350) Bagheri, F., Khori, V., Alizadeh, A. M., Khalighfard, S., Khodayari, S., and Khodayari, H. (2016) Reactive oxygen species-mediated cardiac-reperfusion injury: Mechanisms and therapies. *Life Sci.*

(351) Granger, D. N., and Kvietys, P. R. (2015) Reperfusion injury and reactive oxygen species: The evolution of a concept. *Redox Biol. 6*, 524–51.

(352) Perrotta, I., and Aquila, S. (2015) The role of oxidative stress and autophagy in atherosclerosis. *Oxid. Med. Cell. Longev. 2015*, 130315.

(353) Konradi, J., Mollenhauer, M., Baldus, S., and Klinke, A. (2015) Redox-sensitive mechanisms underlying vascular dysfunction in heart failure. *Free Radic. Res. 49*, 721–742.

(354) Tsutsui, H., Kinugawa, S., and Matsushima, S. (2011) Oxidative stress and heart failure. *Am. J. Physiol. Heart Circ. Physiol. 301*, H2181-90.

(355) Sag, C. M., and Santos, C. X. C. (2014) Redox regulation of cardiac hypertrophy. *J. Mol. Cell. Cardiol. 73*, 103–111.

(356) Maulik, S. K., and Kumar, S. (2012) Oxidative stress and cardiac hypertrophy: a review. *Toxicol. Mech. Methods 22*, 359–366.

(357) Takimoto, E., and Kass, D. A. (2007) Role of Oxidative Stress in Cardiac Hypertrophy and Remodeling. *Hypertension 49*.

(358) Seddon, M., Looi, Y. H., and Shah, A. M. (2007) Oxidative stress and redox signalling in cardiac hypertrophy and heart failure. *Heart 93*, 903–7.

(359) Takano, H., Zou, Y., Hasegawa, H., Akazawa, H., Nagai, T., and Komuro, I. (2003) Oxidative stress-induced signal transduction pathways in cardiac myocytes: involvement of ROS in heart diseases. *Antioxid. Redox Signal. 5*, 789–94.

(360) Madamanchi, N. R., and Runge, M. S. (2013) Redox signaling in cardiovascular health and disease. *Free Radic. Biol. Med. 61*, 473–501.

(361) Penna, C., Mancardi, D., Rastaldo, R., and Pagliaro, P. (2009) Cardioprotection: a radical view Free radicals in pre and postconditioning. *Biochim. Biophys. Acta 1787*, 781–93.

(362) Pagliaro, P., and Penna, C. (2015) Redox signalling and cardioprotection: translatability and mechanism. *Br. J. Pharmacol. 172*, 1974–95.

(363) He, F., and Zuo, L. (2015) Redox Roles of Reactive Oxygen Species in Cardiovascular Diseases. *Int. J. Mol. Sci. 16*, 27770–80.

(364) Tikoo, K., Lau, S. S., and Monks, T. J. (2001) Histone H3 Phosphorylation Is Coupled

to Poly-(ADP-Ribosylation) during Reactive Oxygen Species-Induced Cell Death in Renal Proximal Tubular Epithelial Cells. *Mol. Pharmacol. 60*.

(365) Rahman, I., Marwick, J., and Kirkham, P. (2004) Redox modulation of chromatin remodeling: impact on histone acetylation and deacetylation, NF-kappaB and pro-inflammatory gene expression. *Biochem. Pharmacol. 68*, 1255–67.

(366) Gu, X., Sun, J., Li, S., Wu, X., and Li, L. (2013) Oxidative stress induces DNA demethylation and histone acetylation in SH-SY5Y cells: potential epigenetic mechanisms in gene transcription in Aβ production. *Neurobiol. Aging 34*, 1069–79.

(367) Franco, R., Schoneveld, O., Georgakilas, A. G., and Panayiotidis, M. I. (2008) Oxidative stress, DNA methylation and carcinogenesis. *Cancer Lett. 266*, 6–11.

(368) Kloypan, C., Srisa-art, M., Mutirangura, A., and Boonla, C. (2015) LINE-1 hypomethylation induced by reactive oxygen species is mediated via depletion of S-adenosylmethionine. *Cell Biochem. Funct. 33*, 375–85.

(369) Xin, Y.-J., Yuan, B., Yu, B., Wang, Y.-Q., Wu, J.-J., Zhou, W.-H., and Qiu, Z. (2015) Tet1-mediated DNA demethylation regulates neuronal cell death induced by oxidative stress. *Sci. Rep. 5*, 7645.

(370) O'Hagan, H. M., Wang, W., Sen, S., Destefano Shields, C., Lee, S. S., Zhang, Y. W., Clements, E. G., Cai, Y., Van Neste, L., Easwaran, H., Casero, R. A., Sears, C. L., and Baylin, S. B. (2011) Oxidative damage targets complexes containing DNA methyltransferases, SIRT1, and polycomb members to promoter CpG Islands. *Cancer Cell 20*, 606–19.

(371) Niu, Y., DesMarais, T. L., Tong, Z., Yao, Y., and Costa, M. (2015) Oxidative stress alters global histone modification and DNA methylation. *Free Radic. Biol. Med.*

(372) Masson, N., Singleton, R. S., Sekirnik, R., Trudgian, D. C., Ambrose, L. J., Miranda, M. X., Tian, Y.-M., Kessler, B. M., Schofield, C. J., and Ratcliffe, P. J. (2012) The FIH hydroxylase is a cellular peroxide sensor that modulates HIF transcriptional activity. *EMBO Rep. 13*, 251–7.

(373) Hamed, M. Y., Keypour, H., Silver, J., and Wilson, M. T. (1988) Studies of the reactions of iron(II) ascorbate mixtures with molecular oxygen in solution. *Inorganica Chim. Acta 152*, 227–231.

(374) Chowdhury, R., McDonough, M. A., Mecinović, J., Loenarz, C., Flashman, E., Hewitson, K. S., Domene, C., and Schofield, C. J. (2009) Structural basis for binding of hypoxia-inducible factor to the oxygen-sensing prolyl hydroxylases. *Structure 17*, 981–9.

(375) Invitrogen. (2009) Amplex® Red Hydrogen Peroxide/Peroxidase Assay Kit. Molecular Probes, Eugene OR.

(376) Neal, A., Rountree, A., Kernan, K., Van Yserloo, B., Zhang, H., Reed, B. J., Osborne, W., Wang, W., and Sweet, I. R. (2016) Real-time imaging of intracellular hydrogen peroxide in pancreatic islets. *Biochem. J. 473*.

(377) Scientific, T. (2011) Pierce ® BCA Protein Assay Kit. *Test*. Thermo Fisher Scientific, Rockford, IL.

(378) Life Technologies. (2011) mirVana™ miRNA Isolation Kit. *Lab. Tech.* Life Technologies, Carlsbad, CA.

(379) RevTsc, A. (2010) High Capacity cDNA Reverse Transcription Kits for 200 and 1000

Reactions Protocol (Rev E). *Manual*. Applied Biosystems, Foster City CA.

(380) Rao, V. H., Kandel, A., Lynch, D., Pena, Z., Marwaha, N., Deng, C., Watson, P., and Hansen, L. A. (2012) A positive feedback loop between HER2 and ADAM12 in human head and neck cancer cells increases migration and invasion. *Oncogene 31*, 2888–98.

(381) Liu, W., Xie, Y., Ma, J., Luo, X., Nie, P., Zuo, Z., Lahrmann, U., Zhao, Q., Zheng, Y., Zhao, Y., Xue, Y., and Ren, J. (2015) IBS: an illustrator for the presentation and visualization of biological sequences. *Bioinformatics 31*, 3359–61.

(382) Kawamura, A., Tumber, A., Rose, N. R., King, O. N. F., Daniel, M., Oppermann, U., Heightman, T. D., and Schofield, C. (2010) Development of homogeneous luminescence assays for histone demethylase catalysis and binding. *Anal. Biochem. 404*, 86–93.

(383) Zhang, D., Yoon, H.-G., and Wong, J. (2005) JMJD2A is a novel N-CoR-interacting protein and is involved in repression of the human transcription factor achaete scute-like homologue 2 (ASCL2/Hash2). *Mol. Cell. Biol. 25*, 6404–14.

Appendix 1: HPLC-MS analysis of H3K9me3 peptides for use in *in vitro* assays

A)

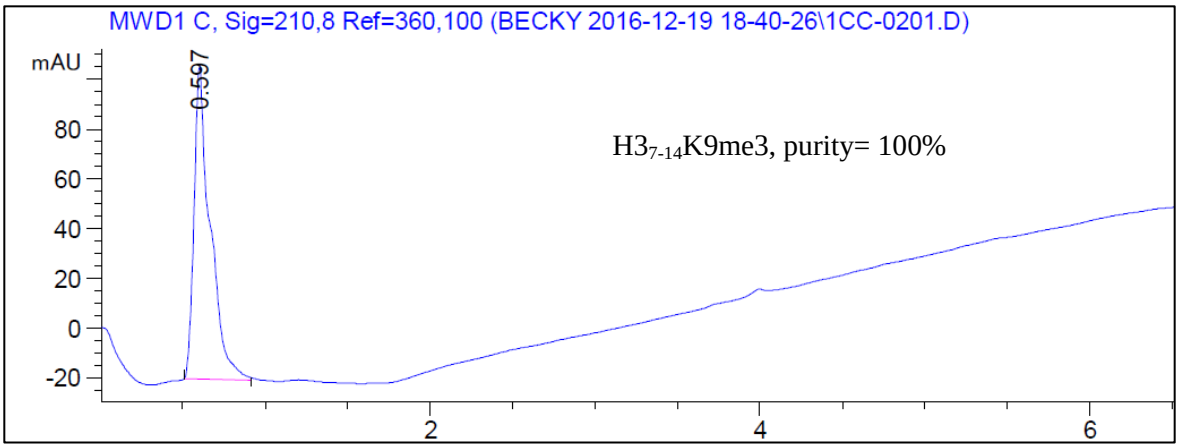

B)

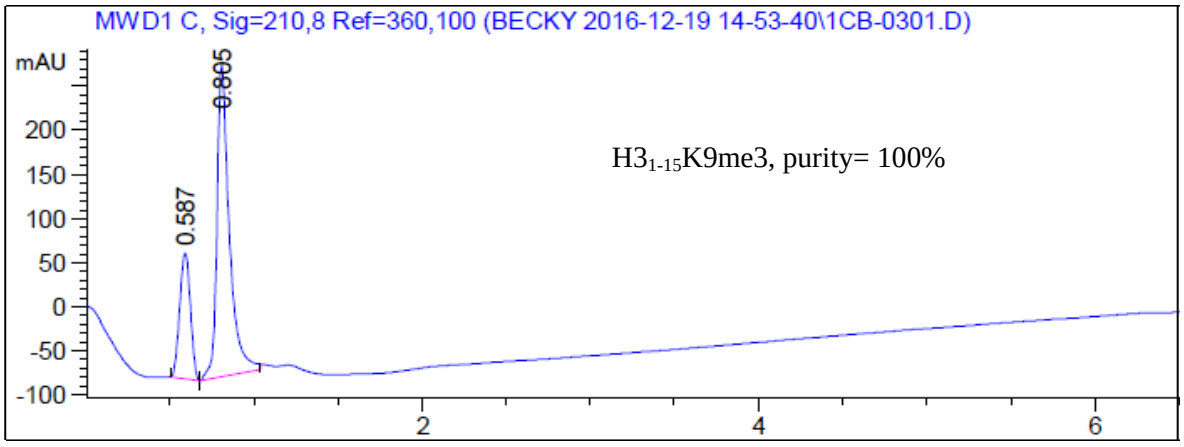

Figure A1. UV chromatographs (absorption at 210 nm) from the High Performance Liquid Chromatography/ Liquid Chromatography-Mass Spectrometry (HPLC/LC-MS) analysis of **A)** H3$_{7-14}$K9me3 and **B)** H3$_{1-15}$K9me3 peptide synthesised for use in *in vitro* assays (Chapter 2). Peptides were only available for analysis dissolved in 50 mM HEPES, pH 7.5. Integration of the peaks was used to assess the purity of the synthesised peptides. **A)** H3$_{7-14}$K9me3 co-eluted at 0.597 min with HEPES buffer as a single peak, as confirmed by inspection of the mass spectrum (not shown), and integration confirmed 100% purity of the peptide. **B)** H3$_{1-15}$K9me3 eluted at 0.805 min, as confirmed from the mass spectrum (not shown). The peak at 0.587 min was found to be HEPES buffer from analysis of the MS spectrum; hence the peptide peak represents 100% of the peptide content of the sample.

Appendix 2: Measurement of O_2 concentration in cell culture medium

In experiments to assess the effect of hypoxia on the cellular activity of KDM4A (Chapter 3), an OxyLite™ dissolved oxygen probe (Oxford Optronix) was used to measure oxygen concentration in the cell culture media (DMEM). F-KDM4A U2OS cells were incubated at varying concentrations of O_2 in hypoxic workstations (0.1, 1.0, 5.0 and 21% O_2, 37 °C, 5.0% CO_2, 24 h, Chapter 7.2.3). Immediately before cells were fixed for immunofluorescence experiments (Chapter 7.2.6), the oxygen probe was inserted into the hypoxic chamber and allowed to equilibrate for approx. 2 min, then used to measure the dissolved oxygen concentration in the media above cells in 3 separate wells across the 96 well plate. An average of these measurements was taken. Measurements were performed on three separate days to produce 3 biological repeats (Figure A2).

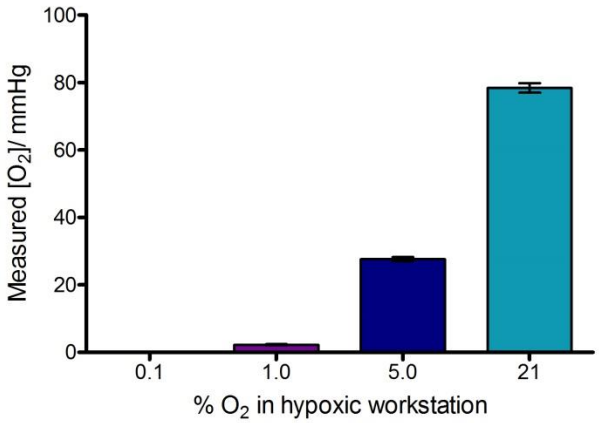

% O_2 in workstation	Measured [O_2]/ mmHg
0.1	0.117 ± 0.062
1.0	2.22 ± 0.189
5.0	27.6 ± 0.633
21	78.4 ± 1.41

Figure A2. Dissolved O_2 concentration in cell culture medium after 24 h incubation in hypoxic chambers. Measurements were taken using an OxyLite™ dissolved oxygen probe (Oxford Optronix). N=3 biological repeats, error bars denote sd. Note: cells incubated at 21% O_2 were contained in a standard cell culture incubator.

Appendix 3: Evaluation of the efficiency of oligonucleotide primers used in RT-qPCR experiments

Oligonucleotide primers for use in the RT-qPCR quantification of gene expression in F-KDM4A U2OS cells exposed to varying degrees of hypoxia were evaluated for efficiency according to the procedure described by Pfaffl[269]. cDNA from various samples was mixed to give an average of all conditions, then a dilution series of cDNA was tested against 300 nM primers (Chapter 7.2.8). The resultant Ct values were plotted against log([cDNA]/ng.μL^{-1}) (Figure A3.1, Figure A3.2) and the slope of the line used to calculate the primer efficiency (Equation A3.1). Only primers with efficiency values between 1.8 and 2.2 were deemed sufficiently efficient for use in RT-qPCR experiments. The linear Ct range was also determined, and any Ct values obtained in subsequent RT-qPCR experiments that fell outside of this range were rejected.

$$Efficiency = 10^{\frac{1}{(ABS(Slope\ Ct_{min}:Ct_{max},log[cDNA]_{min}\ log:[cDNA]_{\max}))}} \qquad \textbf{A3.1}$$

Where:

ABS = Absolute value

Slope = The gradient of the linear regression line through a defined set of points

Ct_{min} = minimum Ct value obtained in the linear range

Ct_{max} = maximum Ct value obtained in the linear range

$Log[cDNA]_{min}$ = log of the minimum cDNA concentration for which Ct is in the linear range

$Log[cDNA]_{max}$ = log of the maximum cDNA concentration for which Ct is in the linear range

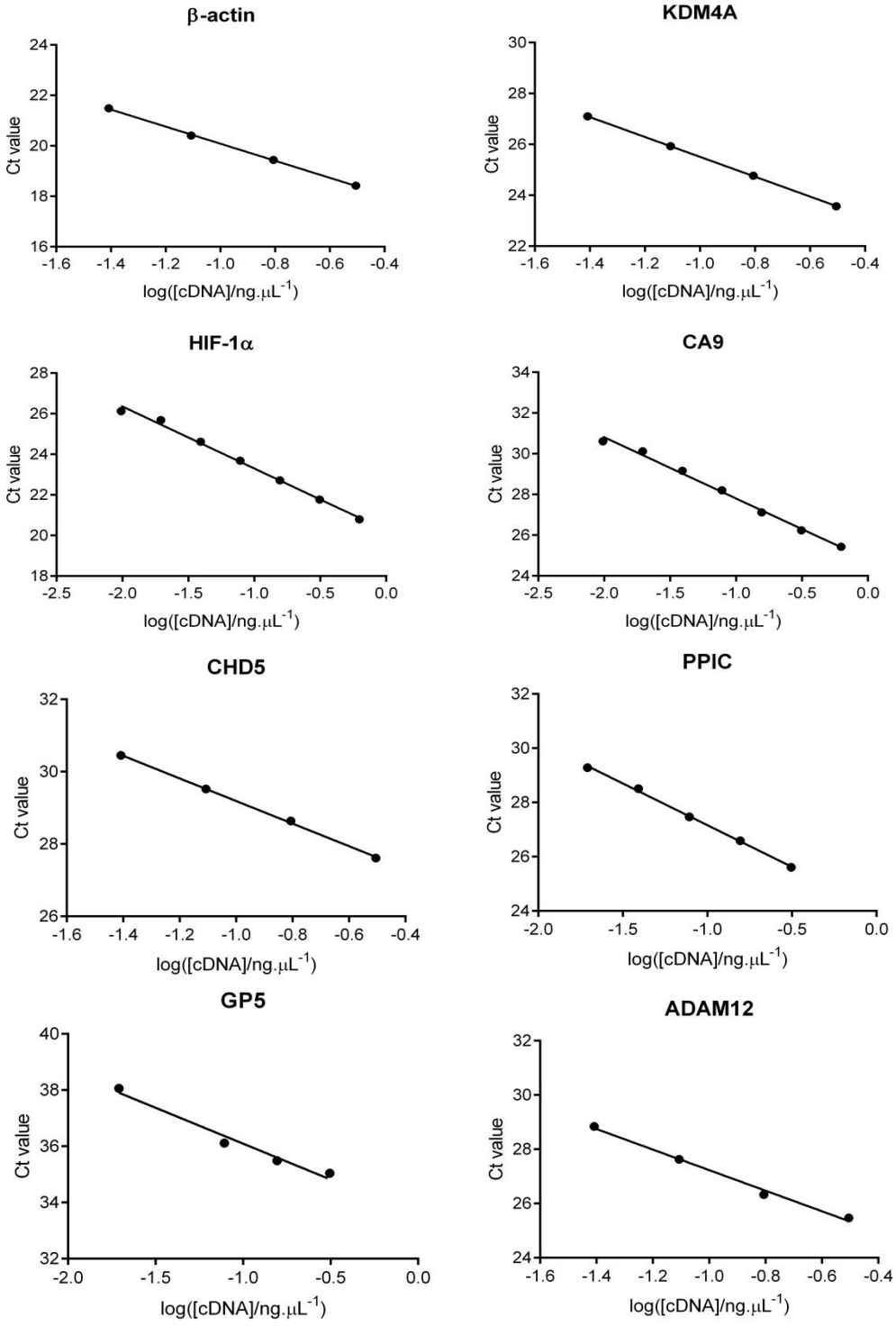

Figure A3.1 Efficiency tests of oligonucleotide primers used for RT-qPCR analysis (Chapter 3. 4, Chapter 7.2.8) of **B)** *KDM4A*^{264}, **C)** *HIF-1α** **D)** the HIF target gene *CA9** and **E-H)** the putative KDM4A target genes *CHD5*^{264}, *PPIC*^{264}, *GP5*^{264} and *ADAM12*^{380}. **A)** β-*actin** was used as a housekeeping control gene**.** Graphs were produced in GraphPad Prism v5.04 and fitted to a linear regression model. Data was collected and processed using CFX Manager™ Software v3.1 (Bio-Rad) and analysed in Microsoft Excel. * Primers were kindly donated by Dr Mun Chiang Chan, Ratcliffe Laboratory, NDM, University of Oxford.

Table A3.1 Calculated efficiencies and valid Ct ranges of the oligonucleotide primers tested and used in RT-qPCR experiments (Chapter 3.4, Chapter 7.2.8).

Primer set	Calculated Efficiency	Valid Ct range
β-actin	1.976	18.42 – 35.43
KDM4A	1.804	23.57 – 27.10
HIF-1α	2.126	20.80 – 26.13
CA9	2.151	25.43 – 30.61
CHD5	2.012	27.61 – 30.45
PPIC	2.114	25.61 – 29.28
GP5	2.043	35.04 – 38.06
ADAM12	1.836	25.57 – 28.84

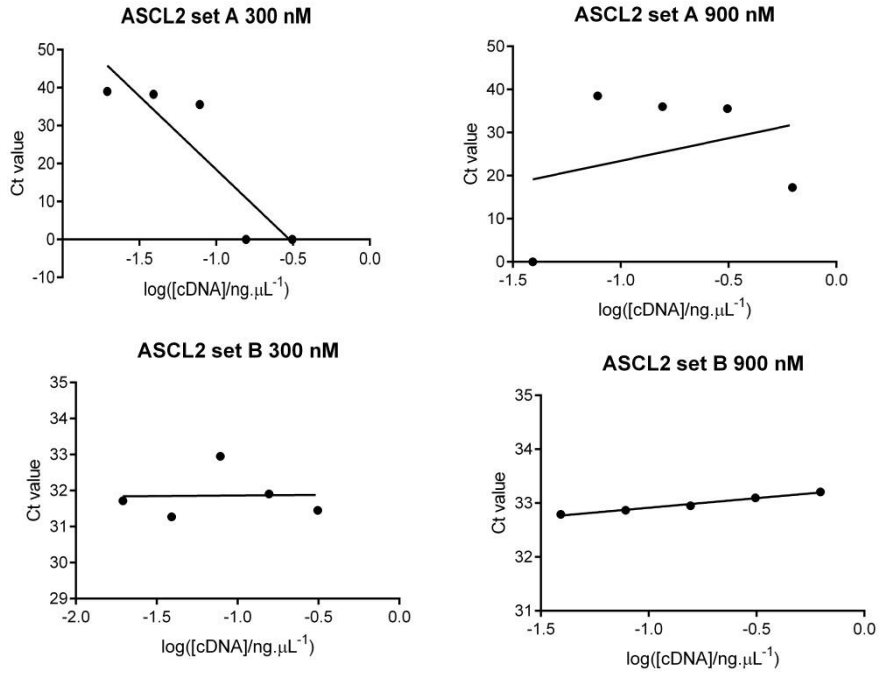

Figure A3.2 Efficiency tests of published oligonucleotide primers for the KDM4A target gene *ASCL2*. Two different sets of primers, **A, B)** set A^{264} and **C, D)** set B^{383}, were tested at **A, C)** 300 nM **B, D)** 900 nM against varying cDNA concentrations. Graphs were produced in GraphPad Prism v5.04 and fitted to a linear regression model. Data was collected and processed using CFX Manager™ Software v3.1 (Bio-Rad) and analysed in Microsoft Excel.

Table A3.2 Calculated efficiencies the oligonucleotide primers tested for the measurement of *ASCL2* expression. The efficiencies calculated were outside the acceptable range of 1.8–2.2, hence were not used in further experiments. (Chapter 3.4, Chapter 7.2.8).

Primer set	Calculated Efficiency
ASCL2 set A 300 nM	1.047
ASCL2 set A 900 nM	1.245
ASCL2 set B 300 nM	3.087
ASCL2 set B 900 nM	650.675

β-actin was chosen for use as a housekeeping gene. RT-qPCR experiments using cDNA from F-KDM4A U2OS cells incubated in 0.1–21% O_2 (Chapter 7.2.3. Chapter 7.2.8) revealed similar Ct values arising from RT-qPCR analysis of *β-actin* across the samples tested (Figure A3.3), suggesting that treatment of cells with doxycycline and incubation in hypoxia has no significant effect on *β-actin* expression.

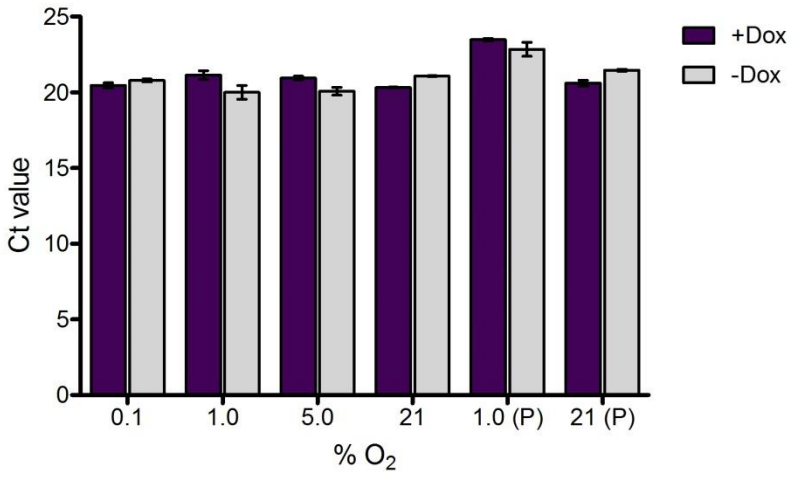

Figure A3.3 Ct values from the RT-qPCR analysis of *β-actin* expression in cDNA samples from F-KDM4A U2OS cells treated ± dox and incubated in various O_2 concentrations. N = 3 biological repeats, error bars represent sd. Graphs were produced in GraphPad Prism v5.04. Data was collected and processed using CFX Manager™ Software v3.1 (Bio-Rad) and analysed in Microsoft Excel.

References:

(1) Mallette, F. A., and Richard, S. (2012) JMJD2A promotes cellular transformation by blocking cellular senescence through transcriptional repression of the tumor suppressor CHD5. *Cell Rep. 2*, 1233–43.

(2) Rao, V. H., Kandel, A., Lynch, D., Pena, Z., Marwaha, N., Deng, C., Watson, P., and Hansen, L. A. (2012) A positive feedback loop between HER2 and ADAM12 in human head and neck cancer cells increases migration and invasion. *Oncogene 31*, 2888–98.

(3) Zhang, D., Yoon, H.-G., and Wong, J. (2005) JMJD2A is a novel N-CoR-interacting protein and is involved in repression of the human transcription factor achaete scute-like homologue 2 (ASCL2/Hash2). *Mol. Cell. Biol. 25*, 6404–14.

Appendix 4: Publications arising from work described in this thesis

1) Hancock, R. L., Masson, N., Dunne, K., Flashman, E., and Kawamura, A. (2017) The activity of JmjC histone lysine demethylase KDM4A is highly sensitive to oxygen concentrations. *ACS Chem. Biol.* acschembio.6b00958. Just accepted.

2) Wilkins, S. E., Abboud, M. I., Hancock, R. L., and Schofield, C. J. (2016) Targeting Protein-Protein Interactions in the HIF System. *ChemMedChem 11*, 773–86.

3) Hancock, R. L., Dunne, K., Walport, L. J., Flashman, E., and Kawamura, A. (2015) Epigenetic regulation by histone demethylases in hypoxia. *Epigenomics 7*, 791–811.